



**POZNAN UNIVERSITY OF TECHNOLOGY**  
**Faculty of Chemical Technology**

**DOCTORAL DISSERTATION**

**Martino Di Serio**  
**UNIVERSITY OF NAPLES FEDERICO II**  
**Department of Chemical Sciences**

**Catalysis, Kinetics, and Chemical Reactor Engineering**  
**for Alkoxylation Reactions**

**DISSERTATION SUPERVISOR**  
**D.Sc. Wiesław Hreczuch**

**Poznan 2024**



### **Acknowledgements**

I would like to express my sincere thanks to my promoter Wieslaw Hreczuch, D.Sc., for assisting me in the creation of this dissertation.

I also thank my wife Amina and my daughters Roberta and Stefania for their patience, understanding, and support that has allowed me to devote myself with continuity and intensity to my work.





# Table of contents

<b>Aim and Description of the Dissertation.....</b>	<b>1</b>
<b>Part I-State of Art in the Alkoxylation Reactions</b>	
<b>Chapter 1.- Introduction.....</b>	<b>3</b>
1.1 Ethylene Oxide and Propylene Oxide.....	4
<b>Chapter 2 – Reaction Mechanisms and Catalysis.....</b>	<b>9</b>
2.1 Non catalyzed reaction.....	9
2.2 Distribution of Oligomers.....	11
2.3 Acid Catalysts.....	16
2.4 Basic Catalysts.....	24
<b>Chapter 3.- Kinetics of the alkoxylation reaction of fatty alcohols catalyzed by metal alkaline hydroxides.....</b>	<b>33</b>
3.1 Experimental.....	33
3.2 Results and discussion.....	38
3.2.1 Density.....	38
3.2.2 Solubility.....	40
3.2.3 Kinetic runs.....	46
3.2.4 Well mixed Stirred Feed Batch Reactor Modell and kinetic parameters determination.....	54
3.3 Conclusions.....	58
<b>Chapter 4 Industrial Alkoxylation Reactors.....</b>	<b>59</b>
4.1 Description of Industrial Alkoxylation Reactors.....	59
4.2 Mathematical model of Venturi Loop Reactor (VLR).....	62
4.3 Mathematical model of Spray Tower Loop Reactor (STLR).....	66
4.4 Safety in ethoxylation processes.....	71

<b>4.5 Conclusions.....</b>	<b>76</b>
-----------------------------	-----------

## **Part II- Process Intensification in the Alkoxylation Reactions**

<b>The novelty of present dissertation.....</b>	<b>77</b>
<b>Chapter 5 Enhanced Loop Reactor (ELR).....</b>	<b>79</b>
<b>5.1 Mathematical model of Enhanced Loop Reactor (ELR).....</b>	<b>79</b>
<b>5.2 Conclusions.....</b>	<b>85</b>
<b>Chapter 6- Alkoxylation in continuous reactors.....</b>	<b>87</b>
<b>6.1 Discussion and perspectives on continuous alkoxylation reactors.....</b>	<b>88</b>
<b>6.2 Conclusions.....</b>	<b>101</b>
<b>Chapter 7- Alkoxylation in milli and micro reactors.....</b>	<b>103</b>
<b>7.1 Laminar flow model for micro and milli reactors.....</b>	<b>104</b>
<b>7.2 Physicochemical properties.....</b>	<b>108</b>
<b>7.3 Simulation and parameter estimation activities in laminar regimes.....</b>	<b>112</b>
<b>7.3.1 Application of the model to experimental ethoxylation data ....</b>	<b>112</b>
<b>7.3.2 Simulation of larger reactors.....</b>	<b>117</b>
<b>7.4 Simulation of reactors working in plug-flow regimes.....</b>	<b>118</b>
<b>7.5 Conclusions.....</b>	<b>121</b>
<b>Chapter 8 - Conclusions summarizing the scientific achievements of the Candidate and being the basis of the dissertation. ....</b>	<b>123</b>
<b>List of Symbols.....</b>	<b>125</b>
<b>Literature.....</b>	<b>131</b>

**Appendix 1 The Author's published output including  
the material described in the dissertation, Part II.....138**

Article 1. Cypyright.....139  
Article 1. Content.....140  
Article 2 – 4 Copyright.....154  
Article 2. Content.....156  
Article 3. Content.....164  
Article 4. Content.....173  
Article 5. Copyright.....176  
Article 5. Content.....177

**Appendix 2. Declarations of co-authors on the substantive  
contribution to the articles. Articles 1 to 5.....194**

Statements to the Article 1.....195  
Statements to the Article 2.....199  
Statements to the Article 3.....203  
Statements to the Article 4.....208  
Statements to the Article 5.....209

# Aim and Description of the Dissertation

In this dissertation the main aspects related with the Alkoxylation Reactions for the synthesis of nonionic surfactants are reported.

The work is divided in two parts. Part I is an introduction to the subject of the work and an analysis of the state of knowledge in the field of oxyalkylation also covering the author's earlier works, before his professorial promotion, and **Part II** where the recent results obtained by the candidate on the reactor engineering and intensification of ethoxylation technology, **constituting the essential research part of the submitted doctoral thesis**, were reported.

The following layout of Part I has been chosen: after a description of the properties of the principal alkylene oxides (ethylene and propylene oxide) (chap.1), a general survey on the catalysts used in the syntheses are described with the related reaction mechanisms in chap. 2. A deep report was then done in chap. 3 on the kinetics of the alkoxylation reaction of fatty alcohols catalyzed by metal alkaline hydroxides. Subsequently, the mathematical models developed for the simulation of classical industrial reactors is described in chap. 4., also addressing the problems related to safety.

The Part II is the doctoral student's original work contribution in teamwork where he played a leading or pivotal role, conducted after professorial promotion in June 2017. Part II describes the most work of the candidate in the sector of intensification of the process with the improve of the classical reactors and in evaluation of the possibility to change the process from semi batch to continuous: in the chap. 5 the model developed for the new Enhanced Loop Reactor (ELR) was reported (DiSerio, M., Russo, V., Santacesaria, E., & Tesser, R., 2021). In chap.6 a review on continuous reactors for alkoxylation described in patents and scientific literature was reported (Tesser, R., Russo, V., Santacesaria, E., Hreczuch, W., & DiSerio, M., (2020). In chap. 7 the possibility to use micro or milli reactor in process intensification for ethoxylation reaction was presented (M Di Serio, 2019), *Frontiers in Chemical Engineering* 1, 2.).

The issues presented in the work are new and belong to the original achievements of the author or made in a team where he played a leading or important role, especially in the field of mathematical modelling, kinetic calculations and creation of advances in reactor engineering towards increase of productivity and safety of the oxyalkylation processes.

The work answers fundamental questions about how progress can be made in increasing the efficiency and safety of the oxyalkylation process, by the postulated

solutions to make the synthesis process continuous and to realise it in a milli- or micro-reactor system. The theses postulated are verified by detailed documented kinetic calculations and mathematical modelling.

The aim of the dissertation is to provide the scientific basis and rationale for further work on the industrialisation of oxyalkylation processes towards a continuous synthesis node and the use of microreactor technology in this field.

# Part I- State of art in the alkoxylation reactions

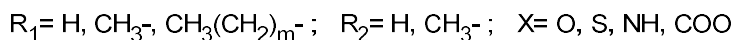
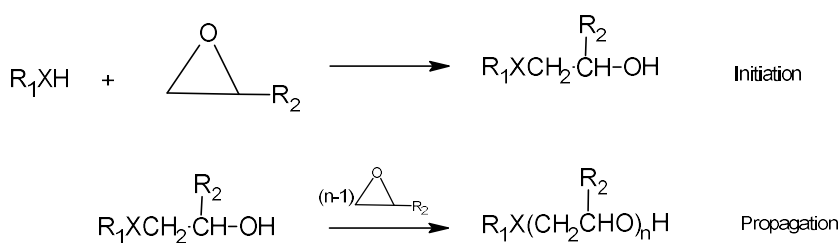
## Chapter 1.- Introduction

Alkoxylation reactions involve the reaction of epoxides (generally ethylene oxide or propylene oxide) with an organic molecule containing an active hydrogen such as alcohols, phenols, carboxylic acids, mercaptans, and amines (Schachat and Greenwald 1967; Edwards 1998; Santacesaria, Iengo, and Di Serio, 1999).

A large part of the use of alkoxylation reactions is the production of non-ionic surfactants or ethylene oxide / propylene oxide copolymers (Santacesaria, di Serio, and Tesser, 2008)

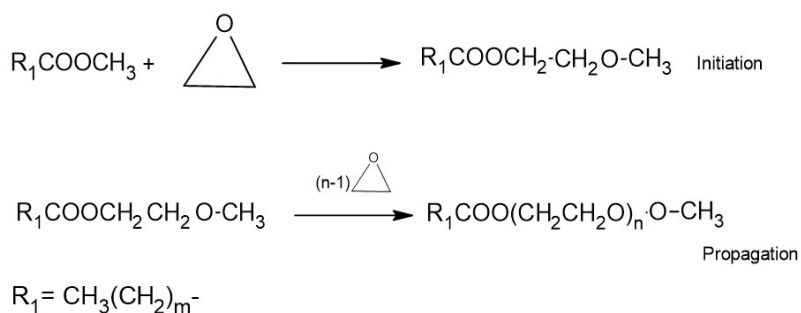
The products of alkoxylation reactions are of great interest for the industry. The size of the global surfactant market was \$ 41.3 billion in 2019 with a share of 37% for non-ionic surfactant. Other important industries using oxyalkylation include the production of glycols, alkyl-ether solvents, and high molecular weight polyethers in processing into polyurethanes and others.

The reactions can give rise to oligomers because the reaction product itself contains an active hydrogen (see scheme 1-1)



**Scheme 1-1.**

With suitable catalysts, also ethoxylation reactions of esters are possible (Szymanowski 2008; Di Serio et al. 2015), and in this case with oligomer production (see for example, scheme 1-2).



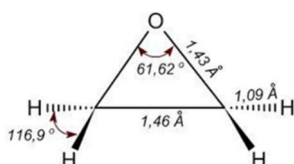
**Scheme 1-2.**

In this chapter the physico-chemical properties of the most used alkylene oxide (ethylene oxide and propylene oxide) are summarized.

## 1.1 Ethylene Oxide and Propylene Oxide

Oxirane rings can easily react under acid, basic and neutral conditions.

Ethylene oxide (EO) is an ether having the oxygen atom in a three-membered ring (Schachat & Greenwald, 1967).



**Scheme 1-3**

The C—O—C bond angle for an epoxide must be 60°, a considerable deviation from the tetrahedral bond angle of 109.5°. Thus, epoxides have angle strain, making them more reactive than other ethers.

The principal chemo-physical properties of ethylene and propylene oxide are summarized in Tab. 1.1-1

From the Tab. 1.1-1 it is evident that both epoxides are highly reactive in air, and they have to be managed very carefully. It is to point out that the explosion limit of ethylene oxide is between 2.6 and 100 vol%, that it means that it is possible to also have the decomposition of ethylene oxide in absence of an oxidant if there is present an enough ignition energy (1000 mJ).

The boiling point of ethylene oxide is 10.5 °C while for propylene oxide we have 34 °C (a boiling point similar to that of diethyl ether), for this reason, ethylene oxide can

be commercialized only in gas cylinder while for propylene oxide it is possible use also glass bottles, naturally avoid high temperature.

The heat of reaction of the two epoxide is very high (mainly for ethylene oxide, 2300 kJ/kg) and for this reason the main industrial technologies for the alkoxylation reaction, as we will see later, use the feed batch approach using Nitrogen for reducing the concentration of epoxides in gaseous atmosphere.

However, the safety problem in the use of alkylene oxides are also linked with their toxicity. In Tab. 1.1-2 and 1.1-3 the info cards of ECHA (European Chemical Agency) for ethylene oxide and propylene oxide are reported.

**Tab. 1.1-1 Chemo-physical properties of ethylene and propylene oxide**




	Ethylene Oxide	Propylene Oxide
Molar mass, g/mol	44.05	58.08
Melting Point (101.3 kPa), °C	-112.5	-111.9
Boiling Point (101.3 kPa), °C	10.5	34.2
Flash Point, °C	-57	-37
Critical Temperature, °C	196.0	209.1
Critical Pressure, kPa	7191	4920
Critical Density, Kg/m <sup>3</sup>	313	312
Critical compressibility factor	0.2588	0.2284
Auto ignition temperature in air at 101.3 kPa, °C	445	449
Explosive limits in air (STP):		
.-Lower, vol %	2.6	1.7
.-Upper, vol %	100	37.0
Heat of combustion (25°C 101.3 kPa), kJ/kg	-29647	-33035
Heat of Polymerization, kJ/Kg	-2324	-1500
Heat of fusion, kJ/kg	117.5	112.6
Heat of solution in water at 25°C, kJ/kg	-143	-45
Heat of formation of the ideal gas (25°C), kJ/kg	-1195	-1600
Heat of formation of liquid Alkylene Oxide (25°C), kJ/kg	-1766.5	-2080
Cubic expansion coefficient at 20°C, 1/K	0.00158	0.00151
Solubility of Alkylene Oxide in water at 20°C, wt%	73	40
Density at 20°C, kg/m <sup>3</sup>	0.875	0.83
Vapor pressure (kPa at 20°C)	145.9	57.7
Flashpoint of 1% aqueous solution, °C	31	23

- (a) Ethylene Oxide Product Stewardship Guidance Manual. American Chemistry Council (2017) <https://www.americanchemistry.com/EO-Product-Stewardship-Manual-3rd-edition/>
- (b) Guidelines for the distribution of Propylene Oxide. Propylene Oxide/Propylene Glycols Cefic Sector Group (2019). [https://www.petrochemistry.eu/wp-content/uploads/2019/04/CEFIC-PO\\_GuidelinesForTheDistributionOf-BROCH\\_V04-pbp.pdf](https://www.petrochemistry.eu/wp-content/uploads/2019/04/CEFIC-PO_GuidelinesForTheDistributionOf-BROCH_V04-pbp.pdf)



The two substances are classified toxic, cancerogenic (1B) and mutagenic (1B), moreover ethylene oxide is classified also as toxic for the reproduction, possible endocrine disrupting. The exposure thresholds value for Systemic Effects and Local System of ethylene oxide<sup>1</sup> are (Long Term Exposition) DMEL<sup>2</sup> = 1.8 mg/m<sup>3</sup> and (Acute/Short Term exposition) DNEL<sup>3</sup> = 10 mg/m<sup>3</sup>, in the case of propylene oxide<sup>4</sup> there aren't threshold value reported for Systemic Effect (Low hazard) while the values for Local Effect (irritation, respiratory tract) are (Long Term Exposition) DNEL = 2.4 mg/m<sup>3</sup> and (Acute/Long Term Exposition) DNEL = 170 mg/m<sup>3</sup>.

**Tab. 1.1-2 Info card ECHA (Last updated: 19/04/2021) of ethylene oxide<sup>5</sup>**

<b>Hazard classification &amp; labelling</b>	
<p><b>Substance identity</b></p> <p><b>EC / List no.:</b> 200-849-9</p> <p><b>CAS no.:</b> 75-21-8</p> <p><b>Mol. formula:</b> C<sub>2</sub>H<sub>4</sub>O</p>	<div style="text-align: center;">  </div> <p>Danger! According to the harmonised classification and labelling (ATP14) approved by the European Union, this substance is toxic if swallowed, causes severe skin burns and eye damage, is toxic if inhaled, may cause genetic defects, may cause cancer, may damage fertility and is suspected of damaging the unborn child, causes damage to organs through prolonged or repeated exposure, is an extremely flammable gas, causes serious eye damage, may cause respiratory irritation and may cause drowsiness or dizziness.</p>
	<p>Additionally, the classification provided by companies to ECHA in REACH registrations identifies that this substance may damage fertility or the unborn child, is an extremely flammable gas and may react explosively even in the absence of air, contains gas under pressure and may explode if heated and causes skin irritation.</p>
	

<sup>1</sup> <https://echa.europa.eu/brief-profile/-/briefprofile/100.000.773>

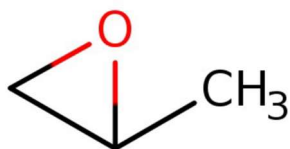
<sup>2</sup> Derived Minimal Effect Level (DMEL) is defined as a level of exposure below which the risk levels of cancer become tolerable.

<sup>3</sup> Derived No-Effect Level (DNEL) is defined as the level of chemical exposure above which humans should not be exposed.

<sup>4</sup> <https://echa.europa.eu/brief-profile/-/briefprofile/100.000.800>

<sup>5</sup> <https://echa.europa.eu/substance-information/-/substanceinfo/100.000.773> (Last updated: 19/04/2021)

Tab. 1.1-3 Info card ECHA propylene oxide (Methyloxirane)<sup>6</sup>



EC / List no.:	200-879-2
CAS no.:	75-56-9
Index number:	603-055-00-4
Molecular formula:	C <sub>3</sub> H <sub>6</sub> O

#### Hazard classification & labelling



Danger! According to the harmonized classification and labelling (ATP09) approved by the European Union, this substance is toxic in contact with skin, is toxic if inhaled, may cause genetic defects, may cause cancer, is an extremely flammable liquid and vapor, is harmful if swallowed, causes serious eye irritation and may cause respiratory irritation.



Additionally, the classification provided by companies to ECHA in REACH registrations identifies that this substance is harmful to aquatic life and causes skin irritation.

<sup>6</sup> <https://echa.europa.eu/brief-profile/-/briefprofile/100.000.800> (Last updated 19/04/2021)



## Chapter 2 – Reaction Mechanisms and Catalysis

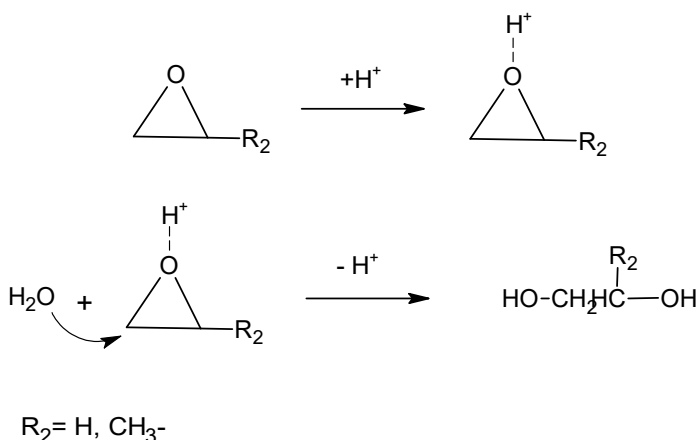
The reaction rate of alkoxylation depends on the alkylene oxide used, substrate structure, temperature, catalyst. Ethylene oxide is mostly more reactive than propylene oxide. The opposite is true for double metal cyanide catalyst applications, where propylene oxide is much more reactive. However, this area is beyond discussion in this dissertation.

### 2.1 Non catalyzed reaction

The initiation reaction with some substrates can start when the right temperature is achieved. The reactivity of substrate can be linked with its Bronsted acidity or nucleophilicity.

Water reacts with ethylene oxide and propylene oxide at 190-200°C without catalyst to produce ethylene glycol (Yue et al., 2012) and propylene glycol (Martin & Murphy, 2000), respectively. The alkylene oxide reacts with  $H^+$  present in the water to form an activated species that reacts with water to produce the glycol (see scheme 2.1-1).

The reaction is an autocatalytic substitution reaction where  $H_2O$  is the nucleophilic specie but, because its autoprotolysis, it also forms the electrophile specie. The formed glycol can react with alkylene oxide to form oligomers with the same mechanism.



**Scheme 2.1-1.**

The formation of the higher homologues is inevitable because alkylene oxide reacts with alkylene glycols more quickly than with water (Rebsdats & Mayer, 2000). The

yields of oligomers can be reduced using an excess of water. In Industry, a 20-fold molar excess is usually employed (Rebsdats & Mayer, 2000), and a selectivity around 90% of ethylene glycol or propylene glycol is obtained (around 10% of mono-, di-, and triethylene glycols).

Also, carboxylic acids can react with ethylene oxide without the presence of catalyst, as can be seen in Fig. 2.1-1 (Di Serio, di Martino, and Santacesaria 1994).

For this reaction a mechanism with the formation of an activated intermediate has been proposed (scheme 2.1-2) (Di Serio, di Martino, and Santacesaria 1994)

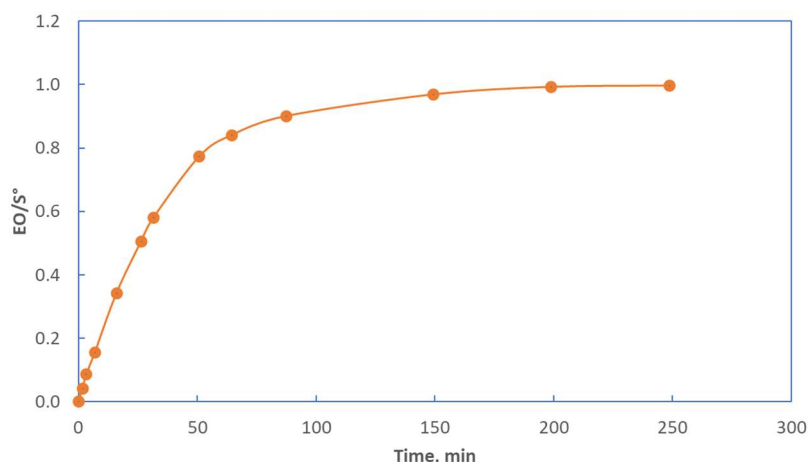
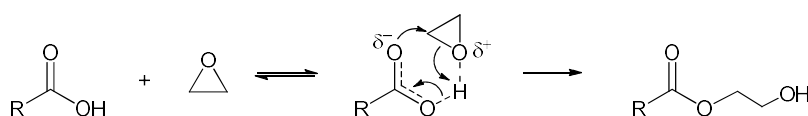


**Fig. 2.1-1.** Ethoxylation of lauric acid performed at 150 °C and 4 atm in the absence of catalyst (Di Serio, di Martino, and Santacesaria 1994)



**Scheme 2.1-2**

In the case of fatty acid, the reaction without catalyst gives only the first adduct because the nucleophilicity of the product is not sufficient for further reactions.

Fatty amines react with ethylene oxide without catalyst because the high nucleophilicity of ammine group (Enikolopiyan, 1976)(see scheme 2.1-3):



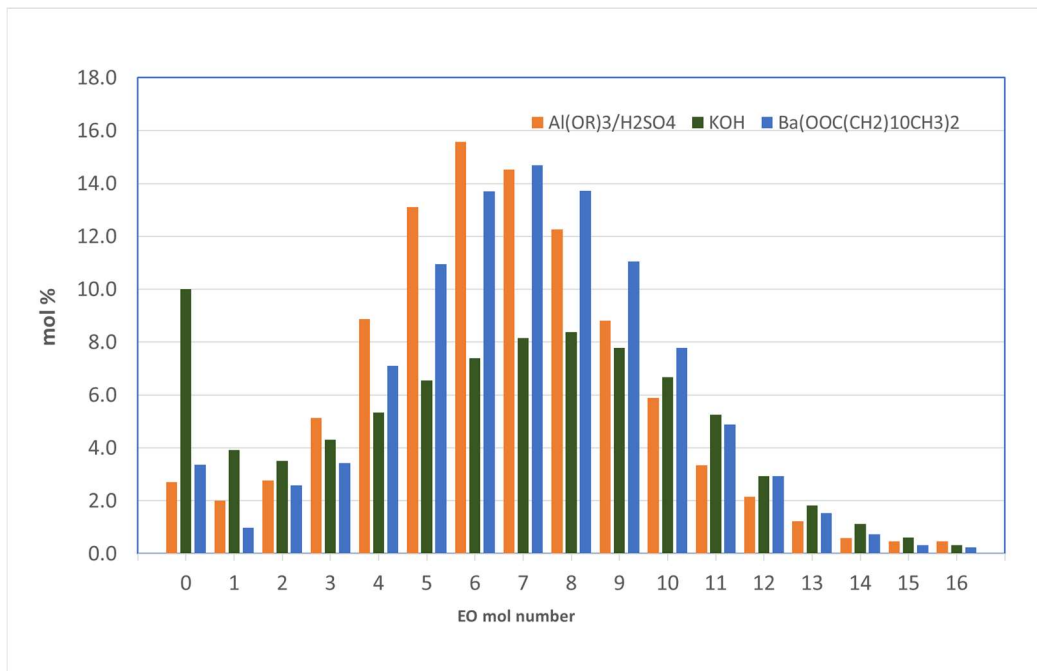


**Fig. 2.2-1.** Oligomer distribution in ethoxylation of dodecanol using different catalysts ( $\text{Al}(\text{OR})_3/\text{H}_2\text{SO}_4$  (Edwards, 1998),  $\text{KOH}$  and  $\text{Ba}(\text{OOC}(\text{CH}_2)_{10}\text{CH}_3)_2$  (Santacesaria et al., 1992b) ) for a molar ratio ethylene oxide reacted/ initial dodecanol equal to 7 ( $\text{EO}/\text{S}^\circ=7$ ).

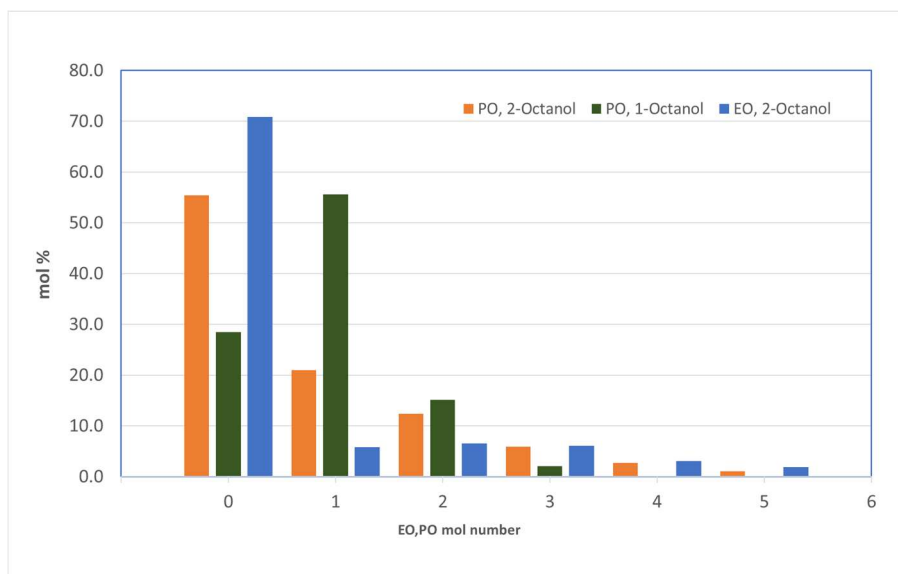
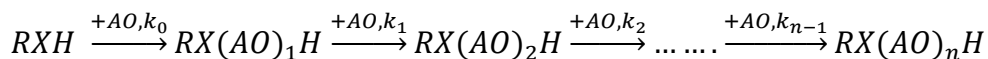


**Fig. 2.2-2.** Oligomer distribution in ethoxylation (EO) and propoxylation (PO) of 1-octacanol and 2-octanol ( $\text{EO},\text{PO}/\text{S}^\circ= 0.85\text{-}0.88$ ) catalyzed by  $\text{KOH}$  (DiSerio, Vairo, et al., 1996).

Considering the reaction scheme 2.2-1



### Scheme 2.2-1

the differences on oligomer distribution are function of the reactivity of starter (RXH) and of oligomers with the allylene oxide (AO).

From previous reaction scheme, if the probability of reaction rate of substrate is equal to that of all oligomers the molar oligomer distribution can be calculated by the molar ratio of alkylene oxide reacted /initial mol starter ( $v = AO/S^\circ$ ) using the Poisson equation as was demonstrated by Flory (Flory, 1940).

$$x_i = \frac{n_{RX(AO)_iH}}{n_{S^\circ}} = e^{-v} \frac{v^i}{i!} \quad (2.2-1)$$

Where,

$x_i$  = molar fractions of the oligomer  $i$ ,

$n_{RX(AO)_iH}$ , = mol of oligomer  $i$

$n_{S^\circ}$  = initial mol of starter

In Fig. 2.2-3 an example of oligomer distribution described by Flory equation is reported. If the probability of reaction of substrate is different from that of oligomers, the oligomer distribution as function of  $v = AO/S^\circ$  and molar fraction of residual starter ( $x_0$ ) can be calculates using the Weibull-Nycander equation (Schachat & Greenwald, 1967):



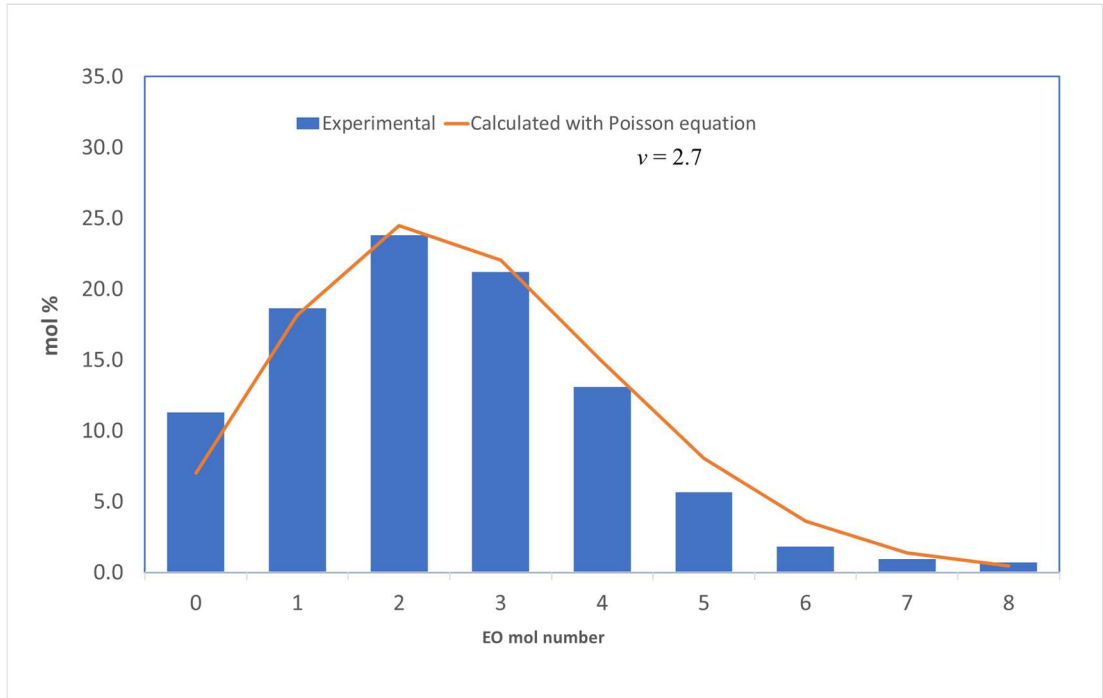


**Fig. 2.2-3.** Oligomer distribution in ethoxylation of C<sub>12</sub>-C<sub>14</sub> alcohol (EO/S°= 2.7) catalyzed by Mg/Al catalyst (Li et al., 2021).

$$x_i = \frac{c^{i-1}}{(c-1)^i} \left\{ x_0 - x_0^c \sum_{j=0}^{i-1} \frac{1}{j!} [(c-1) \ln x_0]^j \right\} \quad (2.2-2)$$

where

$$c = \frac{v+x_0-1}{x_0-\ln x_0-1} \quad (2.2-3)$$

The value of  $c$  in the case of validity of reaction scheme 2.2-1 is linked with the initiation and propagation reaction probability.

In Fig. 2.2-4 an example of oligomer distribution described by Weibull-Nycander equation is reported.

In more general case where all reaction probabilities are different for substrate and every oligomer, the oligomer distribution is given by the Natta-Mantica equation (Natta & Mantica, 1952)

$$x_i = (-1)^i \prod_{j=1}^{i-1} c_j \sum_{j=0}^i x_0^{c_j} \left[ \prod_{\substack{k=0 \\ k \neq j}}^i (c_j - c_k) \right]^{-1} \quad (2.2-4)$$

where  $c_j$  is the ratio between the probability of reaction of oligomer  $i$  and substrate.

In Fig. 2.2-5 an example of oligomer distribution that it is not described by Weibull-Nycander equation, but it is well represented by Natta-Mantica Equation.

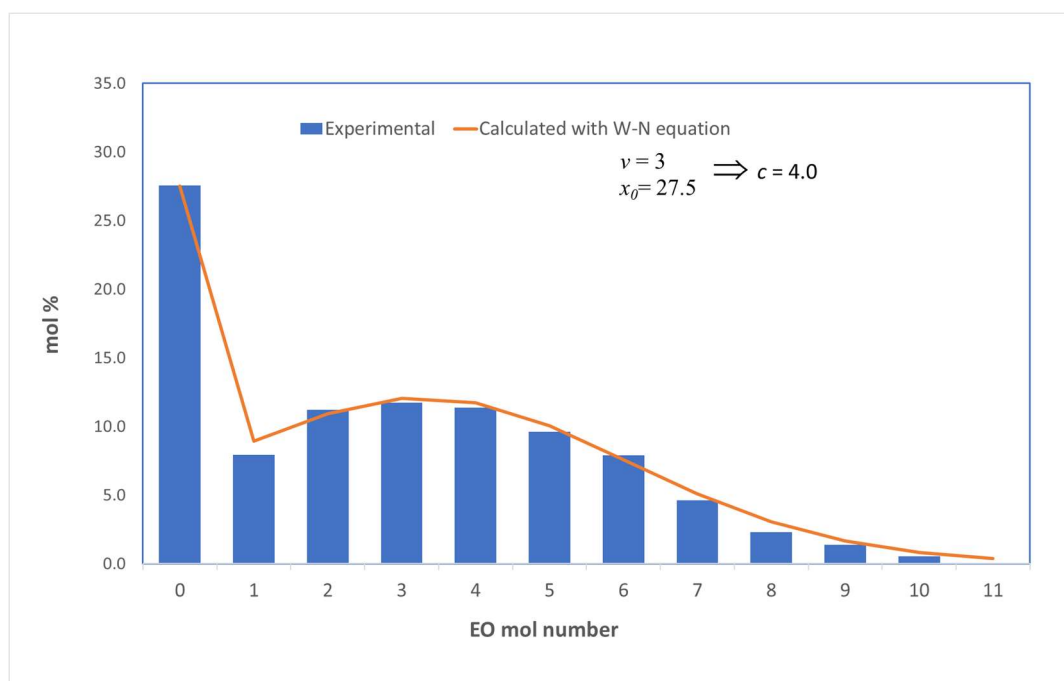


**Fig. 2.2-4.** Oligomer distribution in ethoxylation of dodecanol alcohol (EO/S°= 3) catalyzed by KOH (T=106°C; P<sub>EO</sub> =2 atm; KOH 2 % by mol) (Santacesaria et al., 1992a).

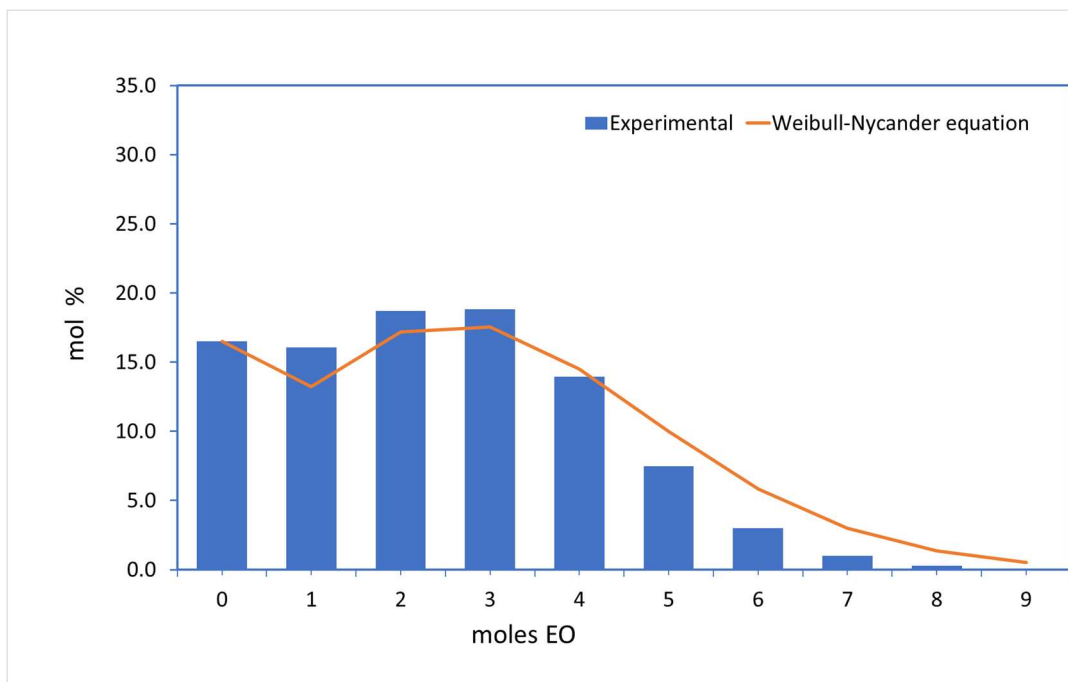


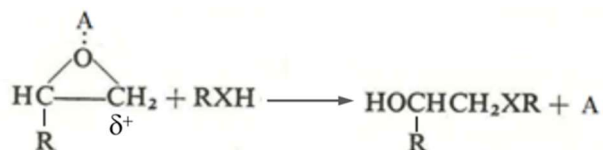
**Fig. 2.2-5.** Oligomer distribution in ethoxylation of dodecanol alcohol ( $EO/S^\circ = 2.8$ ) catalyzed by a Calcium/mineral acid catalyst ( $T=140-160^\circ\text{C}$ ;  $P_{EO} = 3 \text{ atm}$ ; Cat. 1% by wt) (Li et al., 2021).

## 2.3 Acid Catalysts

The difference in oligomer distribution in alkoxylation is strictly linked with the reaction mechanism.

### *Cationic Mechanism*

Both strong Lewis and Bronsted acids can activate the oxirane ring with a cationic mechanism:



**Scheme 2.3-1**

Where A is  $\text{H}^+$  or the active species of a Lewis acid catalyst, as example  $\text{SbCl}_5$ .

Generally, with the acid catalysts the mechanism is intermediate between  $S_N1$  and  $S_N2$ ; the order of the mechanism depends on catalyst, reaction condition and substrates (steric effect, electronic effect, etc.)(Santacesaria, Iengo, and Di Serio 1999). However these influences are less important than in the case of basic catalysts, and the reactivity of substrates is quite equal to that of oligomers, as a matter of fact  $c$  values of Weibull-Nycander equation (2.2-3) is near 1 (Poisson oligomer distribution, see fig. 2.3-1) or, in general, less than 2 (Schachat & Greenwald, 1967).

Because the influence of steric effect of the substrate is less important than in the case of basic catalysts, acid catalysts are used to ethoxylate the secondary alcohols (Baker & Thompson, 1967; Rakutani et al., 1999). For example, in the case of 2-octanol ethoxylation catalyzed by KOH a  $c$  value of Weibull-Nycander equation equal to 11 is derived on experimental data (DiSerio, Vairo, et al., 1996) while by using  $SnCl_4$  as catalyst  $c$  is 1.2 (Baker & Thompson, 1967). In fig. 2.3-2 the calculated oligomer distribution is reported for comparison when  $\nu = EO/S^\circ = 1.0$ .

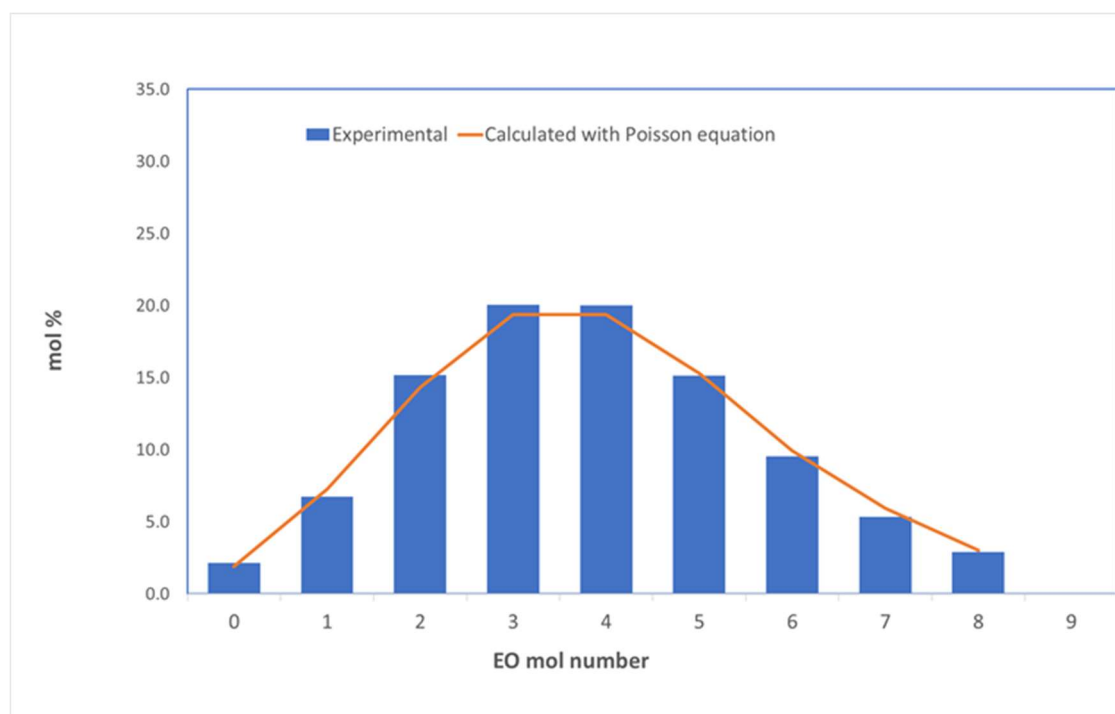


**Fig. 2.3-1.** Oligomer distribution in ethoxylation of hexyl alcohol ( $EO/S^\circ = 4.04$ ) catalyzed by  $SbCl_5$  (Schachat & Greenwald, 1967).

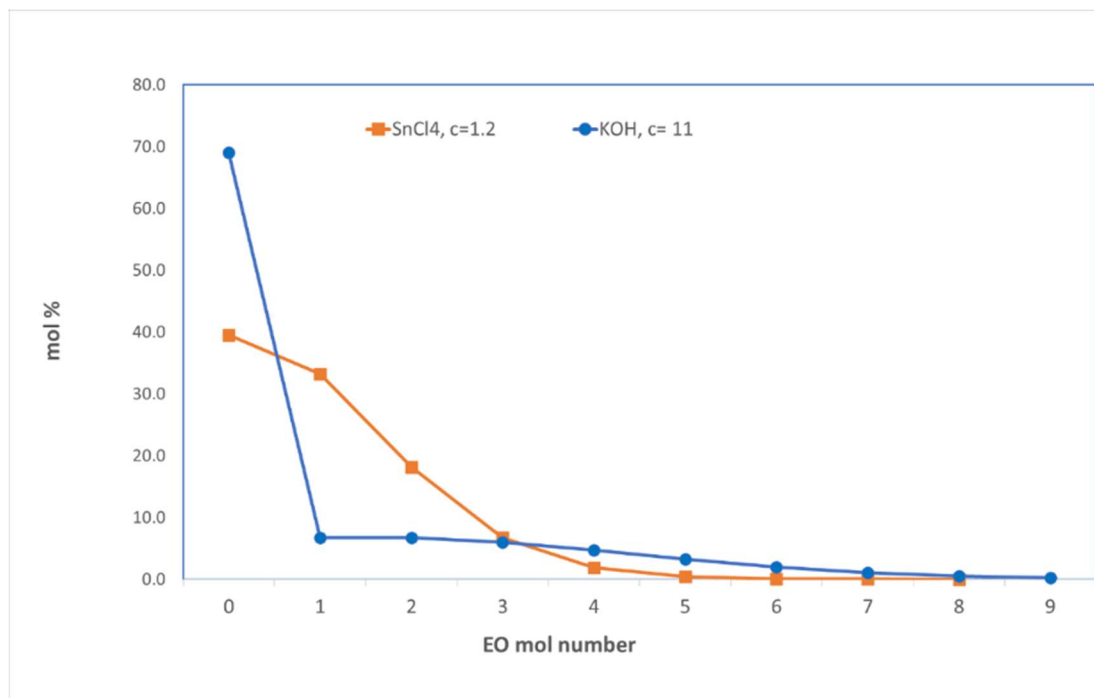
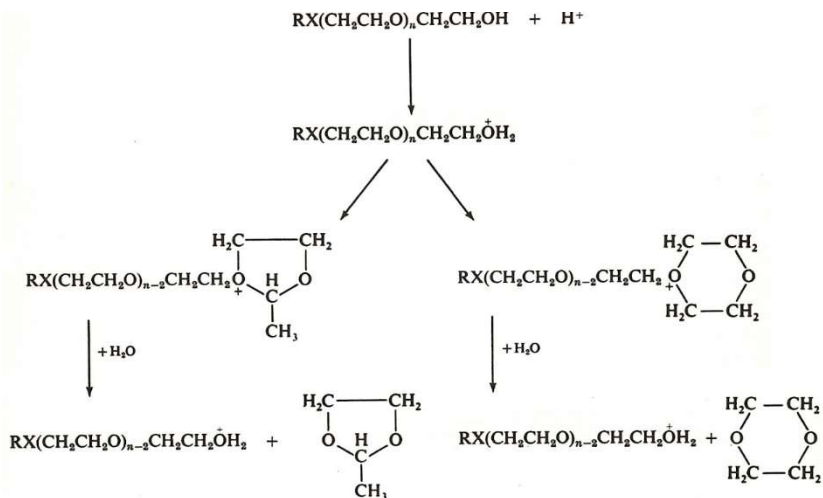


**Fig. 2.3-2.** Oligomer distribution in ethoxylation of 2-octanol calculated with Weibull-Nycander equation for  $v=EO/S^\circ=1$  and two different catalysts (KOH and  $SnCl_4$ ) using the  $c$  parameter derived from experimental data (Baker & Thompson, 1967; DiSerio, Vairo, et al., 1996).

The acid catalyst is industrially used only in case of ethoxylation of secondary alcohols (Baker and Thompson 1967; Rakutani, Onda, and Inaoka 1999) because these catalysts also promote the formation of by-products, with the following mechanism (see scheme 2.3-2, (Schachat and Greenwald 1967)).

The formation of by-products is minimized by synthesizing products with  $EO/S^\circ$  maximum equal to 3. To obtain product with higher  $EO/S^\circ$  value, secondary unreacted alcohol is removed by distillation, and the ethoxylation is continued using a basic catalyst (Rakutani, Onda, and Inaoka 1999).



**Scheme 2.3-2** (from (Schachat & Greenwald, 1967))

Lewis's acid catalyst (transition metals) can promote the ethoxylation also through a non-ionic coordination-insertion mechanism. The alkylene oxide molecule coordinated with a dative bond of oxygen to the metal atom is inserted between the metal and the coordinated substrate. In general, this type of catalysts in ethoxylation of primary alcohols give place to a narrow range oligomer distribution (Santacesaria, Iengo, et al., 1999).

Different type of catalysts has been proposed in the literature (Edwards, 1998) and in Tab. 2.3-1 a selection of these is reported.

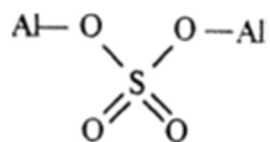
**Tab. 2.3-1. Narrow range acid catalysts (Transition Metals)**

Catalyst	Reference
Metal acetylacetonates (Al <sup>3+</sup> , Cr <sup>3+</sup> , Fe <sup>3+</sup> , Mn <sup>3+</sup> , Sn <sup>2+</sup> , Ti <sup>4+</sup> , Zn <sup>2+</sup> , Zr <sup>3+</sup> )	(Ploog, 1988b)
Al(i-OPr) <sub>3</sub> + H <sub>2</sub> SO <sub>4</sub>	(Edwards 1987; Di Serio, Iengo, et al. 1996)
Al(i-OPr) <sub>3</sub> + H <sub>3</sub> PO <sub>4</sub>	(Edwards, 1988)
Al alkoxide + H <sub>2</sub> SO <sub>4</sub> + catalytic amount of water	(Edwards, 1989)
Al alkoxide + citric or tartaric acid	(Behler et al., 1994)
Ti(OR) <sub>4</sub> or Zr(OR) <sub>4</sub> + H <sub>2</sub> SO <sub>4</sub>	(Ploog 1988a; Di Serio et al. 1998)

The kinetics and reaction mechanism of  $\text{Al}(\text{CH}_3(\text{CH}_2)_{11}\text{O})_3 + \text{H}_2\text{SO}_4$  Catalyst was deeply studied (Di Serio, Iengo, et al. 1996; Improta, Di Serio, and Santacesaria 1999).

The presence of sulfuric acid strongly increases the activity of ethoxylation reaction in respect to the use of  $\text{Al}(\text{CH}_3(\text{CH}_2)_{11}\text{O})_3$  alone, see fig. 2.3-3.

IR and  $^{27}\text{Al}$ -NMR characterization indicated that in solution bridging bidentate coordinated sulphate species are predominant.



Theoretical calculation showed that the presence of the sulphate group in a bridging bidentate coordination, because its electron-withdrawing effect makes aluminum atoms more positively charged, consequently, more electrophilic. This effect favors the reaction of ring opening of oxirane, in initiation and propagation stage (see scheme 2.3-3).

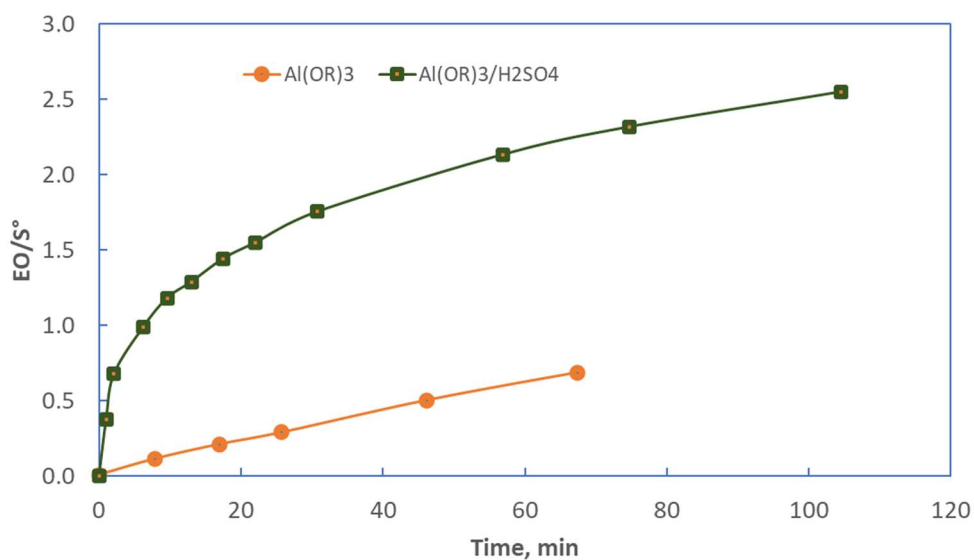
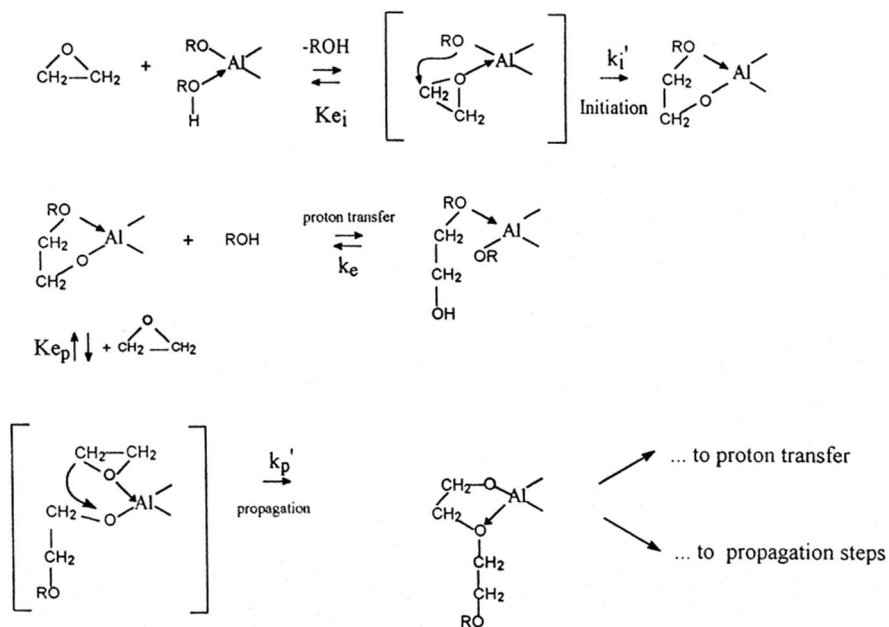


**Fig. 2.3-3.** Ethoxylation of dodecanol acid at 150 °C and 2 atm in the presence of aluminum alkoxide ( $\text{Al}(\text{OR})_3$ ) or aluminum alkoxide sulphate catalyst ( $\text{Al}(\text{OR})_3/\text{H}_2\text{SO}_4 = 1/1$ ). Cat= 1.5% mol. (DiSerio, Iengo, et al., 1996).

In reaction scheme 2.3-3, the first step is coordination of the ethylene oxide adduct to an aluminum atom, displacing a dodecanol molecule.



**Scheme 2.3.3** from (Improta et al., 1999)

The electrophilicity of active aluminum atoms weakens the OC bonds in the oxirane moiety, making the opening of the oxirane ring much easier. The chain can grow further (propagation) or exchange the proton with a free hydroxyl group (proton transfer). Theoretical computations show that, after the insertion reaction has occurred, the ethoxylated chain folds on itself to coordinate the etheral oxygen atom to aluminum. This bonding interaction provides a stabilization, decreasing the probability of a successive ethylene oxide coordination, and thus decreasing the reaction rate, as can be seen in fig. 2.3-3. However, this effect favors the initiation stage with a consequent higher starter consumption and narrow range oligomer distribution (see fig. 2.3-4).



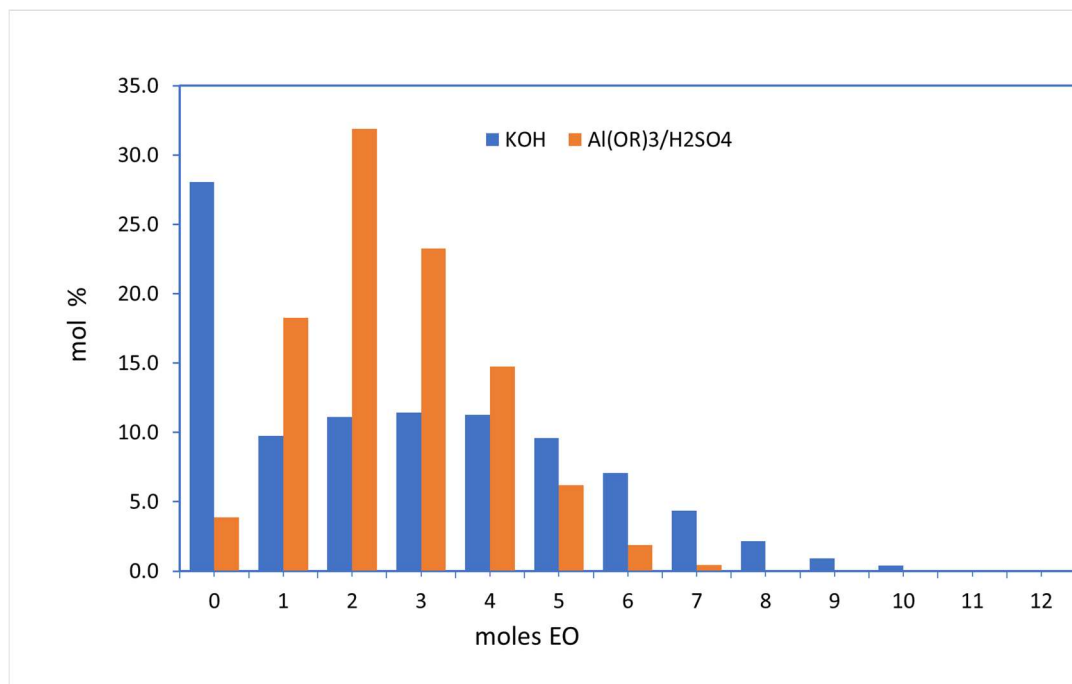


**Fig. 2.3-4.** Oligomer distribution in ethoxylation of dodecanol ( $EO/S^\circ=2.5$ ) with two different catalysts (KOH and  $Al(OR)_3/H_2SO_4 = 1/1$ ) (Di Serio, Iengo, et al. 1996).

It has been demonstrated that also double metal cyanide (DMC) catalysts ( $M^1x[M^2(CN)_6]yL$  ( $M^1 = Zn^{2+}, Fe^{2+}$  or  $Ni^{2+}$ ,  $M^2 = Fe^{3+}$  or  $Co^{3+}$ ,  $L = H_2O, F^-, Cl^-, Br^-, I^-$ , alcs., glycols, ethers or polyethers), generally used in the polyether polyols synthesis, can be used as very active catalyst in ethoxylation of fatty alcohol (rate of reaction ( $g_{EO}/(g_{cat}g_{sub} h)$ ) at  $130-140^\circ C$ ,  $0.3-0.5$  MPa with KOH = 3.4, with DMC = 23.8) giving place narrow oligomer distribution. In this case the reaction mechanism should be different from that described, because non deactivation has been observed during the reaction until an  $EO/S^\circ = 4.5$  (Janik & Chruściel, 2015). Moreover, the catalyst is very active also in the ethoxylation of secondary alcohols, obtaining a narrow oligomer distribution and low by-products concentration until a value of  $EO/S^\circ = 6$  (Hreczuch et al., 2016)(see fig. 2.3-5).

For this type of catalyst, a coordinative cationic polymerization mechanism has been proposed (see scheme 2.3-4 for propoxylation reaction (Zhang et al., 2007)). From the proposed mechanism, it can be assumed that the narrow range distribution is due to the rapid exchange (steps 5 and 7 in scheme 2.3-4)

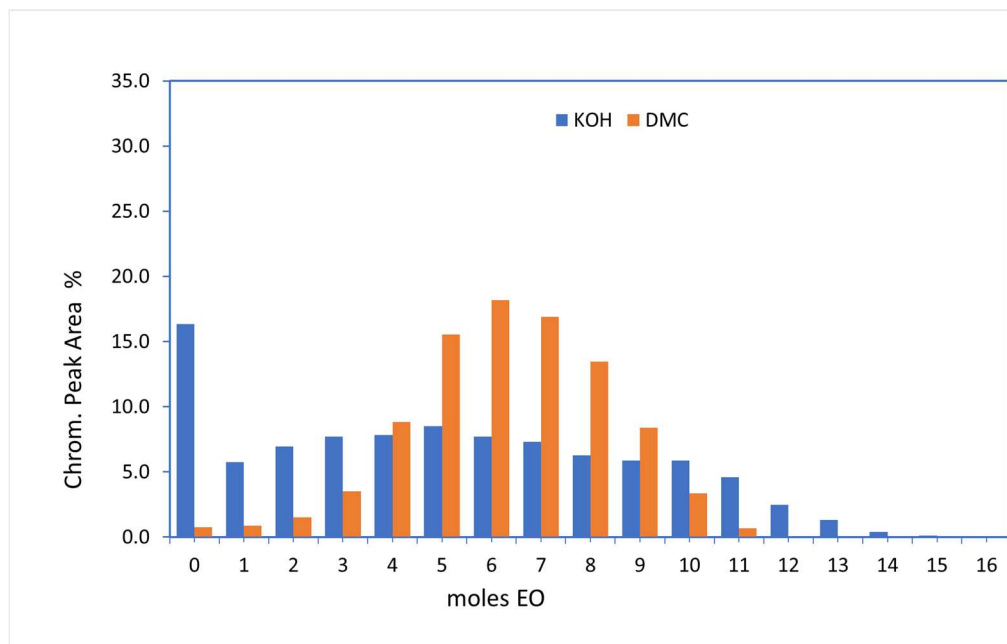
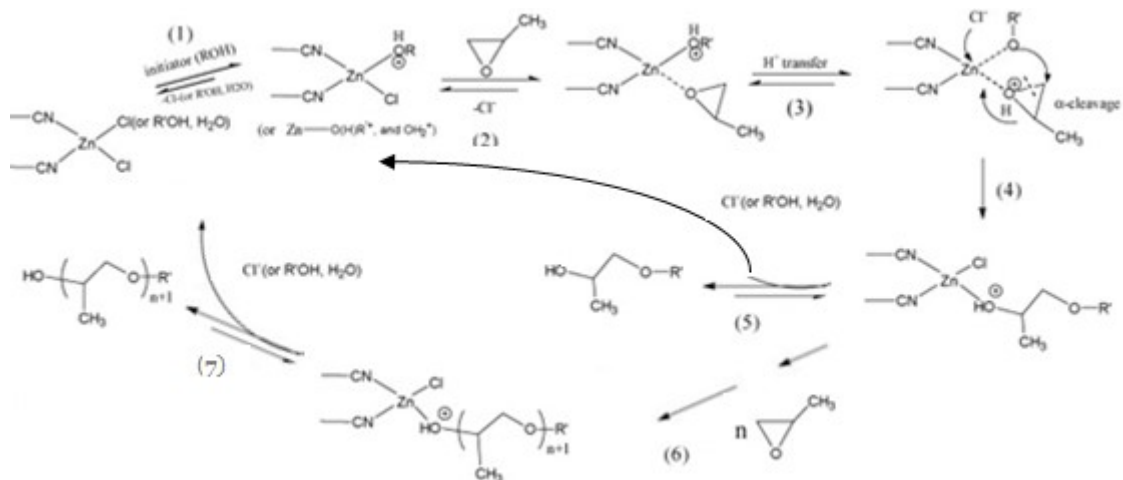


**Fig. 2.3-5.** Oligomer distribution in ethoxylation of 2-ethyl hexanol obtained with KOH and DMC catalyst for  $EO/S^{\circ}=6$  (Hreczuch et al., 2016).



**Scheme 2.3-4** Polymerization mechanism for propoxylation reaction with DMC catalyst (from (Zhang et al., 2007))

## 2.4 Basic Catalysts

Basic catalysts are the most used in the industry. These catalysts are hydroxides, oxides, or methyl alkoxides of alkaline or alkaline earthy metals. The most used are NaOH and KOH. The kinetic behavior and the consequent oligomer distribution depends strongly by the used substrate, because in this case the reaction mechanism is  $S_N2$  between alkylene oxide and the ionic couple formed in the reaction mixture (Schachat & Greenwald, 1967).

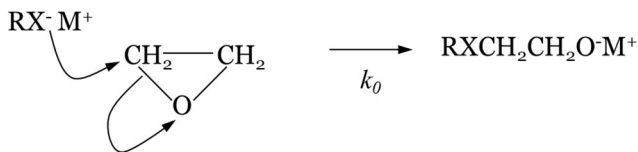
In the case of basic catalyst, the reaction scheme is more complex than that of scheme 2.2-1. The first stage in the reaction is the ionic couple formation, as an example, for an alkaline metal hydroxide:



### Scheme 2.4 -1

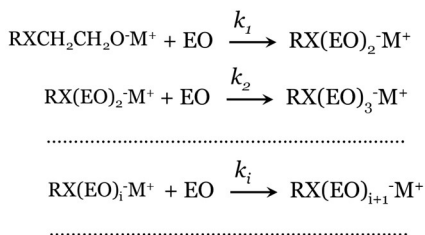
In general, before the addition of alkylene oxide the reactor is purged with nitrogen to remove oxygen (for safety reason) e and water (to reduce the formation of by-products).

The ionic couple reacts with alkylene oxide (initiation reaction), and in the case of ethylene oxide we have:



Scheme 2.4-2

Then the propagation reactions are possible:



### Scheme 2.4-3

Considering that a SN2 reaction mechanism is operative the general reaction rate equation is

$$r_i = k_i [RX(EO)_i^- M^+] [EO] \quad (\text{Eq. 2.4-1})$$

However, the oxyalkylene anions are involved also in proton-transfer reactions:



### Scheme 2.4-4

And the following general equilibrium equation can be written:

$$K_{ei} = \frac{[RXH][RX(EO)_i^- M^+]}{[RX^- M^+][RX(EO)_i H]} \quad (\text{Eq. 2.4-2})$$

The values of  $k_i$  and  $K_{ei}$  are strongly linked with the acidity of substrate and oligomers. As a matter of fact, strong acid molecules give place to a weak nucleophilic anion even if favors their formation. The values of  $k_i$  and  $K_{ei}$ , influence the reaction rate and the oligomer distribution.

In fig. 2.4-1 the consumption of ethylene oxide vs reaction time, for 3 different substrates (dodecanol, nonylphenol and dodecanoic acid) is reported, using KOH as catalyst.

Dodecanol shows a quasi-linear trend of the ethylene oxide consumption, nonylphenol has two consecutive linear trends, with an increase in reaction rate in the second trend. Dodecanoic acid has an initial curve that arrive at a plateau followed by a linear trend. Also, in this case the reaction rate increases with respect to the initial reaction rate.

The behavior of dodecanol can be explained considering that the formed oligomers being linear alcohols, have quite the same nucleophilicity of initial substrate that is an alcohol (see scheme 2.4-5).

The consequence is that the reactivity of ion pair of substrate and oligomers is the same ( $k_0 = k_1 = \dots = k_i = \dots = \dots$ ) A Poisson distribution of oligomer could be forecasted by this observation and reaction scheme 2.2-1 but the obtained oligomer distribution (see fig. 2.2-4) can be described only with the use of Weibul-Nicander equation ( $c=4.0$ ).

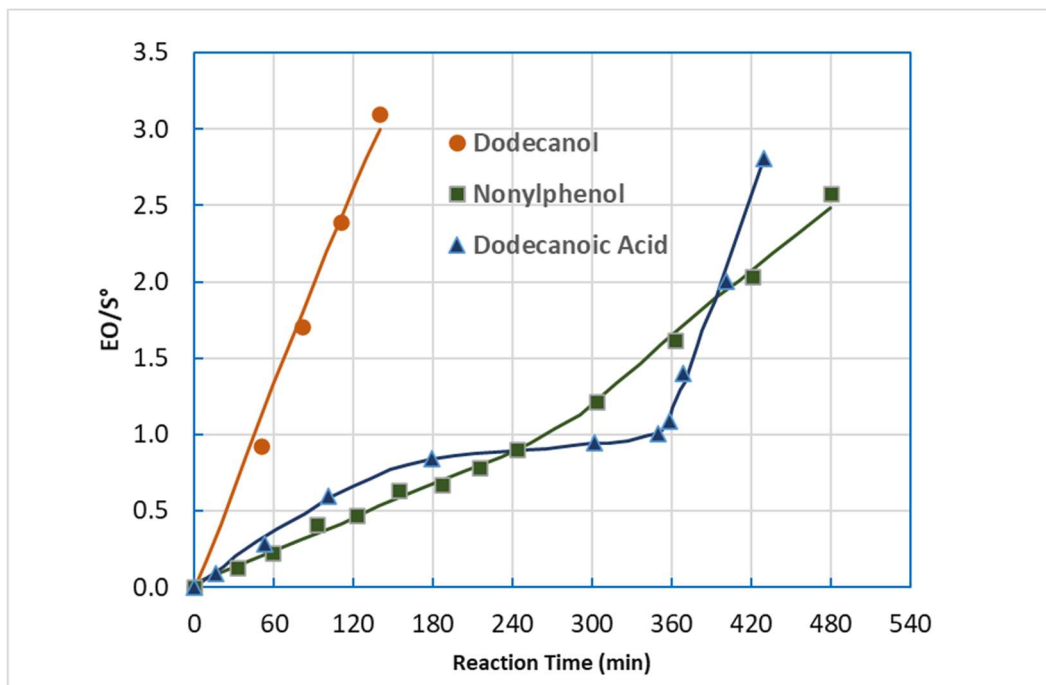
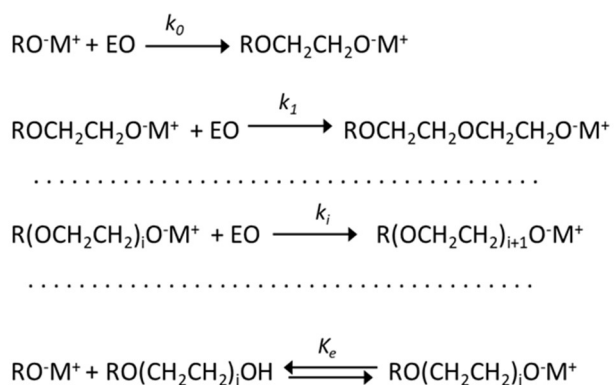


**Fig. 2.4-1.** EO consumption for 3 different substates Dodecanol (106 °C,  $P_{EO}$ = 2 atm, KOH= 2 % by mol), Nonylphenol (73°C,  $P_{EO}$ = 1atm, KOH= 1.9% by mol), Dodecanoic Acid ( $T$ = 120°C,  $P_{EO}$ = 4 atm, KOH= 1% by mol) (Santacesaria et al. 1990; Di Serio, di Martino, and Santacesaria 1994; Santacesaria et al. 1992a).



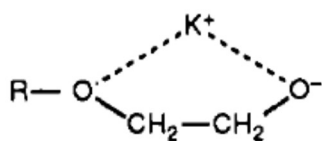
**Scheme 2.4-5**

In the case of described kinetic mechanism of basic catalyst, if the propagation kinetic and Equilibrium proton-transfer constant are independent from the molecular weight of the oligomers ( $k_1 = k_2 = \dots = k_i = \dots = k_p$  and  $K_{e1} = K_{e2} = \dots = K_{ei} = \dots = K_e$ ) the parameter  $c$  of Weibul-Nicander equation is given by the following equation:

$$c = \frac{k_0}{k_p} K_e \quad (\text{Eq. 2.4-3})$$

In the case of dodecanol  $k_0 = k_p$  and so  $c = K_e$

The value of  $K_e > 1$  can be justified considering that the oligomers can stabilize the ionic couple because the presence of ether oxygen in the structure (Bialowas & Szymanowski, 2004; Santacesaria et al., 1992b):



Scheme 2.4-6

This type of interaction can justify also the behavior of barium-based catalysts that give place to narrow range oligomers distributions (see for example Fig. 2.4-2)

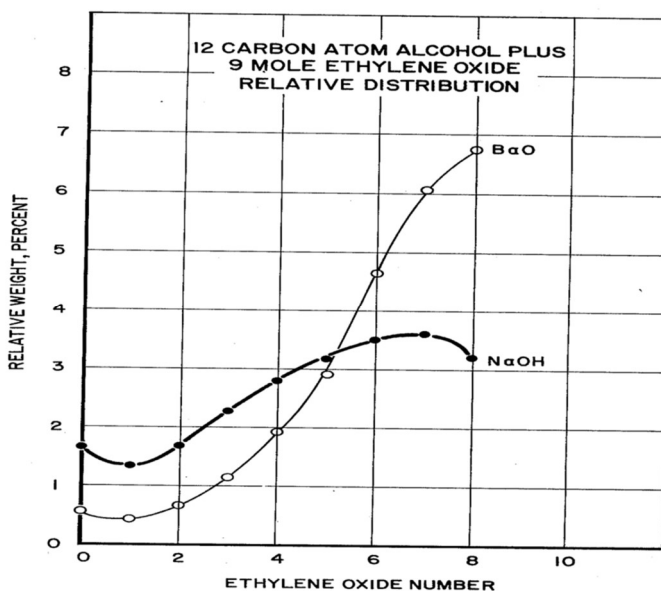
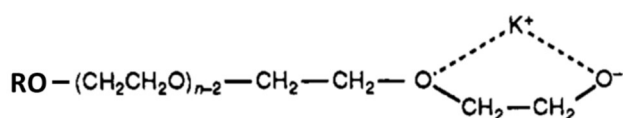


Fig. 2.4-2. Comparison of Oligomers Distribution obtained in tehoxylation of dodecanol using NaOH or BaO as catalyst at EO/S=9 (Yang, 1980).

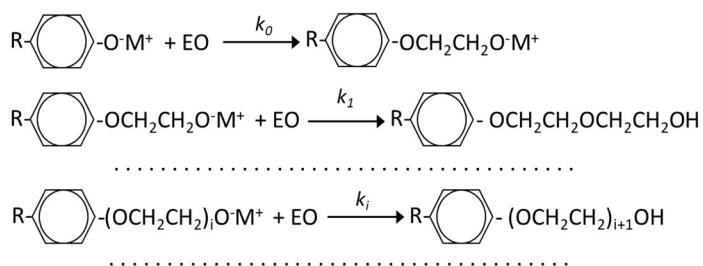
In the case of barium, has been demonstrated that the equilibrium constants of scheme 2.4-5 are different until the 4<sup>th</sup> oligomer ( $K_{e1} \neq K_{e2} \neq K_{e3} \neq K_{e4} = K_{e5} = \dots = K_e$ ) (Santacesaria et al., 1992b). The first constant ( $K_{e1}$ ) has about the same value as for potassium, then we have decreasing values until  $K_{e4}$  which is 60% lower. This low value of the proton-transfer equilibrium constant is responsible for the narrow range distribution compared to potassium. The different behavior of barium compared to potassium can be explained by assuming a tight structure for the potassium ion pairs. Therefore, potassium can interact only with the last uncharged oxygen before the negative charge of the anion, giving rise to complexes of the same stability for every oligomer (see scheme 2.4-7).



**Scheme 2.4-7**

On the contrary, the second charge of barium may interact with more than one oxygen, giving rise to complexes different from scheme 2.4-7; that is, barium cation ionic pairs of oligomers may be more solvated than the corresponding potassium ionic couples.

The ethoxylation of nonylphenol (a phenol) gives place to oligomers (alcohols) that are less acid (and so higher nucleophilic) than the starter:



**Scheme 2.4-8**

It can be noted in fig. 2.4-1 that the increase in reaction rate starts after  $\text{EO}/\text{RXH}^\circ \cong 1$ . This correspond to quite total consumption of the nonylphenol before the start of propagation reaction ( $k_0 < k_p$ ), as can be seen in fig. 2.4.3 (240 min).

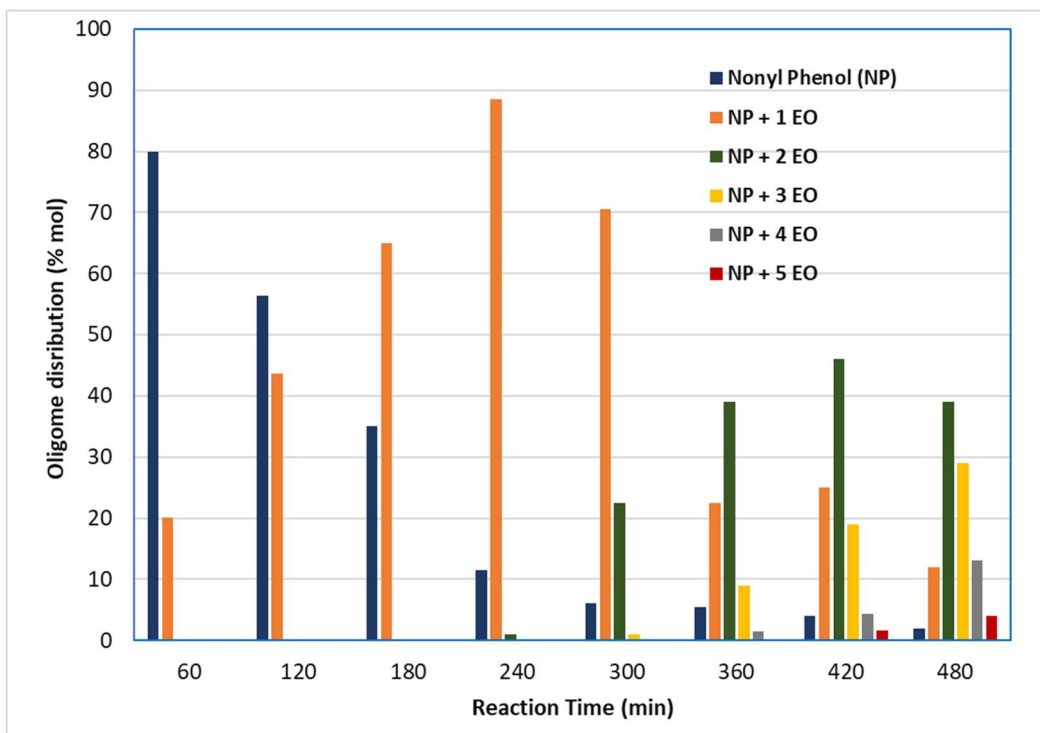


Fig. 2.4-3. Oligomer distribution in Ethoxylation of Nonyphenol (73°C,  $P_{EO}$  = 3 atm, KOH = 1.9% by mol) (Santacesaria et al., 1990).

Notwithstanding the propagation constant is higher than the initiation constant the reaction of the starter is favored because being more acid the proton-transfer equilibria 2.2-4 is shifted to the left ( $K_e < 1$ ).

The behavior of ethoxylation of fatty acids catalyzed by basic catalysts is peculiar. As can be seen from fig. 2.4-1 the consumption of Ethylene oxide reaches a plateau when the ratio EO/Substrate is equal to 1, after a long induction period the reaction rate increase and becomes constant. This trend can be again justified considering the acidity of fatty acids is enough to catalyze the ethoxylation reaction without catalyst (see fig. 2.2-1), when the concentration of fatty acid became low ( $EO/Substrate \cong 1$ ) the reaction rate became very low even because the activity of carboxylate anion (that are poor nucleophilic character) is low ( $k_0 \ll k_p$ ). In this situation, until there is the presence of fatty acids the equation 2.4-4 is completely shifted to the left ( $K_e < 1$ ) and because the low concentration of alkoxyate the propagation reactions is poorly active. This fact can be seen clearly in fig. 2.4-4, where until 353 min. an accumulation of first oligomer is observed.



After the complete consumption of fatty acids, the formation of alkoxyate is possible and the propagation reaction is fully operative.

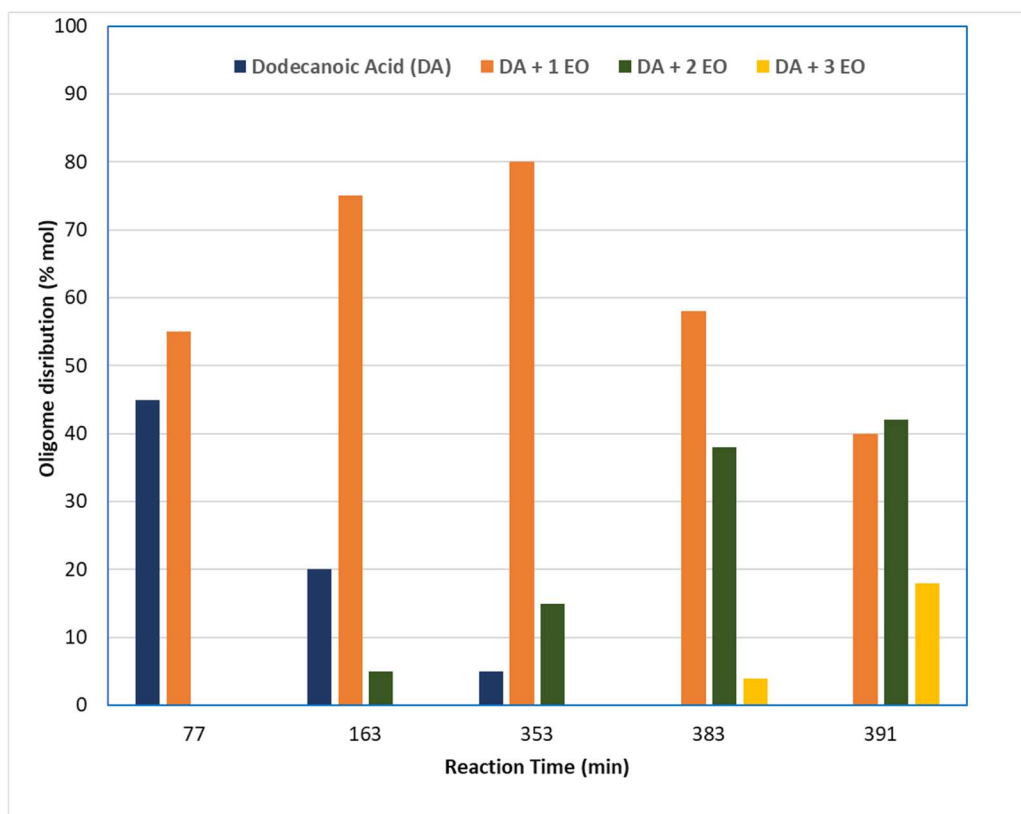
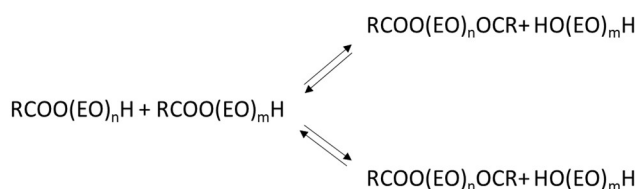


**Fig. 2.4-4.** Oligomer distribution (monoesters) obtained in the ethoxylation of dodecanoic acid ( $T=120^{\circ}\text{C}$ ,  $P_{\text{EO}}=4\text{ atm}$ ,  $\text{KOH}=1\%$  by mol) (Di Serio, di Martino, and Santacesaria 1994).

The ethoxylation reactions of fatty acids catalyzed by basic catalysts have another important peculiarity. The ethoxylation reaction of fatty acid give place to a monoester that have also an alcoholic functional group, these products in the presence of a basic catalyst can give place to the transesterification reaction reducing diesters and polyglycols:



**Scheme 2.4-9**

The importance of the phenomena can be seen in fig. 2.4-5 were the molar ratio diester/(diester + monoester) determined in run reported in fig. 2.4-1 are reported

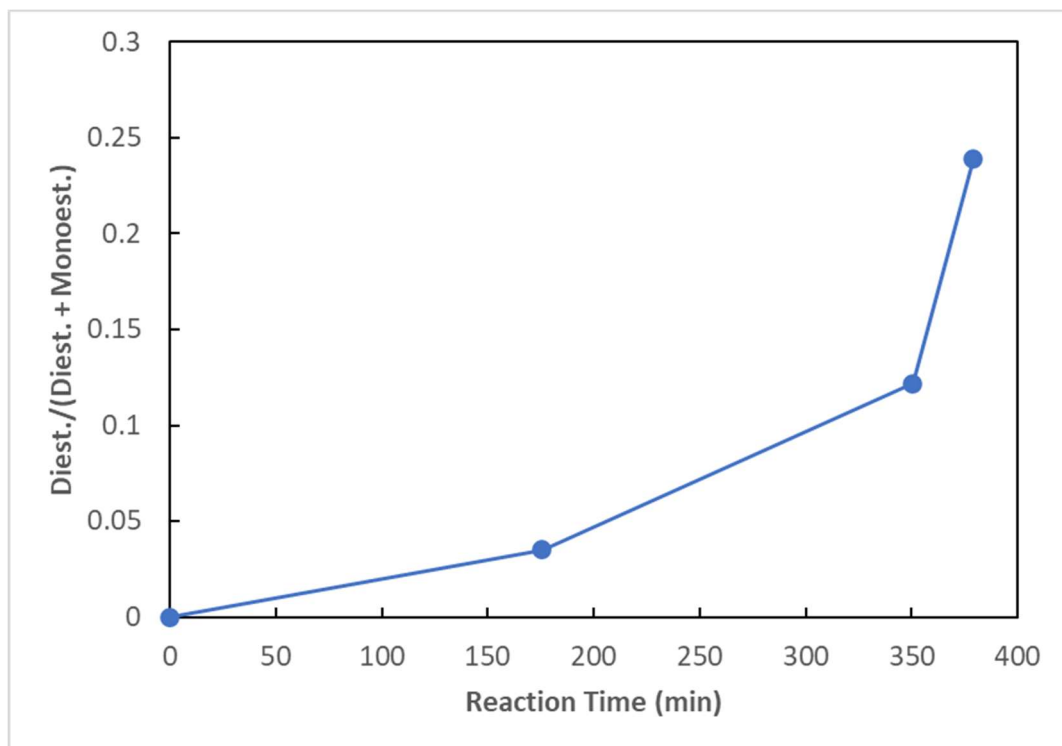


**Fig. 2.4-4.** Molar Ratio Diester (D)/(Diester (D) + Monoester (M)) determined in dodecanoic acid ethoxylation at 120°C, 4 bar, 1% by mol KOH ((Di Serio, di Martino, and Santacesaria 1994).



## Chapter 3.- Kinetics of the alkoxylation reaction of fatty alcohols catalyzed by metal alkaline hydroxides.

In this chapter we present the results obtained in the study of alkoxylation kinetics of fatty alcohols catalyzed by alkaline catalyst like KOH, NaOH or related alkoxides, that is, nowadays, the most used technology for surfactant synthesis.

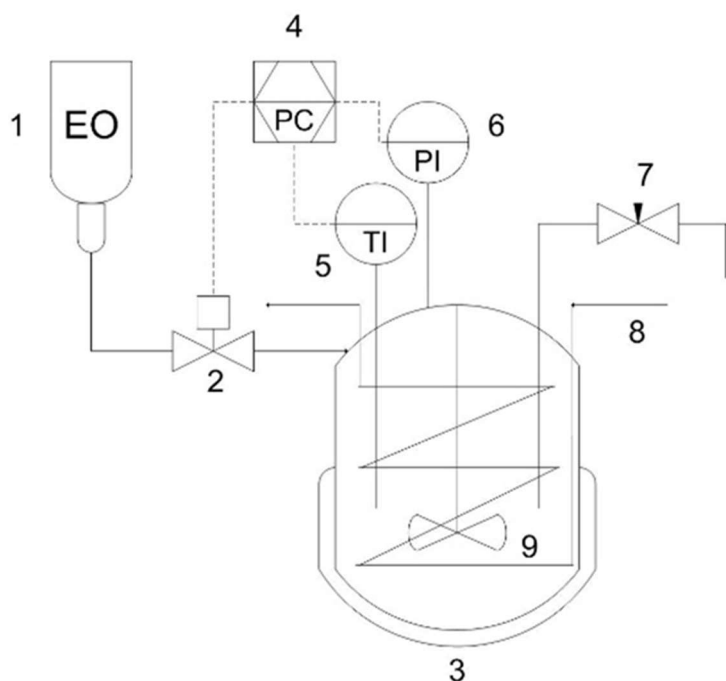
### 3.1 Experimental

#### *Reaction*

The reaction is studied in laboratory by using well-mixed semi batch reactors (See Fig. 3.1.1).

Either ethylene oxide (EO) or propylene oxide (PO) is gradually added to the solution of an alkaline catalyst (MOH or MOR) in the liquid initiator previously heated to the reaction temperature, normally maintained in the range of 120-200°C. Before the adding of alkylene alkoxide the reactor is flushed with N<sub>2</sub> to remove oxygen of Air and water or low boiling alcohol that is formed during the preheating stage in the formation of fatty alcohols alkoxide (see scheme 2.4-1). The gas phase pressure is kept constant at a level of 0.2-0.5 MPa through continuously feeding the alkylene oxide reagent by opening an automated control valve. The reactions are highly exothermic ( $\sim 83.7 \text{ kJ/mol}^{-1}$ ) and require efficient heat transfer to avoid the danger of leakage particularly dangerous due to the possible intervention, at high temperature, of explosive side reactions related to the decomposition of ethylene oxide or propylene oxide (Pekalski et al. 2004). The presence of internal cooling coil is useful to extinguish the reaction in case of loss of control. EO and PO, under the above temperature conditions, evaporate rapidly and are partitioned between gas and liquid phases. The reaction occurs in the liquid phase between the starter and the gaseous reactant dissolved in the starter. To study the reaction kinetics, it is important, first, to create a large gas-liquid interface area to avoid mass transfer limitation. The high gas-liquid interface was achieved by using a perforated stirrer.

The EO bottle is on a scale and is weighed during testing, allowing measurement of the alkylene oxide added to the reactor. The reactor is also equipped with a line for taking samples during kinetic runs.



10

**Fig. 3.1-1.** Scheme of the laboratory reactor for studying polyalkoxilation reactions. 1=EO bottle, 2=on-off solenoid valve, 3= Jacketed reactor, 4=Computer interface, 5= Thermocouple, 6=Pressure transducer, 7= Line for samples, 8= Freezing coil, 9-10 = Magnetic driven holed stirrer.

### *Samples Analysis*

For the analysis of samples of the reaction mixtures taken at different times, two analytical methods were used (HPLC (Santacesaria et al., 1992a) and GC (DiSerio, Vairo, et al., 1996)).

In the case of dodecanol ethoxylation, samples were derivatized with 3,5-dinitrobenzoyl chlorides (Desbène et al., 1987) and analyzed by the HPLC technique. The elution gradient technique was used (solvent A (99/1 (v/v) = n-heptane/CH<sub>2</sub>Cl<sub>2</sub>-2-propanol (95/5)), solvent B (50/50 (v/v) = n-heptane/CH<sub>2</sub>Cl<sub>2</sub>-2-propanol (95/5)). Solvent B was increased from 0 to 100% during the first 50 min., then only B was fed for 15 min. and from 65 to 80 min. B was reduced from 100 to 0%.

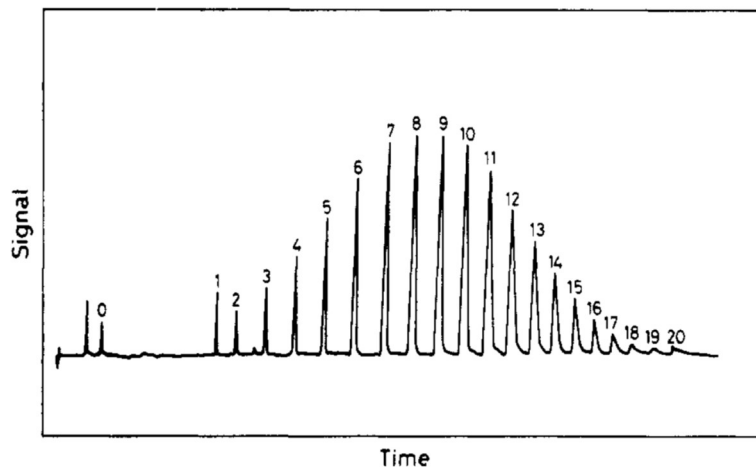
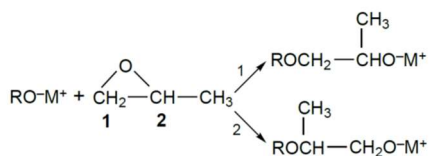


**Fig. 3.1-2.** Example of chromatogram obtained by HPLC. Numbers are related to the EO adducts in the molecule. The first peak is the excess of derivatizing agent. Reprinted with permission from (Santacesaria et al., 1992a). Copyright 1992 American Chemical Society.

The solvent feed rate was 1 cm<sup>3</sup>/min. A 25 X 0.4 cm column of Lichrospher 100 Diol supplied by Merck Co was used, and the UV detector was fixed at 254 nm. The different oligomers were recognized by injecting standard monodisperse samples provided by Nikkol Chem. Co. Figure 3.1-2 shows an example of the chromatograms obtained.

The ethoxylated and propoxylated oligomers of 1-octanol or 2-octanol were analyzed by gas chromatographic technique. A 0.2 μL portion of solution (0.03 g of the reaction sample dissolved in 4 cm<sup>3</sup> CHCl<sub>3</sub>) was injected onto a 25 m × 0.32 mm i.d., HP1 column (100% dimethylpolysiloxane rubber) and analyzed by taking the temperature to 80 °C for 1.5 min. and then heating at a rate of 10 °C/min. to 320 °C. FID detector maintained at 350 °C was used. Oligomer response factors were calculated as suggested by literature (Milwidsky & Gabriel, 1982) and were verified based on the mass balance of epoxide consumption.

Propylene oxide molecule could generate primary or secondary alcohols when ring opening occurs as a result of nucleophilic attachments to the methylene (1) or methyne (2) group (see scheme 3.1-1):



**Scheme 3.1-1** Possible propoxylation reaction pathway

To investigate this aspect the propoxylated samples of 1 and 2-octanol were analyzed by  $^{13}\text{C}$  NMR using a 270 MHz Bruker apparatus operating at 67 MHz, determining the signal areas concerning primary alcohol ( $\delta$ ) 62.4 ppm and secondary alcohol ( $\delta$ ) 66.0 ppm of samples dissolved in  $\text{CDCl}_3$ . Acquisition times of 6 s were applied with no delay between pulses. The pulse angle was  $90^\circ$  and the spectral amplitude was 1360 Hz. Data were processed with an exponential weighting function (weight) 0.3 Hz before transformation to reduce noise. Chemical changes were referenced to tetramethylsilane as an external reference. In Fig. 3.1-2 the  $^{13}\text{C}$  NMR spectra of sample obtained with propoxylation of 1-octanol are reported, the concentration of primary alcohol determined with NMR is equal to that obtained with GC analysis, moreover in the propoxylation of 2-octanol no signals of primary alcohol were observed in  $^{13}\text{C}$  NMR spectra. These results confirmed those for propylene oxide polymerization (Schilling & Tonelli, 1986) and for methanol and isopropanol propoxylation (Gee et al., 1959, 1961), that demonstrated that the reaction at the methyne group is negligible in comparison with that occurring at the methylene group.

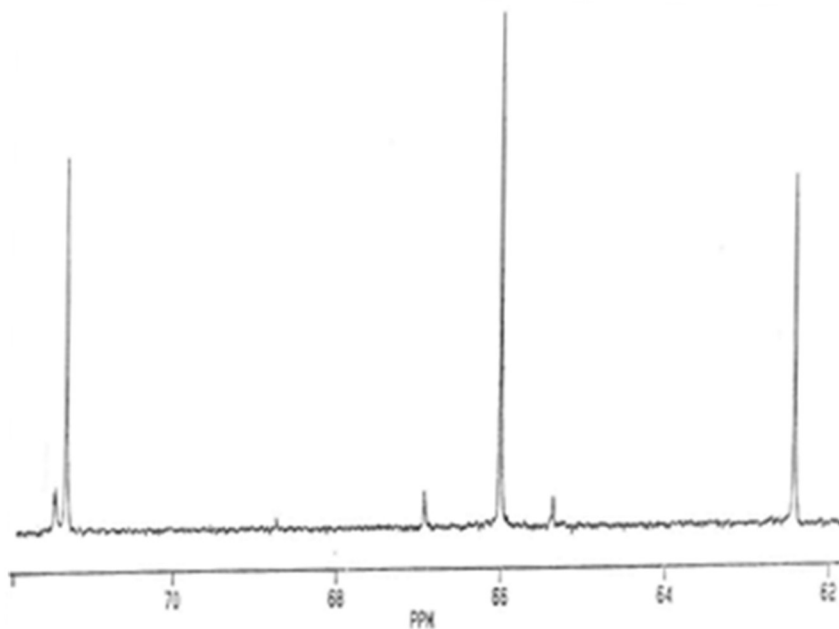


**Fig. 3.1-2.**  $^{13}\text{C}$  NMR spectra of sample obtained in propoxylation of 1-octanol.

### Density Measurement

The reaction produces oligomer mixtures that have different mean molar mass and different density of starter with a consequent increase of liquid volume. To describe the kinetic of the system it is necessary to know how the density changes with the temperature and composition of liquid phase. For this objective density measurements of starter and products with different AO/S ratio at different temperatures, were done using a pycnometer.

The density of alkylene oxides ( $\rho_{AO}$ ) can be calculated with the method proposed by Yen and Woods (Yen & Woods, 1966) using the critical parameters ( $z_c$  critical compressibility factor, critical density,  $T_c$  critical temperature (K)) reported in Table 1.1-1:

$$\frac{\rho_{AO}}{\rho_c} = 1 + A \left(1 - \frac{T}{T_c}\right)^{\frac{1}{3}} + B \left(1 - \frac{T}{T_c}\right)^{\frac{2}{3}} + C \left(1 - \frac{T}{T_c}\right)^{\frac{4}{3}} \quad (\text{Eq. 3.1-1})$$

$$A = 17.4425 - 214.578z_c + 989.625z_c^2 - 1522.06z_c^3$$

$$B = -3.28257 + 13.6377z_c + 107.4844z_c^2 - 384.211z_c^3$$

$$C = 60.209 - 402.063z_c + 501.0z_c^2 + 641z_c^3$$

### Alkylene oxides Solubility

Ethylene oxide and propylene oxide solubility runs were carried out in thermostatic autoclaves by introducing a weighed amount of dodecanol or its ethoxylated derivatives ( $W_S$ ). Weighed amounts of ethylene oxide or propylene oxide ( $W_{AO}$ ) were then added at a prefixed temperature, and equilibrium pressures (P) were measured by a pressure transducer. The vapor phase had been considered ideal in calculations because the low considering pressure and the volume of alkylene oxides and substrates are considering additive. On this basis the following balance equations can be written:

$$V_R = V_G + V_L \quad (\text{Eq. 3.1-2})$$

$$V_L = V_{AOL} + V_S \quad (\text{Eq. 3.1-3})$$

$$V_G = n_{AOG} \frac{RT}{P_{AO}} \quad (\text{Eq. 3.1-4})$$

$$V_{AOL} = n_{AOL} \frac{PM_{AO}}{\rho_{AO}} \quad (\text{Eq. 3.1-5})$$



$$V_{SL} = \frac{W_S}{\rho_S} \quad (\text{Eq. 3.1-6})$$

$$\frac{W_{AO}}{PM_{AO}} = n_{AOG} + n_{AOL} \quad (\text{Eq. 3.1-7})$$



$$n_{AOL} = \frac{V_R \frac{W_{AO}}{PM_{AO}} \frac{RT}{P_{AO}} \frac{W_S}{\rho_S}}{\left( \frac{PM_{AO}}{\rho_{AO}} \frac{RT}{P_{AO}} \right)} \quad (\text{Eq. 3.1-8})$$

$$n_S = \frac{W_S}{PM_S} \quad (\text{Eq. 3.1-9})$$

$$x_{AO} = \frac{n_{AOL}}{n_{AOL} + n_S} \quad (\text{Eq. 3.1-10})$$

$$[AO] = \frac{n_{AOL}}{V_L} \quad (\text{Eq. 3.1-11})$$

## 3.2 Results and discussion

### 3.2.1 Density

Values of measured density of dodecanol and corresponding oligomers as function of temperature are reported in fig. 3.2-1.

The data of fig. 3.3-1 can be interpolated with the following polynomial empirical expression:

$$\rho_S \left( \frac{g}{cm^3} \right) = A + B \frac{AO_R}{S^\circ} + C \left( \frac{AO_R}{S^\circ} \right)^2 + D \left( \frac{AO_R}{S^\circ} \right)^3 + E\vartheta \quad (\text{Eq. 3.2-1})$$

Table 3.2-1 presents the value of parameters of equation (3.2-1) for dodecanol (Santacesaria et al., 2018) and for 1 and 2-octanol (DiSerio, Vairo, et al., 1996) alkoxyated products.

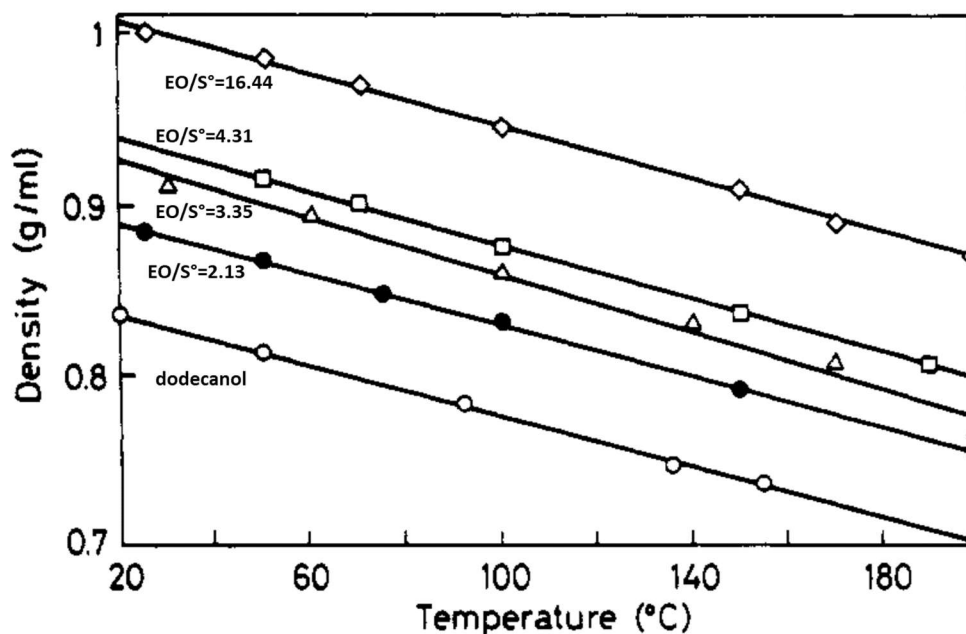


Fig. 3.2-1 Density of dodecanol and its oligomers as function of temperature Reprinted with permission from (Santacesaria et al., 1992a) Copyright 1992 American Chemical Society.

Table 3.2-1 Parameters of Eq. 3.2-1 for calculation of density ( $\text{g/cm}^3$ ) dodecanol (Santacesaria et al., 2018) and for 1 and 2 octanol (DiSerio, Vairo, et al., 1996) alkoxyated products and range of applicability.

Substrate	AO	A	B	C	D	E	$\text{AO}_R/\text{S}^\circ$ max
Dodecanol	EO	0.860	$2.50 \times 10^{-2}$	$-4.76 \times 10^{-4}$	$-2.59 \times 10^{-5}$	$-7.7 \times 10^{-4}$	15
1-Octanol	EO	0.860	0.07	-	-	$-9.0 \times 10^{-4}$	1
1-Octanol	PO	0.860	0.05	-	-	$-9.0 \times 10^{-4}$	1
2-Octanol	EO	0.826	0.14	-	-	$-7.0 \times 10^{-4}$	1
2-Octanol	PO	0.826	0.06	-	-	$-7.0 \times 10^{-4}$	1

### 3.2.2 Solubility

Alkylene oxide is partitioned between the liquid and vapor phase, and the partition coefficient changes according to the organic substrate used, temperature, pressure, and extent of the reaction. Reaction products are oligomers of different molecular weights that is, the reaction environment gradually changes and alkylene oxide solubility changes consequently. It is of great importance, therefore, to know the alkylene oxide solubility in the reaction mixture at any time because the reaction rate directly depends on the alkylene oxide concentration in the liquid phase.

The solubility of alkylene oxides can be determined as described in section 3.1 or predicted using predictive methods as UNIFAC (Fredenslund et al., 1977).

In table 3.2-2 the measured solubilities of dodecanol and ethoxylated dodecanol are reported.

The results of Table 3.3-2 are reported in Figure 3.3-2 in the form of natural logarithm of partition coefficients  $K = \text{PEO}/x\text{EO}$  versus  $103/T$ .

As can be seen, because the obtained linear trend, the ethylene oxide solubility complies with Henry's law in all the considered cases.

The data of Fig. 3.2-2 can be described with a polynomial equation.

$$\ln K = 6.544 - 0.13774 \frac{EO_R}{S^\circ} + 7.6328 \cdot 10^{-3} \left( \frac{EO_R}{S^\circ} \right)^2 - 1.2751 \cdot 10^{-4} \left( \frac{EO_R}{S^\circ} \right)^3 + \frac{-17066 - 3.1084 \frac{EO_R}{S^\circ}}{T} \quad (\text{Eq. 3.2-2})$$

**Table 3.2-2** Ethylene Oxide Partition Data at Different Temperatures in 1-Dodecanol and Ethoxylated Dodecanol with Different Average Numbers of Ethylene Oxide. Reprinted with permission from (DiSerio et al., 1995) . Copyright 1995 American Chemical Society.

$x_{EO}$	$P_{EO}$ (atm)			$x_{EO}$	$P_{EO}$ (atm)		
	70 °C	99 °C	150 °C		70 °C	99 °C	150 °C
Dodecanol							
0.036			0.55	0.248	1.15		
0.039		0.33		0.278		1.95	
0.059	0.35			0.295	1.35		
0.072			0.90	0.310		2.25	
0.077		0.54		0.338	1.55		
0.105			1.31	0.347		2.55	
0.112		0.73		0.375	1.71		
0.130	0.68			0.386		2.70	
0.136			1.70	0.409	1.90		
0.161		1.01		0.417		3.15	
0.165			2.07	0.439	2.07		
0.193	0.90		2.42	0.467	2.21		
0.204		1.34		0.492	2.37		
0.231			2.94	0.521	2.5		
0.242		1.65					
Dodecanol + 4.3EO							
0.094			0.72	0.336		1.40	
0.102		0.40		0.355			2.80
0.134	0.43			0.370		1.58	
0.154			1.03	0.381	1.08		
0.187		0.73		0.399		1.80	
0.203			1.38	0.426		2.00	
0.237	0.64			0.434	1.24		
0.248			1.70	0.478	1.40		
0.259		1.00		0.515	1.55		
0.287			2.08	0.542	1.68		
0.300		1.20		0.567	1.81		
0.317	0.89			0.589	1.95		
0.323			2.45	0.600	2.00		
Dodecanol + 15EO							
0.200	0.24	0.47	1.17	0.520			4.00
0.300		0.70	2.00	0.600	1.06	2.35	
0.400	0.47	1.06	2.70	0.800	2.35		

However, this equation cannot be used for extrapolation that needs the use of thermodynamic model. Two models have been considered: NRTL (Renon & Prausnitz, 1968) and WILSON (Wilson, 1964). With these two models it is possible to calculate the activity coefficients  $\gamma_{AO}$  in liquid phase and consequently the equilibrium alkylene oxide liquid concentration using the following relation:

$$x_{AO} = \frac{P_{AO}}{\gamma_{AO} P_{AO}^0} \quad (\text{Eq. 3.2-3})$$

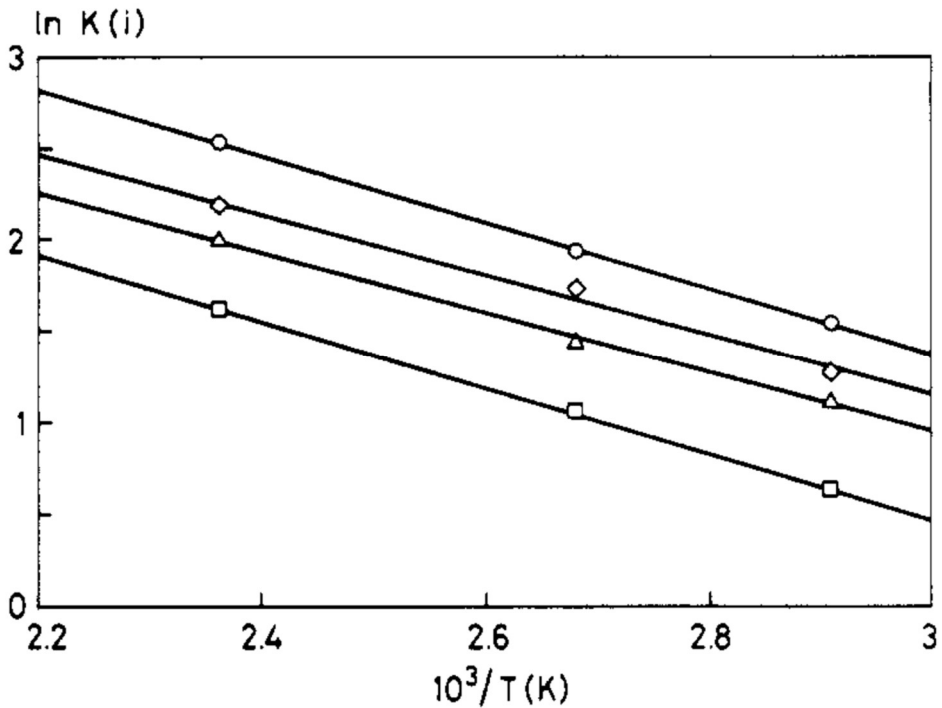


**Fig. 3.2-2.** Van't Hoff type plot for the Henry solubility constant ( $K$ , atm) of ethylene oxide in 1-dodecanol and in ethoxylated dodecanol with different average number of EO adducts. Number of adducts: (O) 0, (◇) 2.1, (△) 4.3, (□) 14.5. Reprinted with permission from (Santacesaria et al., 1992a) Copyright 1992 American Chemical Society.

Where the vapour pressure of alkylene oxides  $P_{AO}^0$  can be calculated using the Antoine Equation (Prausnitz & Anderson, 1980):

$$P_{EO}^0 (atm) = \frac{e^{16.74 - \frac{2568}{T-29.01}}}{760} \quad (\text{Eq. 3.2-4})$$

$$P_{PO}^0 (atm) = \frac{e^{15.32 - \frac{2108}{T-64.87}}}{760} \quad (\text{Eq. 3.2-5})$$

The solutions are considered as pseudo binary mixture alkylene oxide – substrate characterized by the medium mol of ethylene oxide reacted per mol of substrate ( $AO_R/S^\circ$ ). The NRTL equation for a binary system can be written as follows:

$$\ln\gamma_{AO} = x_S^2 \left[ \Gamma_{S,AO} \left( \frac{e^{-0.3\Gamma_{AO,S}}}{x_{AO} + x_S e^{-0.3\Gamma_{AO,S}}} \right)^2 + \frac{\Gamma_{AO,S} e^{-0.3\Gamma_{S,AO}}}{(x_S + x_{EO} e^{-0.3\Gamma_{S,AO}})^2} \right] \quad (\text{Eq. 3.2-6})$$

$$\Gamma_{AO,S} = A_{AO,S} + B_{AO,S} \frac{AO_R}{S^\circ} + C_{AO,S} \left( \frac{AO_R}{S^\circ} \right)^2 \quad (\text{Eq. 3.2-7})$$

$$\Gamma_{S,AO} = A_{S,AO} + B_{S,AO} \frac{EO_R}{S^\circ} + C_{S,AO} \left( \frac{EO_R}{S^\circ} \right)^2 \quad (\text{Eq. 3.2-8})$$

The data of table 3.2-2 were used to determine by regression analysis the parameters of Equations 3.2-7 and 3.2-8 for the systems ethylene oxide – dodecanol and ethylene oxide – ethoxylated products of dodecanol, and the obtained values are reported in the following equations (the dependence from temperature of the parameters have been found negligible):

$$\Gamma_{EO,S} = 3.713 - 0.3387 \frac{EO_R}{S^\circ} - 0.01748 \left( \frac{EO_R}{S^\circ} \right)^2 \quad (\text{Eq. 3.2-9})$$

$$\Gamma_{S,EO} = -2.394 - 1.453 \frac{EO_R}{S^\circ} - 0.00380 \left( \frac{EO_R}{S^\circ} \right)^2 \quad (\text{Eq. 3.2-10})$$

In table 3.2-3 the median errors between the experimental solubilities values and the ones calculated with NRTL model for dodecanol and its ethoxylates are reported. As can be seen, they are in the range 16-20 %.

**Table 3.2-3** Average Percent Errors Obtained for the Different Binaries Applying the UNIFAC, Wilson, and NRTL method, respectively. Reprinted with permission from (DiSerio et al., 1995) . Copyright 1995 American Chemical Society.

substrate	mean error (%)		
	UNIFAC	NRTL	Wilson
dodecanol	18	18	19
dodecanol + 4.3EO	35	16	16
dodecanol + 15EO	10	20	7

The Wilson equations for calculating the AO activity coefficient is the following:

$$\ln\gamma_{AO} = -\ln(x_{AO} + x_S\Lambda_{AO,S}) + x_S \left[ \frac{\Lambda_{AO,S}}{x_{AO} + x_S\Lambda_{AO,S}} - \frac{\Lambda_{S,AO}}{x_{AO}\Lambda_{S,AO} + x_S} \right] \quad (\text{Eq. 3.2-11})$$

Where parameters  $\Lambda_{AO,S}$  and  $\Lambda_{S,AO}$  are linked with the molecular weight of substrate through the following equations

$$\Lambda_{AO,S} = A_{AO,S} + B_{AO,S} \frac{AO_R}{S^\circ} + C_{AO,S} \left( \frac{AO_R}{S^\circ} \right)^2 \quad (\text{Eq. 3.2-12})$$

$$\Lambda_{S,AO} = A_{S,AO} + B_{S,AO} \frac{EO_R}{S^\circ} + C_{S,AO} \left( \frac{EO_R}{S^\circ} \right)^2 \quad (\text{Eq. 3.2-13})$$

The coefficients of equations 3.2-12 and 3.2-13 can be derived by regression on experimental data. The following equations have been obtained by regression on data of table 3.2-2

$$\Lambda_{EO,S} = 13.00 - 0.9611 \frac{EO_R}{S^\circ} - 0.01967 \left( \frac{EO_R}{S^\circ} \right)^2 \quad (\text{Eq. 3.2-14})$$

$$\Lambda_{S,EO} = -0.4069 + 0.04714 \frac{EO_R}{S^\circ} - 0.001340 \left( \frac{EO_R}{S^\circ} \right)^2 \quad (\text{Eq. 3.2-15})$$

The agreement obtained between experimental data of table 3.2-2 and those calculated with WILSON equation are reported in table 3.2-3. As can be seen the performance of WILSON equation is better than that of NRTL equation, being the error in the interval 7-18%.

The WILSON equation was used also to determine its capacity in the extrapolation. In table 3.2-4 the calculated solubility has been compared with the experimental ones determined in a range of temperatures (120-190 °C) different from that of data used for the determination of parameters equations 3.2-14 and 3.2-15 (70-150°C). As can be seen the mean error is around 22%, showing sufficient affordability of WILSON equation in extrapolation.

The use of a polynomial equation or of NRTL or WILSON equation is possible only when the solubility experimental data are available. When there is a lack of these data it is possible use UNIFAC Method to calculate the alkylene oxide activity coefficient. UNIFAC Method is a predictive method that to calculate the activity coefficients of components of a liquid mixture uses a contribute functional groups approach (Fredenslund et al., 1977).

**Table 3.2-4** Comparison of Experimental Data (Hall & Agrawal, 1990) for Dodecanol at High Temperature with Those Calculated with the Wilson Equations (Eqs, 3.2-12, 3.2-15, 3.2-15). Reprinted with permission from (DiSerio et al., 1995) . Copyright 1995 American Chemical Society.

<i>P</i> (atm)	<i>T</i> (°C)	[EO] <sub>i</sub> (mol/L)	
		expt	calcd
2.07	171.1	0.41	0.55
2.07	190.6	0.30	0.43
1.38	162.8	0.35	0.43
0.69	162.8	0.19	0.22
2.07	148.8	0.59	0.79
2.07	123.8	0.96	1.20

In Table 3.2-3 the agreements of this method in the prediction of equilibrium of ethylene oxide-dodecanol, ethylene oxide – ethoxylated dodecanol are reported. As can be seen, the mean value (21 %) is acceptable.

To verify the applicability of UNIFAC for propylene oxide too, the propylene oxide solubility at 100 °C, in dodecanol, was measured. The experimental values obtained are compared with the calculated ones with UNIFAC in Figure 3.2-3. The same figure also shows the agreement obtained for ethylene oxide. From the observed results we can conclude that UNIFAC for both ethylene oxide and propylene oxide is a useful method to calculate the alkylene oxide concentration in liquid phase in absence of experimental data.

In table 3.2-5 the calculated concentration of EO an PO in 1 and 2-octanol and the corresponding monoethoxylated products, at different condition are reported.

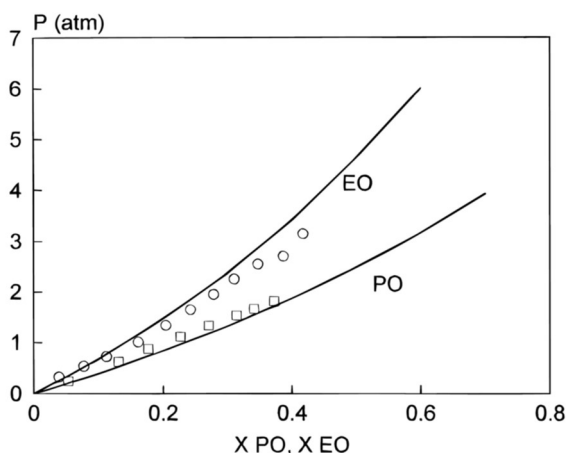


**Fig. 3.2-3.** Equilibrium pressure of epoxide as a function of the liquid molar fraction in dodecanol at 100 °C (dots are experimental; lines are calculated with UNIFAC). Reprinted with permission from (DiSerio, Vairo, et al., 1996). Copyright 1995 American Chemical Society.



**Table 3.2-5** Epoxide Concentrations Calculated by UNIFAC. Reprinted with permission from (DiSerio et al. 1996). Copyright 1996 American Chemical Society.

substrate	epoxide	concn (mol/cm <sup>3</sup> × 10 <sup>3</sup> )			
		100 °C	120 °C	130 °C	160 °C
1-octanol	EO	1.4	0.91	0.77	
1-octanol + 1EO	EO	1.4	0.86	0.73	
1-octanol	PO	2.7	1.8	1.4	
1-octanol + 1PO	PO	2.5	1.2	1.0	
2-octanol	EO	1.4	0.89	0.79	0.42
2-octanol + 1EO	EO	1.6	1.0	0.87	0.49
2-octanol	PO	2.6	1.6	1.3	
2-octanol + 1PO	PO	2.0	1.2	0.99	

### 3.2.3 Kinetic runs

The list of the kinetic runs analyzed in this chapter is reported in Table 3.2-6. Three different starter (dodecanol, 1-octanol and 2-octanol) and two alkylene oxides (ethylene oxide and propylene oxide) were used.

The ethoxylation of dodecanol and 1-octanol, showed a similar behaviour. The reaction rate is constant along the time (figures 3.2-4 ,3.2-6 (a) and broad oligomer distributions are observed (figures 3.2-5, 3.2-6 (b))

The ethylene oxide consumption in ethoxylation of 2-octanol has a different behaviour. In this case we can observe (Fig. 3.2-7 (a)) an increase of reaction rate with the increase of EO/S along the time, moreover the oligomer distribution is very broad with and high starter residue (Fig. 3.2-7 (b))

In the case of propoxylation of 1-octanol (run 11-13 of table 3.2-6) we can observe an opposite trend. The propoxylation rate decreases with the increase of PO/S value (see Figure 3.2-8). In this case the initiation reaction involves the reaction of a primary alcohol with PO that give place to a secondary alcohol with a lower reactivity. In this case the oligomer distribution is narrow with a low starter residue.

The behaviour of propoxylation of 2-octanol is similar to that of ethoxylation of 1-octanol or dodecanol (see Figure 3.2-9). In this case we have a constant reaction rate (lower than in the case of ethoxylation) because the initiation reaction is between a secondary alcohol with PO like the propagation ones. Also, the oligomer distribution is very similar to that of 1-octanol ethoxylation.

**Table 3.2-6** Kinetic runs catalyzed by KOH.

Run	Substrate	AO	Temperature °C	Catal. % mol	Pressure atm	Ref
1	dodecanol	EO	106	2.0	2	I
2	dodecanol	EO	128	1.0	2	I
3	dodecanol	EO	128	1.0	1	I
4	dodecanol	EO	100	2.0	2	I
5	dodecanol	EO	68.5	3.0	2	I
6	1-octanol	EO	120	2.0	2	II
7	2-octanol	EO	100	2.0	2	II
8	2-ocatnol	EO	120	2.0	2	II
9	2-octanol	EO	130	2.0	2	II
10	2-octanol	EO	160	2.0	2	II
11	1-octanol	PO	100	2.0	2	II
12	1-octanol	PO	120	2.0	2	II
13	1-octanol	PO	130	2.0	2	II
14	2-octanol	PO	100	2.0	2	II
15	2-octanol	PO	120	2.0	2	II
16	2-octanol	PO	130	2.0	2	II

I (Santacesaria et al., 1992a); II (DiSerio, Vairo, et al., 1996)

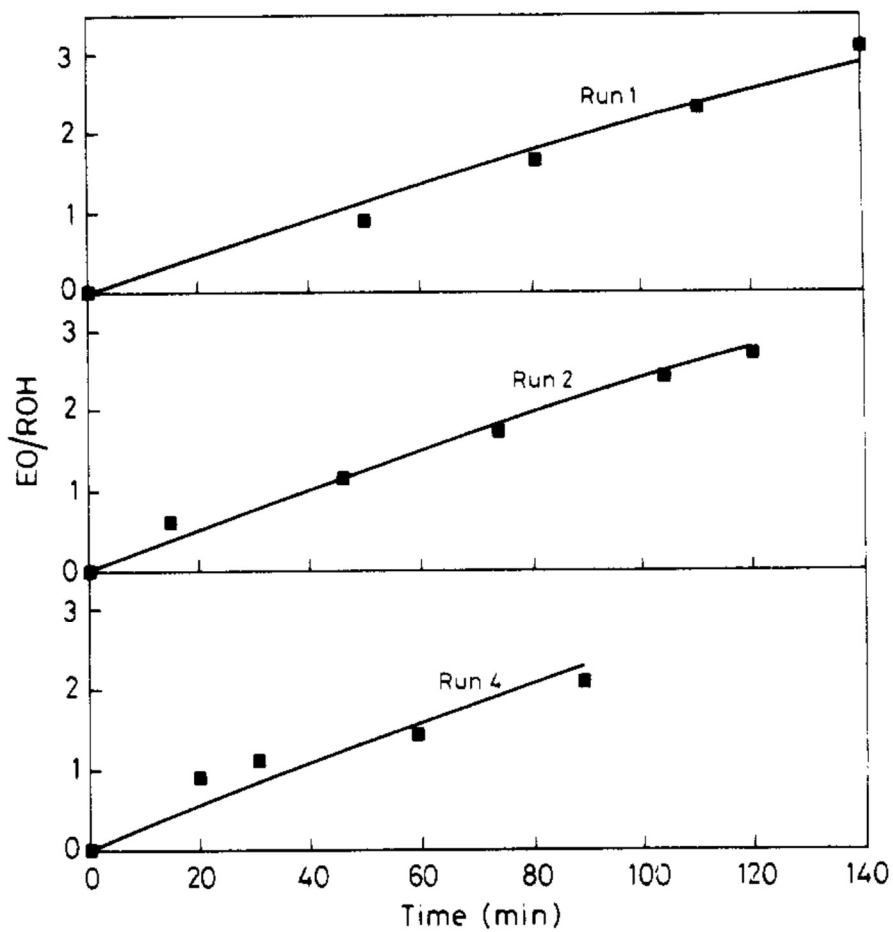


**Fig. 3.2-4.** Ethylene oxide consumption related to the initial moles of alcohol (EO/ROH) in the ethoxylation of dodecanol (reaction condition see Tab. 3.2-6). Dots are experimental, line calculated. Reprinted with permission from (Santacesaria et al. 1992) Copyright 1992 American Chemical Society.

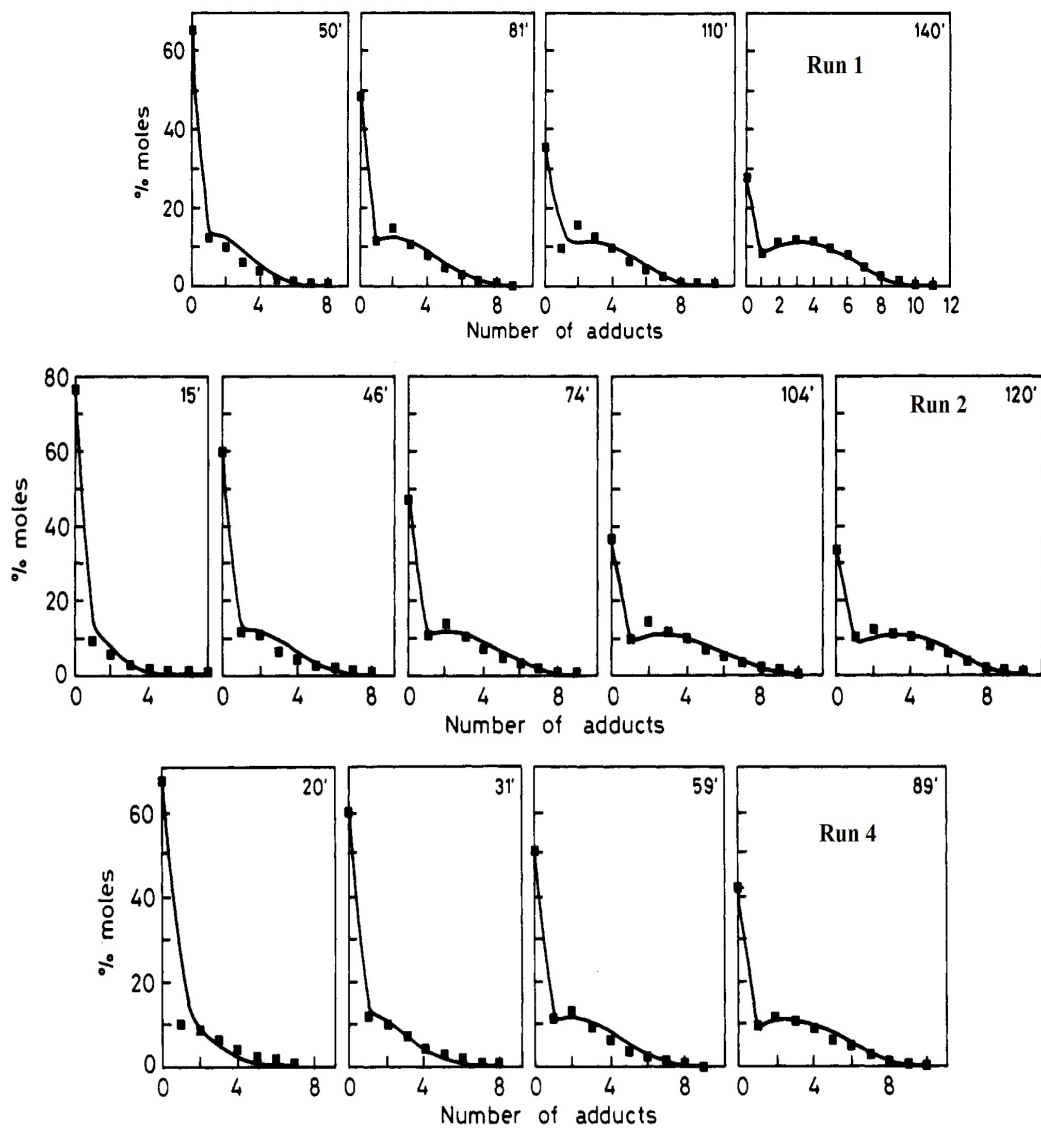


**Fig. 3.2-5.** Experimental (dots) and calculated (line) oligomer distributions of ethoxylation of dodecanol (run 1, 2 and 4 of tab. 3.2-6) at different reaction times. Adapted with permission from (Santacesaria et al. 1992) Copyright 1992 American Chemical Society.

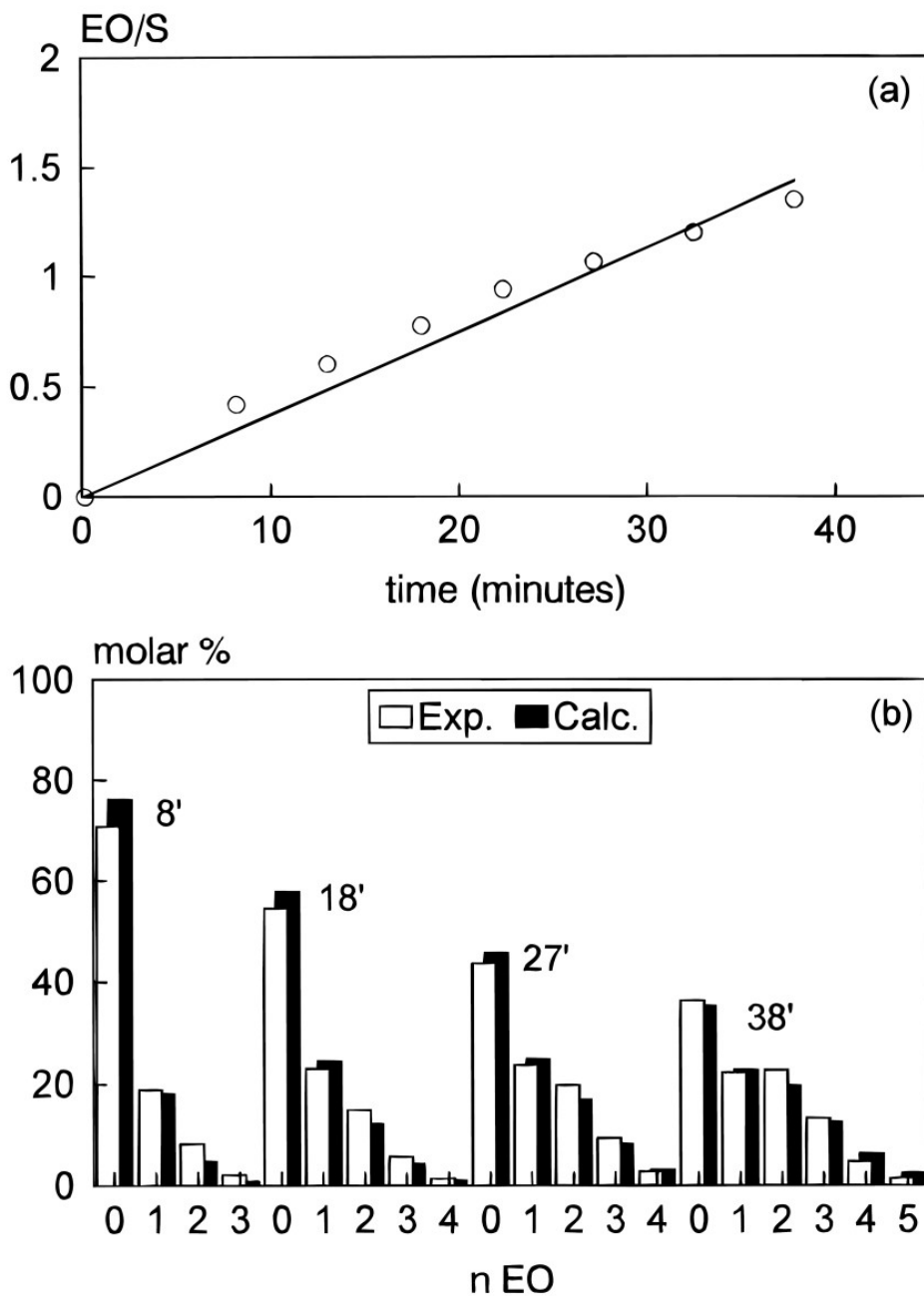


**Fig. 3.2-6.** (a) Ethylene oxide consumption related to the initial moles of alcohol (EO/S) in the ethoxylation of 1-octanol (run 6, Tab. 3.2-6). Dots are experimental, line calculated. (b) Experimental and calculated oligomer at different reaction times. Reprinted with permission from (DiSerio, Vairo, et al., 1996) Copyright 1996 American Chemical Society.

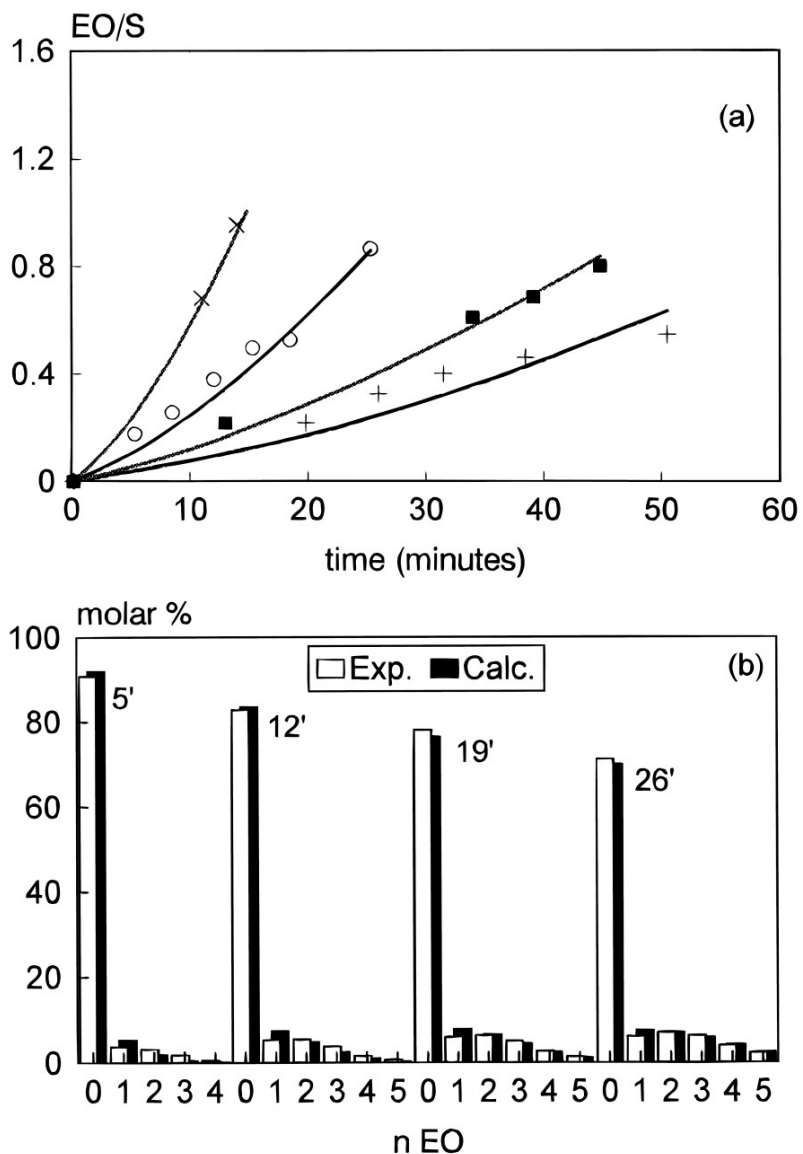


**Fig. 3.2-7.** (a) Ethylene oxide consumption related to the initial moles of alcohol (EO/S) in the ethoxylation of 2-octanol (+ run 7, ■ run 8, ○ run 9, x run 10 of Table 3.2-6)). Dots are experimental, line calculated. (b) Experimental and calculated oligomer distributions at different reaction times. Reprinted with permission from (DiSerio, Vairo, et al., 1996) Copyright 1996 American Chemical Society.

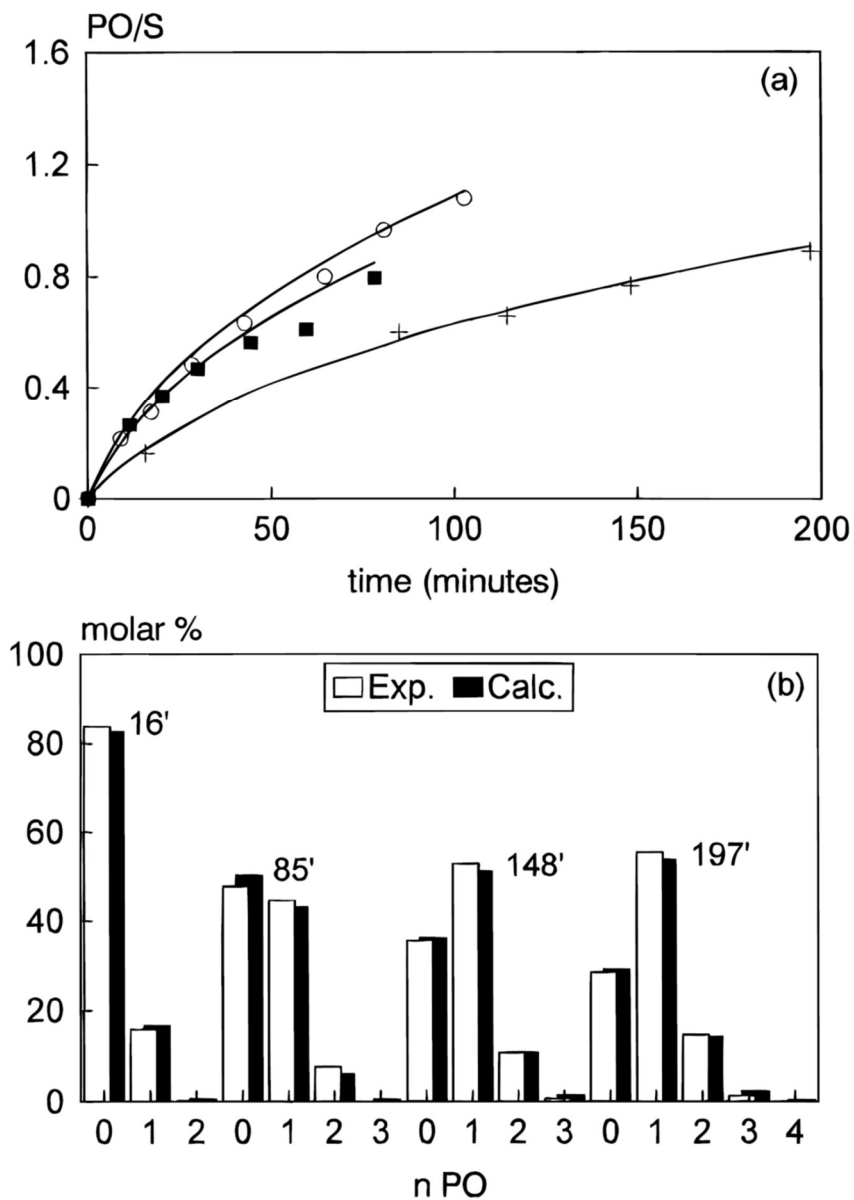


**Fig. 3.2-8.** (a) Propylene oxide consumption related to the initial moles of alcohol (PO/S) in the propoxylation of 1-octanol (+ run 11, ■ run 12, O run 113, of Table 3.2-6). Dots are experimental, line calculated. (b) Experimental and calculated oligomer distributions at different reaction times. Reprinted with permission from (DiSerio, Vairo, et al., 1996) Copyright 1996 American Chemical Society.

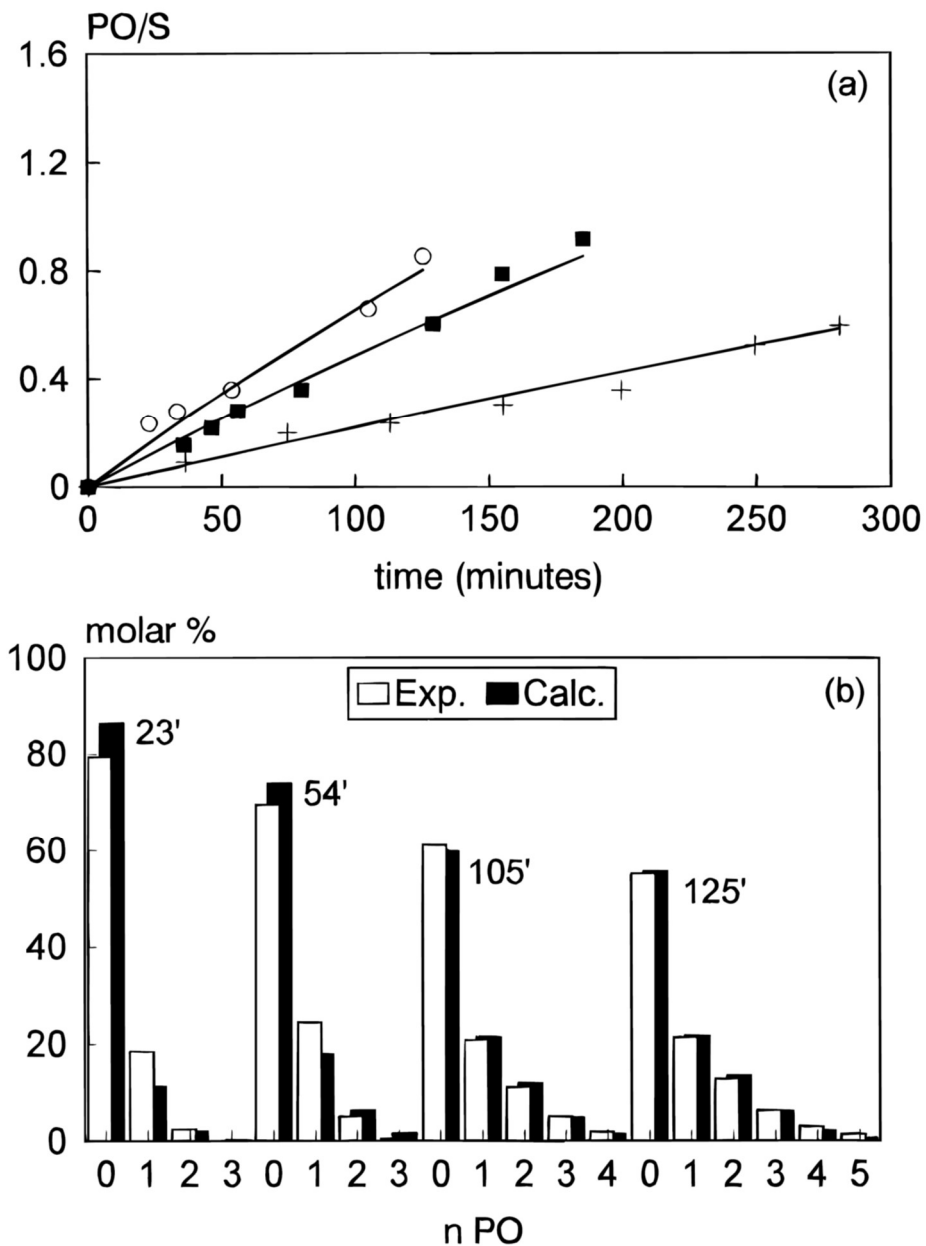


**Fig. 3.2-9.** (a) Propylene oxide consumption related to the initial moles of alcohol (PO/S) in the propoxylation of 2-octanol (+ run 14, ■ run 15, ○ run 16, of Table 3.2-6). Dots are experimental, line calculated. (b) Experimental and calculated oligomer distributions at different reaction times. Reprinted with permission from (DiSerio, Vairo, et al., 1996) Copyright 1996 American Chemical Society.



### 3.2.4 Well mixed Stirred Feed Batch Reactor Modell and kinetic parameters determination

To determine the kinetic parameters of the ethoxylation and propoxylation reaction runs described previously it is necessary to apply a mathematical model of the used reactor.

The reactor used in kinetic studies can be considered as well mixed feed batch, isotherm, and isobar reactor.

The mass balance equations of liquid phase, considering the reaction scheme 2.4.5 are the following:

$$\frac{dn_{ROH}}{dt} = -r_0 \quad \text{initiation reaction} \quad (\text{Eq. 3.2-16})$$

$$\frac{dn_{RO(AO)_1H}}{dt} = (r_0 - r_1)V_L$$

$$\frac{dn_{RO(AO)_2H}}{dt} = (r_1 - r_2)V_L$$

..... propagation reactions ( $i=1, \dots$ )  
(Eq. 3.2-17)

$$\frac{dn_{RO(AO)_iH}}{dt} = (r_{i-1} - r_i)V_L$$

$$\frac{dn_{AO_R}}{dt} = V_L \sum_i r_i \quad \text{total mol AO reacted} \quad (\text{Eq. 3.2-18})$$

$$V_L = V_{SL} + V_{AOL} \approx V_{SL} = \frac{W_{S^0} + n_{AO_R} P_{MAO}}{\rho_{SL}} \quad \text{Liq. Volume} \quad (\text{Eq. 3.2-19})$$

Considering the general reaction rate equation of alkoxylation (Eq. 2.4-1) we have:

$$r_0 = k_0[RO^-M^+][AO]; r_1 = k_1[RO(AO)_1^-M^+][AO]; \dots \dots; r_i = k_i[RO(AO)_i^-M^+][AO] \quad (\text{Eq. 3.2-20})$$

To solve the differential equation 3.2-16 – 3.2-18, the concentration of alkylene oxide of Equations 3.2-20 can be derived from the data or by the methods described

previously, while the concentrations of different ionic couples are linked with the concentration of oligomers through the equilibrium equations (Eq. 2.4-2).

Considering the validity of assumption that in the case of basic catalysts (alkaline hydroxide or alkoxide) the equilibrium constant is independent from the oligomer length (and temperature) but depends only from the different stability of ionic couple formed with the starter and oligomers, we have:

- 1) Ethoxylation of a primary alcohol starter:  $K_{e1} = K_{e2} = \dots = K_{ei} = \dots = K_e = K_{11}$
- 2) Ethoxylation of a secondary alcohol starter:  $K_{e1} = K_{e2} = \dots = K_{ei} = \dots = K_e = K_{21}$
- 3) Propoxylation of a primary alcohol starter:  $K_{e1} = K_{e2} = \dots = K_{ei} = \dots = K_e = K_{12}$
- 4) Propoxylation of a secondary alcohol starter:  $K_{e1} = K_{e2} = \dots = K_{ei} = \dots = K_e = K_{22}$

And we can write:

$$K_e = \frac{[ROH][RO(AO)_i^- M^+]}{[RO^- M^+][RO(AO)_i H]} \quad i = 1, \dots \quad (\text{Eq. 3.2-21})$$

From Eq. 3.2-6 we have:

$$[RO(AO)_i^- M^+] = K_e \frac{[RO(AO)_i H]}{[ROH]} [RO^- M^+] \quad i = 1, \dots \quad (\text{Eq. 3.2-22})$$

considering, that:

$$B^\circ = \sum_{i=1, \dots} [RO(AO)_i^- M^+] + [RO^- M^+] = \quad (\text{Eq. 3.2-23})$$

$$= K_e \frac{[RO^- M^+]}{[ROH]} \sum_{i=1, \dots} [RO(AO)_i H] + [RO^- M^+] =$$

$$= \frac{[RO^- M^+]}{[ROH]} \left( K_e \sum_{i=1, \dots} [RO(AO)_i H] + [ROH] \right)$$

⇓

$$[RO^- M^+] = B^\circ [ROH] / (K_e \sum_{i=1, \dots} [RO(AO)_i H] + [ROH]) \quad (\text{Eq. 3.2-24})$$

In the case of alkoxylation of fatty alcohols described previously we have 4 different situations:

- 1) Ethoxylation of a primary alcohol starter: the product is a primary alcohol like the starter.
- 2) Ethoxylation of a secondary alcohol starter: the product is a primary alcohol primary contrary to the starter which is secondary.
- 3) Propoxylation of a primary alcohol starter: the product is a secondary alcohol contrary to the starter which is primary.
- 4) Propoxylation of a secondary alcohol starter: the product is a secondary alcohol like the starter.

In the case of alkoxylation of fatty alcohols catalyzed by bases the reactivity depends only by the alkylene oxide and by the hydroxyl types of alcohol (see paragraph 2.4), and we have the following situation for the values of kinetic constants:

- 1) Ethoxylation of a primary alcohol starter:  $k_0 = k_1 = k_2 = \dots = k_i = \dots = k_p = k_{11}$
- 2) Ethoxylation of a secondary alcohol starter:  $k_0 = k_{21} \neq k_1 = k_2 = \dots = k_i = \dots = k_p = k_{11}$
- 3) Propoxylation of a primary alcohol starter:  $k_0 = k_{12} \neq k_1 = k_2 = \dots = k_i = \dots = k_p = k_{22}$
- 4) Propoxylation of a secondary alcohol starter:  $k_0 = k_1 = k_2 = \dots = k_i = \dots = k_p = k_{22}$

The kinetic and equilibrium constants of described model for ethoxylation reaction of dodecanol of Table 3.2-6 obtained by mathematical regression on data of Figures 3.2-4-3.2-5 are reported in Table 3.2.7. In the case of ethoxylation and propoxylation of 1 and 2 octanol the constants were determined by regression on data reported in Figure 3.2-6 and 3.2-9 obtaining the values reported in Table 3.2-8

The results obtained by simulation with these constants are in very high agreement with the experimental data as can be seen in Figures 3.2-4-3.2-9, confirming the correctness hypothesis done on the kinetic model.

**Table 3.2-7** Kinetic Constants for the Ethoxylation of Dodecanol and Proton Transfer Equilibria Constant (Santacesaria et al., 1992a).

Kinetic Constant	$\ln A$ (cm <sup>3</sup> mol <sup>-1</sup> s <sup>-1</sup> )	$E$ (kcal/mol)
$k_{11}$	$20.3 \pm 0.3$	$13.3 \pm 0.2$
Proton Transfer equilibrium constant		
$K_{11} = 4.8$		

From data of Table 3.2-7 and 3.2-8, it can be observed that the kinetic constant of ethoxylation of primary alcohols is very poor influenced by the length of carbon atoms chain, contrary to proton transfer equilibrium constants. It is to point out that the kinetic constant obtained  $k_{11}$  are in good agreement with reported by other authors (See Figure 3.2-10).

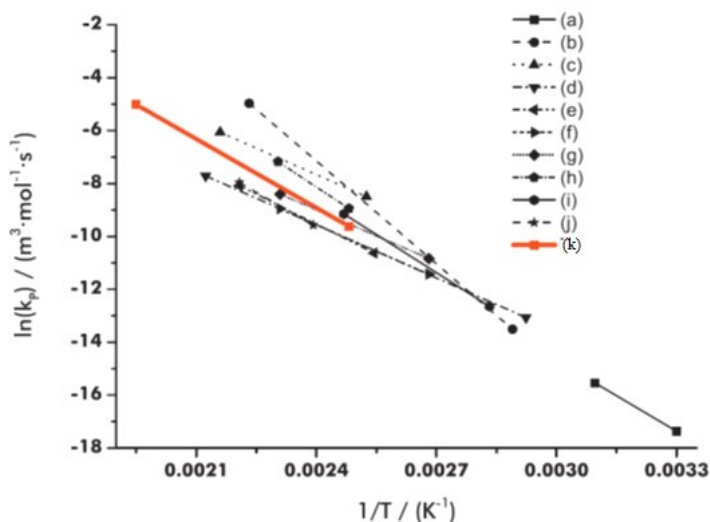
**Table 3.2-8** Kinetic Constants for the Ethoxylation and Propoxylation of 1-Octanol and 2-Octanol, respectively, and Proton Transfer Equilibria Constants for Four Cases. Reprinted with permission from (DiSerio, Vairo, et al., 1996) Copyright 1996 American Chemical Society.

kinetic constants	$\ln A$ ( $\text{cm}^3 \text{mol}^{-1} \text{s}^{-1}$ )	$E$ (kcal/mol)
$k_{11}$	$20.52 \pm 0.25$	$13.0 \pm 1.8$
$k_{12}$	$22.69 \pm 0.03$	$15.6 \pm 0.5$
$k_{21}$	$23.83 \pm 0.14$	$16.8 \pm 1.0$
$k_{22}$	$25.10 \pm 0.19$	$19.0 \pm 1.9$

Proton Transfer Equilibrium Constants			
$\text{Ke}_{11}$	$\text{Ke}_{12}$	$\text{Ke}_{21}$	$\text{Ke}_{22}$
$2.0 \pm 0.3$	$3.5 \pm 0.4$	$2.2 \pm 0.2$	$2.5 \pm 0.3$

The activation energy increases in the case of ethoxylation of secondary alcohol and in the propoxylation reaction. The ratio between rate of addition of ethylene oxide to a primary alcohol with respect to propylene oxide  $k_{11}/k_{12}$  is always  $>1$ ; on the contrary, the ratio between the rate of addition of propylene oxide to a secondary alcohol vs. ethylene oxide  $k_{22}/k_{21}$  is always  $<1$ .



**Fig. 3.2-10.** kinetic constant of ethoxylation of a primary alcohol determined by several authors (a) (Gee et al., 1959), (b)(Santacesaria et al., 1990), (c)(Hall & Agrawal, 1990), (d)(Santacesaria et al., 1992a), (e) (DiSerio et al., 1994), (f) (DiSerio et al., 1995), (g) (DiSerio, Vairo, et al., 1996), (h) (DiSerio et al., 2002) (i) (Amaral & Giudici, 2011), (j) (Rupp et al., 2013b) (k) (Rupp et al., 2013b) Reprinted with permission from (Rupp et al., 2013b) Copyright 2013 Elsevier B.V.

### 3.3 Conclusions

The adopted kinetic model can be applied to ethoxylation and propoxylation of primary and secondary alcohol to describe the evolution of alkylene oxide consumption and of oligomers distribution. This opens the possibility to use the model and the kinetic constants to describe the behaviour of industrial reactors

## Chapter 4 Industrial Alkoxylation Reactors

Different reactor technologies can be employed to produce non-ionic surfactants via alkoxylation reaction. In the present chapter, the most advanced reactors are deeply illustrated and compared for what concerns the working principle and the main performance.

### 4.1 Description of Industrial Alkoxylation Reactors

These devices, described in the present chapter, are different, basically, according to (i) production capacity and (ii) the desired final alkoxylation degree. A first category is represented by Semibatch Stirred Tank Reactors (SSTR) mainly employed for small-scale productions. This type of reactor can differ according to the strategy adopted for the heat exchange system that can be (i) internal coil, (ii) external jacket, and (iii) circulation loop with an external heat exchanger device. The second category of alkoxylation reactors is represented by the Venturi Loop Reactor (VLR or Buss reactor) that was initially designed as hydrogenator. In this reactor, gaseous hydrogen was sucked by the Venturi tube and dispersed into the liquid phase. It has successively been adapted to alkoxylation in which EO or PO are sucked as liquid into the Venturi tube and there vaporize with an exceptional increase of volume. This gas is pressurized into the mixer and gives place to a very high gas–liquid interface area inside the reactor. Due to this aspect, the reactor can be considered as a well-mixed gas–liquid reactor and treated with models similar to the CSTR reactors. Another type of reactor is the Spray Tower Loop Reactors (STLR or Pressindustria-Scientific Design reactors) in which the circulating liquid phase is sprayed in an atmosphere of gaseous alkoxide. According to this configuration, the liquid is the dispersed phase while gas is the continuous one.

The chapter is dedicated to the description of models that were proposed to describe quantitatively the mentioned reactors for the ethoxylation of fatty alcohols. The model is characterized by a general validity and can be easily adapted to each specific reactor configuration.

From an historical point of view, the first reactor used for conducting alkoxylation reactions are the semibatch stirred tank reactors (SSTR) normally employed for small scale production and for low to moderate alkoxylation degree. According to the need of heat removal rate, different strategies of thermal exchange system can be installed in the reactor. By considering the scheme reported in Figure 4.1-1

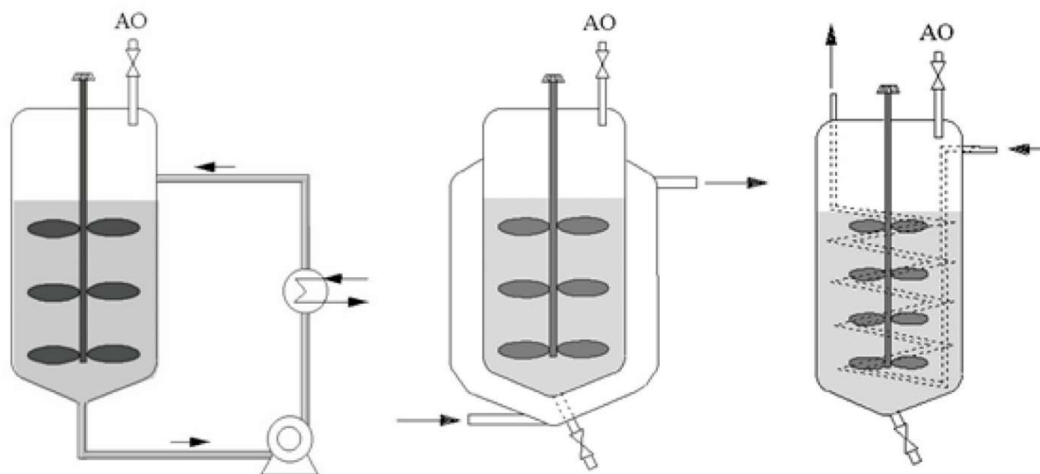


**Fig. 4.1-1.** Semibatch Stirred Tank Reactors (SSTR): circulation loop SSTR (left); jacketed SSTR (centre); internal coiled SSTR (right) (Santacesaria et al., 2018).

From the first used stirred jacketed, during the time, new reactor types with enhanced efficiency and productivity have been proposed on the market. The increase in safety, productivity and selectivity has been the driving force for the new reactor designs (DiSerio, 2019; DiSerio et al., 2005; Salzano et al., 2007a) and we can consider the technological improvement in the alkoxylation reactors as a clear example of the process intensification (Stankiewicz & Moulijn, 2000).

Notwithstanding the new quite recent proposals for continuous reactor (Tesser et al., 2020), described in the Chapter 5 the ethoxylated or propoxylated products synthesis is still largely based on fed-batch reactors technology in various configurations.

A first classification of these reactors is possible by considering the dispersed phase (Dimiccoli et al., 2000). The ethylene oxide (EO) or propylene oxide (PO) are bubbled in the liquid phase (stirred tank reactor, STR, or Venturi Loop Reactor, VLR, (see Figure 4.1-2) or the liquid is sprayed in an atmosphere of gaseous ethylene (Spray Tower Loop Reactor, STLR) (see Figure 4.1-3).

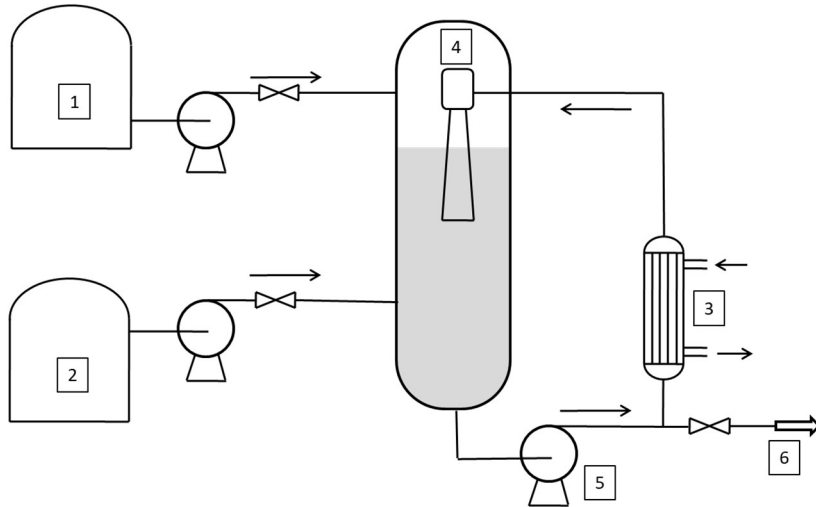


**Fig. 4.1-2.** Venturi Loop Reactor (VLR). 1-2: tanks, 3: heat exchanger; 4: ejector; 5: recirculating pump; 6: outlet stream. (DiSerio et al., 2021).

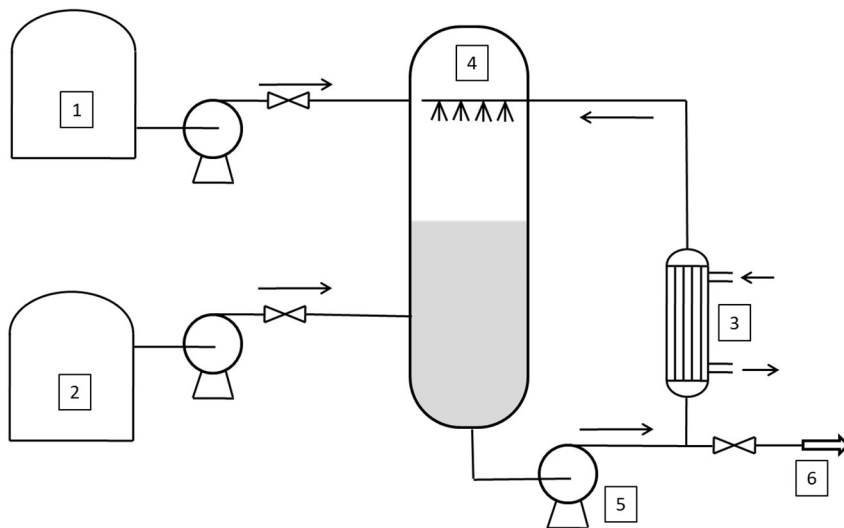


**Fig. 4.1-3.** Flowsheet of the Spray Tower Loop Reactor (STLR). 1-2: tanks, 3: heat exchanger; 4: spray nozzles; 5: recirculating pump; 6: outlet stream. (DiSerio et al., 2021).

The STLR can be arranged vertically, as depicted in Figure 4.1-3, or alternatively, in horizontal way. A horizontal spray reactor can be equipped with a higher number of



spray nozzles even if a moderate increase in volume is so allowed. In general, the heat exchanger is located outside the reactor, on the circulation line, and a liquid recirculation pump is present, also in the case of the simple mixed reactor.

The main problem for this process is the difficulty in eliminating or minimizing mass-transfer and heat-transfer limitations, which are generally associated with conventional stirred tank alkoxylation reactors. The use of Venturi Loop Reactor (VLR) or Spray Tower Loop Reactor (STLR) can solve these problems, and as we will see below these reactors are safer in respect to stirred reactor.

## 4.2 Mathematical model of Venturi Loop Reactor (VLR)

In the VLR, the pumped liquid passes through a nozzle that provides a high velocity jet of fluid to create suction of the gas. In a mixing tube, the high velocity jet attaches itself to the mixing tube wall, resulting in a rapid dissipation of kinetic energy, which creates an intensive mixing with the production of a fine dispersion of gas bubbles in the liquid phase. The two-phase mixture that “jets” into the reaction autoclave also causes intensive mixing. The consequence is a very high value of mass-transfer coefficient ( $k_l a = 0.2\text{-}1.5\text{ s}^{-1}$ ). Considering that the Hatta number of ethoxylation reactions is less than 1, a Venturi Loop Reactor can be simulated by assuming it as a well-stirred isothermal reactor (see figure 4.2-1) (DiSerio et al., 2005):

*EO in gaseous phase:*

$$\frac{dn_{EO,G}^{\square}}{dt} = F_{EO} - J_{EO}V_L \quad (4.2-1)$$

where

$$J_{EO} = k_l a ([EO]_0 - [EO]_b) \quad (4.2-2)$$

*EO in liquid phase:*

$$\frac{d[EO]_b}{dt} = J_{EO} - R \quad (4.2-3)$$

where in general  $R = \sum_{j=0}^n k_j [RO(EO)_j^- M^+] [EO]_b$  but in the case of ethoxylation of linear fatty alcohol, because the kinetic constant is independent by the ethoxylation grade, we can write:

$$R = k[Cat][EO]_b \quad (4.2-4)$$

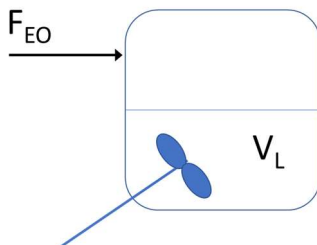


**Fig. 4.2-1.** Scheme of a Well Stirred Reactor.

The ratio of mols of ethylene oxide reacted/ initial moles of fatty alcohol is given by the following equation:

$$\frac{\frac{n_{EO}}{n_{ROH^o}}}{dt} = R \frac{V_L}{ROH^o} \quad (4.2-5)$$

$V_L$  changes during the reaction time and can be calculated by the equation:

$$V_L = \left[ n_{ROH^o} \rho_S^{-1} \left( MW_{ROH^o} + \frac{n_{EO}}{n_{ROH^o}} MW_{EO} \right) \right] \quad (4.2-6)$$

Also  $[EO]_0$  change as function of EO pressure ( $P_{EO}$ ) and EO repartition constant ( $H_{EO,S}$ ):

$$[EO]_0 = \frac{P_{EO}}{H_{EO,S}} \quad (4.2-7)$$

$P_{EO}$  can be determined by considering ideal the gaseous phase:

$$P_{EO} = n_{EO,G} \frac{RT}{(V_R - V_L)} \quad (4.2-8)$$

$\rho_S$  and  $H_{EO,S}$  that are function of temperature and ethoxylation grade can be calculated as described in the Cap. 3.

For safety reason air must be eliminated from the reactor before the EO feed (the explosive range of EO-air mixtures is from 2.6 to 100%). For eliminating the danger, the reactor is purged with Nitrogen. The presence of Nitrogen is useful also to avoid the decomposition of EO that can occur even in absence of air. Moreover, Nitrogen limits the formation of EO by-products that influence the quality of the final product.

For these reasons the molar gaseous fraction of EO ( $y_{EO}$ ) must be  $<0.50$  (Leuteritz, 1992).

To achieve the safety condition safe an initial nitrogen pressure in the range 1-7 bar is generally used, and the initial number of moles of Nitrogen present into the reactor can be calculated with the following equation:

$$n_{N_2,0} = n_{N_2,G} + n_{N_2,L} = P_{N_2,0} \left( \frac{V_R - V_L}{RT} \right) + \frac{P_{N_2,0}}{H_{N_2,S}} V_L \rho_S = P_{N_2,0} \left( \frac{V_R - V_L}{RT} + \frac{V_L \rho_S}{H_{N_2,S}} \right) \quad (4.2-9)$$

The value of  $H_{N_2,S}$  (the solubility of nitrogen in the substrate) is approximately  $2.34 \cdot 10^7$  bar g mol<sup>-1</sup> (estimated values (DiSerio et al., 2005)).

The quantity of Nitrogen in the reactor increases during the reaction because it is introduced also with the feed of EO, because liquid EO is stored in a tank under nitrogen pressure to prevent decomposition and a certain amount of  $N_2$  is dissolved in the EO. The mol of Nitrogen added with EO feed can be calculated with the following relationship:

$$\frac{dn_{N_2}}{dt} = \frac{F_{EO} MW_{EO} (P_{ST} - P_{EO}^0)}{H_{N_2,EO}} \quad (4.2-10)$$

At 298 K, The solubility of nitrogen in ethylene oxide ( $H_{N_2,EO}$ ) is  $9.72 \cdot 10^4$  bar g mol<sup>-1</sup> and the vapor pressure of EO ( $P_{EO}^0$ ) is 1.74 bar. Consequently, the total pressure in the reactor, considering the equation 4.2-8 and 4.2-9 will be:

$$P = P_{N_2} + P_{EO} = \frac{n_{N_2}}{\left( \frac{V_R - V_L}{RT} + \frac{V_L \rho_S}{H_{N_2,S}} \right)} + n_{EO,G} \frac{RT}{V_R - V_L} \quad (4.2-11)$$

In Fig. 4.2-2 the simulation results obtained with the mathematical model previously described for an isothermal reactor operating with an EO feed rate of 1000 kg/hour, are reported in Fig. 4.2-2. The related operating conditions are listed in Table 4.2-1 and in caption of the figure.

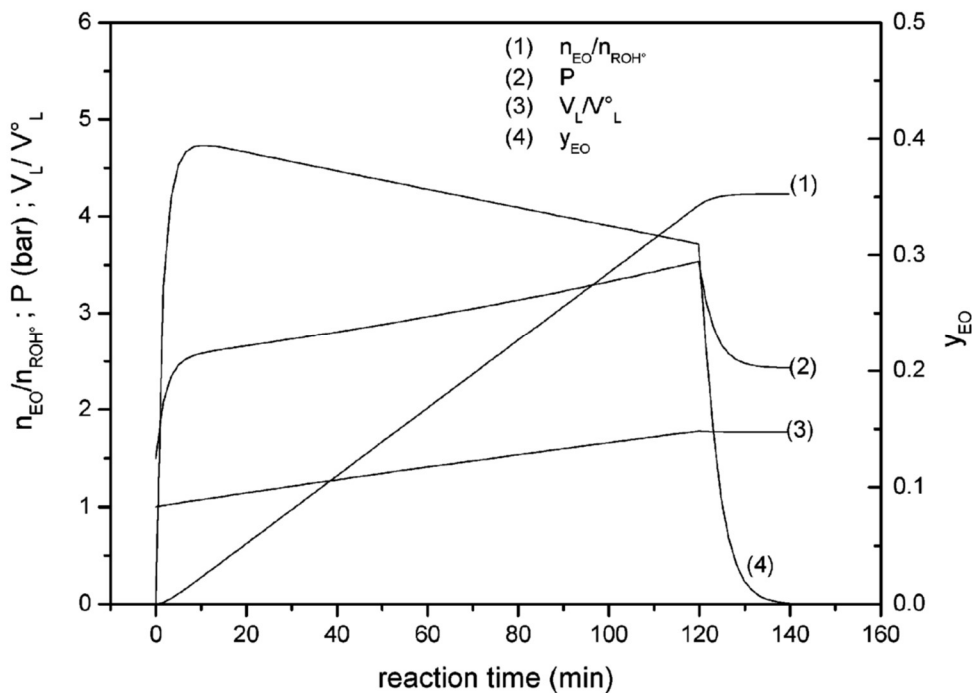


**Fig. 4.2-2.** Calculated values of total pressure,  $y_{EO}$ , and  $V_L/V_L^0$  in the ethoxylation of dodecanol in a Venturi loop reactor at EO fed 1000 kg/h, T 453 K, and  $k_{La}$  0.5 s<sup>-1</sup>. The other reaction conditions are reported in Table 4.2-1. Reprinted with permission from (DiSerio et al., 2005) Copyright 2005 American Chemical Society.

As can be seen, in Figure 4.2-2 the total Pressure has a strong increase at the start of the feed, along the time the total pressure decreases (because increase the ethylene oxide dissolved in the liquid for the increasing of liquid volume).

When the feed of EO is stopped the total pressure decreases quickly but it arrives at a final value that is higher than the initial one. This is due to the fact the total amount of nitrogen in the reactor is slightly increased but mainly because the gaseous volume is reduced. The molar fraction of EO in the gaseous phase increases continuously (but in chosen conditions it is always <0.5), when the feed of EO is stopped this value arrive to 0 in 20 minutes. This phase is called cooking and is very important for assure the absence of EO in the reactor gaseous phase before its discharge.

**Table 4.2-1.** Characteristics of the Reactor and the Related Operating Conditions of the Reported Simulations

$V_R$	reactor volume (m <sup>3</sup> )	10
$ROH^\circ$	dodecanol charged (kg)	2000
$CAT$	catalyst (KOH) (kg)	6.5
$k$	kinetic constant (cm <sup>3</sup> mol <sup>-1</sup> s <sup>-1</sup> )	$6 \cdot 10^8 \exp(-6640/T)$
$P_{N_2,0}$	initial pressure of N <sub>2</sub> (bar)	1.5
$P_{ST}$	pressure of EO storage tank (bar)	4.0
	time of EO alimentation (min)	120

### 4.3 Mathematical model of Spray Tower Loop Reactor (STLR)

In STLR, the sprayed liquid is dispersed in the form of small liquid drops flying into the alkylene oxide gaseous atmosphere. Drops emerging from an efficient spray nozzle resulted as internally well-mixed drops, leading to a very high mass-transfer rate, and if the average flight time of the drops is long enough, these drops are completely saturated at the end of their flight (Dimiccoli et al., 2000; Santacesaria, di Serio, et al., 1999). The reaction occurs in the liquid column and can be neglected the drops contribution to the reaction, since the flight time is extremely short if compared to the residence time in the liquid column and to the relatively low liquid holdup in the gas phase (Dimiccoli et al., 2000; Santacesaria, di Serio, et al., 1999). The liquid column can then be modeled assuming it as a plug-flow reactor in transient conditions as the concentration of dissolved alkoxide changes with time and along the column itself.

Hence, in these reactors, mass transfer and chemical reaction occur separately in two distinct zones: the mass-transfer zone, corresponding to the zone of drops flying across the gaseous atmosphere, and the reaction zone, corresponding to the slowly flowing liquid-phase collected at the bottom of the reactor and recirculated back to the spray nozzle (DiSerio et al., 2005).

The liquid column in the reactor can be assumed with a plug-flow behavior but is in transient conditions as the concentration changes both along the time and along the axial direction. For modeling purposes, the reactor can be better schematized as a series of well mixed cells or liquid portions distributed along the liquid column, according to the well-known compartmental models (Egedy et al., 2013; Haag et al., 2018). In the scheme reported in Figure 4.3-1 the cells scheme related to STLR configuration is reported.

From this scheme it is possible to appreciate the characteristics of the reactor.

The model is certainly general and provides the possibility to impose a user-defined number of compartments, depending on the axial dispersion degree that would describe the system.

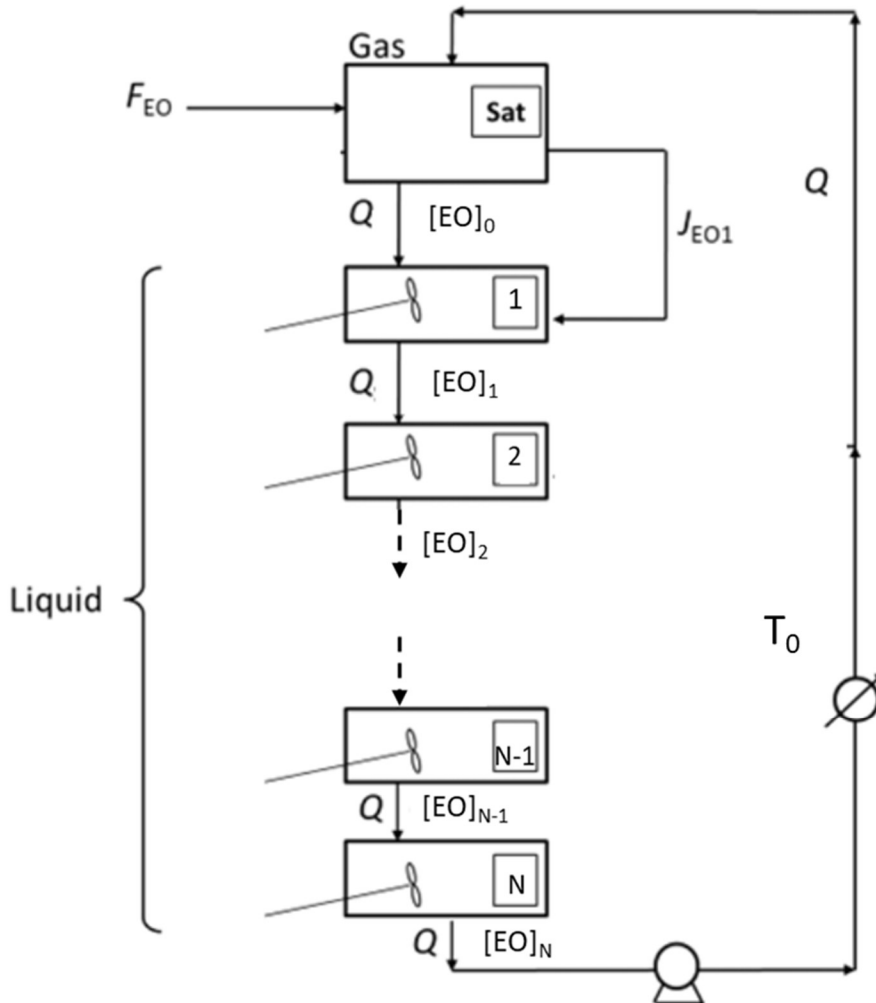


Fig. 4.3-1. Scheme of a simplified STLR model.

For the development of a general model based on the scheme reported in Figure 4.3-1, some assumptions can be adopted, as in the following points:

- 1) The spray nozzle is considered with a full efficiency in saturation. In the spray chamber, the entering liquid is fully saturated with EO. This simplifying

assumption can be removed by introducing an empirical multiplying factor (less than unity) to simulate lower saturation efficiency.

- 2) The flow of liquid phase in the liquid column is simulated as a series of CSTR reactors (cells or compartments). The different distribution of cells volume can be used to represent different reactor configuration and fluid-dynamic conditions. For instance, as for the general tank-in-series model, depending on the axial dispersion degree, it is possible to choose a different number of compartments. In detail, a plug-flow fluid-dynamics can be simulated by a theoretically infinite number of cells, while a stirred tank with only one compartment. Thus, a high number of equal cells is used for a STLR (10-20). The first stage is in contact with gaseous phase also the additive mass transfer  $J_{EO1}$  could be considered, even if in the case of STLR this contribute is very low because the low interface area of liquid column with gaseous phase.
- 3) The expansion of the system volume, that occurs as ethoxylation proceeds, is assumed as equally distributed on all the cells in the reactor.
- 4) The overall volumetric circulation flowrate,  $Q$ , is assumed constant.
- 5) The feed of liquid EO from the external tank is assumed as completely vaporized in the saturation chamber of the reactor.
- 6) Some properties of the reacting mixture and EO are assumed as constants or averaged with temperature, such as specific heat of reactive mixture ( $C_p = 2.5$  J/(g K)), heat of vaporization of EO ( $\lambda_{EO} = 0.15$  W/(m K) at 298K), specific heat of liquid EO ( $C_{pEO} = 1973$  J/(kg K) at 298K) .
- 7) The reactor is perfectly insulated and no heat exchange with the surroundings is present.

The heat exchanger installed on the circulation line is assumed with infinite exchange capacity and the outlet temperature is fixed at a predefined value  $T_S$ . Alternatively, in order to gain more accuracy, a more rigorous exchanger model can be introduced into the overall compartment modeling scheme. Referring to the scheme in Figure 4.3-1, the mass balance for EO in the gaseous phase of the reactor is:

$$\frac{dn_{EO,G}}{dt} = F_{EO} + Q([EO]_N - [EO]_0) - J_{EO1}V_1 \quad (4.3-1)$$

Where the mass transfer flows are defined by the following relation:

$$J_{EO1} = k_{L1}a_1([EO]_0 - [EO]_1) \quad (4.3-2)$$

Another important relation if the account for the overall quantity of reacted EO. This equation can be written as follows:

$$\frac{dn_{EO}}{dt} = \sum_{j=1}^N V_j R_j \quad (4.3-3)$$

Where:

$$R_j = k[Cat][EO]_j \quad (4.3-4)$$

As said before, the liquid EO is stored in a tank pressurized with an inert gas (usually nitrogen) and is fed to the reactor directly from this tank. Also, in the case of STLR the inert gas dissolved into liquid EO is continuously fed to the reactor resulting in an accumulation of inert during the operation, and the balance on inert gas is described by equation (4.2-10). The following differential equations represent the mass balances for cell 1 (Eq. 4.3-5) and the following cells (from 2 to N) (Eq. 4.3-6)

$$\frac{dn_{EO,1}}{dt} = Q([EO]_0 - [EO]_1) - R_1 V_1 + J_{EO} V_1 \quad (4.3-5)$$

$$\frac{dn_{EO,2}}{dt} = Q([EO]_1 - [EO]_2) - R_2 V_2 \quad (4.3-6)$$

$$\dots$$

$$\frac{dn_{EO,N}}{dt} = Q([EO]_{N-1} - [EO]_N) - R_N V_N$$

Further equations are necessary to estimate the temperature along the reactor. The energy balance of the saturation chamber is described by the following equation:

$$T_{sat} = \frac{Q\rho C_P T_0 + F_{EO} MW_{EO} C_P \overset{\square}{\square} T_{TANK} - F_{EO} MW_{EO} \lambda_{EO}}{Q\rho C_P + F_{EO} MW_{EO} C_P \overset{\square}{\square}} \quad (4.3-7)$$

In analogy with the material balance equations, the energy balance on the compartments can be written. For the first cell the energy balance assumes the following form:

$$\frac{dT_1}{dt} = -\frac{R_1 \Delta H}{\rho C_P} + \frac{Q}{V_1} (T_{SAT} - T_1) \quad (4.3-8)$$

The temperature of the bottom cells can be described by the following ODEs:

$$\frac{dT_2}{dt} = -\frac{R_2 \Delta H}{\rho C_P} + \frac{Q}{V_2} (T_1 - T_2) \quad (4.3-9)$$

$$\dots$$



$$\frac{dT_N}{dt} = -\frac{R_N \Delta H}{\rho C_P} + \frac{Q}{V_N} (T_{N-1} - T_N)$$

The group of relations consisting of the model represent a system of coupled ordinary differential equations that must be integrated in time starting from a suitable initial condition for each of the related dependent variables. However, the mentioned ODEs system cannot be solved without the addition of other algebraic constitutive equations that describe auxiliary variables such as pressure, liquid, and gas volume, EO solubility, reactive mixture density, kinetic expression, and related parameters (Eq. 4.2.6 – 4.2.11).

In Figure 4.3-2 the simulation of a STLR is reported

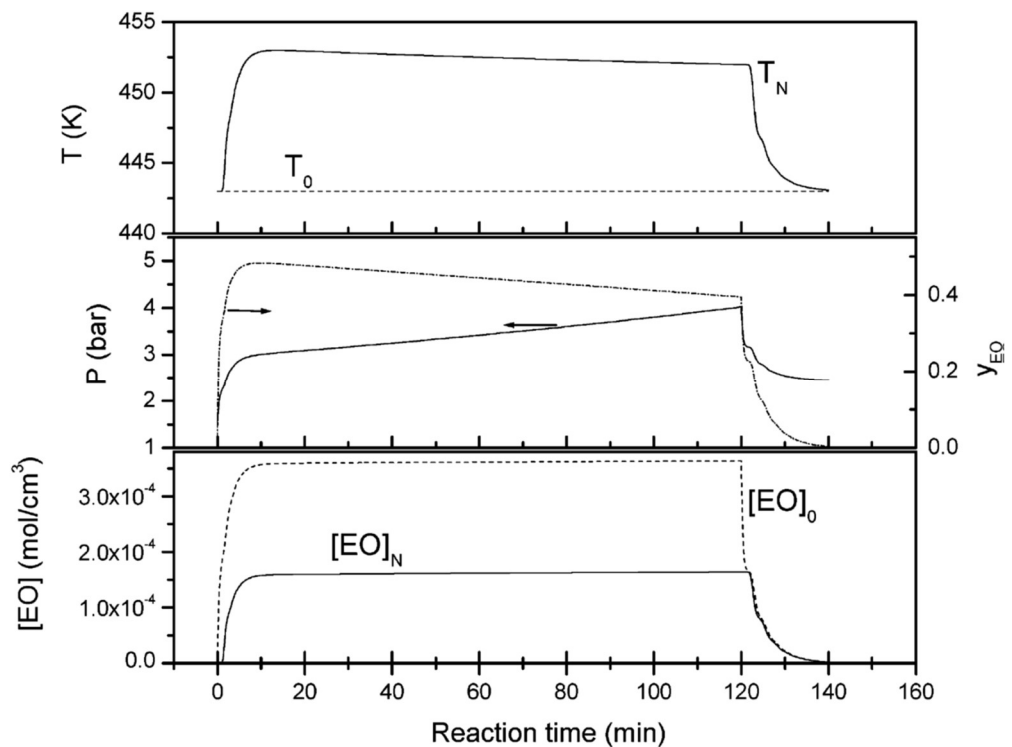


**Fig. 4.3-2.** Calculated values of total pressure ( $P$ ), gaseous molar EO fraction ( $y_{EO}$ ), temperature ( $T$ ), and EO concentration at the top of the liquid column and the bottom of the reactor (0 and N, respectively) in the ethoxylation of dodecanol in a spray tower loop reactor at EO fed = 1000 kg/h and  $Q = 3.17 \cdot 10^4 \text{ cm}^3/\text{s}$  (114 m<sup>3</sup>/h). The other reaction conditions are reported in Table 4.2.1. Reprinted with permission from (DiSerio et al., 2005) Copyright 2005 American Chemical Society.

## 4.4 Safety in ethoxylation processes

The safety aspects are fundamentals in alkoxylation processes, mainly in ethoxylation ones. The main problems that can arise during the ethoxylation processes were listed by Gustin (Gustin, 2000):

- *A gas phase explosion hazard related to the flammability of EO in the presence of air or oxygen.*
- *A gas phase explosion hazards due to EO vapour instability. Similar to acetylene, propargyl chloride, nitrous oxide, nitrogen chloride, chlorine oxides, hydrogen azide or chlorine azide, EO gives decomposition flames with pressure effects in vessels, even in the absence of oxygen.*
- *A liquid phase decomposition hazard, since the decomposition of liquid EO may be initiated by high temperatures, hot spot or catalysts. The reaction of decomposition of EO can propagate in liquid phase if high concentration of EO is present. The thermal stability of EO liquid is influenced by temperature, the material of construction and the presence of impurities.*
- *A runaway reaction hazard when EO is reacted with other chemicals in ethoxylation processes, if EO is allowed to accumulate in reaction vessels, due to improper operating conditions. Also concentrated EO solutions may self-heated runaway if the temperature is not controlled or if a catalyst is present.*
- *A toxic hazard since EO is highly toxic and may cause a cancer. Diluted EO solution can cause severe burns.*

The use of reliable kinetic data and reactor model can be useful to reduce the risk in ethoxylation plants by simulating the reacting system in not right operative conditions, in presence of default of control systems or mechanical ruptures. This simulation can be used to find operative procedures or dedicated devices to reduce significantly the risk in ethoxylation operations (Santacesaria et al., 1995) .

In this section we will report 2 examples of use of reactor simulation in the prediction of consequences of not correct operations or defaults. The first example is the prediction of the maximum productivity of a reactor being in safety condition in respect to the possible gas phase explosion (DiSerio et al., 2005) . The second one is a consequence-based analysis for the definition of safety distances for damage to surrounding equipment and the people working on-site or even outside the industrial plant (Salzano et al., 2007b).

we will consider the VLR (Venturi Loop Reactor) and STLR (Spray Tower Loop Reactor) described previously. The mixed reactor is not considered because it is less safe. The

presence of the stirrer may cause the gas mixture to ignite (formation of a dipole between the stirrer and the reactor wall and overheating of the mechanical seal) or, if the mechanical seal is damaged or fails, ethylene oxide may escape from the reactor, or the seal lubricant may be released into the reactor. In both reactor types mentioned, there are no rotating metallic devices present and the efficiency of heat transfer is ensured by an external thermal exchanger. Both reactors give high productivity.

In Figures 4.4-1 and 4.4-2, simulations of VLR and STLR operating with an EO feed rate of 1000 kg/h have been shown. The productivity of the system could obviously be increased by increasing the EO feed rate. However, the increase has a limitation due to the maximum values of pressure that can be reached in the reactor and  $y_{EO}$ , which must always be  $<0.5$ . Figure 4.4-1 shows the maximum values of pressure,  $y_{EO}$ , and  $n_{EO}/n_{ROH^*}$ , calculated from simulations performed with the same operating conditions as in Table 4.2-1 at different values of EO feed for the Venturi Loop Reactor.

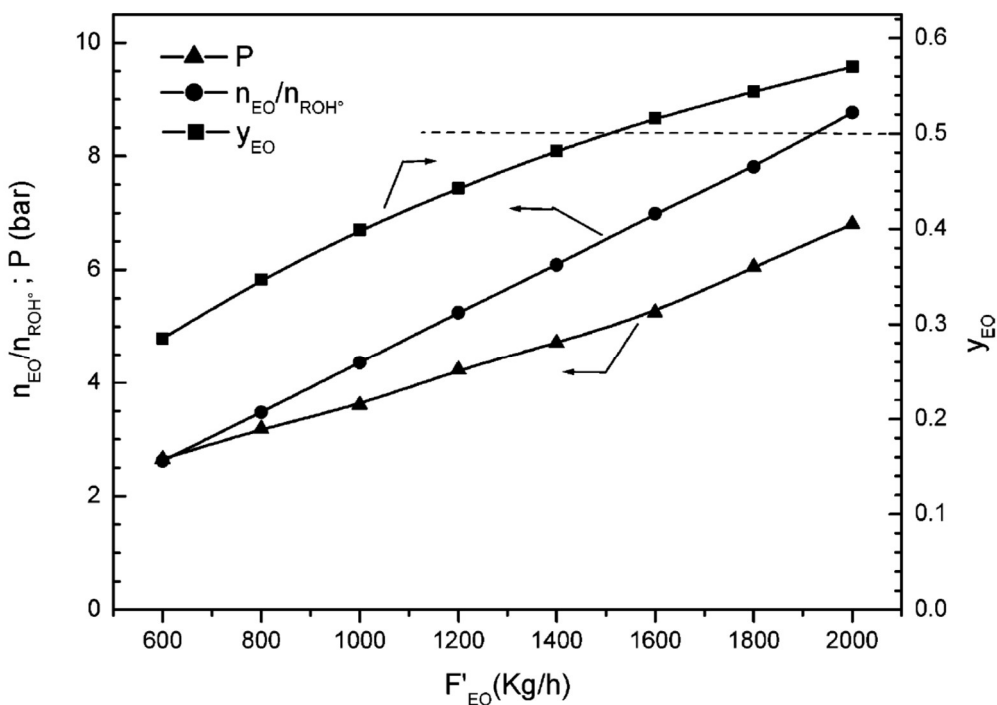


**Fig. 4.4-1.** Calculated maximum values of  $n_{EO}/n_{ROH^*}$ , total pressure, and  $y_{EO}$  in the ethoxylation of dodecanol in a Venturi loop reactor as a function of EO fed,  $T=453$  K, and  $k_{La}= 0.5$  s $^{-1}$ . Reprinted with permission from (DiSerio et al., 2005) Copyright 2005 American Chemical Society.

As can be seen, increasing the EO feed rate obviously increases the degree of ethoxylation. However, the maximum total pressure and the maximum mole fraction of ethylene oxide in the gas phase also increase. The maximum values of  $y_{EO} > 0.5$  are obtained at an EO feed rate  $> 1500$  kg/h. Since these EO molar fraction values are outside the safety zone, EO feed rates above 1500 kg/h cannot be used. This drawback can be solved by increasing the initial pressure of the inert gas, but in this case the maximum total pressure reached in the reactor will also increase.

In the case of STLR, the temperature profile in the spray tower loop reactor depends on the reaction rate, the temperature of the liquid at the outlet of the heat exchanger ( $T_0$ ), and the flow rate of the recirculation liquid ( $Q$ ) (see Eq. 4.3.7-4.3.9). By fixing  $T_0$ , a  $Q$  value can be found that provides the required value of the reactor bottom temperature ( $T_N$ ).

In Figure 4.4-2, the maximum total pressure and maximum mole fraction of EO are plotted as a function of ethylene oxide feed rate, in a spray tower ring reactor operating under pseudo-isothermal conditions  $T_0=452$  K,  $T_N= 454$  K. The other reaction conditions are as shown in Table 4.2-1.

The required  $Q$  values are also shown in Figure 4.4-2. As can be seen, the performance of STLR is quite similar to that of VLR in terms of the maximum achievable productivity ( $F_{EO}= 1500$  kg/h of EO) under the optimal reaction conditions ( $y_{EO} < 0.5$ ). To achieve maximum productivity in STLR, a high recirculation flow rate is required. The power input required for a spray tower ring reactor is of the same order of magnitude as that for a very efficient stirred reactor (self-aspirating stirrer, for example) and is, therefore, greater than that for a Venturi Loop reactor.

The high  $Q$  values in the runs shown in Figure 4.4-2 are necessary because the reactor operates under isothermal conditions.  $Q$  can be greatly lowered when we accept an internal temperature profile in the liquid column. For example, Figure 4.3-2 shows a simulation of a run performed by setting  $T_0 = 443$  K and  $T_N = 453$  K, for an  $F_{EO} = 1000$  kg/h. The other reaction conditions are as in Table 4.2.1. In Figure 4.3-2, the EO concentration and temperature of liquid feed to the spray ( $[EO]_0$  and  $T_0$ , respectively) and at the bottom ( $[EO]_N$  and  $T_N$ , respectively) of the reactor, the total pressure and the molar are plotted for the EO fractions in the gas phase. To achieve a temperature, rise below the fixed limit ( $T_N= 453$  K), we must use  $Q= 3.17.104$  cm<sup>3</sup>/s (114 m<sup>3</sup>/h), which is 5 times lower than that reported for a pseudo-isothermal condition (1.6.105 cm<sup>3</sup>/s; see Figure 4.4-2). Using the lower flow rate of the liquid circuit obviously offers great advantages for lower energy consumption.

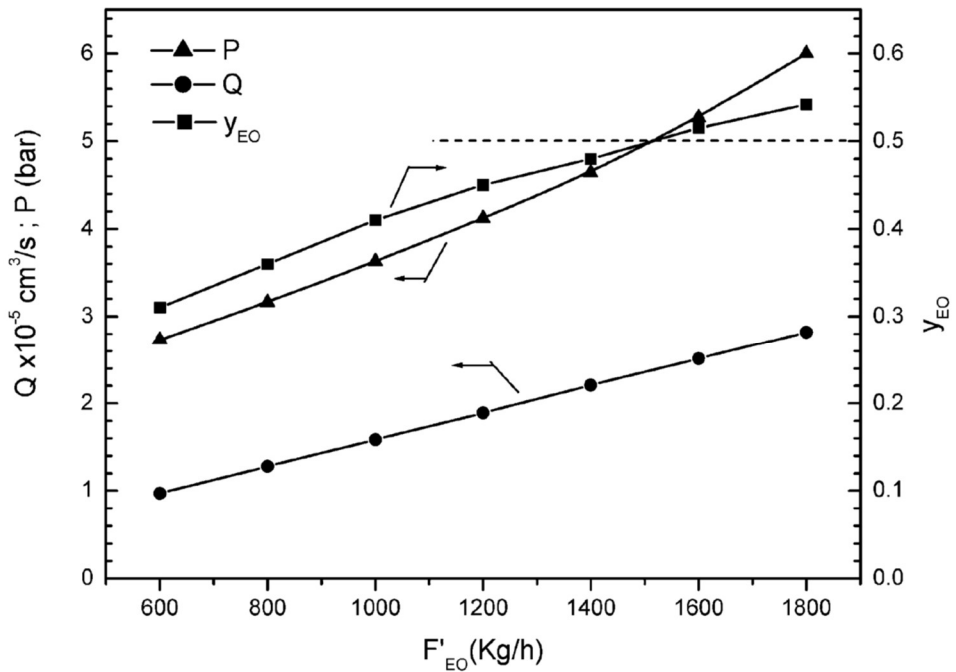


**Fig. 4.4-2.** Calculated maximum values of total pressure and  $y_{EO}$  in the ethoxylation of dodecanol in a spray tower loop reactor operating in pseudo-isothermal conditions as a function of EO fed. The figure also shows the required rates of loop flow (Q) to have pseudo-isothermal condition  $T_0 = 452 \text{ K}$  and  $T_N = 454 \text{ K}$ . The other reaction conditions are reported in Table 4.2-1. Reprinted with permission from (DiSerio et al., 2005) Copyright 2005 American Chemical Society.

With a lower  $T_0$  and Q, however, there is an increase in maximum total pressure and maximum molar gaseous EO concentration. In fact, in the example shown (Figure 4.3-2), a value of  $y_{EO_{max}} = 0.48$  is obtained instead of 0.41 for an  $F_{EO} = 1000 \text{ kg/h}$ . With these reaction conditions an increase in productivity is not possible because an increase in EO flow rate results in achieving molar fractions of EO in the gas greater than 0.5.

Also, the maximum partial pressure of  $P_{EO}$  is important for the safety. The increase of  $P_{EO}$  gives place to an increase in Ethylene Oxide concentration in liquid phase (this concentration is higher in VLR than in STLR). The dissolved EO can have strong consequence in the case of accidental liquid release from the reactor. The total amount of EO in the liquid phase because the increase of liquid volume is higher at the end of reaction than at the beginning. In Table 4.4-2 the EO amount in a VLR reactor operating as described in Table 4.4-1 are reported at the initial and final stage of the reaction ( $EO/S=4.4$ ), as function of  $P_{EO}$  and reaction temperature T. Moreover, in Table 4.4-2 the calculated maximum distances for flammable could and for toxic

dispersion are indicated (Salzano et al., 2007b). As can be seen both  $P_{EO}$  and  $T$  have great influence in the safety distance that increase with the increase of  $P_{EO}$  while decrease with the increase of  $T$ . This behavior can be explained considering the effects of the two parameters on EO solubility.

**Table 4.4-1** Chemical and geometric characteristics of alkoxylation reactors analyzed in this work and the typical range of operation conditions VLR process. Reprinted with permission from Copyright (Salzano et al., 2007b) 2007 Elsevier B.V.

Reactor volume (m <sup>3</sup> )	10
Height (m)	2.5
Dodecanol initially charged (kg)	2000
Time of EO feed (min)	About 120
Initial pressure of N <sub>2</sub> (bar)	1.5
Total reactor pressure (bar)	4.0–5.0
Partial EO pressure (bar)	1.0–3.0
Temperature (°C)	125.0–180.0
Pressure of EO storage tank (bar)	4.0–5.0

**Table 4.4-2** Total flammable mass available for explosion ( $m_{EO,expl}$ ) and maximum distance for flammable cloud (for flash fire,  $x_{ff}^*$ ) and for toxic dispersion (IDLH,  $x_{tox}^*$ ). Reprinted with permission from Copyright(Salzano et al., 2007b) 2007 Elsevier B.V.

$T$ (K)	$P_{EO} = 1$ bar			$P_{EO} = 2$ bar			$P_{EO} = 3$ bar		
	$m_{EO,expl}$ (kg)	$X_{ff}^*$ (m)	$x_{tox}^*$ (m)	$m_{EO,expl}$ (kg)	$x_{ff}^*$ (m)	$x_{tox}^*$ (m)	$m_{EO,expl}$ (kg)	$x_{ff}^*$ (m)	$x_{tox}^*$ (m)
2000 kg									
398	54.1	35.3	130.7	108.3	49.7	175.3	151.6	58.3	201.8
423	33.3	27.4	106.0	66.7	39.2	142.8	80.4	43.0	165.5
453	17.2	18.8	79.2	40.1	30.3	114.9	48.8	33.5	133.9
4000 kg									
398	85.5	44.4	167.3	171.1	61.6	223.4	239.5	71.9	256.8
423	52.5	34.8	136.0	105.0	49.0	182.3	143.4	56.8	210.8
453	27.0	24.4	102.1	63.0	38.2	147.0	86.8	44.7	170.9

Wind velocity = 3 m s<sup>-1</sup>.

## 4.5 Conclusions

In this chapter we have seen the great advantage that right simulation models can give in the design and conduction of ethoxylation reactors, also for safety purposes.

As a result, research has been undertaken in chapter 5 on the development of innovative synthesis node for the alkoxylation process, particularly in the modelling and development of new, efficient, and safe reactor for this process.

# PART II - Process Intensification in the Alkoxylation Reactions

## The novelty of the presented dissertation:

In the second part the following novelty of dissertation is reported:

1. Presentation of the idea of new Enhanced Loop Reactor (ELR) and comparing its performance with both state-of-the-art systems: Spray Tower Loop Reactor (STLR) and Venturi Loop Reactor (VLR), based on the developed mathematical simulations of the reactors.  
As a result, research has been undertaken on the development of innovative synthesis nodes for the alkoxylation process, particularly in the modelling and development of new, efficient and safe reactors for this process.  
Based on the comparison of simulation results of the performance of known STLR and VLR reactor systems and the developed concept of a hybrid ELR synthesis node, the advantages of the new solution were demonstrated.  
The novelty is the development and application of a suitable mathematical model to describe the operation of the compared reactors as well as the concept of the new ELR synthesis node.
2. Critical analysis of the most recent efforts reported in both, the scientific and patent literature dealing with the alkoxylation processes in continuous mode, as published with the participation of the doctoral candidate in the form of a review article. Novelty is the first extensive examination, comparison and discussion of-the-state of the art of such proposals, considering a possible industrial perspective in terms of productivity of the systems. This complements the original research work contained in Chapter 5 and leads to the description of the research work in Chapter 7, devoted to the further development of the technology of oxyalkylation towards microreactors.
3. Elaborating on the data collected in the microreactors, where for the first time a laminar flow model was used to study the kinetics of ethoxylation of the analyzed system. For this purpose, a dedicated mathematical algorithm was developed and successfully applied for continuous ethoxylation using microreactors, under dynamic conditions.

The research part of the dissertation presented in point 1 and 3 represents a novelty in the description of the state of the art and is the achievement of the team in which the doctoral candidate made a leading or significant contribution.

The dissertation part described in point 2 is a literature study of the achievements of other authors as well and is essential for laying the groundwork for further advances in microreactor-based oxyethylation technology, as investigated in point 3.





## Chapter 5 Enhanced Loop Reactor (ELR)

As we seen (par. 4.4) Venturi Loop Reactor assures greater productivity than Spray Loop Reactor with lower energy, however Venturi loop reactor has some drawbacks related to the rigid geometrical parameters that must be satisfied as concerns the dimensions of the reactor, the liquid level, and the nozzle length. As a matter of fact, the plants where VLR technology is used have in general two reactors: the first one works in the initial stage of the reaction (when the liquid level is low), and the other one is used for achieving high ethylene oxide/substrate molar ratio that corresponds to high increase in volume. Moreover, in the case of large reactors, the behavior of VLR can also become like that of STLR in terms of the power input required for liquid recirculation. So, the choice of the better technology is linked to the specific industrial need. To overcome these problems, Desmet-Ballestra launched a Hybrid Spray-Venturi Loop Reactor (HSVLR) or Enhanced Loop Reactor (ELR) that merges the advantages of the Venturi Loop Reactor with those of the Spray Tower Loop Reactor. The development of a mathematical model for the description of the ELR is reported in this chapter (DiSerio et al., 2021).

### 5.1 Mathematical model of Enhanced Loop Reactor (ELR)

The ELR (see Fig. 5.1-1) has been simulated considering it as a STLR reactor on which, in the lower part of the reactor, is placed an ejector. In this case the total recirculating flow ( $Q$ ) is divided, after the heat exchanger, in two streams: one of which is fed to the spray nozzle ( $Q_S$ ) and the second to the ejector ( $Q_B$ ). Furthermore, the liquid flowing in the ejector suck up the gas from the reactor head and disperses it in the liquid phase in the form of bubbles which, rising upwards in the liquid column, further stir the liquid phase.

In this case the ELR, when the ethoxylation reaction is started, behaves like a STLR and when the liquid level reaches a prefixed value, circulation flow is splitted and the ejector is started. In this phase the behavior of the ELR is more like a VLR. This reactor configuration has the effect to merge the two most important advantage of both STLR and VLR: it is possible start the production with a very low quantity of substrate (like in the case of STLR) and a high efficiency in mass transfer is achieved with low power input (like in the case of VLR).

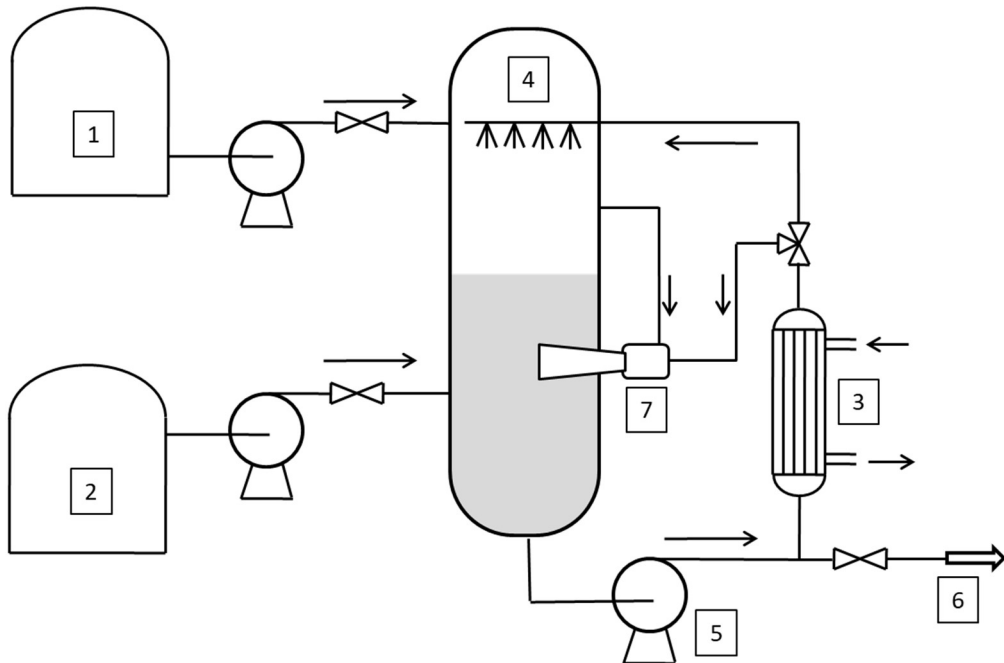


**Fig. 5.1-1.** Sketch of the Enhanced Loop Reactor (ELR). 1-2: tanks; 3: heat exchanger; 4: spray nozzles; 5: recirculating pump; 6: outlet stream; 7: ejector.

In the case of ELR, for modeling purposes, the reactor can be schematized in Figure 5.1-2 the cells scheme related to ELR configuration is reported.

From this scheme it is possible to appreciate the characteristics of the reactor. After the heat exchanger on the circulation line, the flow is splitted into two portions: one of these is fed to the spray and the other one is sent to the ejector placed in the lower part of the reactor.

As revealed in Figure 5.1-2, four cells were assumed as an example of discretization. The model is certainly general and provides the possibility to impose a user-defined number of compartments, depending on the axial dispersion degree that would describe the system, as in the general tank-in-series model. In the specific case, we assumed four cells as the liquid phase is well mixed by the ejector present in the bottom of the reactor. Thus, due to the mixing efficiency of the ejector, the liquid column is assumed as constituted by four separate cells which behavior is that of a dynamic CSTR reactor: the first upper cell 1 receive the liquid more or less saturated with EO in the spray chamber; the majority of the liquid is located in the cells 2 that is well mixed by the ejector; two additional relatively small cells 3 and 4 are located in the lower part of the reactor and become important in the final part of the operations, when the height of the liquid column is increased significantly. More

generally, a higher number of cells can be considered both above and below the central cell 2 associated to the ejector.

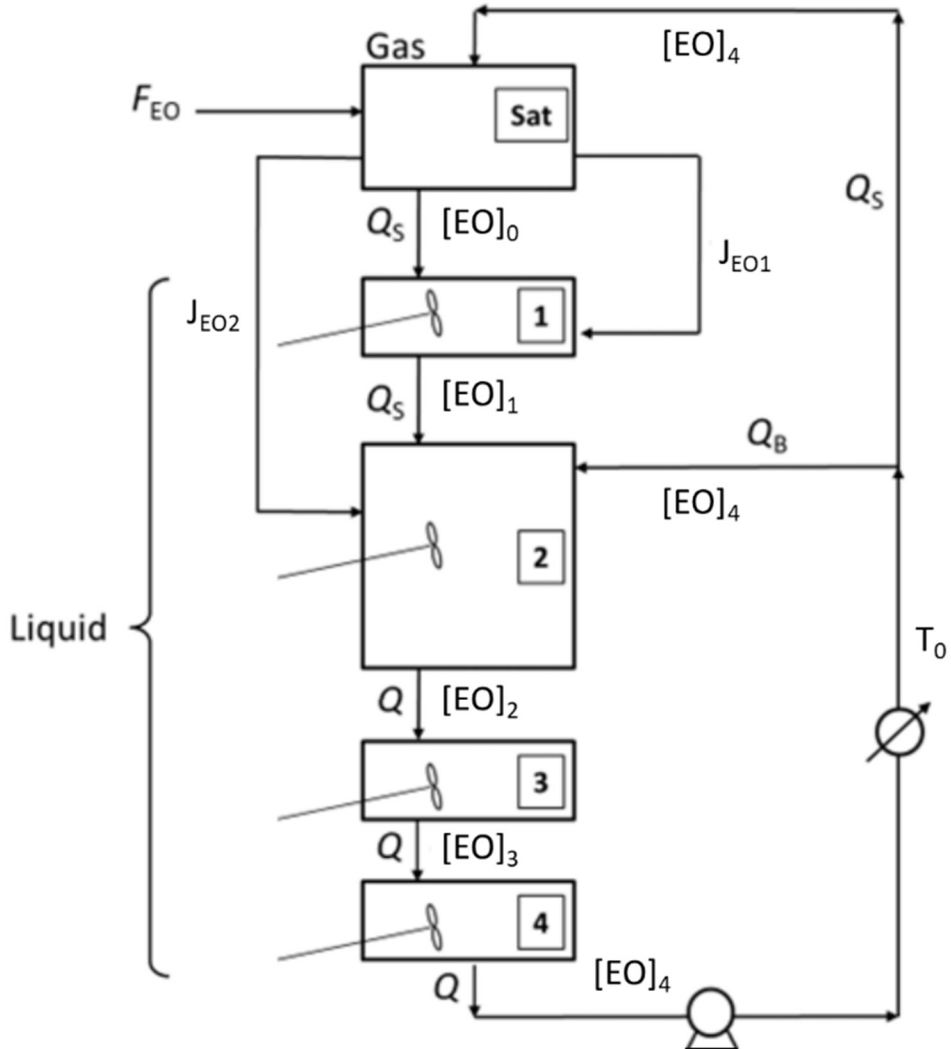


Fig. 5.1-2. Modelling scheme to describe the Enhanced Loop Reactor (ELR).

In the scheme of Figure 5 1-2 also gas-liquid mass transfer flows are reported: the first,  $J_{EO1}$  is related to the spray chamber in which gaseous EO is transferred from gas-phase to liquid droplets emerging from nozzles; the second,  $J_{EO2}$ , is due to the gas suction from ejector that transfer EO directly to the liquid phase of cell 2.

Further improvements in the reactor model schematized in Figure 5.1-2 can consist in a different distribution of compartments volume and, moreover, introducing additional compartments for simulating the liquid holdup of various portions of the circulation line and the volume inside the exchanger (process side).

For the development of a general model based on the scheme reported in Figure 5.1-2, the same assumptions of STLR reactor can be adopted (see par. 4.3).

Referring to the scheme in Figure 5.1-2, the mass balance for EO in saturation section of the reactor is:

$$\frac{dn_{EO,G}}{dt} = F_{EO} + Q_S([EO]_N - [EO]_0) - J_{EO} V_1 - J_{EO2} V_2 \quad (5.1-1)$$

Where the mass transfer flows are defined by the following relations:

$$J_{EO1} = k_{L1} a_1 ([EO]_0 - [EO]_1) \quad (5.1-2)$$

$$J_{EO2} = k_{L2} a_2 ([EO]_0 - [EO]_2) \quad (5.1-3)$$

Material balance on cells is slightly different from one cell to another. The following differential equations represent the mass balances for cell 1 (Eq. 5.1-4), cell 2 (Eq. 5.1-5) and cells 3 and 4 (Eq. 5.1-6).

$$\frac{dn_{EO,1}}{dt} = Q_S([EO]_0 - [EO]_1) - R_1 V_1 + J_{EO} V_1 \quad (5.1-4)$$

$$\frac{dn_{EO,2}}{dt} = Q_S([EO]_1 - [EO]_2) + Q_B([EO]_0 - [EO]_2) - R_2 V_2 + J_{EO} V_2 \quad (5.1-5)$$

$$\frac{dn_{EO,j}}{dt} = Q([EO]_{j-1} - [EO]_j) - V_j R_j \quad (5.1-6),$$

where  $R_j$  is given by equation (4.3-4).

The overall quantity of reacted EO is given by the equation (4.3-3), the initial inert amount by equation (4.2-9), the balance on inert gas is described by equation (4.2-10) and the total pressure by equation (4.2-11).

In analogy with the material balance equations, the energy balance on the compartments can be written. For the first cell the energy balance assumes the following form:

$$\frac{dT_1}{dt} = -\frac{R_1 \Delta H}{\rho C_P} + \frac{Q_S}{V_1} (T_{SAT} - T_1) \quad (5.1-7)$$

For the central cell number 2 the energy balance is slightly different:

$$\frac{dT_2}{dt} = -\frac{R_2\Delta H}{\rho C_P} + \frac{Q_S}{V_2}(T_1 - T_2) + \frac{Q_B}{V_2}(T_0 - T_2) \quad (5.1-8)$$

The temperature of the two last bottom cells can be described by the two following ODEs:

$$\frac{dT_3}{dt} = -\frac{R_3\Delta H}{\rho C_P} + \frac{Q}{V_3}(T_2 - T_3) \quad (5.1-9)$$

$$\frac{dT_4}{dt} = -\frac{R_4\Delta H}{\rho C_P} + \frac{Q}{V_4}(T_3 - T_4) \quad (5.1-10)$$

The group of relations consisting of the model represent a system of coupled ordinary differential equations that must be integrated in time starting from a suitable initial condition for each of the related dependent variables. However, the mentioned ODEs system cannot be solved without the addition of other algebraic constitutive equations that describe auxiliary variables such as pressure, liquid, and gas volume, EO solubility, reactive mixture density, kinetic expression, and related parameters, etc.

A further equation is necessary to estimate the temperature of the saturation chamber from an energy balance. This equation is as follows:

$$T_{sat} = \frac{Q_S \rho C_P T_0 + F_{EO} M W_{EO} C_{P_{EO}} T_{TANK} - F_{EO} M W_{EO} \lambda_{EO}}{Q_S \rho C_P + F_{EO} M W_{EO} C_{P_{EO}}} \quad (5.1-11)$$

The comparison of the different reactors was done considering reactor with the same total volume and using the same total recirculating flow (see Figure 5.1-3 and 5.1-4, in the caption the adopted simulation conditions are reported).

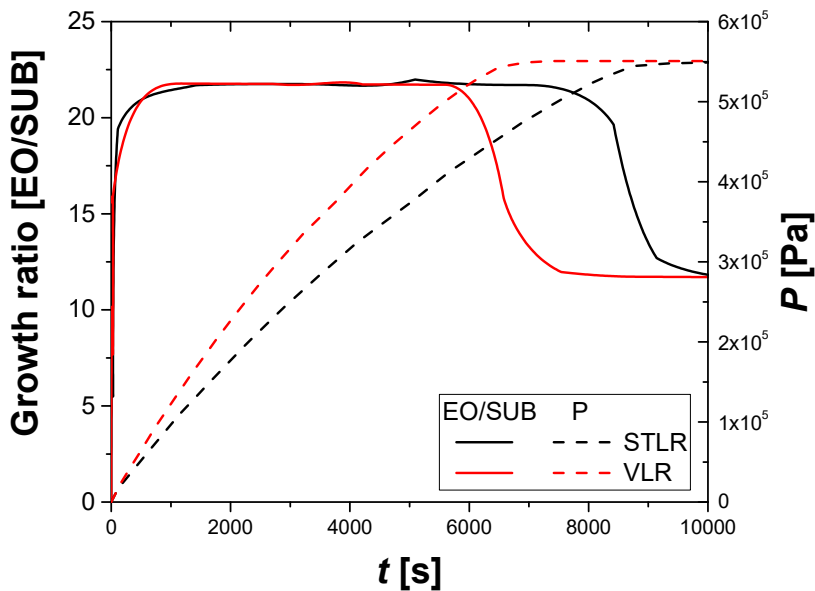


**Fig. 5.1-3.** Calculated values of growth ratio and total pressure, in VLR, STLR operating in the same conditions. Reactor volume: 20 m<sup>3</sup>; total recirculating flow: 210 m<sup>3</sup>/h; maximum operating pressure: 5.5 bar; initial Nitrogen pressure: 1.2 bar; starter (dodecanol) :500 Kg; catalyst (KOH): 8 Kg; exiting heat exchanger temperature: T<sub>0</sub> = 178°C; final growth ratio:20.5.(DiSerio et al., 2021).

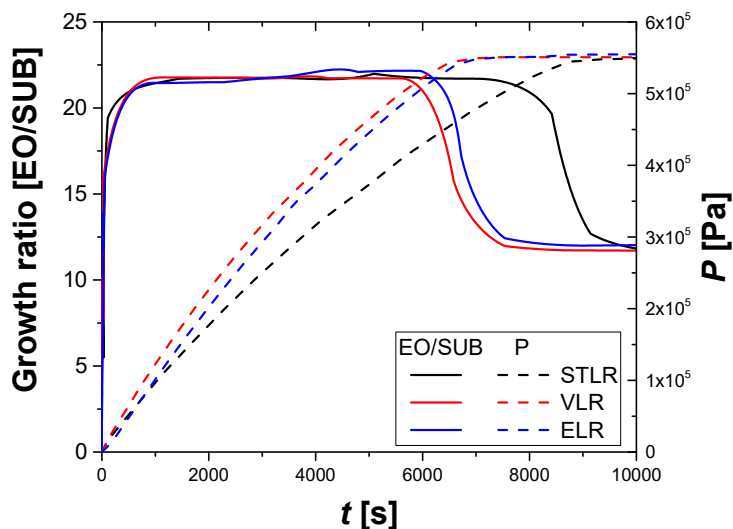


**Fig. 5.1-4.** Calculated values of growth ratio and total pressure, in VLR, STLR, ELR operating in the same conditions. Reactor volume: 20 m<sup>3</sup>; total recirculating flow: 210 m<sup>3</sup>/h; maximum operating pressure: 5.5 bar; initial Nitrogen pressure: 1.2 bar; starter (dodecanol) :500 Kg; catalyst (KOH): 8 Kg; exiting heat exchanger temperature: 178°C; final growth ratio:20.5 (Di Serio et al., 2021)

As the simulations were conducted to keep a constant pressure of the system, the growth ratio approaches to a plateau value when the consumption of ethylene oxide decreases, indicating the stop of the ethylene oxide feed. Thus, the overall pressure decreases reaching the set value of the inert gas.

The performance

The performance of the VLR strongly depends on the liquid column height inside the reactor relative to the position of the venturi tube end. Because there is an increase in liquid volume during the reaction and consequently an increase in liquid column height, several venturi tubes of different lengths are positioned inside the reactor and operated at different times.

In Figure 5.1-4 the performance of the ELR is reported. In this case the total recirculating flow was divided in two parts when liquid volume in the reactor was 3 m<sup>3</sup>. The one that supplied the spray nozzle was the 25% of the total while the remaining amount supplied the ejector.

## 5.2 Conclusions

In conclusion, the ELR has the same performances of the VLR, as they provide a similar mixing to the liquid phase, thus a similar ethylene oxide content. However, the Enhanced Loop Reactor has a high flexibility of the gas-liquid contacting devices that permit constant performances of the reactor during all the course of the production process and mass growth ratio in the system up to 80.





## Chapter 6- Alkoxylation in continuous reactors

As it was presented in the previous chapters, the alkoxylation reaction is conducted in semi-batch modality even if this technology is intrinsically characterized by a relatively low productivity. As the demand of surfactants production is increasing, it is natural to shift toward a continuous process. In the present chapter, the most recent efforts dealing with the alkoxylation processes in continuous mode are reported, analyzing critically the results reported in both the scientific and patent literature.

The shift from the traditional semi-batch process to the continuous ones could really represent the start of a new era in the alkoxylation technologies (Santacesaria et al., 2018). Moreover, a continuous process must be designed to operate under high pressure, and this could represent a further advantage for the safety due to the absence of a vapor phase (DiSerio et al., 2005) rich in alkoxide that could be more susceptible to ignition. The adoption of a sufficiently high pressure can ultimately keep the alkoxide in liquid state at the process temperature realizing high concentration with an improvement also of the reaction rate.

In the scientific and patent literature both traditional reactors, like the tubular ones, and more innovative reactor configurations, like microreactors, have been proposed for the continuous alkoxylation reactions. These last are particularly suitable for exothermic and multiphase reactions, thanks to the high heat and mass transfer exchange rate (Kralisch et al., 2012). Moreover, very recently, also stirred tank reactors in series or in combination with PFRs have been proposed as suitable for a continuous alkoxylation production process. In fact, whereas innovative microreactors showed superior performances in terms of heat/mass transfer efficiency and in theoretical productivity, many authors still proposed the use of traditional reactor devices accepting the drawbacks (lower productivity, lower heat transfer efficiency) but gaining in the possibility for large-scale applications. On the other hand, the exploitation of microdevices advantages can be achieved through the concept of numbering-up (instead of scale-up) that involves, however, a complex setting and control. Hybrid emerging technologies, like for example annular thin film reactor (tube-in-tube arrangement) of corrugated plates heat exchanger reactor, could represent a good perspective in the industrial consolidation of continuous alkoxylation.

In the present chapter the state-of-the-art of such reactor arrangement is examined, compared, and extensively discussed, also considered for a possible industrial perspective in terms of productivity of different systems.

## 6.1 Discussion and perspectives on continuous alkoxylation reactors

From a literature survey of the last decades, several attempts in performing the alkoxylation process in continuous devices have been made. In Table 6.1-1 examples of the reaction conditions adopted by different authors are summarized and compared, also in terms of system productivity expressed as the quantity of product obtained per unit of time and per unit of reactor volume.

By Using tubular reactors, even working under optimized process conditions of pressure and temperature, there are problems for what concerns the thermal control of the system. This fact has been solved by lowering the ethylene oxide concentration by splitting the feed at different points along the tubular reactor. This solution leads to drawbacks and difficulties due to the necessity of a very complex process control system, particularly in the case of high numbering-up (replication of multiple reactor modules) (Hinz & Dexeimer, 2002; Hubel et al., 2005; Nikbin et al., 2018; Umbach & Stein, 1971a).

A possible solution to control of temperature can be the use of a coiled tubular reactor as suggested in a pioneering work of Umbach and Stein (Umbach & Stein, 1971a). In their investigation these authors have tested ethoxylation and propoxylation reactions in two types of tubular reactors consisting in a stainless-steel tube of different diameters (6 and 9 mm) arranged as coils. With this experimental setup, the authors were able to obtain a complete conversion of alkoxides in very short residence times, in the range 15-150 sec, which is much lower than the resident time characteristic of discontinuous processes. The system is operated under high pressure (60-100 bar) to maintain ethylene or propylene oxide in liquid state while the temperature of the feed is quite low (60-70 °C).

The two reactors are designed with a very high L/D ratio (respectively 2500 and 1400) for a better performance in heat removal, nevertheless a rather high temperatures were reached along the reactor with a characteristic profile. The achieved temperature peaks obtained with different systems tested by the authors, can be observed in Figure 6.1-1.

As it can be seen, the maximum temperatures reached were in the range of 240-300 C. Even if only reactions with low alkoxylation degrees were tested in this

investigation (2-4 moles of alkoxide per mole of substrate), the productivities obtained resulted very interesting, giving place to a product throughput up to 100-120 kg/h that corresponds to a monthly production of 60-70 ton and with a specific productivity of 120000 kg/(h m<sup>3</sup>).

**Table 6.1-1** – Summary of the typical reaction conditions and related results for different alkoxylation processes performed in continuous reactors ( $\tau$ : residence time;  $P$ : productivity). \* mol %.(Tesser et al., 2020)

Reactor	Alcohol (Alkoxide)	$C_{CAT}$ , w%	Type of cat.	Alcohol/Alkoxide	$T_{MAX}$ , °C	$\tau$ , s	$P$ , kg/(h m <sup>3</sup> )	Ref.
Coiled tubes	C <sub>12-14</sub> (EO/PO)	0.10	NaOCH <sub>3</sub>	1:1-1:6 mol/mol	287	25	120000	Umbach and Stein 1971
Coiled tubes	Sucrose (EO/PO)	0.40	KOH	11.4:5.8 w/w	180	600	-	Hinz and Dexheimer 2002
Microchannels	Butanol (EO/PO)	3.00*	KOCH <sub>3</sub>	1:35 mol/mol	190	200	-	Hubel 2010
Microchannels	Octanol (EO)	0.66*	KOH	1:3-1:6-1:9 mol/mol	240	50	12600	Rupp et al. 2013
Falling film multipipe	n-nonyl phenol (EO)	0.60	NaOH	1:7 mol/mol	220	160	22000	Aigner et al. 2016
Stirred compartments	Polyoxypropylenetriol (PO)	0.05	DMC	1:4.2 w/w	120	15000	324	Yamada et al. 2006
CSTR	C <sub>13</sub> (EO)	0.18	La(PO <sub>4</sub> )	1:1.4 w/w	170	7200	450	McDaniel and Reese 2007a
Two CSTR	C <sub>12-16</sub> (EO)	0.0144	DMC	1:1.4 w/w	130	12960	255	McDaniel and Reese 2007b
Two CSTR	Nonylphenol ethoxylate (EO)	0.0133	DMC	1:1.9 w/w	130	13320	195	McDaniel and Reese 2008b
CSTR+PFR	C <sub>26</sub> diol (EO/PO)	0.3	DMC	1:9 w/w	140	21600	150	Villa et al. 2014
CSTR+PFR	Glycerol alkoxyolate (PO)	0.0058	DMC	1:4.2 w/w	125	8700	372	Verwijs et al. 2008
CSTR+PFR	Glycerol (EO/PO)	0.4	DMC	1:10.3 w/w	160	25200	130	Weston et al. 2012
Two CSTR	Glycerol (EO/PO)	0.002	DMC	1:2.7:33.1 w/w (EO/PO)	140	-	653	Lai et al. 2019

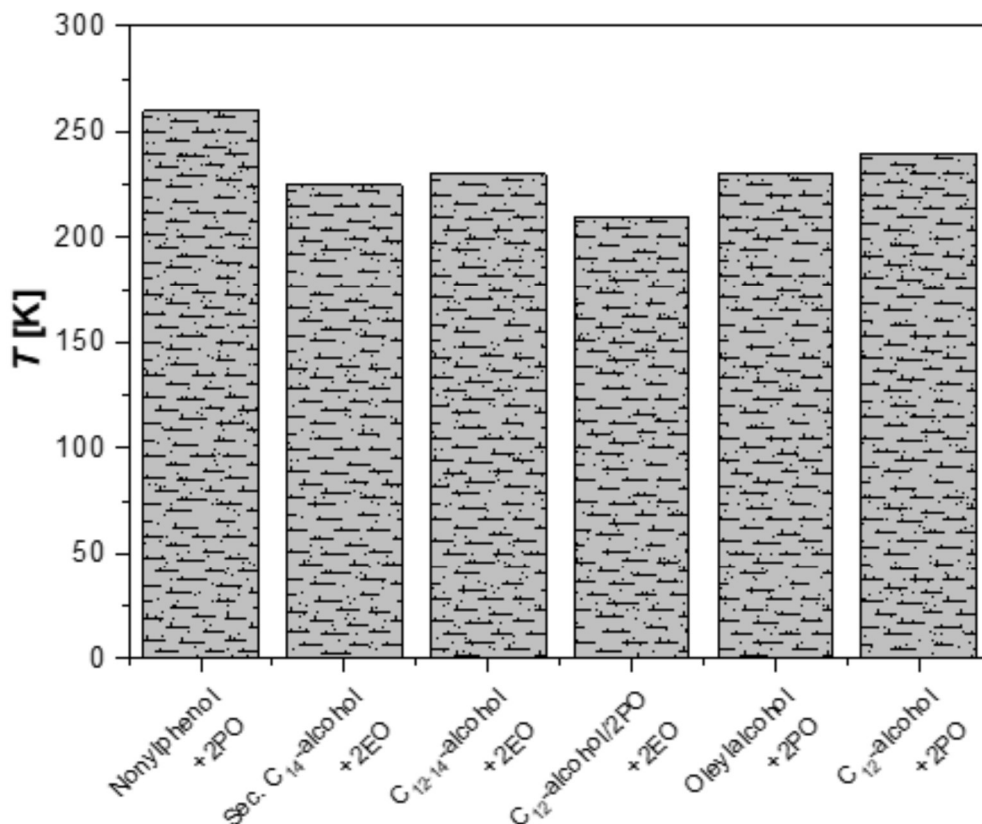
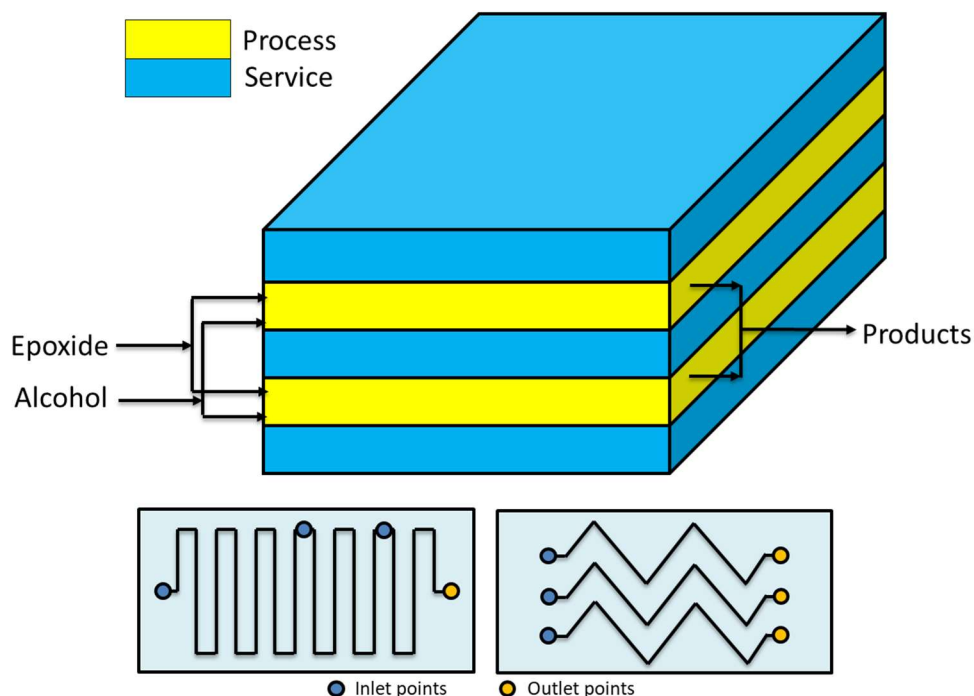


Fig. 6.1-1 – Temperature peaks for the ethoxylation of fatty alcohols, (Umbach & Stein, 1971a).

The same concept has been developed for sucrose-based polyether production, in the patent by Hinz et al. (Hinz & Dexeimer, 2002). These authors used concentrated aqueous solution of sucrose (60% by weight) as substrate to be epoxidized and various mixture of EO and PO as epoxides mixture. The employed catalyst was KOH at 0.4 wt%. For example, by using two reactor modules connected in series, with a thermostating fluid respectively at 140 and 180°C and with a feed ratio of sucrose solution and epoxides equal to 11.4:5.8 they obtain an average ration of (EO, PO)/sucrose of around 5.2 mol/mol. The adopted reaction pressure was 36.5 bar.

The concept of using a reactor of high  $L/D$  ratio, for maximizing the heat removal efficiency, can be further stressed by passing to microreactors. Hubel et al. patented in 2010 used different microchannel devices to perform the alkoxylation of alcohols (Hubel et al., 2005). The authors stated that microdevices are characterized by a very high efficiency in both mass and heat transfer. In this way, it is possible to run the reaction in safe conditions by using microplates, whose microchannels (capillaries of a 600  $\mu\text{m}$  hydraulic diameter) are optionally coated with catalysts, where alcohol and

epoxide are mixed directly at the entrance of the plate (see Figure 6.1-2). In this way, the two solutions get totally mixed and temperature peaks are avoided. The described setups allow working in different configurations, characterized by the presence of heating/cooling plates that are alternated to plates where catalyst is present. The configurations differ in how the epoxide is fed to the reactor. In fact, it is possible to either feed the entire stream to the first plate or feed the mentioned stream in different point of the microreactor, keeping its concentration almost constant along the axial coordinate. The authors claim that a system like that can work at a temperature up to 400°C and at a pressure up to 800 bar, to keep the reaction media in liquid phase. From the different examples that the author reported, it is interesting to observe that by working with a residence time of 200 s at 190 °C and 120 bar it is possible to achieve 99.6 % conversion. Different EO/butanol molar ratios were used between 9 and 65. The microreactors showed in Figure 6.1-2 have two possible channels structures for the reaction side, that differ in the geometry (one is zig-zagged, the other step-wised) and the possibility to feed fresh reactants also along different positions of the channel itself.



**Fig. 6.1-2.** Microreactor designed by Hubel et al. 2010. Maximum working pressure: 800bar; working temperature: -10 to 300°C; channels diameter: 600µm. Inspired by Hubel et al. 2010 (Tesser et al., 2020).

Moreover, the authors claim that a relatively high ethoxylation degree can be achieved in the micro structured device described above. A molar ratio EO/alcohol of 35 with a polydispersity index of 1.06 were achieved by using the conditions reported in Table 1 and potassium methoxide (3% mol) as catalyst. In this way a very low concentration of unreacted EO (<10 ppm) was found in the reactor outlet stream.

Rupp et al. (Rupp et al., 2013b) studied octanol ethoxylation by using a single microchannel reactor immersed in a thermostatic bath. These authors performed an extensive experimental and modeling investigation on the possibility to continuously produce ethoxylated octanol, to a various degree, in a short residence time with interesting productivity results. The reactors used in this study are characterized by  $L/D$  ratio in the range 2000-4600 and are constituted by microchannels with diameters of respectively 250 and 876  $\mu\text{m}$ . The feed to the reactor consists in two separate streams: one contains octanol and dissolved catalysts (potassium octanoate) and the other is ethylene oxide in the desired ratio. Just before the reactor a micromixer (SIMM V2 by IMM, Mainz) is installed to ensure a complete mixing and homogenization of the reactants. As before, the pressure was kept in the range 90-100 bar by means of a back-pressure regulator for ensure a liquid-phase reaction and the kinetic investigation of these authors covered the temperature range 130-240°C. In these operative conditions, a residence time of 50 seconds resulted enough to reach a complete conversion of ethylene oxide and to obtain an ethoxylation degree on octanol in the range 3-9. In this specific experimental device, the maximum throughput was 0.5  $\text{cm}^3/\text{min}$  that is very low, however the productivity, defined as the amount of product obtained per hour and per  $\text{m}^3$  of reactor, is on the contrary very high: 12600  $\text{kg}/(\text{h}\cdot\text{m}^3)$ .

The problem of the low productivity of microreactors in the alkoxylation reaction has been recently faced and solved by the Microinova Engineering GmbH, using a micro structured chemical reactor developed by the Institut für Mikrotechnik Mainz (IMM) GmbH with innovative fabrication techniques reported in (Kralisch et al., 2012). The reactor is built with the concept of modularity which allows the manufacture of different reactors according to the requirements of the process (see sketch in Figure 6.1-3). Microinova has designed and built an alkoxylation plant with a productivity of 20  $\text{Kg}/\text{hr}$ . This plant is now on stream and a new plant with a productivity of 200  $\text{kg}/\text{h}$  is in assembling. The authors claim that working with their multiple plates microreactor, it is possible to scale down the reaction times from 12 h to 1 min, keeping the same product characteristics, with an intensification factor of about 700.

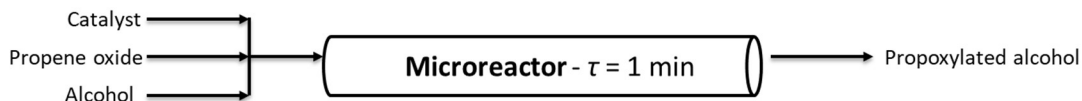


**Fig. 6.1-3.** Microinnova alkoxylation plant scheme. (Tesser et al., 2020).

Other kind of reactors are also present in the literature which structure is more traditional with respect to the already presented microchannel or microstructured reactors. For example, Yamada et al. (Yamada et al., 2006) patented a tubular reactor constituted by different plates stirred by dynamic impellers. Both the epoxide and initiator/catalyst mixture are fed from the bottom and the vessel is kept under pressure by an external vessel pressurized with nitrogen. The reactor can be operated also by feeding ethylene oxide in the different stirred sections of the reactor body (see Figure 6.1-4 A). A second configuration is also shown, where the mentioned reactor is placed in a loop (see Figure 6.1-4 B). This last setup could be particularly interesting as a heat exchanger can be installed on the circulation line improving the reaction heat removal. In the patent of Yamada et al. (Yamada et al., 2006) different examples are reported and among them is worth to note a case in which a reactor configuration like the scheme of Figure 6.1-4 A was used. The reactor (6.5 cm of internal diameter) was constituted by 10 compartments each of them of 100 cm<sup>3</sup> and operated at 120°C and 15 bar. The authors worked with the double metal cyanide catalysts (DMC), zinc hexacyanocobaltate complex, patented firstly by General Tire's in 1960s and widely used in alkoxylation reactions (McDaniel 2007). The stirring speed was 900 rpm, DMC was used as catalyst with a concentration of 0.05 wt% in the initiator. The feed was 2 g/min of polyoxypropylentriol as initiator and PO was adopted as epoxide. This last was fed at a rate of 1.68 g/min to each 1°, 3°, 5°, 7° and 9° compartments. After 30 minutes of operation the reactor reached stationary conditions with a complete conversion of PO and with a polydispersity index of 1.12 and with a productivity of 624 kg/(h m<sup>3</sup>).

The strategy to employ CSTR reactor for continuous ethoxylation, instead of tubular reactor, have been extensively studied by McDaniel and Reeser ((McDaniel, 2011; McDaniel & Reese, 2008, 2009, 2010). Two interesting examples are reported here to illustrate the approach based on CSTR reactor. In a first example, a single CSTR reactor of around 1900 cm<sup>3</sup> of volume and equipped with thermal and pressure controls, was used to conduct ad ethoxylation at 170°C at 3 bar with La(PO<sub>4</sub>) as catalyst (McDaniel, 2011) The scheme of this reactor is reported in Figure 6.1-5.



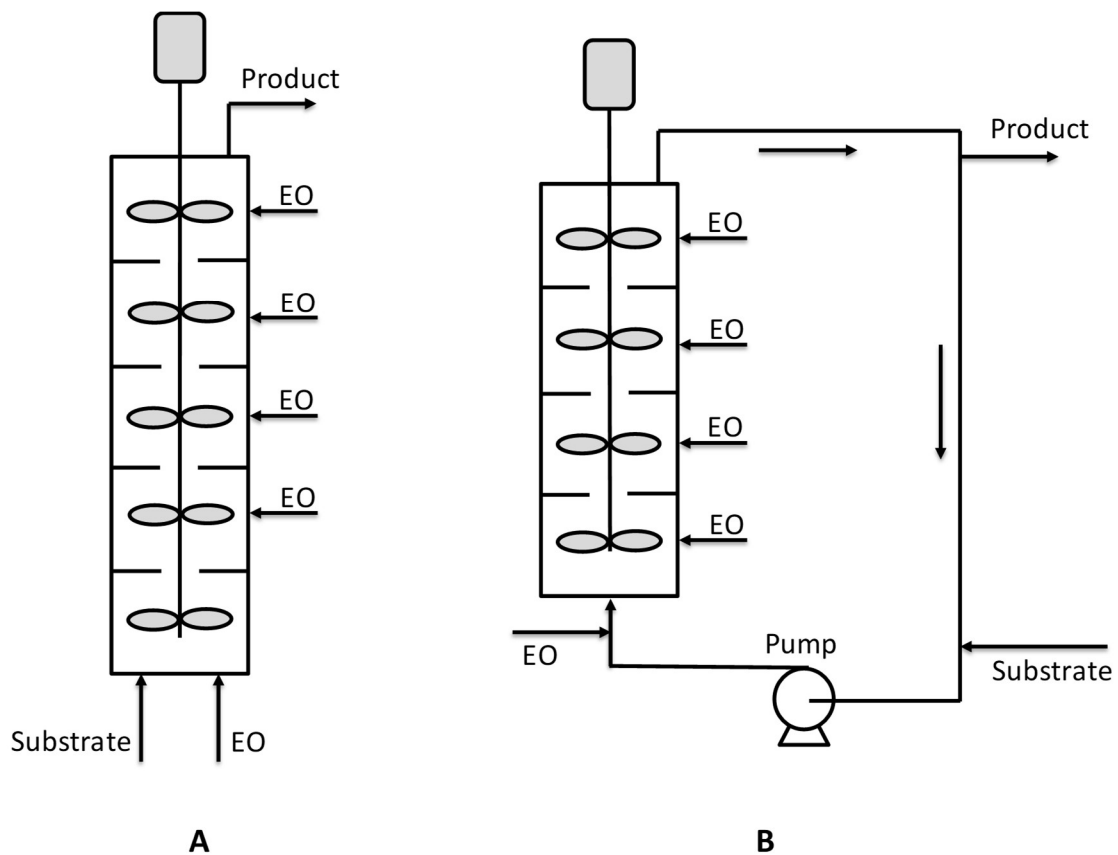


**Fig. 6.1-4.** Scheme of reactors patented by Yamada et al. 2006. A – continuous reactor with different stirred compartments; B – continuous reactor with stirred compartments operated inside a circulation loop. Inspired by Yamada et al. 2006. (Tesser et al., 2020).

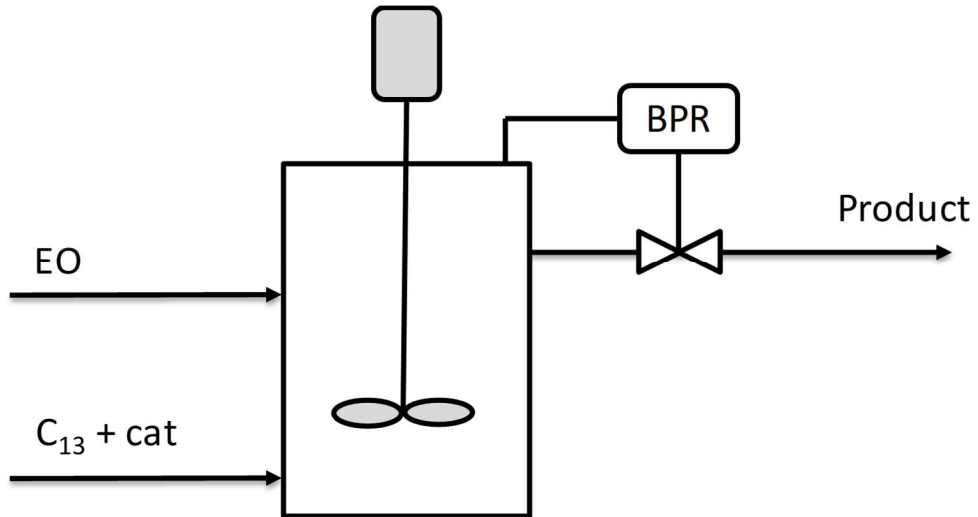


**Fig. 6.1-5.** Scheme of single CSTR reactor for ethoxylation. Inspired by (McDaniel 2011, Tesser et al., 2020).

The reactor, initially charged with an ethoxylated  $C_{13}/EO=6.5$ , was fed with 8.34 g/min. of EO and 5.83 g/min. of a mixture  $C_{13}/catalyst$ . With a residence time of 2 h a complete conversion of EO was reached and the product was characterized with a polydispersity index of 1.12. In a second example, the strategy of multiple-stage reactors in series with intermediate feed of EO was adopted (McDaniel & Reese, 2010). The scheme is illustrated in Figure 6.1-6.

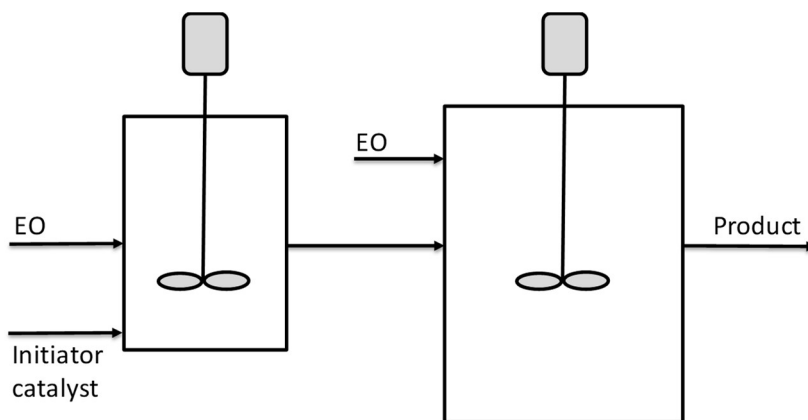


**Fig. 6.1-6.** Scheme of CSTR reactors in series for ethoxylation. Inspired by (McDaniel & Reese, 2010, Tesser et al., 2020).

The two reactors schematized in Figure 6.1-6 have a volume of, respectively, 4.5 and 9 liters. DMC was used as catalyst with a concentration of 144 ppm. The first reactor was fed with 23.95 g/min. of initiator (ethoxylate of Neodol 25) and catalyst in a first stream and with 16.7 g/min. of EO in a second stream. A further feed of 16.7 g/min. of EO was fed to the second bigger reactor. An overall molar ethoxylation degree of 6.6 was obtained with a residence time of 1.5 hours in the first reactor and 2.1 hours in the second. Finally, a polydispersity index of 1.10 was obtained for the product stream. The same apparatus described in Figure 6 was used by McDaniel (McDaniel and Reeser 2008 a, b) for the continuous ethoxylation of a different initiator, based on nonylphenol ethoxylate and with DMC catalyst. At 130°C and 3.5 bar a productivity of 195 kg/(h\*m<sup>3</sup>) was obtained.

Villa et al. (Verwijns et al., 2008; Villa et al., 2014; Weston et al., 2015) showed another interesting aspect of DMC catalyst that could favor their industrial application. These catalysts are thermally deactivated, fact that increases the safety of the process. By working with this catalyst, it is possible to reduce the maximum temperature that the system can reach. In Figure 6.1-7 (left), it is possible to observe that KOH leads to a higher temperature than DMC. Moreover, starting from different initial temperatures, it is possible to reach different maximum temperatures (Figure 6.1-7, right plot). As it is evident, a slope of temperature increase is still present but very smooth. Thus, it is possible to take all the safety procedures to stop the reaction.

These authors reported different example in their patent and, as example, a reaction in liquid phase under pressure adopting a CSTR reactor enclosed in a circulation loop and a tubular reactor used as digester of the unreacted monomer (PO). By using a glycerol alkoxylate as initiator and propylene oxide as monomer an overall productivity of 372 kg/(h\*m<sup>3</sup>) was obtained at relatively low temperature (110°C in CSTR and 125°C in PFR).

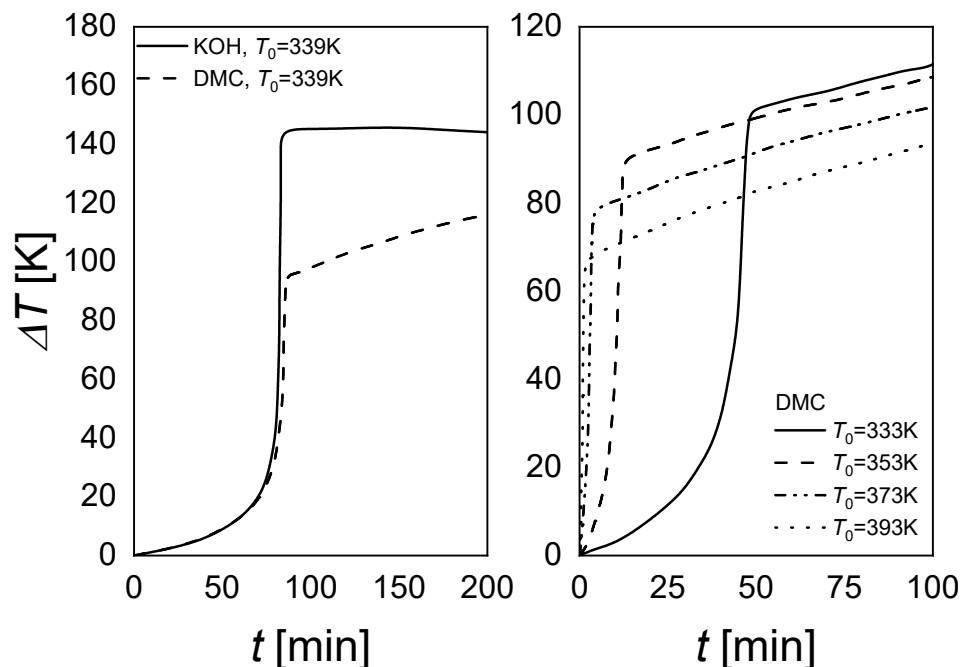


**Fig. 6.1-7.** Comparison of the maximum achievable temperature for KOH and DMC catalyst (right). DMC performances at different initial temperature values (left). (Tesser et al., 2020).

For what concerns reactor configuration, in the patent of Villa et al. (Villa et al., 2014) different loop continuous systems are proposed and, among them, particularly promising is represented schematically in Figure 6.1-8. In an example reported by these authors, two reactors (CSTR and PFR) with volume, respectively, of 28 and 25 L were used to process a diol of 400 Da and obtain a product of 4000 Da that corresponds to an EO/S molar ratio of about 80. The catalyst concentration of 25 ppm and reaction temperature of 140°C were used as other conditions. A high circulation flow rate of 7500 kg/h was adopted to minimize temperature and concentration differences ( $\max \Delta T = 1^\circ\text{C}$ ). With a residence time of 3 hours in each reactor the authors obtained a residual EO concentration in the loop of 0.3% and a product with a polydispersity index of 1.11.

In 2016, Aigner et al. filed a patent claiming a new reactor technology dedicated to the continuous alkoxylation reaction of a generic substrate with active hydrogen atoms (Aigner et al., 2016). The reactor is designed as a concentric tubular reactor in which an annular space is obtained for performing the reaction continuously (see sketch in Figure 6.1-9).

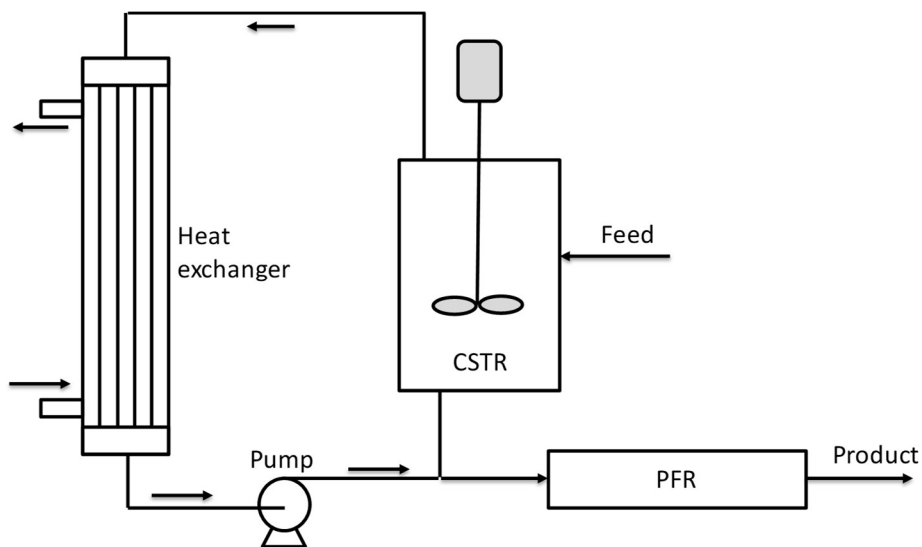
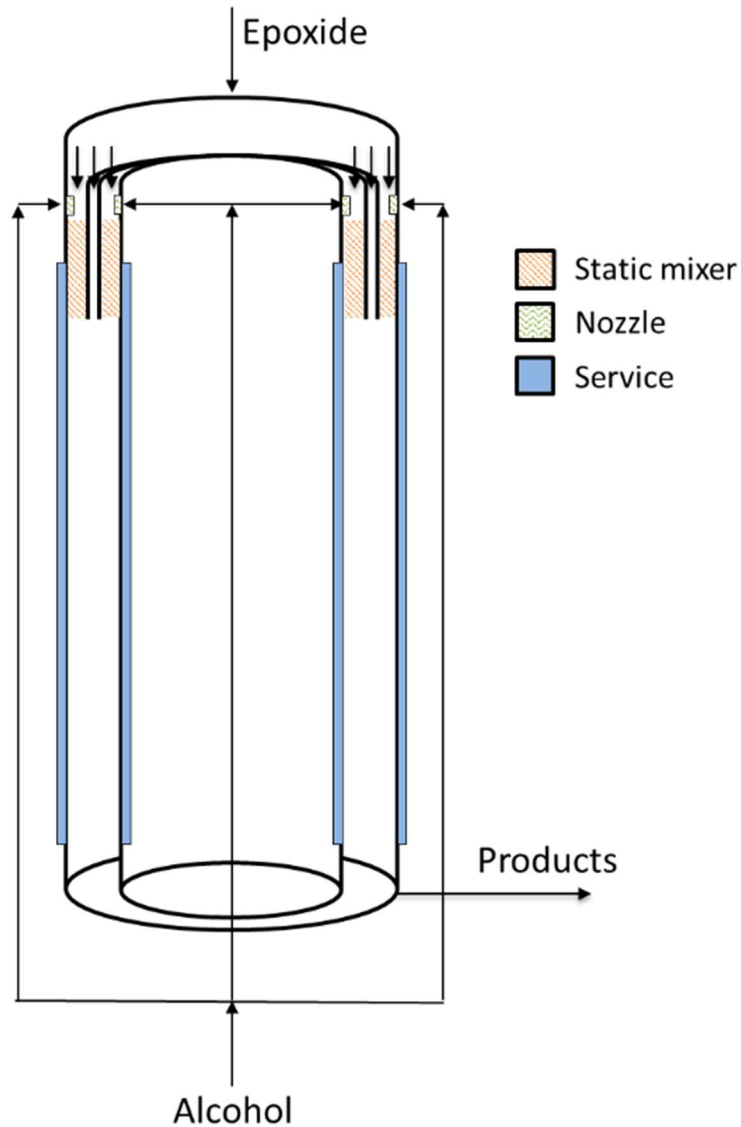


Fig. 6.1-8. Scheme of reactors combination proposed by Villa et al. 2014 (Tesser et al., 2020).

In this way the annular gap reaction volume (width 6.5 mm, diameter 5 inches, length 5 m) is very similar to a thin film with enhanced properties of thermal exchange and able to achieve safe operation. Such a reactor system is characterized by a  $L/D$  ratio of about 770 and can achieve a product throughput of 250 kg/h (7 moles of EO per mole of n-nonyl phenol) in correspondence to a residence time of roughly 160 sec and with a productivity of 22000 kg/(h\*m<sup>3</sup>). The authors claim the possibility to complete the reaction either in a separate tank or in the same reactor by introducing a higher volume at its bottom. In this way, products of different properties can be produced. Despite this reactor was built in a quite complex way, it opens the perspective of a real industrial utilization in the field of alkoxylation technology.



**Fig. 6.1-9.** Concentric tubular reactor with annular space. Inspired by Aigner et al. 2016 (Tesser et al., 2020).

In the patent of Lai et al. (Lai et al. 2019) two CSTR reactors connected in series, allowed to obtain a polyolether constituted by EO/PO copolymer (Hreczuch et al. 2016) using DMC as catalysts (20 ppm) at a temperature of 140 °C. Glycerol was used as starter and in the final product a weight ratio PO/EO of 12 was obtained.

Another very interesting reactor configuration was proposed by Nikbin et al. (Nikbin et al., 2018). The continuous reactor was assembled as three concentric tubes (tube-in-tube setup) schematically represented in Figure 6.1-10. In the inner, small diameter tube, alkoxide is fed and can be distributed along the reactor axis at different axial position; in the intermediate annular section, the reaction zone, the starter is fed and the reaction occurs with alkoxide coming from holes in the inner tube. Between the larger external tube and the intermediate one, the cooling fluid is fed allowing an optimal temperature control.

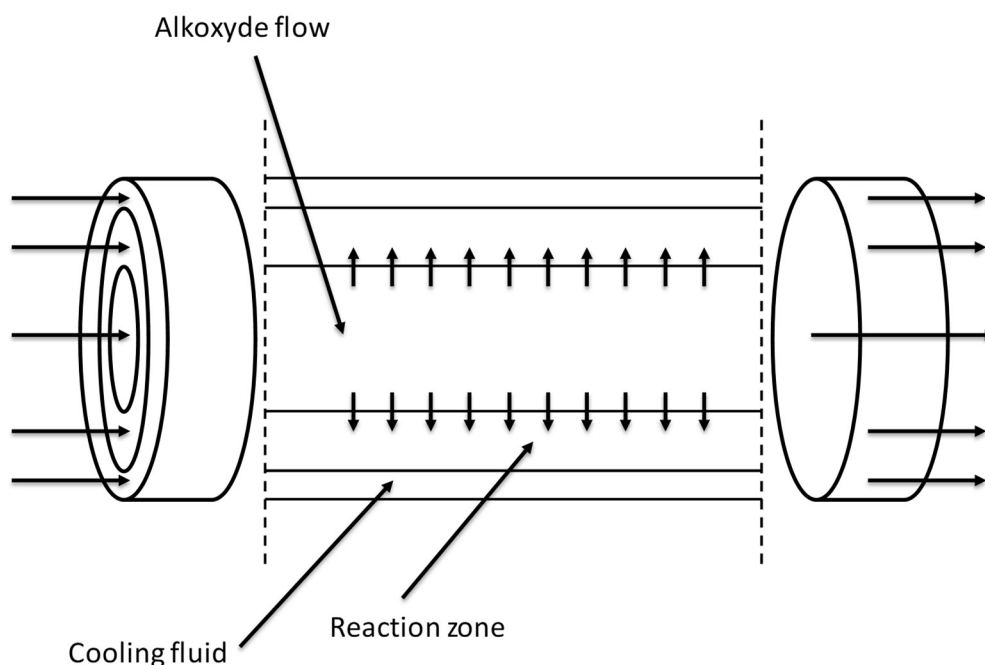


**Fig. 6.1-10.** Tubular tube-in-tube reactor proposed by Nikbin et al. 2018. Inspired by Nikbin et al. 2018 (Tesser et al., 2020).

With this configuration, the authors described the use of a very long reactor (200 m) with a volume of 50 m<sup>3</sup>. The reactor was operated in three sections to demonstrate the flexibility of the operation: in the first 50 m PO was fed through the holes of internal tube; in the next 104 m EO was added in the same way and the remaining 46 m were used as cooking section.

## 6.2 Conclusions

The chapter is devoted to continuous alkoxylation, a promising perspective nowadays available for performing alkoxylation reactions. It has been demonstrated that specifically designed continuous reactors can furnish very good performances in terms of productivity and for ensuring safe operation in the adopted conditions. The reactors are characterized by sufficient flexibility to achieve different alkoxylation degree being, in this way, suitable for different productions. The obtained productivity is sufficiently high to guarantee, also considering reactor modularity, the possibility of useful industrial applications. Employing these emerging technologies, a new era in alkoxylation technology could start in a near future. In perspective, more experimental and theoretical activities are indeed necessary to confirm the interesting data that emerged from the preliminary literature reports. This could allow to achieve the conceptualization of new open process windows for the alkoxylation reaction, realizing prototypes solving the numbering-up issues (Hessel et al., 2014).





## Chapter 7- Alkoxylation in milli and micro reactors

In the Chapter 6 the possibility to use microreactors to ensure good productivities and good control was claimed. Microreactors are particularly suitable for very exothermic reactions, i.e., alkoxylation, involving also multiphase reactions, thanks to the high heat and mass transfer exchange. Such reactors were tested in the literature, in the case of 1-octanol ethoxylation promoted by KOH as catalyst, showing good performances in terms of reaction conversion and thermal control, allowing to work at relatively high temperatures (240°C) (Rupp et al., 2013a, 2013c). Rupp et al. published a paper using an experimental setup allowing to work under pressure (90-100 bar), thus with a single liquid phase. A microdevice characterized by an inner diameter of 250  $\mu\text{m}$  was used, adjusting the length of the device to ensure the desired residence time. For further details, please check the literature (Rupp et al., 2013c). Even though in the adopted experimental conditions it was demonstrated that the flow-pattern is laminar (Hermann et al., 2016), the collected data were simulated first with a simple plug-flow model approach (Rupp et al., 2013c) and successively with a complex model based of CFD calculation. The approximation to plug-flow certainly leads to a non-rigorous determination of the parameters related to the intrinsic kinetics of the reaction, on the other hand the use of a complex CFD model gives some problem in the use it for design purpose or to fit experimental data. To solve these aspects, in the present thesis chapter a laminar-flow model was applied to the description of the experimental data collected by Rupp et al. and compared with the results obtained with a plug-flow model. In the Rupp et al. runs an isothermal condition was hypothesized and proven with dimensionless analysis.

In this chapter, the isothermicity of the runs is proven by also introducing an energy balance into the model. The results obtained using a plug-flow model reactor and a laminar-flow model in the simulation of Rupp et al. runs have been reported in the chapter (Russo et al., 2023). Moreover, the model has been used to design a flow ethoxylation reactor with a productivity interesting for industrial applications (Russo et al., 2023).

## 7.1 Laminar flow model for micro and milli reactors

The experimental apparatus used in Rupp et al. paper (Rupp et al., 2013c) consists in a microreactor working under pressure, to warrant the existence of a unique liquid phase, characterized by a laminar flow regime. The authors conducted 1-octanol ethoxylation in the presence of KOH as homogeneous catalyst.

The development of the design equation of the laminar flow reactor model (LFR) implies the definition and solution of material balance on the microstructured reactor, comprising the following terms:

- Flow term: related to the convection of reactants/products by laminar flow profile.
- Diffusive term: representative of the transport of matter by the concentration gradient along the radial coordinate.
- Kinetic term: represented by the reaction rate, indicating the generation/consumption term.

Therefore, the equation takes the form reported in Eq. 7.1-1.

$$u(y) \frac{\partial c_i(z, y)}{\partial z} = D_i \left( \frac{\partial^2 c_i(z, y)}{\partial y^2} + \frac{1}{y} \frac{\partial c_i(z, y)}{\partial y} \right) + v_i r(z, y) \quad (7.1-1)$$

With,  $u(y)$  fluid velocity [m/s],  $c_i$  concentration of specie  $i$  [mol/m<sup>3</sup>],  $z$  axial coordinate [m],  $D_i$  molecular diffusivity of component  $i$  [m<sup>2</sup>/s],  $y$  radial coordinate [m],  $v_i$  stoichiometric coefficient of component  $i$  and  $r$  reaction rate [mol/(m<sup>3</sup>\*s)].

Being the flow laminar, the velocity profile assumes a parabolic trend with the radial coordinate,  $y$ , that can be described by Eq. 7.1-2.

$$u(y) = u_{\max} \left[ 1 - \left( \frac{y}{R} \right)^2 \right] = 2\bar{u} \left[ 1 - \left( \frac{y}{R} \right)^2 \right] \quad (7.1-2)$$

The mass balance reported in Eq. 1 can be written in a more compact and practical form adopting mathematical rearrangements.

For instance, axial coordinate  $z$  can be converted to residence time  $\tau$ :

$$\tau = \frac{V}{\dot{V}} = \frac{LA}{\dot{V}} = \frac{L}{u} \quad (7.1-3)$$

with  $A$  the cross-sectional area [ $\text{m}^2$ ],  $L$  the reactor length [ $\text{m}$ ],  $V$  the reactor volume [ $\text{m}^3$ ],  $V'$  the volumetric flowrate [ $\text{m}^3/\text{s}$ ] and  $\bar{u}$  the average flow velocity [ $\text{m}/\text{s}$ ]. Thus,

$$\tau = \frac{z}{\bar{u}} \quad (7.1-4)$$

Deriving Eq. 6.1-4, it is possible to obtain:

$$\partial z = \bar{u} \partial \tau \quad (7.1-5)$$

Concentration can be expressed in terms of reactant conversion starting from its definition:

$$c_i = c_{i,0}(1 - x_i) \quad (7.1-6)$$

with,  $c_{i,0}$  the feed concentration of component  $i$ .

Deriving Eq. 7.1-6, it is possible to obtain:

$$\partial c_i = \partial (c_{i,0}(1 - x_i)) = c_{i,0} \partial (1 - x_i) = -c_{i,0} \partial x_i \quad (7.1-7)$$

Finally, it can be possible to introduce a dimensionless reactor radius coordinate,  $\lambda$ :

$$\lambda = \frac{y}{R} \quad (7.1-8)$$

Deriving Eq. 7.1-8 it is possible to obtain:

$$\partial y = R \partial \lambda \quad (7.1-9)$$

Thus, the velocity profile becomes:

$$u(y) = 2\bar{u} [1 - \lambda^2] \quad (7.1-10)$$

Inserting Eqs. 7.1-5, 7.1-7, 7.1-9 and 7.1-10 in Eq. 7.1-1, it is possible to obtain the following mass balance equation:

$$-2\bar{u}(1 - \lambda^2) \frac{c_{i,0}}{\bar{u}} \frac{\partial x_i}{\partial \tau} = -D_i \left( \frac{c_{i,0}}{R^2} \frac{\partial^2 x_i}{\partial \lambda^2} + \frac{c_{i,0}}{R^2} \frac{1}{\lambda} \frac{\partial x_i}{\partial \lambda} \right) + v_i r \quad (7.1-11)$$

Rearranging, the following form can be derived:

$$2(1 - \lambda^2) \frac{\partial x_i}{\partial \tau} = \frac{D_i}{R^2} \left( \frac{\partial^2 x_i}{\partial \lambda^2} + \frac{1}{\lambda} \frac{\partial x_i}{\partial \lambda} \right) - v_i \frac{r}{c_{i,0}} \quad (7.1-12)$$

The reactant conversion, more specifically  $x_{EO}$ , shows a parabolic trend with the reactor radius coordinate. For instance, depending on the radial position, different flow velocities are expected due to Eq. 7.1-2: at the reactor center, the liquid flow shows the highest velocity, thus a low conversion, while at the pipe radius the fluid velocity approaches zero, leading to a higher conversion.

The following boundary and initial conditions were imposed to solve the partial differential equation system.

$$x_{i,0}(\forall \lambda) = 0 \quad (7.1-13)$$

$$\left. \frac{\partial x_i}{\partial \lambda} \right|_{\lambda=0} = 0 \quad (7.1-14)$$

$$\left. \frac{\partial x_i}{\partial \lambda} \right|_{\lambda=1} = 0 \quad (7.1-15)$$

For instance, at  $\tau=0$ , the ethylene oxide conversion was assumed zero. Both at the reactor center and walls, the first derivative of conversion along the dimensionless radius coordinate was considered zero, for symmetry reasons.

As the experimental data collected at the pipe outlet represent an average of the ethylene oxide conversion profile along the radius, an average conversion must be defined, using the integral average approach:

$$\overline{x_{EO}} = \frac{\int_0^1 x_{EO}(\lambda) u(\lambda) 2\pi\lambda d\lambda}{\int_0^1 u(\lambda) 2\pi\lambda d\lambda} \quad (7.1-16)$$

By introducing Eq. 7.1-2 in Eq. 7.1-16, the following expression can be obtained:

$$\overline{x_{EO}} = \frac{\int_0^1 x_{EO}(\lambda) 2(1-\lambda^2) 2\pi\lambda d\lambda}{\int_0^1 2(1-\lambda^2) 2\pi\lambda d\lambda} \quad (7.1-17)$$

As revealed, the average ethylene oxide conversion is independent on the average fluid velocity.

Reaction rate was fixed as a first order equation with respect to both ethylene oxide and catalyst concentration, as reported in the literature (Rupp et al., 2013c):

$$r = k C_{EO} C_{cat} \quad (7.1-18)$$

Where, the catalyst and the feed ethylene oxide concentrations were calculated starting from the definition of  $\varepsilon_0$  and  $K$ , representing respectively the feed ethylene oxide/octanol molar ratio and the catalyst/octanol molar ratio.

$$C_{EO,0} = \frac{1}{M_{EO} + M_O / \varepsilon_0} \rho_{mix,0} \quad (7.1-19)$$

$$C_{cat} = \frac{K / \varepsilon_0}{M_{EO} + M_O / \varepsilon_0} \rho_{mix,0} \quad (7.1-20)$$

The kinetic constant dependence with temperature was taken into consideration by imposing the modified Arrhenius equation, Eq. 7.1-21.

$$k = k_{ref} \exp \left( -\frac{E_a}{R_g} \left( \frac{1}{T} - \frac{1}{T_{ref}} \right) \right) \quad (7.1-21)$$

Where,  $T_{ref}=473K$ .

Temperature variation was included by solving simultaneously the dimensionless energy balance equation reported in Eq. 7.1-22. The mathematical derivation is totally symmetrical compared to the mass balance, thus not reported here.

$$2(1 - \lambda^2) \frac{\partial T}{\partial \tau} = \frac{\lambda_{mix}}{R^2} \left( \frac{\partial^2 T}{\partial \lambda^2} + \frac{1}{\lambda} \frac{\partial T}{\partial \lambda} \right) - \frac{\Delta_r H \cdot r}{c_{p,mix} \rho_{mix}} \quad (7.1-22)$$

Where the reaction enthalpy value was equal to  $\Delta_r H = -92000$  J/mol (Di Serio et al., 2021).

The initial and boundary conditions needed to solve Eq. 7.1-22 are reported in Eqs. 7.1-23-7.1-25.

$$T_0(\forall \lambda) = T_{fed} \quad (7.1-23)$$

$$\left. \frac{\partial T}{\partial \lambda} \right|_{\lambda=0} = 0 \quad (7.1-24)$$

$$T|_{\lambda=1} = T_w \quad (7.1-25)$$

For instance, at  $\tau=0$ , the temperature was assumed to be constant at a set value. At the reactor center, the first derivative of temperature along the dimensionless radius coordinate was considered zero, for symmetry reasons, while temperature at the reactor walls was considered constant at a fixed value, as milli/micro reactors are characterized by high heat transfer efficiency.

The partial differential equation (PDE) system describing the single liquid phase reactor was solved adopting the *pdepe* function implemented in Matlab R2020a. Parameter estimations were conducted using *particleswarm* algorithm provided in Matlab, imposing the objective function calculation as it follows.

$$F_{obj} = \frac{1}{N_{data}} \sqrt{\sum_{i=1}^{N_{data}} \left( \frac{x_{EO,EXP} - \bar{x}_{EO,CALC}}{x_{EO,EXP}} \right)^2} \quad (6.1-26)$$

## 7.2 Physicochemical properties

Several physicochemical properties are needed to be implemented within the model, in particular liquid density and viscosity.

Liquid density dependency with temperature ( $T$ ), the initial ethylene oxide/substrate ratio ( $\varepsilon_0$ ) and ethylene oxide conversion ( $x_{EO}$ ) was taken from the literature (Rupp et al., 2013c). Rupp et al. precisely determined the mentioned functionalities, by collecting experimental data and proposing semi-empirical equations, listed below as used in the model, Eqs. 7.2-1, 7.2-2.

$$\rho_{prod} = 1062 - 231.2(0.82^{x_{EO} \cdot \varepsilon_0}) \quad (7.2-1)$$

$$\rho_{mix} = \rho_{prod} + 8.69(1 - x_{EO})\varepsilon_0 - 0.36(1 - x_{EO})\varepsilon_0^2 + \\ - 0.10(T - 273) - 0.0021(T - 273)^2 - 0.101(T - 273)(1 - x_{EO})\varepsilon_0 \quad (7.2-2)$$

Ethylene oxide and 1-octanol viscosities were determined using ChemCAD database (Chemstations, n.d.), adopting the following expression.

$$\ln(\eta_i) = (A_i + B_i / T + C_i \ln(T)) \quad (7.2-3)$$

The coefficients for ethylene oxide and 1-octanol are listed in Table 7.2-1.

**Table 7.2-1** – Viscosity coefficients of ethylene oxide and 1-octanol.

Component	$A_i$	$B_i$	$C_i$
Ethylene oxide	-8.521	634.2	-0.3314
1-octanol	-50.674	4725.1	5.2499

Both specific heat and heat conductivities of the mixtures were calculated starting from the related values of pure ethylene oxide and alcohol. Both were taken as a function of the temperature from ChemCAD database (Chemstations, n.d.), Eqs. 7.2-4 – 7.2-7.

$$c_{p,EO} = 1.45 \cdot 10^5 - 758.87 \cdot T + 2.8261 \cdot T^2 - 0.00306 \cdot T^3 \quad (7.2-4)$$

$$c_{p,O} = 5.14 \cdot 10^6 - 54970 \cdot T + 228.72 \cdot T^2 - 0.40331 \cdot T^3 + 0.00025844 \cdot T^4 \quad (7.2-5)$$

$$\lambda_{EO} = 0.26957 - 0.0003984 \cdot T \quad (7.2-6)$$

$$\lambda_O = 0.220444 - 0.00018378 \cdot T \quad (7.2-7)$$

Both the specific heat and heat conductivity of the mixture were calculated as weighted average of the pure components.

$$c_{p,mix} = c_{p,EO} \frac{c_{EO,0}}{c_{EO,0} + c_{O,0}} \frac{1000}{M_{EO}} + c_{p,O} \frac{c_{O,0}}{c_{EO,0} + c_{O,0}} \frac{1000}{M_O} \quad (7.2-8)$$

$$\lambda_{mix} = \lambda_{EO} \frac{c_{EO,0}}{c_{EO,0} + c_{O,0}} + \lambda_O \frac{c_{O,0}}{c_{EO,0} + c_{O,0}} \quad (7.2-9)$$

To use the previous described model, molecular diffusivity must be estimated as one of the key parameters in correctly predicting the concentration gradients along the pipe radius.

At this purpose, ethylene oxide diffusivity was determined using the Scheibel correlation (Poling et al., 2001), Eq. 7.2-10.

$$D_{EO} = \frac{\alpha_{EO} T}{\eta_{mix} V_{mix}^{1/3}} \quad (7.2-10)$$

where,  $\alpha_{EO} = 1.751 \cdot 10^{-16}$ .



The Scheibel correlation shows the dependence of the diffusion coefficient with the absolute temperature. Therefore, both the viscosity and the molar volume of the liquid mixture must be known. During the ethoxylation reaction, ethylene oxide is consumed, and oligomers are formed, consisting in chains of ethylene oxide added to one alcoholic molecule (i.e., 1-octanol). Thus, both the viscosity and the molar volumes of the liquid mixture are a natural function of the conversion degree.

Moreover, depending on the feed ethylene oxide/substrate molar ratio, different oligomers distribution can be obtained.

The molar volume can be easily calculated from the density liquid mixture, that was experimentally measured by Rupp et al. (Rupp et al., 2013c), obtaining a function of both  $x_{EO}$ ,  $T$  and  $\varepsilon_0$ , using Eq. 7.2-11.

$$V_{mix} = \frac{M_{mix}}{\rho_{mix}} \quad (7.2-11)$$

With, the molecular weight of the mixture is defined as a function of the ethylene oxide conversion degree and the feed ethylene oxide/1-octanol molar ratio, as in Eq. 7.2-12.

$$M_{mix} = M_O + \varepsilon_0 x_{EO} M_{EO} \quad (7.2-12)$$

The liquid mixture viscosity was calculated weighting the ethylene oxide and the oligomer viscosity, by respectively the ethylene oxide conversion and the related complementary to one.

$$\ln(\eta_{mix}) = \ln(\eta_{EO})x_{EO} + \ln(\eta_{oligomer})(1 - x_{EO}) \quad (7.2-13)$$

The oligomers viscosity was calculated using the Orrick and Erbar method (Poling et al., 2001), using the mixture density and molecular weight above mentioned, Eq. 7.2-12.

$$\ln(\eta_{oligomer}) = (A_{oligomer} + B_{oligomer} / T) + \ln(\rho_{mix} M_{mix}) \quad (7.2-14)$$

The correlation was tested for 1-octanol, obtaining less than 1% deviation with the data retrieved from ChemCAD database.

To simplify the mathematical treatment, data were simulated varying both  $T$  and  $\varepsilon_0$ , first at zero conversion, then varying the ethylene oxide conversion. The results are reported in Figure 7.2-1, revealing a strong dependency of the diffusion coefficient with the conversion degree, as the viscosity of the product increases with conversion.

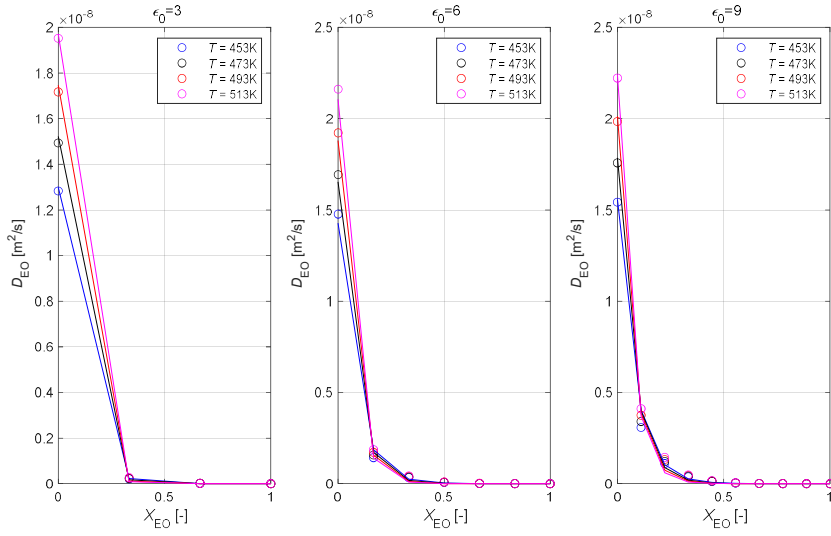


**Fig. 7.2-1.** Evolution of ethylene oxide molecular diffusivity as a function of temperature, ethylene oxide conversion and initial ethylene oxide/1-octanol molar ratio. Symbols represent the calculated values with Eq. 6.4-7, lines the fitted values (V. Russo et al. 2023).

The simulated data were fitted to introduce in the model a simple equation, obtaining the fits reported in Figure 6.2-1 and the coefficients reported in Eqs. 7.2-15 and 7.2-16.

$$D_{EO,0} = (-8.32 \cdot 10^{-9} + 377 \cdot 10^{-12} \varepsilon_0) + (111 \cdot 10^{-12} + 307 \cdot 10^{-15} \varepsilon_0) T \quad (7.2-15)$$

$$D_{EO} = D_{EO,0} \exp(-67.75 \cdot 10^{-3} T x_{EO}) \quad (7.2-16)$$

As revealed, a good fit was obtained in every case.

## 7.3 Simulation and parameter estimation activities in laminar regimes

### 7.3.1 Application of the model to experimental ethoxylation data

The developed laminar flow mode was applied to describe the kinetic data collected by Rupp et al. (Rupp et al., 2013c). The fit obtained is reported in Figures 7.3-1 and 7.3-2.

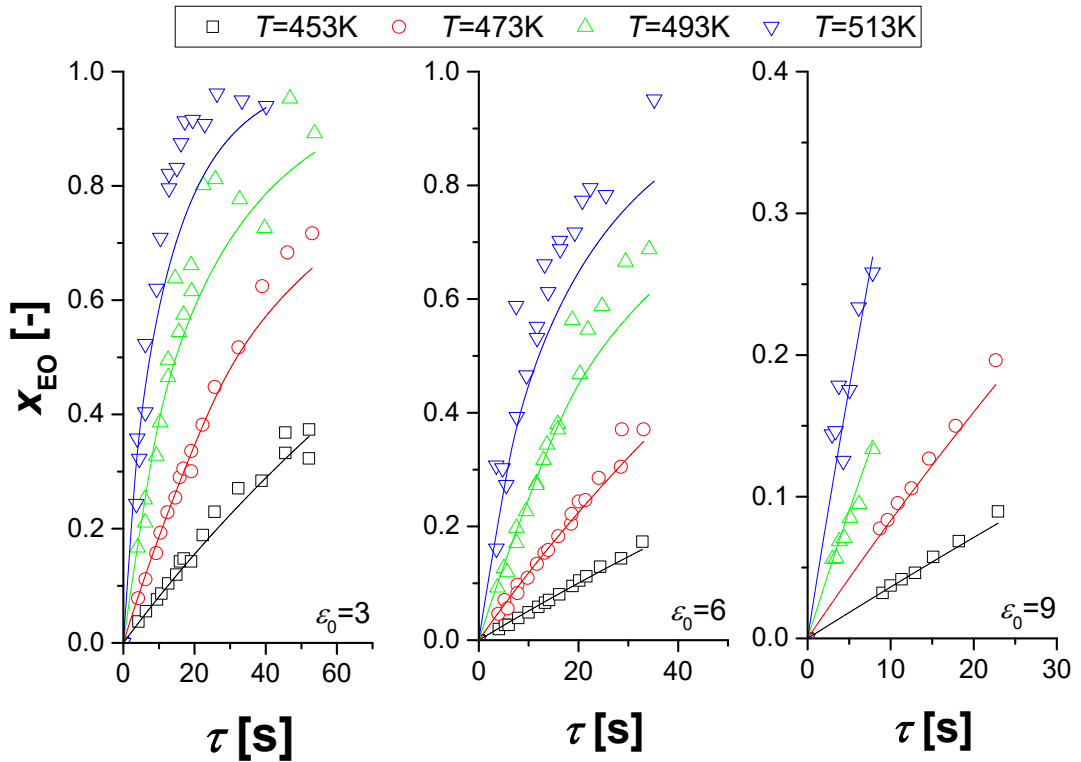


**Fig. 7.3-1.** Data fitted to experiments in which both residence time and initial ethylene oxide/1-octanol molar ratio were varied as a function of temperature, ranging from 453-513K. Symbols represent the experimental data, lines the calculated values (V. Russo et al. 2023).

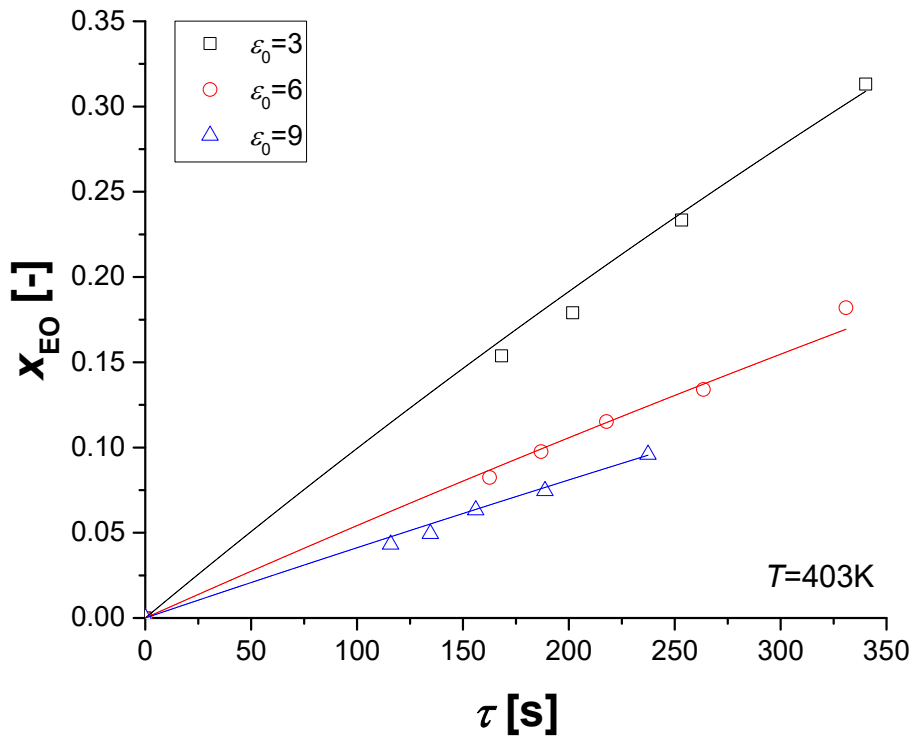


**Fig. 7.3-2.** Data fit for experiments where both residence time and initial ethylene oxide/1-octanol molar ratio are varied at 403K. Symbols represent the experimental data, lines the calculated values (V. Russo et al. 2023).

The model describes adequately the experimental data in every case, varying both temperature and the feed composition, showing high flexibility of the model.

Temperature profiles were monitored in every case, verifying that working at constant wall temperature, negligible temperature gradients are calculated expected, both at  $T=453$  and  $513$ K (Figures 7.3-3 and 7.3-4), while wide conversion gradients are expected at high residence times at both temperatures.

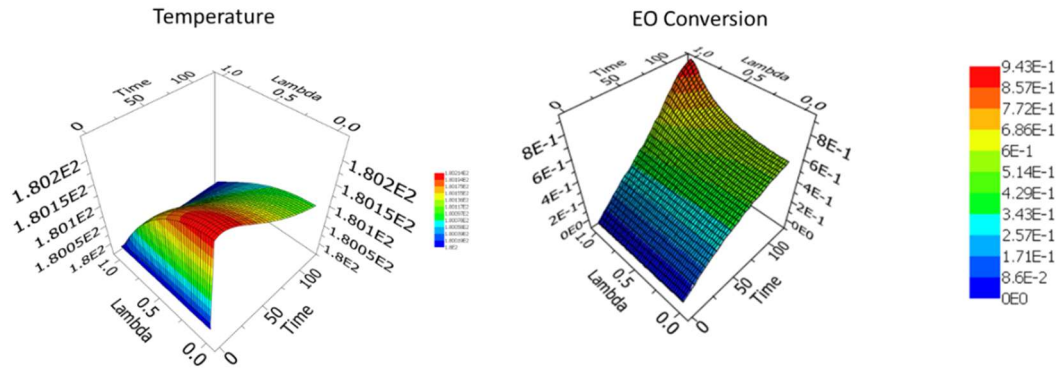


**Fig. 7.3-3.** Temperature and EO conversion trends along the residence time and the dimensionless radial coordinate, fixing  $\epsilon_0=3$ ,  $\text{cat}=0.66\% \text{ mol/mol}$ ,  $T_{\text{feed}}=453\text{K}$  (V. Russo et al. 2023).

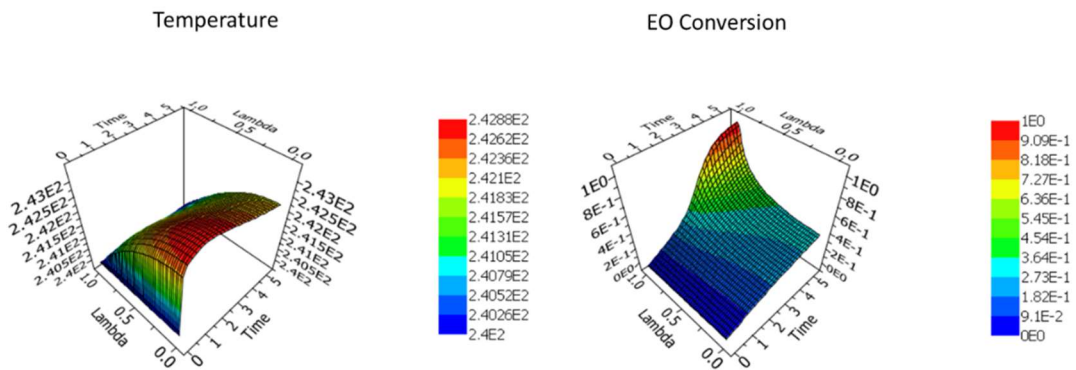


**Fig. 7.3-4.** Temperature and EO conversion trends along the residence time and the dimensionless radial coordinate, fixing  $\epsilon_0=3$ ,  $\text{cat}=0.66\% \text{ mol/mol}$ ,  $T_{\text{feed}}=513\text{K}$  (V. Russo et al. 2023).

The estimated activation energy value and the reference kinetic constant are reported in Table 7.3.1.

**Table 6.3-1** Results of the parameter estimation activity.

	Value	Units
$E_a$	$(81.1 \pm 0.8) \cdot 10^3$	J/mol
$k_{\text{ref}}(T_{\text{ref}}=473\text{K})$	$(1.2 \pm 0.1) \cdot 10^{-3}$	$\text{m}^3/(\text{mol s})$

As revealed, the confidence interval associated with each parameter is reasonable showing high statistical significance of the obtained parameters.

The obtained parameters were compared with those reported in the literature (Figure 7.3-5, showing that the highest deviation with the ones reported by Rupp et al. can be observed at high temperatures, i.e., at  $T=513$  K a 47% of difference can be calculated.

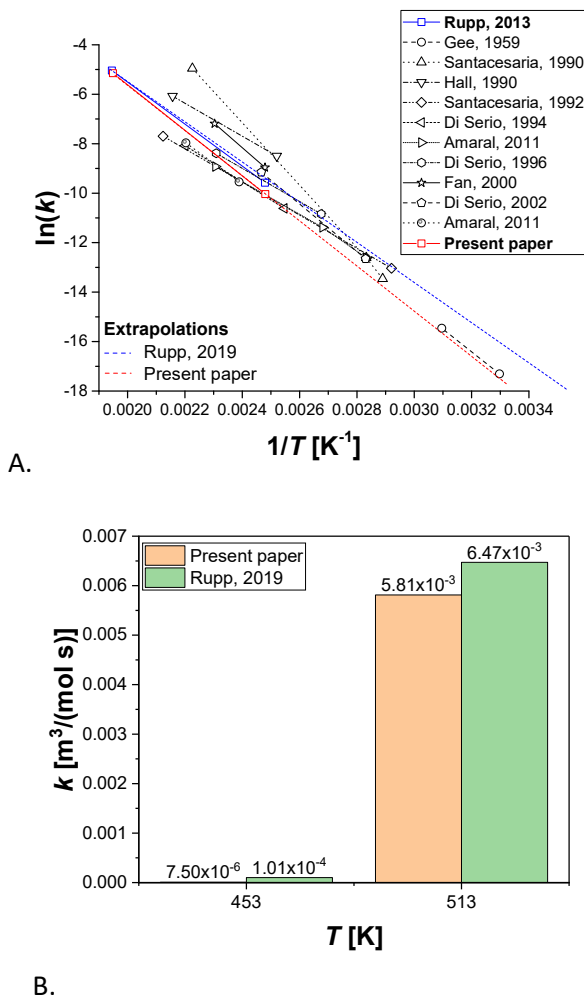


**Fig. 7.3-5.** A. Comparison between the Arrhenius plot of different papers. B. Comparison between the kinetic constants obtained in the present paper and by Rupp et al. 2013 (V. Russo et al. 2023).

Finally, the performance of the laminar flow model was compared with a classical plug-flow fluid-dynamics. As revealed in Figure 7.3-6, at  $T=493$  K, the laminar flow reactor predicts strong conversion gradients, reaching ethylene oxide full conversion at the reactor's wall. The highest difference with the plug-flow model is expected at higher residence times.

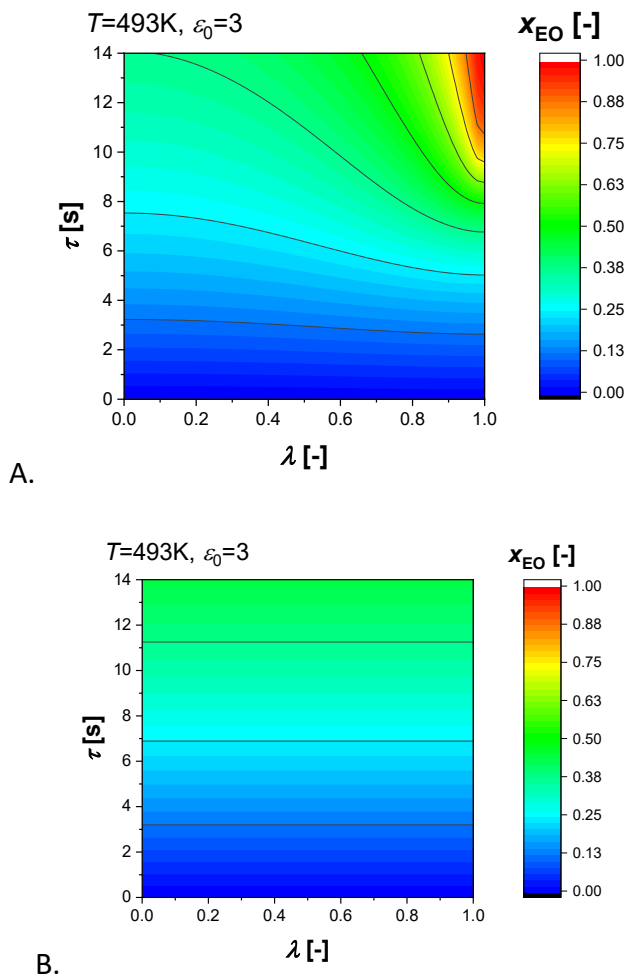


**Fig. 7.3-6** – Comparison between laminar flow model (A) and plug flow model (B) simulations, imposing  $T_{\text{feed}}=493\text{K}$ ,  $\varepsilon_0=3$ ,  $\text{cat}=0.66\%$  mol/mol (V. Russo et al. 2023).

### 7.3.2 Simulation of larger reactors

Rupp et al. showed that the use of microreactors assure the control of the temperature inside the reactor and they have also a great productivity (500-fold increase compared to the stirred tank reactor). However, the numbering up does not seem to be an industrial solution (45000 tube of 0.5 mm x 10 m are necessary).

The increase of tube diameter could improve the productivity, but it could lead to hot spot for the lowering of heat transfer efficiency. Thus, simulations were conducted using larger reactors, characterized by an internal diameter of 9 mm (Figure 7.3-7), imposing  $T_{\text{feed}}=453$  K,  $\varepsilon_0=3$ ,  $\text{cat}=0.1\%$  mol/mol,  $L=50$  m. Several simulations were conducted lowering the catalyst load, but the system was always characterized by a runaway behavior.

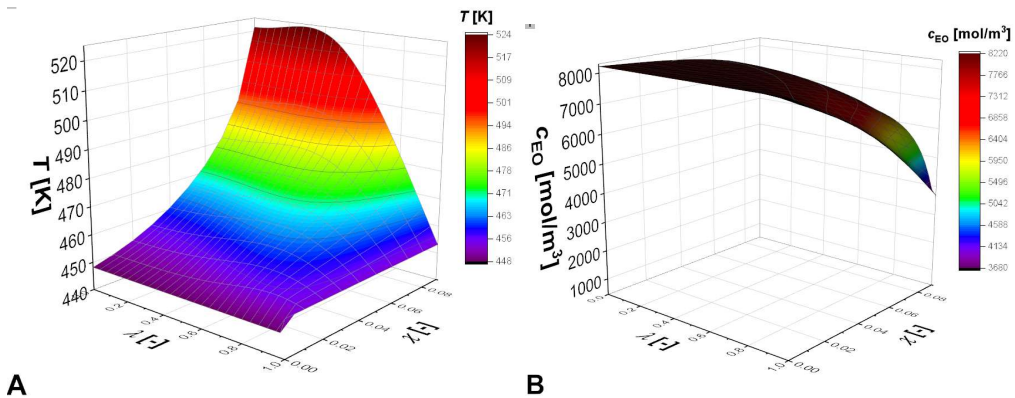


**Fig. 7.3-7.** Temperature and ethylene oxide concentration trends along the dimensionless axial coordinate and the dimensionless radial coordinate for a reactor characterized by 9 mm inner diameter, imposing  $T_{\text{feed}}=453$ K,  $\varepsilon_0=3$ ,  $\text{cat}=0.1\%$  mol/mol (V. Russo et al. 2023).

As revealed, high temperature gradients are expected to occur when the diffusion path increases, leading to possible runaway risks.

Finally, an additional simulation was conducted simulating the performance of the system obtainable adopting always an inner diameter of 9 mm, thus simulating an industrial pipe, but with a lower EO feed ( $\varepsilon_0=1$ ), assuming to add subsequently ethylene oxide at different reactors length (Figure 7.3-8).



As revealed, also in this case the system is in runaway. Thus, the necessity to work under plug-flow regime to ensure better thermal control is needed.

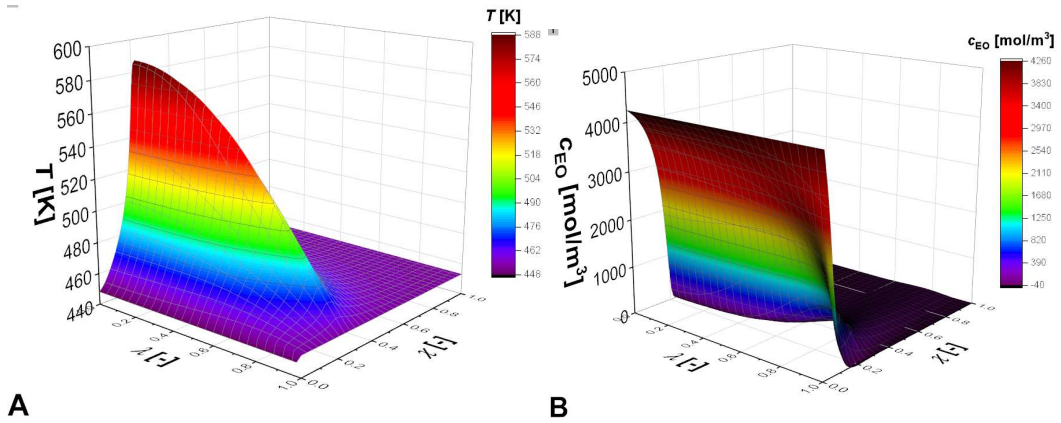


**Fig. 7.3-8.** Temperature and ethylene oxide concentration trends along the dimensionless axial coordinate and the dimensionless radial coordinate for a reactor characterized by 9.0mm inner diameter, imposing  $T_{feed}=443K$ ,  $\varepsilon_0=1$ ,  $cat=0.1\%$  mol/mol (V. Russo et al. 2023).

## 7.4 Simulation of reactors working in plug-flow regimes

A plug-flow model was implemented to simulate reactors working in conditions near to ideality. The mass and energy balance equations adopted are reported in Eqs. 7.4-1 and 7.4-2.

$$\frac{u}{L} \frac{\partial c_{EO}}{\partial \chi} = v_i r \quad (7.4-1)$$

$$\frac{u}{L} \frac{\partial T}{\partial \chi} = - \frac{\Delta r H \cdot r + UA(T - T_w)}{c_{p,mix} \rho_{mix}} \quad (7.4-2)$$

As revealed, the only unknown parameter of the model is the overall heat transfer coefficient ( $U$ ). To have an order of magnitude for a classical industrial pipe (9 mm internal diameter), data from the literature were taken to estimate the order of magnitude of this coefficient. Umbach reported the temperature profile along the

axial coordinate for a coiled tube reactor characterized by a residence time of 25 s, a reactor length of 12.5 m and a diameter of 9 mm, working with a jacket temperature range between 185-235°C (Umbach & Stein, 1971b). The authors reported that by working with  $\varepsilon_0=1$  and a catalyst loading of 0.1%, a maximum temperature peak of 280°C was recorded.

The developed mode was applied, estimating  $U=0.4 \text{ kW}/(\text{m}^2 \text{ K})$ , value in line with the order of magnitude reported in the literature, being between 0.2-1.0  $\text{kW}/(\text{m}^2 \text{ K})$  (Bell, K.J., 1983).

In this way, the parameter was fixed, and several simulations were conducted, imposing  $\varepsilon_0=3$ , a pipe diameter of 9 mm, a fluid velocity of 0.05 m/s and a catalyst loading of 0.1%, working with a feed temperature of 210°C. The length of the pipe was fixed at 50 m. The result of the simulation is reported in Figure 7.4-1.

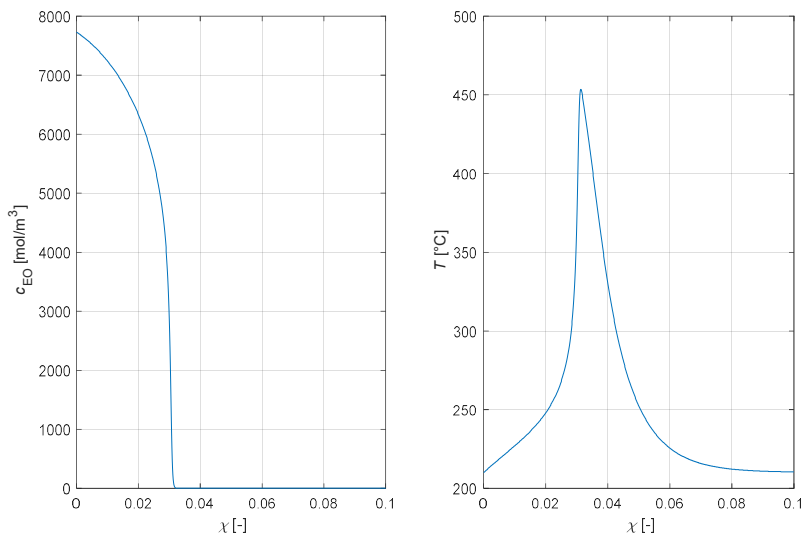


**Fig. 7.4-1.** EO concentration and temperature profiles for a reactor working at  $T_{\text{feed}}=210^\circ\text{C}$ ,  $u=0.05 \text{ m/s}$ ,  $\varepsilon_0=3$ , catalyst concentration of 0.1%, reactor diameter of 9mm and length of 50 m (V. Russo et al. 2023).

As revealed, temperature increase cannot be considered acceptable, thus, the EO feed was divided in three points, feeding  $\varepsilon_0=1$  at the entrance of the pipe, and injecting other two equivalents in terms of ethylene oxide content at 10 and 20 % of the pipe. Ethylene oxide was fed at room temperature in an adiabatic mixer. The

results shown in Figure 7.4-2 clearly demonstrate that it is possible to work at high conversion in safe conditions.

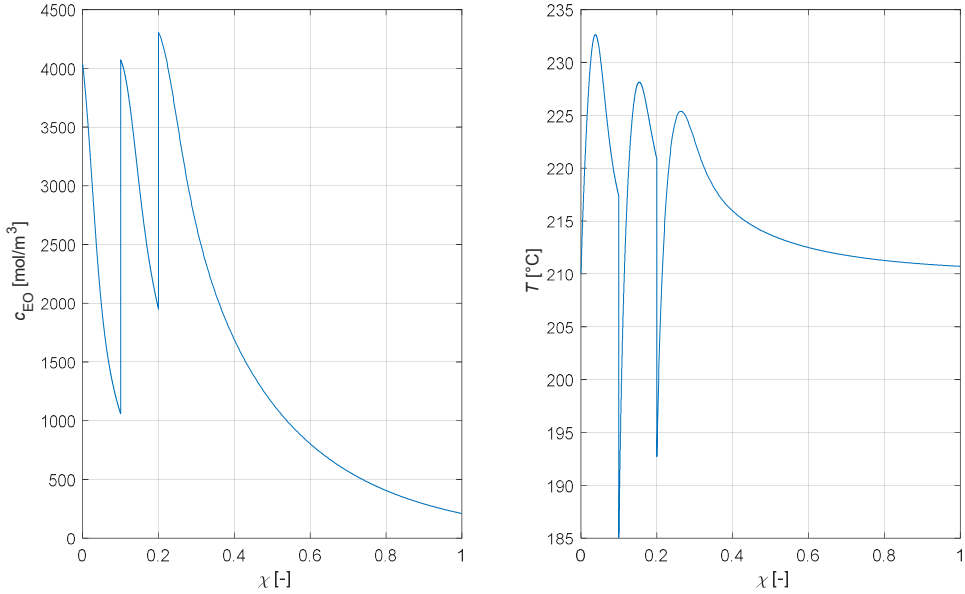


**Fig. 7.4-2.** EO concentration and temperature profiles for a reactor working at  $T_{\text{feed}}=210^\circ\text{C}$ ,  $u=0.05\text{m/s}$ , catalyst concentration of 0.1%, reactor diameter of 9mm and length of 50m. Ethylene oxide feed is split into three streams, at 0, 10 and 20% of the pipe (V. Russo et al. 2023).

## 7.5 Conclusions

In the present chapter, a laminar flow reactor model was developed and successfully applied to describe the experimental data reported in the literature. The experimental data, derived from previous work, have been used to estimate reliable kinetic parameters. The exothermicity of the system was proved by additional simulations.

Larger reactors were considered, checking the possibility to conduct the operation at the industrial scale, demonstrating the high flexibility of the model and its power in predicting the alkoxylation system.

Final simulations were conducted using a plug flow model showing that it is possible to work at high conversion and in safe conditions by using a multi-feed approach, splitting the ethylene oxide stream in different positions of the pipe.

These results open the way to deeper experimental and theoretical investigation to arrive at a final industrial configuration for a continuous ethoxylation reactor.



## **Chapter 8 - Conclusions summarizing the scientific achievements of the Candidate and being the basis of the dissertation.**

The candidate has been studying alkoxylation reactions since the beginning of his scientific career. The results obtained (especially in kinetic study of alkoxylation reactions) have been described in the first part of the dissertation together with the state of the art of literature in the field of kinetics and catalysis of alkoxylation reactions.

Building on this knowledge as innovative work in this dissertation, the results obtained by the candidate in the intensification of the alkoxylation process are reported.

In particular, a mathematical model was developed that can simulate the behavior of new fed-batch reactor in which the peculiarities of both spray tower and jet-loop reactors are found. The reactor showed similar productivity to that of jet-loop reactors but retains the ability to work with a very low amount of initial sublayer thus allowing a very high final alkylene oxide/substrate ratio.

Process intensification certainly comes from transforming processes from a fed-batch mode to a continuous mode. Proposals from both the scientific and patent literature are given in the dissertation.

Among the various proposals from the literature, micro- and milli-reactors are certainly promising. Simulation models of both micro and milli-reactors have been developed in the dissertation. The simulations show that microreactors provide excellent temperature control but are characterized by low throughput; in contrast, for milli-reactors both have high throughput, which is interesting for industrial applications, but temperature control is nontrivial for these systems. The use of the simulation model made it possible to identify the best reactor configuration and operating modes to ensure good productivity while keeping temperature under control.

These results of the dissertation will be the basis for the design, first of pilot plants and then of continuous industrial alkoxylation processes.

Among the co-authored publications listed below, those that contribute novel insights into the progression of knowledge involve the doctoral candidate personally

programming the models and simulating the synthesis processes under specific conditions. The candidate then compared these simulations to experimental data from other authors published in the literature. The candidate creatively participated in conceptualizing and planning the work, as well as in calculating and interpreting the results, which were published with his co-authorship. These contributions have been synthesized in this doctoral dissertation, representing compilation of the Author's recent advances in the chemistry and chemical engineering of oxyalkylation reactions.

### **Summary of the Author's published output including the material described in the dissertation, Part II.**

1. Russo, V., Tesser, R., Hreczuch, W., & **DiSerio, M.** (2023). Design of a continuous device for ethoxylation reaction: The choice between micro and milli scale. *Chemical Engineering Research and Design*. 194 (2023) 550–562, <https://doi.org/10.1016/j.cherd.2023.04.051>.
2. **DiSerio, M.**, Russo, V., Santacesaria, E., & Tesser, R. (2021). The Evolution of the Fed Batch Ethoxylation Reactors to Produce the Non-Ionic Surfactants. *Frontiers in Chemical Engineering*, Vol. 3, Article 644719, <https://doi.org/10.3389/fceng.2021.644719>.
3. Tesser, R., Russo, V., Santacesaria, E., Hreczuch, W., & **DiSerio, M.** (2020). Alkoxylation for Surfactant Productions: Toward the Continuous Reactors. *Frontiers in Chemical Engineering*, Vol. 2, Article 7. <https://www.semanticscholar.org/paper/Alkoxylation-for-Surfactant-Productions%3A-Toward-the-Tesser-Russo/a6b82dc93b5bf66cf4bd12f4e54c1c2dc9a34ef4>
4. **M DiSerio** (2019), Chemical reaction engineering as a bridge between nano and macro world, *Frontiers in Chemical Engineering*, Vol. 1, Article 2, <https://www.frontiersin.org/articles/10.3389/fceng.2019.00002/full>.
5. Santacesaria, E., Tesser, R., & **DiSerio, M.** (2018). Polyethoxylation and polypropoxylation reactions: Kinetics, mass transfer and industrial reactor design. *Chinese Journal of Chemical Engineering*, 26(6), 1235–1251. <https://doi.org/10.1016/j.cjche.2018.02.020>.

## List of Symbols

$A$	Cross sectional area
$A_{AO,S}$	Coefficient in Eq. 3.2-8
$A_i, B_i, C_i$	Coefficients in Eq. 28
$A, B, C, D, E$	Parameters in Eqs. 3.1-1 and 3.2-1
$A_{oligomer}, B_{oligomer}$	Coefficient in Eq. 41
$AO$	Alkylene Oxide
$AO_R$	Reacted alkylene oxide
$A_{S,AO}$	Coefficients in Eq. 3.2-9
$B^\circ$	Catalyst concentration
$B_{AO,S}$	Coefficient in Eq. 3.2-8
$B_{S,AO}$	Coefficient in Eq. 3.2-8
$C_{AO,S}$	Coefficient in Eq. 3.2-8
$Cat$	Catalyst
$C_{cat}$	Catalyst concentration
$C_{EO,0}$	Initial ethylene oxide concentration
$C_{EO}$	Ethylene oxide concentration
$C_i$	Ratio between the probability of reaction of oligomer $i$ and substrate
$C_i$	Concentration of species $i$
$C_{i,0}$	Feed concentration of component $i$
$C_{O,0}$	Initial octanol concentration
$C_p$	Specific heat of reactive mixture
$C_{p,EO}$	Ethylene oxide specific heat
$C_{p,mix}$	Specific heat of the mixture
$C_{p,O}$	Octanol specific heat
$C_{pEO}$	Specific heat of liquid ethylene oxide
$C_{S,AO}$	Coefficient in Eq. 3.2-9
$D$	Reactor diameter
$D_{EO}$	Ethylene oxide diffusivity
$D_{EO,0}$	Initial ethylene oxide diffusivity
$D_i$	Molecular diffusivity of component $i$
$E$	Activation energy
$E_a$	Activation energy of reaction
$EO$	Ethylene Oxide
$EO_R$	Reacted ethylene oxide
$F_{EO}$	Ethylene oxide feed



$F_{obj}$	<i>Objective function</i>
$H_{EO,S}$	<i>Ethylene oxide repartition constant</i>
$H_{N_2,EO}$	<i>Solubility of nitrogen in ethylene oxide</i>
$H_{N_2,S}$	<i>Solubility of nitrogen in the substrate</i>
$[i]$	<i>Concentration of <math>i</math> in liquid phase</i>
$J_{EO}$	<i>Gas-liquid mass transfer rate</i>
$K$	<i>Catalyst/octanol molar ratio</i>
$K$	<i>Henry solubility constant</i>
$k$	<i>Kinetic constant of reaction</i>
$k_0$	<i>Kinetic constant initial reaction rate</i>
$k_i$	<i>Kinetic constant of reaction rate <math>i</math></i>
$k_{la}$	<i>Mass-transfer coefficient</i>
$k_p$	<i>Kinetic constant of propagation reaction rate</i>
$k_{11}$	<i>Kinetic constant of Ethoxylation of a primary alcohol</i>
$k_{12}$	<i>Kinetic constant of Ethoxylation of a secondary alcohol</i>
$k_{21}$	<i>Kinetic constant of Propoxylation of a primary alcohol</i>
$k_{22}$	<i>Kinetic constant of Propoxylation of a secondary alcohol</i>
$K_e$	<i>Equilibrium constant</i>
$k_{ref}$	<i>Reference kinetic constant of reaction</i>
$L$	<i>Reactor length</i>
$M_{EO}$	<i>Ethylene oxide molecular weight</i>
$M_{mix}$	<i>Molecular weight of the mixture</i>
$M_O$	<i>Octanol molecular weight</i>
$MOH/MOR$	<i>Alkaline catalysts</i>
$MW_{EO}$	<i>Molecular weight of ethylene oxide</i>
$MW_i$	<i>Molecular weight of <math>i</math></i>
$MW_{ROHO}$	<i>Molecular weight of fatty alcohols</i>
$N$	<i>Moles</i>
$n_{AOG}$	<i>Mols of alkylene oxide in gas phase</i>
$n_{AOL}$	<i>Mols of alkylene oxide in liquid phase</i>
$n_{AOR}$	<i>Mols of alkylene oxide reacted</i>
$n_{RX(AO)iH}$	<i>mol of oligomer <math>i</math></i>
$n_s^0$	<i>Initial mols of substrate</i>
$n_s$	<i>Mols of substrate</i>
$N_{data}$	<i>Number of data</i>
$P$	<i>Pressure</i>
$P^{\circ}_{EO}$	<i>Vapor pressure of ethylene oxide</i>
$P^{\circ}_{AO}$	<i>Vapor pressure of alkylene oxide</i>
$P^{\circ}_{EO}$	<i>Vapor pressure of ethylene oxide</i>
$P^{\circ}_{PO}$	<i>Vapor pressure of propylene oxide</i>

$P_{AO}$	Alkylen oxide pressure
$P_{EO}$	Ethylene oxide pressure
$P_{N_2,0}$	Initial pressure of $N_2$
$P_{ST}$	Pressure of ethylene oxide storage tank
$PM_{AO}$	Alkylen oxide molecular weight
$PM_S$	Substrates molecular weight
$PO$	Propylene Oxide
$Q$	Volumetric flowrate
$Q_B$	Flow to the ejector
$Q_S$	Flow to the spray nozzle
$r$	Reaction rate
$r_0$	Initial reaction rate
$r_p$	Propagation reaction rate
$r_i$	Reaction rate $i$
$R$	Reactor radius
$R_g$	Ideal gas constant
$ROH$	Fatty alcohols
$S^0$	Initial mol of substrate
$S$	Substrate
$t$	Time
$T$	Temperature (K)
$T_0$	Temperature of the liquid at the outlet of the heat exchanger
$T_c$	Critical temperature
$T_{feed}$	Feed temperature
$T_{MAX}$	Maximum temperature
$T_N$	Reactor bottom temperature
$T_{ref}$	Reference temperature
$T_{sat}$	Saturation temperature
$T_w$	Wall temperature
$U$	Overall heat transfer coefficient
$u$	Fluid velocity
$\bar{u}$	Average flow velocity
$u_{max}$	Maximum fluid velocity
$v$	Molar oligomer distribution
$V_{AOL}$	Dissolved alkylene oxide liquid volume
$V_G$	Gas Phase volume
$V_L$	Liquid phase volume
$V_{mix}$	Molar volume of the mixture
$V_S$	Substrates volume
$V_{SL}$	Liquid volume of substrate

$V_R$	Reactor volume
$\dot{V}$	Volumetric flowrate
$W_{AO}$	Weight amounts of ethylene oxide or propylene oxide
$W_{S^*}$	Weight amount of initial substrate
$W_S$	Weight amount of dodecanol or ethoxylated derivatives
$\bar{x}_{EO}$	Ethylene oxide average conversion
$\bar{x}_{EO,CALC}$	Average calculated ethylene oxide conversion
$X_i$	Molar fraction of $i$ in liquid phase
$X_0$	Molar fraction of residual starter
$X_{AO}$	Molar fraction of alkylene oxide
$X_{EO}$	Molar fraction of ethylene oxide
$X_{EO}$	Ethylene oxide conversion
$X_{EO,0}$	Initial ethylene oxide conversion
$X_{EO,EXP}$	Experimental ethylene oxide conversion
$X_i$	Molar fraction of the oligomer $i$
$X_i$	Reactant conversion
$X_S$	Molar fraction of substrates
$y$	Radial coordinate
$y_{EO}$	Ethylene oxide molar gaseous fraction
$z$	Axial coordinate
$Z_c$	Critical compressibility factor

### Greek Letters

$a_{EO}$	Coefficient of Eq. 37
$\Lambda_{AO,S}, \Lambda_{S,AO}$	Parameters in Eq. 3.2-12
$\Lambda_{EO,S}, \Lambda_{S,EO}$	Parameters in Eqs. 3.2-15, 3.2-16
$\gamma_{AO}$	Activity coefficient in liquid phase
$\gamma_i$	Activity coefficient of $i$
$\Gamma_{AO,S}$	Coefficient of Eq. 3.2-7
$\Gamma_{S,AO}$	Coefficient of Eq. 3.2-7
$\Delta_r H$	Enthalpy of reaction
$\epsilon_0$	Feed ethylene oxide/octanol molar ratio
$\eta_{EO}$	Ethylene oxide viscosity
$\eta_i$	Viscosity of component $i$
$\eta_{mix}$	Viscosity of the mixture
$\eta_{oligomer}$	Oligomer viscosity
$\theta$	Temperature ( $^{\circ}C$ )
$\lambda$	Dimensionless reactor radius coordinate
$\lambda_{EO}$	Ethylene oxide heat of vaporization

$\lambda_{mix}$	<i>Heat conductivities of the mixture</i>
$\lambda_O$	<i>Octanol heat conductivities</i>
$\nu_i$	<i>Stoichiometric coefficient of component i</i>
$\rho_{AO}$	<i>Alkylen oxide density</i>
$\rho_i$	<i>Density of i</i>
$\rho_{mix}$	<i>Density of the Initial mixture</i>
$\rho_{mix,0}$	<i>Density of the Initial mixture</i>
$\rho_{prod}$	<i>Density of the products</i>
$\rho_S$	<i>Substrates density</i>
$\tau$	<i>Residence time</i>
$\chi$	<i>Dimensionless axial coordinate</i>



## Literature

- Amaral, G. M., & Giudici, R. (2011). Kinetics and Modeling of Fatty Alcohol Ethoxylation in an Industrial Spray Loop Reactor. *Chemical Engineering and Technology*, 34(10), 1635–1644. <https://doi.org/10.1002/ceat.201100215>.
- Baker, S. B., & Thompson, W. R. (1967). *Secondary alcohol ethoxylation* (Patent No. US3359331A).
- Behler, A., Raths, H. C., & Ploog, U. (1994). *Narrow range alkoxyate nonionic surfactant prodn. - by alkoxylation of cpds. contg. active hydrogen or ester using metal alcoholate activated with organic carboxylic acid as homogeneous catalyst.* (Patent No. DE4325136).
- Bell, K.J. (1983), *Introduction to heat exchanger design*. In HEAT EXCHANGER DESIGN HANDBOOK, Volume 3 : Thermal and Hydraulic Design of Heat Exchangers, Dusseldorf, VDI-Verlag GmbH, 1
- Bialowas, E., & Szymanowski, J. (2004). *Catalysts for Oxyethylation of Alcohols and Fatty Acid Methyl Esters*. *Ind. Eng. Chem. Res.* 43, 20, 6267–6280 <https://doi.org/10.1021/ie049898h>.
- Chemstations. (n.d.). *ChemCAD v. 7.0*. Retrieved January 3, 2023, from <https://www.chemstations.com/>.
- Desbène, P. L., Desmazières, B., Even, V., Basselier, J. J., & Minssieux, L. (1987). Analysis of non-ionic surfactants used in tertiary oil recovery. Optimisation of stationary phase in normal phase partition chromatography. *Chromatographia*, 24(1), 857–861. <https://doi.org/10.1007/BF02688599>.
- Dimiccoli, A., DiSerio, M., & Santacesaria, E. (2000). Mass Transfer and Kinetics in Spray-Tower-Loop Absorbers and Reactors. *Industrial & Engineering Chemistry Research*, 39(11), 4082–4093. <https://doi.org/10.1021/ie000137y>.
- DiSerio, M. (2019). Chemical Reaction Engineering as a Bridge Between Nano and Macro World. *Frontiers in Chemical Engineering | www.Frontiersin.Org*, 1(2), 31. <https://doi.org/10.3389/fceng.2019.00002>.
- DiSerio, M., di Martino, S., & Santacesaria, E. (1994). Kinetics of Fatty Acids Polyethoxylation. *Industrial & Engineering Chemistry Research*, 33(3), 509–514. <https://doi.org/10.1021/ie00027a006>.
- DiSerio, M., Tesser, R., Felippone, F., & Santacesaria, E. (1995). Ethylene Oxide Solubility and Ethoxylation Kinetics in the Synthesis of Nonionic Surfactants. *Industrial & Engineering Chemistry Research*, 34(11), 4092–4098. <https://doi.org/10.1021/ie00038a052>.
- DiSerio, M., Iengo, P., Gobetto, R., Bruni, S., & Santacesaria, E. (1996). Ethoxylation of fatty alcohols promoted by an aluminum alkoxide sulphate catalyst. *Journal*

- of Molecular Catalysis A: Chemical*, 112(2), 235–251.  
[https://doi.org/10.1016/1381-1169\(96\)00134-3](https://doi.org/10.1016/1381-1169(96)00134-3).
- DiSerio, M., Vairo, G., Iengo, P., Felippone, F., & Santacesaria, E. (1996). Kinetics of Ethoxylation and Propoxylation of 1- and 2-Octanol Catalyzed by KOH. *Industrial & Engineering Chemistry Research*, 35(11), 3848–3853.  
<https://doi.org/10.1021/ie960200c>.
- DiSerio, M., Iengo, P., Vairo, G., & Santacesaria, E. (1998). Narrow-range ethoxylation of fatty alcohols promoted by a zirconium alkoxide sulfate catalyst. *Journal of Surfactants and Detergents*, 1(1), 83–91.  
<https://doi.org/10.1007/s11743-998-0011-9>.
- DiSerio, M., Tesser, R., Dimiccoli, A., & Santacesaria, E. (2002). Kinetics of Ethoxylation and Propoxylation of Ethylene Glycol Catalyzed by KOH. *Industrial & Engineering Chemistry Research*, 41(21), 5196–5206.  
<https://doi.org/10.1021/ie020082v>.
- DiSerio, M., Tesser, R., & Santacesaria, E. (2005). Comparison of different reactor types used in the manufacture of ethoxylated, propoxylated products. *Industrial and Engineering Chemistry Research*, 44(25), 9482–9489.  
<https://doi.org/10.1021/ie0502234>.
- DiSerio, M., Russo, V., Santacesaria, E., & Tesser, R. (2021). The Evolution of the Fed Batch Ethoxylation Reactors to Produce the Non-Ionic Surfactants. *Frontiers in Chemical Engineering*, 3. <https://doi.org/10.3389/fceng.2021.644719>.
- Edwards, C. L. (1987). *Preparation of nonionic surfactants* (Patent No. EP228121).
- Edwards, C. L. (1988). *Preparation of nonionic surfactants* (Patent No. US4721817).
- Edwards, C. L. (1989). *Narrow range alkanol alkoxylates* (Patent No. EP344835).
- Edwards, C. L. (1998). Nonionic Surfactants. In N. M. van Os (Ed.), *Distribution of the Polyoxyethylene Chain Charles*. MARCEL DEKKER, INC.  
<https://doi.org/10.1201/9780203745649>.
- Egedy, A., Varga, T., & Chován, T. (2013). Compartment model structure identification with qualitative methods for a stirred vessel. *Mathematical and Computer Modelling of Dynamical Systems*, 19(2), 115–132.  
<https://doi.org/10.1080/13873954.2012.700939>.
- Enikolopiyan, N. S. (1976). New Aspects of the Nucleophilic Opening of Epoxide Rings. *Pure and Applied Chemistry*, 48(3), 317–328.  
<https://doi.org/10.1351/pac197648030317>
- Flory, P. J. (1940). Molecular Size Distribution in Ethylene Oxide Polymers. *Journal of the American Chemical Society*, 62(6), 1561–1565.  
<https://doi.org/10.1021/ja01863a066>.
- Fredenslund, A., Gmehling, J., & Rasmussen, P. (1977). *Vapor—Liquid Equilibria using UNIFAC: a group-contribution method*. Elsevier.

- Gee, G., Higginson, W. C. E., Levesley, P., & Taylor, K. J. (1959). Polymerisation of Epoxides. Part I. Some Kinetic Aspects of the Addition of Alcohols to Epoxides catalysed by Sodium Alkoxides. *Journal of the Chemical Society*, 1338–1344. <https://doi.org/https://doi.org/10.1039/JR9590001338>
- Gee, G., Higginson, W. C. E., Taylor, K. J., & Trenholme, M. W. (1961). The polymerization of epoxides. Part III. The polymerization of propylene oxide by sodium alkoxides. *Journal of the Chemical Society (Resumed)*, 4298–4303. <https://doi.org/10.1039/jr9610004298>.
- Gustin, J. L. (2000). Safety of ethoxylation reactions. *Hazards XV—The Process, Its Safety and the Environment. Symposium Series No. 147*, 1–13.
- Haag, J., Gentric, C., Lemaitre, C., & Leclerc, J.-P. (2018). Modelling of Chemical Reactors: From Systemic Approach to Compartmental Modelling. *International Journal of Chemical Reactor Engineering*, 16(8). <https://doi.org/10.1515/ijcre-2017-0172>.
- Hall, C. A., & Agrawal, P. K. (1990). Separation of kinetics and mass-transfer in a batch alkoxylation reaction. *The Canadian Journal of Chemical Engineering*, 68(1), 104–112. <https://doi.org/10.1002/cjce.5450680113>.
- Hermann, P. D., Cents, T., Klemm, E., & Ziegenbalg, D. (2016). Simulation study of the ethoxylation of octanol in a microstructured reactor. *Industrial and Engineering Chemistry Research*, 55(49), 12675–12686. [https://doi.org/10.1021/ACS.IECR.6B04110/ASSET/IMAGES/LARGE/IE-2016-04110H\\_0008.JPEG](https://doi.org/10.1021/ACS.IECR.6B04110/ASSET/IMAGES/LARGE/IE-2016-04110H_0008.JPEG)
- Hessel, V., Kralisch, D., & K. N. (2014). *Novel Process Windows: Innovative Gates to Intensified and Sustainable Chemical Processes*. Wiley. <https://doi.org/10.1002/9783527654826>
- Hinz, W., & Dexheimer, E. M. (2002). *Continuous process for the production of sucrose based polyether polyols* (Patent No. US6380367 (B1)).
- Hreczuch, W., Chruściel, A., Dąbrowska, K., DiSerio, M., & Yongqiang, S. (2016). Characteristics of Block Copolymers of Methyl Oxirane and Oxirane Derivatives of 2-Ethylhexanol as Obtained with KOH and Dimetalcyanide Type Catalyst. *Tenside Surfactants Detergents*, 53(3), 259–264. <https://doi.org/10.3139/113.110431>.
- Hubel, R., Markowz, G., Recksik, M., Wewers, D., & Zeller-Schuldes F. (2005). *Alkoxylation in microstructured capillary reactors* (Patent No. US7858829 (B2)).
- Improta, R., DiSerio, M., & Santacesaria, E. (1999). Aluminium alkoxide sulphate catalyst: a computational study. *Journal of Molecular Catalysis A: Chemical*, 137(1–3), 169–182. [https://doi.org/10.1016/S1381-1169\(98\)00114-9](https://doi.org/10.1016/S1381-1169(98)00114-9).



- Janik, J., & Chruściel, A. (2015). Activity and selectivity of alkaline and doublemetal cyanide catalysts in ethoxylation of fatty alcohols. *Przemysł Chemiczny*, 94(8), 1404–1410. <https://doi.org/10.15199/62.2015.8.32>.
- Kralisch, D., Streckmann, I., Ott, D., Krtschil, U., Santacesaria, E., DiSerio, M., Russo, V., de Carlo, L., Linhart, W., Christian, E., Cortese, B., de Croon, M. H. J. M., & Hessel, V. (2012). Transfer of the Epoxidation of Soybean Oil from Batch to Flow Chemistry Guided by Cost and Environmental Issues. *ChemSusChem*, 5(2), 300–311. <https://doi.org/10.1002/cssc.201100445>.
- Lai, J., Wray, W. D., Lenahan, R. A., Reese, J. R., and Morrison, D. M. (2019). *Systems and Processes for Producing Polyether Polyols*. (Patent No. US10258953 (B2)).
- Leuteritz, G. M. (1992). *Process for the safe and environmentally sound production of highly alkylene oxide* (Patent No. U.S. Patent 5,159,092).
- Li, Y., Zhou, J., Zhang, Y., Liang, H., Sun, J., Liu, Y., D’Errico, G., Sun, Y., & DiSerio, M. (2021). Synthesis and Properties of Primary Alcohol Ethoxylates Using Different Catalytic Systems. *ACS Omega*, 6(44), 29774–29780. <https://doi.org/10.1021/acsomega.1c04232>
- Martin, A. E., & Murphy, H. F. (2000). Glycols, Propylene Glycols. In *Kirk-Othmer Encyclopedia of Chemical Technology*. Wiley. <https://doi.org/https://doi.org/10.1002/0471238961.0520082506151811.a01.pub2>.
- McDaniel, K. G. (2011). *High productivity alkoxylation processes* (Patent No. EP2325230 (A1)).
- McDaniel, K. G., & Reese, J. R. I. (2008). *Continuous processes for the production of alkyphenol ethoxylates*. (Patent No. US2008132728 (A1)).
- McDaniel, K. G., & Reese, J. R. I. (2009). *High productivity process for alkyphenol ethoxylates*. (Patent No. US7473677 (B2)).
- McDaniel, K. G., & Reese, J. R. I. (2010). *Continuous processes for the production of ethoxylates* (Patent No. EP2223953 (A1)).
- Milwidsky, B. M., & Gabriel, D. M. (1982). *Detergent Analysis A Handbook for Cost-effective Quality Control*. Wiley.
- Natta, G., & Mantica, E. (1952). The Distribution of Products in a Series of Consecutive Competitive Reactions. *Journal of the American Chemical Society*, 74(12), 3152–3156. <https://doi.org/10.1021/ja01132a057>
- Nikbin, N. N., Villa, C. M., Remacha, M. J. N., Khan, I., Heath, W. H., Pendergast, J. G., J., Forlin, A., & Schaefer, M. (2018). *Alkoxylation Process Using Tubular Reactor* (Patent No. WO2018057438).
- Pekalski, A. A., Zevenbergen, J. F., Braithwaite, M., Lemkowitz, S. M., & Paskan, H. J. (2005). Explosive decomposition of ethylene oxide at elevated condition: effect

- of ignition energy, nitrogen dilution, and turbulence. *Journal of Hazardous Materials*, 118(1–3), 19–34. <https://doi.org/10.1016/J.JHAZMAT.2004.09.029>
- Ploog, U. (1988a). *Use of esters of titanate and/or zirconic acid as ethoxylation or propoxylation catalysts*. (Patent No. EP340593).
- Ploog, U. (1988b). *Use of metal acetyl acetonates as ethoxylation or propoxylation catalysts* (Patent No. DE 3,829,753).
- Poling, B. E., Prausnitz, J. M., O'Connell, J. P., York, N., San, C., Lisbon, F., Madrid, L., City, M., Delhi, M. N., & Juan, S. (2001). *Properties of Gases and Liquids*. McGraw-Hill Education.  
<https://www.accessengineeringlibrary.com/content/book/9780070116825>.
- Prausnitz, J., & Anderson, T. (1980). *Computer calculations for multicomponent vapour-liquid and liquid-liquid equilibria*. Prentice-Hall.
- Rakutani, K., Onda, Y., & Inaoka, T. (1999). No Title. In D. Karsa (Ed.), *Annual Surfactant Review. Secondary alcohol ethoxylates*. CRC Press.
- Rebsdat, S., & Mayer, D. (2000). Ethylene Glycol. In *Ullmann's Encyclopedia of Industrial Chemistry*. Wiley-VCH Verlag GmbH & Co. KGaA.  
[https://doi.org/10.1002/14356007.a10\\_101](https://doi.org/10.1002/14356007.a10_101)
- Reck, R. A. (1967). Polyoxyethylene Alkylamines. In M. Schick (Ed.), *Nonionic Surfactants, Surfactant Science Series, Vol 1* (pp. 187–207), MARCEL DEKKER, INC.
- Renon, H., & Prausnitz, J. (1968). Local Composition in Thermodynamic Excess Function for Liquid Mixtures. *AIChE J.*, 14, 135–140.
- Rupp, M., Ruback, W., & Klemm, E. (2013a). Alcohol ethoxylation kinetics: Proton transfer influence on product distribution in microchannels. *Chemical Engineering and Processing: Process Intensification*, 74, 187–192.  
<https://doi.org/10.1016/J.CEP.2013.09.006>.
- Rupp, M., Ruback, W., & Klemm, E. (2013b). Octanol ethoxylation in microchannels. *Chemical Engineering and Processing*, 74, 19–26.  
<https://doi.org/10.1016/j.cep.2013.09.012>.
- Rupp, M., Ruback, W., & Klemm, E. (2013c). Octanol ethoxylation in microchannels. *Chemical Engineering and Processing: Process Intensification*, 74, 19–26.  
<https://doi.org/10.1016/J.CEP.2013.09.012>.
- Russo, V., Tesser, R., Hreczuch, W., & DiSerio, M. (2023). Process intensification for ethoxylation Reaction: the choice between micro and milli scale. *Chemical Engineering Research and Design*.  
<https://doi.org/10.1016/j.cherd.2023.04.051>.
- Salzano, E., DiSerio, M., & Santacesaria, E. (2007a). The evaluation of risks of ethoxylation reactors. *Process Safety Progress*, 26(4), 304–311.  
<https://doi.org/10.1002/prs.10212>.

- Salzano, E., DiSerio, M., & Santacesaria, E. (2007b). The role of recirculation loop on the risk of ethoxylation processes. *Journal of Loss Prevention in the Process Industries*, 20(3), 238–250. <https://doi.org/10.1016/j.jlp.2007.03.016>.
- Santacesaria, E., di Serio, M., & Iengo, P. (1999). Mass transfer and kinetics in ethoxylation spray tower loop reactors. *Chemical Engineering Science*, 54(10), 1499–1504. [https://doi.org/10.1016/S0009-2509\(99\)00042-1](https://doi.org/10.1016/S0009-2509(99)00042-1).
- Santacesaria, E., DiSerio, M., Garaffa, R., & Addino, G. (1992a). Kinetics and mechanisms of fatty alcohol polyethoxylation. 1. The reaction catalyzed by potassium hydroxide. *Industrial & Engineering Chemistry Research*, 31(11), 2413–2418. <https://doi.org/10.1021/ie00011a001>.
- Santacesaria, E., DiSerio, M., Garaffa, R., & Addino, G. (1992b). Kinetics and mechanisms of fatty alcohol polyethoxylation. 2. Narrow-range ethoxylation obtained with barium catalysts. *Industrial & Engineering Chemistry Research*, 31(11), 2419–2421. <https://doi.org/10.1021/ie00011a002>.
- Santacesaria, E., DiSerio, M., Lisi, L., & Gelosa, D. (1990). Kinetics of nonylphenol polyethoxylation catalyzed by potassium hydroxide. *Industrial & Engineering Chemistry Research*, 29(5), 719–725. <https://doi.org/10.1021/ie00101a002>
- Santacesaria, E., DiSerio, M., & Tesser, R. (1995). Role of ethylene oxide solubility in the ethoxylation processes. *Catalysis Today*, 24(1–2), 23–28. [https://doi.org/10.1016/0920-5861\(95\)00022-8](https://doi.org/10.1016/0920-5861(95)00022-8).
- Santacesaria, E., Iengo, P., & DiSerio, M. (1999). Annual Surfactants Review. In D. K. Karsa (Ed.), *Catalytic and kinetic effects in ethoxylation processes* (1 st, Vol. 2). CRC.
- Santacesaria, E., Tesser, R., & DiSerio, M. (2018). Polyethoxylation and polypropoxylation reactions: Kinetics, mass transfer and industrial reactor design. *Chinese Journal of Chemical Engineering*, 26(6), 1235–1251. <https://doi.org/10.1016/j.cjche.2018.02.020>
- Schachat, N., & Greenwald, H. J. (1967). Mechanism of Ethylene oxide Condensation. In M. J. Schick (Ed.), *Nonionic surfactants, Surfactant Science Series, Vol 1* (pp. 8–32). MARCEL DEKKER, INC.
- Schilling, F. C., & Tonelli, A. E. (1986). Carbon-13 NMR Determination of Poly (propylene oxide) Microstructure. In *Macromolecules* (Vol. 19). <https://pubs.acs.org/sharingguidelines>.
- Stankiewicz, A. I., & Moulijn, J. A. (2000). Process intensification: transforming chemical engineering. *Chemical Engineering Progress*, 96(1), 22–34.
- Tesser, R., Russo, V., Santacesaria, E., Hreczuch, W., & DiSerio, M. (2020). Alkoxylation for Surfactant Productions: Toward the Continuous Reactors. *Frontiers in Chemical Engineering*, 2(7). <https://doi.org/10.3389/fceng.2020.00007>

- Umbach, W., & Stein, W. (1971a). Continuous alkoxylation process. *Journal of the American Oil Chemists Society*, 48(8), 394–397.  
<https://doi.org/10.1007/BF02637359>.
- Umbach, W., & Stein, W. (1971b). Continuous alkoxylation process. *Journal of the American Oil Chemists Society* 1971 48:8, 48(8), 394–397.  
<https://doi.org/10.1007/BF02637359>.
- Verwijs, J. W., Weston, J. W., Papadopoulos, W. J., Elwell, R. J., Villa, C. M., & Papadopoulos, W. J. S. (2008). *Continuous process and system of producing polyether polyols* (Patent No. US7378559 (B2)).
- Villa, C. M., WESTON, J. W., JAIN, P., THOMPSON, L. H., & MASY, J.-P. (2014). *Continuous Loop Flow Process For Polyether Polyol Production* (Patent No. US8912364 (B2)).
- Weston, J. W., VILLA, C. M., MASY, J.-P., & SEAVEY, K. C. (2015). *METHOD FOR CONTINUOUSLY PRODUCING LOW EQUIVALENT WEIGHT POLYOLS USING DOUBLE METAL CYANIDE CATALYSTS* (Patent No. US9074044 (B2)).
- Wilson, G. M. (1964). Vapor-Liquid Equilibrium. XI. New Expression for the Excess Free Energy of Mixing. *J. Am. Chem. Soc.*, 86, 127–130.
- Yamada, K., KASAHARA, N., TOYOTA, Y., SUZUKI, C., IKAI, S., & HATANO, H. (2006). *Method for continuously producing a polyether* (Patent No. US7012164 (B2)).
- Yang, K. (1980). *Barium Oxide Catalyzed Ethoxylation* (Patent No. US4239917).
- Yen, L. C., & Woods, C. C. (1966). A Generalized Equation for Computer Calculation of Liquid Densities. *A.I.Ch.E. Journal*, 12(1), 96–99.  
<https://doi.org/10.1002/aic.690120119>.
- Yue, H., Zhao, Y., Ma, X., & Gong, J. (2012). Ethylene glycol: properties, synthesis, and applications. *Chemical Society Reviews*, 41(11), 4218.  
<https://doi.org/10.1039/c2cs15359a>.
- Zhang, X.-H., Hua, Z.-J., Chen, S., Liu, F., Sun, X.-K., & Qi, G.-R. (2007). Role of zinc chloride and complexing agents in highly active double metal cyanide catalysts for ring-opening polymerization of propylene oxide. *Applied Catalysis A: General*, 325(1), 91–98. <https://doi.org/10.1016/j.apcata.2007.03.014>.

## **Appendix 1**

**The Author's published output  
including the material described in the dissertation, Part II.**

# Article 1 Copyright\_Elsevier



Sign in/Register



RightsLink



## Design of a continuous device for ethoxylation reaction: The choice between micro and milli scale

**Author:** Vincenzo Russo, Riccardo Tesser, Wieslaw Hreczuch, Martino Di Serio

**Publication:** Chemical Engineering Research and Design

**Publisher:** Elsevier

**Date:** June 2023

*© 2023 Institution of Chemical Engineers. Published by Elsevier Ltd. All rights reserved.*

### Journal Author Rights

Please note that, as the author of this Elsevier article, you retain the right to include it in a thesis or dissertation, provided it is not published commercially. Permission is not required, but please ensure that you reference the journal as the original source. For more information on this and on your other retained rights, please visit: <https://www.elsevier.com/about/our-business/policies/copyright#Author-rights>

BACK

CLOSE WINDOW

© 2024 Copyright - All Rights Reserved | [Copyright Clearance Center, Inc.](#) | [Privacy statement](#) | [Data Security and Privacy](#)  
| [For California Residents](#) | [Terms and Conditions](#) Comments? We would like to hear from you. E-mail us at [customer-care@copyright.com](mailto:customer-care@copyright.com)

Article 1. Russo, V., Tesser, R., Hreczuch, W., & DiSerio, M. (2023).  
Design of a continuous device for ethoxylation reaction: The choice between  
micro and milli scale. *Chemical Engineering Research and Design*. 194 (2023) 550–  
562, <https://doi.org/10.1016/j.cherd.2023.04.051>.

An update to this article is included at the end

CHEMICAL ENGINEERING RESEARCH AND DESIGN 194 (2023) 550–562



Available online at [www.sciencedirect.com](http://www.sciencedirect.com)

Chemical Engineering Research and Design

ICHEM E

journal homepage: [www.elsevier.com/locate/cherd](http://www.elsevier.com/locate/cherd)

## Design of a continuous device for ethoxylation reaction: The choice between micro and milli scale



Vincenzo Russo<sup>a</sup>, Riccardo Tesser<sup>a,b</sup>, Wiesław Hreczuch<sup>c</sup>,  
Martino Di Serio<sup>a,d,\*</sup>

<sup>a</sup> Department of Chemical Sciences, University of Naples Federico II, IT-80126 Naples, Italy

<sup>b</sup> CIRCC, Consorzio Interuniversitario Reattività Chimica e Catalisi, IT-70126 Bari, Italy

<sup>c</sup> MEXEO, PL-47-200 Kędzierzyn-Koźle, Poland

<sup>d</sup> IROAST, Kumamoto University, JP-43201-6 Kumamoto, Japan

### ARTICLE INFO

#### Article history:

Received 25 January 2023

Received in revised form 7 April 2023

Accepted 23 April 2023

Available online 25 April 2023

#### Keywords:

Ethoxylation

Microreactors

Modeling

Laminar flow model

Scale-up

### ABSTRACT

A laminar flow model was developed to investigate the reaction kinetics of 1-dodecanol ethoxylation promoted by KOH, elaborating the data collected in microreactors. A generic laminar flow model was coded, and a sensitivity analysis was conducted highlighting the good flexibility of the model to simulate a wide range of conditions. Ethylene oxide diffusivity and liquid mixture viscosity were determined by applying existing correlations, carefully considering the change in viscosity with ethylene oxide conversion, temperature, and feed ethylene oxide/1-octanol ratio. The model was tested on literature data obtaining in every case good results. The obtained kinetic data were demonstrated to be in line with the ones obtained in separate investigations conducted in a fed-batch reactor, demonstrating that there was a real need in adopting the laminar flow reactor approach, as it allowed to retrieve more precise information about the intrinsic kinetics of the ethoxylation reaction, when working with microreactors, compared with the ones obtainable with a plug-flow ideal fluid-dynamic model. The developed model was used to simulate the behavior of a milli-reactor (this device allows to reach sufficient productivity for industrial application) and it was forecasted the possibility to use continuous ethoxylation milli-reactors using fluid-dynamic conditions characterized by a high Reynolds number (> 10000).

© 2023 Institution of Chemical Engineers. Published by Elsevier Ltd. All rights reserved.

## 1. Introduction

The ethoxylation of fatty alcohol is an important process to produce non-ionic surfactants. Ethylene oxide reacts rapidly with long-chain alcohols, a reaction promoted by a strong base catalyst, reaching almost full selectivity to the desired products, as no-side reactions are favored in the presence of base catalysts. The reaction occurs via anionic polymerization,

where ethylene oxide molecules are added to a growing poly-ether chain, leading to a statistical distribution of the products. The alkoxylation reactions are generally performed in semi-batch reactors (Di Serio et al., 2025), also in series, in which the catalyst and the substrate (alkyl phenols, fatty alcohols or acids) are initially charged while epoxide (ethylene or propylene oxide) is added during the reaction course. This synthesis strategy is due to the high reactivity of alkoxides and to the high heat involved in the alkoxylation reaction. The use of semi-batch reactors, however, has some drawbacks that can be summarized in the following points: (i) the reactor volume is relatively high; this aspect could represent a serious problem for safety issues due to the high quantity of alkoxide present in

\* Corresponding author at: Department of Chemical Sciences, University of Naples Federico II, IT-80126 Naples, Italy.

E-mail address: [diserio@unina.it](mailto:diserio@unina.it) (M. Di Serio).

<https://doi.org/10.1016/j.cherd.2023.04.051>

0263-8762/© 2023 Institution of Chemical Engineers. Published by Elsevier Ltd. All rights reserved.



## Nomenclature

$a_{ED}$	Coefficient in Eq. 38
$A$	Cross-sectional area of the pipe, $m^2$
$A_s$	Specific exchange area, $m^2/m^3$
$A_i, B_i, C_i$	Coefficients in Eq. 29
$C_{cat}$	Catalyst concentration, $mol/m^3$
$C_A$	Concentration of reactant A, $mol/m^3$
$C_{A,0}$	Initial concentration of reactant A, $mol/m^3$
$C_{A,AV}$	Average concentration of reactant A, $mol/m^3$
$C_{EO,0}$	Initial ethylene oxide concentration, $mol/m^3$
$C_{EO}$	Ethylene oxide concentration, $mol/m^3$
$C_i$	Concentration of species $i$ , $mol/m^3$
$C_{i,0}$	Feed concentration of component $i$ , $mol/m^3$
$C_{p,mix}$	Specific heat of the mixture, $J/(kg K)$
$C_{p,ED}$	Ethylene oxide specific heat, $J/(kmol K)$
$C_{p,O}$	Octanol specific heat, $J/(kmol K)$
$D_A$	Molecular diffusivity of component A, $m^2/s$
$D_{ED}$	Ethylene oxide molecular diffusivity, $m^2/s$
$D_{EO,0}$	Initial ethylene oxide diffusivity, $m^2/s$
$D_i$	Molecular diffusivity of component $i$ , $m^2/s$
$E_a$	Activation energy, $J/mol$
$F_{obj}$	Objective function, -
$k$	Kinetic constant, $m^3/(mol s)$
$k_A$	Kinetic constant, $1/s$
$k_{ref}$	Kinetic constant at the reference temperature of 473 K, $m^3/(mol s)$
$K$	Feed catalyst/octanol molar ratio
$L$	Reactor length, $m$
$M_{mix}$	Molecular weight of the mixture, $mol/kg$
$M_{EO}$	Ethylene oxide molecular weight, $mol/kg$
$M_O$	Octanol molecular weight, $mol/kg$
$N_{data}$	Number of experimental data
$r$	Reactor radius, $m$
$R$	Reactor radius, $m$
$R_g$	Gas constant, $J/(K mol)$
$T$	Temperature, $K$
$T_{feed}$	Temperature of the feed, $K$
$T_{ref}$	Reference temperature (473 K), $K$
$T_w$	Temperature at the wall, $K$
$U$	Overall heat transfer coefficient, $W/(m^2 K)$
$u$	Fluid velocity, $m/s$
$\bar{u}$	Average flow velocity, $m/s$
$u_{max}$	Maximum fluid velocity, $m/s$
$V_{mix}$	Molar volume of the mixture, $m^3/mol$
$V$	Volumetric flowrate, $m^3/s$
$X_{ED}$	ethylene oxide average conversion
$X_{ED,CALC}$	average calculated ethylene oxide conversion
$X_{EO}$	ethylene oxide conversion
$X_{ED,EXP}$	experimental ethylene oxide conversion
$x_i$	reactant conversion
$y$	radial coordinate
$z$	axial coordinate
<b>Greek Letters</b>	
$\Delta_r H$	Reaction enthalpy, $J/mol$
$\epsilon_O$	Feed ethylene oxide/octanol molar ratio
$\eta_{ED}$	Ethylene oxide viscosity, $Pa s$
$\eta_i$	Viscosity of component $i$ , $Pa s$
$\eta_{mix}$	Viscosity of the mixture, $Pa s$
$\eta_{oligomer}$	Oligomer viscosity, $Pa s$
$\theta$	Dimensionless time
$\lambda$	Dimensionless reactor radius coordinate

$\lambda_{mix}$	Heat conductivities of the mixture, $W m/K$
$\lambda_{EO}$	Ethylene oxide heat conductivity, $W m/K$
$\lambda_O$	Octanol heat conductivity, $W m/K$
$\nu_i$	Stoichiometric coefficient of component $i$
$\rho_{mix}$	Density of the mixture, $kg/m^3$
$\rho_{mix,0}$	Density of the mixture fed to the reactor, $kg/m^3$
$\rho_{prod}$	Density of the products, $kg/m^3$
$\tau$	Residence time, $s$
$\chi$	Dimensionless reactor axial coordinate

## Abbreviations

A	Generic reactant
B	Generic product
CALC	Calculated
cat	Catalyst
ELR	Enhanced Loop Reactor
EO	Ethylene Oxide
EXP	Experimental
O	Octanol
STLR	Spray Tower Loop Reactor
VLR	Venturi Loop Reactor

the reactor at a certain time; (ii) the productivity of the system is quite low for the various steps involved in a semi-batch process; (iii) the safety of the overall process is not optimal, fact due to possible epoxide accumulations that could lead easily to runaways reactions.

A possible solution that could allow overcoming the mentioned drawbacks is the adoption of a continuous reactor that can be properly designed for the achievement of the desired alkoxylation degree. In the scientific and patent literature both traditional tubular reactors and more innovative reactor configurations are proposed as useful solutions. Very recently, several reactor technologies were described and compared dealing with the evolution of fed-batch technology (Di Serio et al., 2021), analyzing the performances of three main fed-batch reactors, namely Venturi Loop Reactor (VLR), Spray Tower Loop Reactor (STLR) and Enhanced Loop Reactor (ELR). Even if the operation is still semi-continuous, the three systems warrant good productivity and low risks in the operation.

Continuous reactors for alkoxylation were reviewed recently (Tesser et al., 2020), highlighting the possibility to use microreactors to ensure good productivity and good control. Microreactors are particularly suitable for very exothermic reactions, i.e., alkoxylation, involving also multiphase reactions, thanks to the high heat and mass transfer exchange. Such reactors were tested in the literature, in the case of 1-octanol ethoxylation promoted by KOH as a catalyst, showing good performances in terms of reaction conversion and thermal control, allowing them to work at relatively high temperatures (240 °C) (Rupp et al., 2013a,b). Even though in the adopted experimental conditions it was demonstrated that the flow pattern is laminar (Hermann et al., 2016), the collected data are normally simulated with a plug-flow model approach (Rupp et al., 2013a). This condition can be easily checked considering that the experiments were performed at low Reynolds numbers ( $< 10$ ). The use of a plug-flow model approximation certainly leads to a non-rigorous determination of the parameters related to the intrinsic kinetics of the reaction. For this purpose, in the present work, a



laminar-flow model was developed and implemented. The model was firstly tested with a dedicated parametric investigation to check its performance and predicting power. Further, the model was applied to describe the mentioned kinetic data collected using a microreactor, comparing the obtained parameters with the ones reported in the literature (Amaral and Giudici, 2011; Di Serio et al., 2002, 1994; Hall and Agrawal, 1990; Rupp et al., 2013a; Santacesaria et al., 2018, 1992, 1990) obtained from fed-batch studies, to verify if the obtained parameters can be considered reliable.

The developed model was used to design the right configuration of a continuous reactor that would allow to work with high productivity avoiding, in contempt, run-away conditions. Milli and microreactors could be two valid alternatives to be tested. Thus, the performance of the laminar flow configuration (suitable for micro reactors) was compared with the ideal plug flow reactor fluid-dynamics (more suitable for milli reactors), in order to find the best configuration for the ethoxylation reaction.

## 2. Methods

### 2.1. Reactor model

The experimental apparatus used in Rupp et al. paper (Rupp et al., 2013a) consists of a microreactor working under pressure, to warrant the existence of a homogeneous liquid phase, characterized by a laminar flow regime. The authors conducted 1-octanol ethoxylation in the presence of KOH as a homogeneous catalyst.

The development of the design equation of a steady-state laminar flow reactor model (LFR) implies the definition and solution of material balance on the microstructured reactor, comprising the following terms:

- Flow term: related to the convection of reactants/products by laminar flow profile.
- Diffusive term: representative of the transport of matter by the concentration gradient along the radial coordinate.
- Kinetic term: represented by the reaction rate, indicating the generation/consumption term.

Therefore, the equation takes the form reported in Eq. 1.

$$u(y) \frac{\partial c_i(z, y)}{\partial z} = D_i \left( \frac{\partial^2 c_i(z, y)}{\partial y^2} + \frac{1}{y} \frac{\partial c_i(z, y)}{\partial y} \right) + v_i r(z, y) \quad (1)$$

With,  $u(y)$  axial fluid velocity [m/s] at different radial positions,  $c_i$  concentration of specie  $i$  [mol/m<sup>3</sup>],  $z$  axial coordinate [m],  $D_i$  molecular diffusivity of component  $i$  [m<sup>2</sup>/s],  $y$  radial coordinate [m],  $v_i$  stoichiometric coefficient of component  $i$  and  $r$  reaction rate [mol/(m<sup>3</sup> s)].

Being the flow laminar, the radial velocity profile assumes a parabolic trend with the radial coordinate,  $y$ , which can be described by Eq. 2.

$$u(y) = u_{\max} \left[ 1 - \left( \frac{y}{R} \right)^2 \right] = 2u \left[ 1 - \left( \frac{y}{R} \right)^2 \right] \quad (2)$$

The mass balance reported in Eq. 1 can be written in a more compact and practical form adopting mathematical rearrangements.

For instance, axial coordinate  $z$  can be converted to residence time  $\tau$ :

$$\tau = \frac{V}{V} = \frac{LA}{V} = \frac{L}{u} \quad (3)$$

with  $A$  cross-sectional area [m<sup>2</sup>],  $L$  the reactor length [m],  $V$  the reactor volume [m<sup>3</sup>],  $V$  the volumetric flow rate [m<sup>3</sup>/s], and  $u$  the average flow velocity. Thus,

$$\tau = \frac{z}{u} \quad (4)$$

Deriving Eq. 4, it is possible to obtain:

$$\partial z = u \partial \tau \quad (5)$$

Concentration can be expressed in terms of reactant conversion starting from its definition:

$$c_i = c_{i,0}(1 - x_i) \quad (6)$$

With,  $c_{i,0}$  the feed concentration of component  $i$ .

Deriving Eq. 6, it is possible to obtain:

$$\partial c_i = \partial(c_{i,0}(1 - x_i)) = -c_{i,0} \partial x_i = -c_{i,0} \partial x_i \quad (7)$$

Finally, it can be possible to introduce a dimensionless reactor radial coordinate,  $\lambda$ :

$$\lambda = \frac{y}{R} \quad (8)$$

Deriving Eq. 8 it is possible to obtain:

$$\partial y = R \partial \lambda \quad (9)$$

Thus, the velocity profile becomes:

$$u(y) = 2u[1 - \lambda^2] \quad (10)$$

Inserting Eqs. 5, 7, 9 and 10 in Eq. 1, it is possible to obtain the following mass balance equation:

$$-2u(1 - \lambda^2) \frac{c_{i,0} \partial x_i}{u} = -D_i \left( \frac{c_{i,0} \partial^2 x_i}{R^2 \partial \lambda^2} + \frac{c_{i,0} 1 \partial x_i}{R^2 \lambda \partial \lambda} \right) + v_i r \quad (11)$$

Rearranging, the following form can be derived:

$$2(1 - \lambda^2) \frac{\partial x_i}{\partial \tau} = \frac{D_i}{R^2} \left( \frac{\partial^2 x_i}{\partial \lambda^2} + \frac{1}{\lambda} \frac{\partial x_i}{\partial \lambda} \right) - v_i \frac{r}{c_{i,0}} \quad (12)$$

By fixing an average reaction time  $\tau = u/L$ , it is possible to introduce a dimensionless reaction time  $\theta = \tau/\tau$ , obtaining the following equation, Eq. 13.

$$2(1 - \lambda^2) \frac{\partial x_i}{\partial \theta} = \frac{D_i \tau}{R^2} \left( \frac{\partial^2 x_i}{\partial \lambda^2} + \frac{1}{\lambda} \frac{\partial x_i}{\partial \lambda} \right) - v_i \frac{r \tau}{c_{i,0}} \quad (13)$$

The reactant conversion, more specifically  $x_{EO}$ , shows a parabolic trend with the reactor radius coordinate. For instance, depending on the radial position, different flow velocities are expected due to Eq. 2: at the reactor center, the liquid flow shows the highest velocity, thus a low conversion, while at the pipe radius, the fluid velocity approaches zero, leading to a higher conversion.

The following boundary and initial conditions were imposed to solve the partial differential equation system.

$$x_{i,0}(y, \lambda) = 0 \quad (14)$$

$$\frac{\partial x_i}{\partial \lambda} \Big|_{\lambda=0} = 0 \quad (15)$$

$$\frac{\partial x_i}{\partial \lambda} \Big|_{\lambda=1} = 0 \quad (16)$$

For instance, at  $\theta = 0$ , the ethylene oxide conversion was assumed zero. Both at the reactor center and walls, the first derivative of conversion along the dimensionless radius coordinate was considered zero, for symmetry reasons.

As the experimental data collected at the pipe outlet represent an average of the ethylene oxide conversion profile along the radius, an average conversion must be defined, using the integral average approach, Eq. 17.

$$\bar{x}_{EO} = \frac{\int_0^1 x_{EO}(\lambda) u(\lambda) 2\pi\lambda d\lambda}{\int_0^1 u(\lambda) 2\pi\lambda d\lambda} \tag{17}$$

By introducing Eq. 2 in Eq. 17, the expression reported in Eq. 18 can be obtained.

$$\bar{x}_{EO} = \frac{\int_0^1 x_{EO}(\lambda) 2(1 - \lambda^2) 2\pi\lambda d\lambda}{\int_0^1 2(1 - \lambda^2) 2\pi\lambda d\lambda} \tag{18}$$

As revealed, the average ethylene oxide conversion is independent of the average fluid velocity.

The reaction rate was fixed as a first-order equation with respect to both ethylene oxide and catalyst concentration, as reported in the literature (Di Serio et al., 2002, 1994; Rupp et al., 2013a), Eq. 19.

$$r = k_{EO} C_{cat} \tag{19}$$

Where, the catalyst and the feed ethylene oxide concentrations were calculated starting from the definition of  $\alpha_0$  and  $K$ , representing respectively the feed ethylene oxide/octanol molar ratio and the catalyst/octanol molar ratio, as in Eqs. 20, 21.

$$C_{EO,0} = \frac{1}{M_{EO} + M_{O}/\alpha_0} \rho_{mix,0} \tag{20}$$

$$C_{cat} = \frac{K/\alpha_0}{M_{EO} + M_{O}/\alpha_0} \rho_{mix,0} \tag{21}$$

The kinetic constant dependence with temperature was taken into consideration by imposing the modified Arrhenius equation, Eq. 22.

$$k = k_{ref} \exp\left(-\frac{E_a}{R_3} \left(\frac{1}{T} - \frac{1}{T_{ref}}\right)\right) \tag{22}$$

Where,  $T_{ref} = 473$  K.

Temperature variation was included by solving simultaneously the dimensionless energy balance equation reported in Eq. 23. The mathematical derivation is totally symmetrical compared to the mass balance, thus not reported here.

$$2(1 - \lambda^2) \frac{\partial T}{\partial r} = \frac{1}{R^2} \left( \frac{\lambda_{mix}}{c_{p,mix} \rho_{mix}} + D_{EO} \right) \left( \frac{\partial^2 T}{\partial \lambda^2} + \frac{1}{\lambda} \frac{\partial T}{\partial \lambda} \right) - \frac{\Delta_r H r}{c_{p,mix} \rho_{mix}} \tag{23}$$

Where the reaction enthalpy value was equal to  $\Delta_r H = -92,000$  J/mol (di Serio et al., 2021). The initial and boundary conditions needed to solve Eq. 23 are reported in Eqs. 24–26.

$$T_0(\forall \lambda) = T_{feed} \tag{24}$$

$$\left. \frac{\partial T}{\partial \lambda} \right|_{\lambda=0} = 0 \tag{25}$$

$$T|_{\lambda=1} = T_w \tag{26}$$

For instance, at  $r = 0$ , the temperature was assumed to be constant at a set value. At the reactor center, the first derivative of temperature along the dimensionless radius coordinate was considered zero, for symmetry reasons, while the temperature at the reactor walls was considered

**Table 1 – Viscosity coefficients of ethylene oxide and 1-octanol.**

Component	$A_i$	$E_i$	$C_i$
Ethylene oxide	-8.521	634.2	-0.3314
1-octanol	-50.674	4725.1	5.2499

constant at a fixed value, as milli/micro reactors are characterized by high heat transfer efficiency.

**2.2. Physicochemical properties**

Several physicochemical properties are needed to be implemented within the model, in particular liquid density and viscosity.

Liquid density dependency with temperature ( $T$ ), the initial ethylene oxide/substrate ratio ( $\alpha_0$ ) and ethylene oxide conversion ( $x_{EO}$ ) was taken from the literature (Rupp et al., 2013a). Rupp et al. precisely determined the mentioned functionalities, by collecting experimental data and proposing semi-empirical equations, listed below as used in the model, Eqs. 27, 28.

$$\rho_{prod} = 1062 - 231.2 (0.82^{x_{EO}/\alpha_0}) \tag{27}$$

$$\rho_{mix} = \rho_{prod} + 8.69(1 - x_{EO})\alpha_0 - 0.36(1 - x_{EO})\alpha_0^2 - 0.10(T - 273) - 0.0021(T - 273)^2 - 0.101(T - 273)(1 - x_{EO})\alpha_0 \tag{28}$$

Ethylene oxide and 1-octanol liquid viscosities were determined using ChemCAD database (Chemstations, 2023), adopting the expression in Eq. 29.

$$\ln(\eta_i) = (A_i + B_i/T + C_i \ln(T)) \tag{29}$$

The coefficients for ethylene oxide and 1-octanol are listed in Table 1.

Both specific heat and heat conductivities of the mixtures were calculated starting from the related values of pure ethylene oxide and alcohol. Both were taken as a function of the temperature from ChemCAD database (Chemstations, 2023), Eqs. 30–33.

$$c_{p,EO} = 1.45 \cdot 10^3 - 758.87 T + 2.8261 T^2 - 0.00306 T^3 \tag{30}$$

$$c_{p,O} = 5.14 \cdot 10^3 - 54970 T + 228.72 T^2 - 0.40331 T^3 + 0.00025844 T^4 \tag{31}$$

$$\lambda_{EO} = 0.26957 - 0.0003984 T \tag{32}$$

$$\lambda_O = 0.220444 - 0.00018378 T \tag{33}$$

Both the specific heat and heat conductivity of the mixture were calculated as weighted average of the pure components, Eqs. 34–35.

**Table 2 – Parameters adopted for the sensitivity study of the laminar flow reactor model.**

Parameter	Value range	Units
$R$	$1.25 \cdot 10^{-4} - 2.5 \cdot 10^{-4}$	m
$D_A$	$1 \cdot 10^{-9} - 1 \cdot 10^{-12}$	m <sup>2</sup> /s
$C_{A,0}$	0.5 – 1.5	mol/m <sup>3</sup>
$C_{R,0}$	0	mol/m <sup>3</sup>
$k_A$	0.01 – 0.05	s <sup>-1</sup>



**Table 3 – Results of the parameter estimation activity.**

	Value	Units
$E_a$	$(81.1 \pm 0.8) \cdot 10^3$	J/mol
$k_{ef} (T_{ref}=473\text{ K})$	$(1.2 \pm 0.1) \cdot 10^{-3}$	$\text{m}^3/(\text{mol s})$

$$c_{p,max} = c_{p,ED} \frac{c_{O,0}}{c_{ED,0} + c_{O,0}} \frac{1000}{M_{ED}} + c_{p,O} \frac{c_{O,0}}{c_{O,0} + c_{O,0}} \frac{1000}{M_O} \quad (34)$$

$$\lambda_{mix} = \lambda_{ED} \frac{c_{ED,0}}{c_{ED,0} + c_{O,0}} + \lambda_O \frac{c_{O,0}}{c_{ED,0} + c_{O,0}} \quad (35)$$

### 2.3. Simulation and parameter estimation activities

The partial differential equation (PDE) system describing the single liquid phase reactor was solved by adopting the *pdepe* function implemented in Matlab R2020a. Parameter estimations were conducted using *particleswarm* evolutionary minimization algorithm provided in Matlab, imposing the objective function calculation as follows, Eq. 36.

$$F_{obj} = \frac{1}{N_{data}} \sqrt{\sum_{i=1}^{N_{data}} \left( \frac{X_{ED,EXP} - X_{ED,CALC}}{X_{ED,EXP}} \right)^2} \quad (36)$$

## 2. Results and discussion

### 2.1. Sensitivity analysis

A sensitivity analysis was conducted to check the flexibility of the developed model, considering a generic reaction  $A \rightarrow B$ , fixing a first-order reaction kinetics, Eq. 37.

$$r = k_A c_A \quad (37)$$

In detail, the influence of several parameters on the reaction conversion was investigated by performing different simulations varying systematically the parameters. The parametric investigation was conducted in isothermal conditions. The adopted parameters, together with the range of investigations are reported in Table 2.

A typical conversion trend obtained in each simulation is reported in Fig. 1, where conversion is plotted vs the dimensionless reactor radial coordinate and the residence time, both as a contour plot (left) and as a parametric plot at different values of  $\lambda$  (right). This simulation was conducted fixing  $D_A = 1 \cdot 10^{-11} \text{ m}^2/\text{s}$ ,  $k = 0.05 \text{ s}^{-1}$ ,  $R = 1.24 \cdot 10^{-4} \text{ m}$  and  $c_{A,0} = 1 \text{ mol/m}^3$ .

The contour plot reported in Fig. 1(left) shows high conversion gradients, as a strong difference in conversion between the reactor center and wall is present, at each level of residence time. The higher the conversion, the steeper the gradients. In the proximity of the reactor wall, conversion is almost always near unity, as the flow velocity is the lowest possible while at the pipe center, the lower conversion is

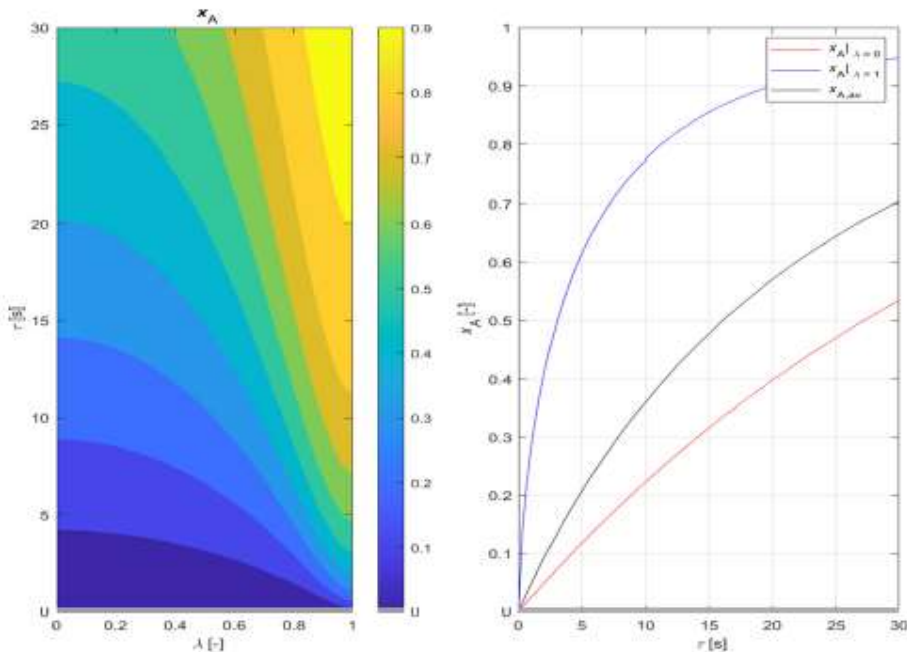


Fig. 1 – Reactant conversion as a function of the residence time and the dimensionless reactor radial coordinate: (left) contour plot; (right) plots at the reactor center, wall, and average conversion. Simulation conditions:  $D_A = 1 \cdot 10^{-11} \text{ m}^2/\text{s}$ ,  $k = 0.05 \text{ s}^{-1}$ ,  $R = 1.24 \cdot 10^{-4} \text{ m}$  and  $c_{A,0} = 1 \text{ mol/m}^3$ .

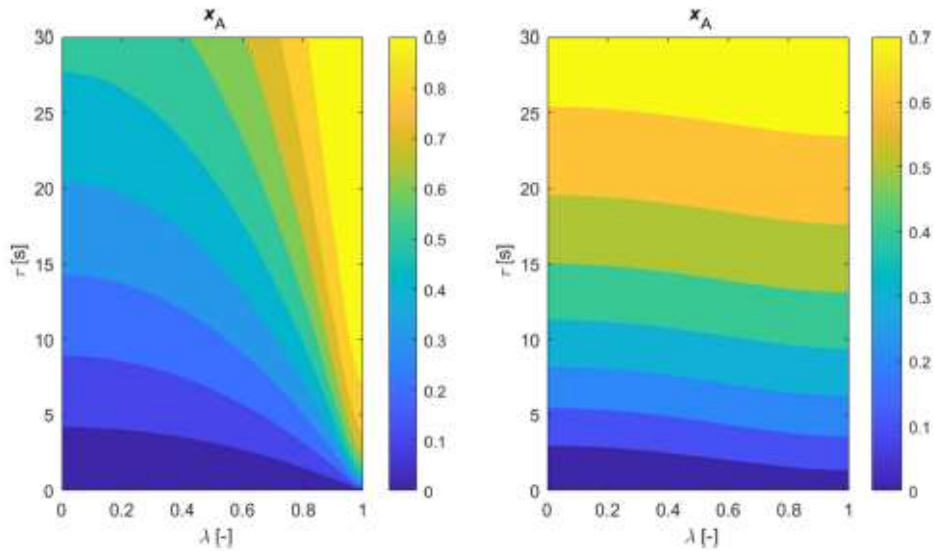


Fig. 2 – Reactant conversion as a function of the residence time and the dimensionless reactor radial coordinate, fixing  $k = 0.05 \text{ s}^{-1}$ ,  $R = 1.24 \cdot 10^{-4} \text{ m}$  and  $c_{A,0} = 1 \text{ mol/m}^3$ , and varying the molecular diffusivity value: (left)  $D_A = 1 \cdot 10^{-12} \text{ m}^2/\text{s}$ ; (right)  $D_A = 1 \cdot 10^{-9} \text{ m}^2/\text{s}$ .

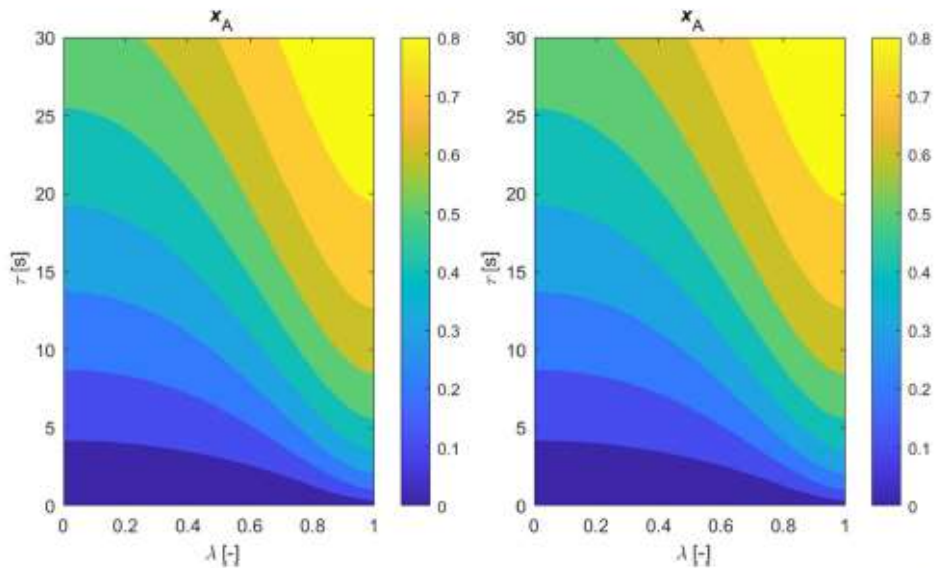


Fig. 3 – Contour plots representing the conversion vs the residence time and the dimensionless reactor radial coordinate, fixing  $k = 0.05 \text{ s}^{-1}$ ,  $D_A = 1 \cdot 10^{-11} \text{ m}^2/\text{s}$  and  $c_{A,0} = 1 \text{ mol/m}^3$ , and varying the pipe radius: (left)  $R = 6.25 \cdot 10^{-5} \text{ m}$ ; (right)  $R = 2.50 \cdot 10^{-4} \text{ m}$ .

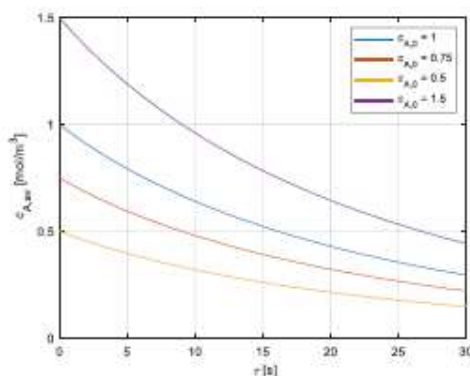


Fig. 4 – Average reactant concentration profiles vs residence time, fixing different feed concentrations.  $D_A = 1 \cdot 10^{-11} \text{ m}^2/\text{s}$ ,  $k = 0.05 \text{ s}^{-1}$ , and  $R = 1.24 \cdot 10^{-4} \text{ m}$ .

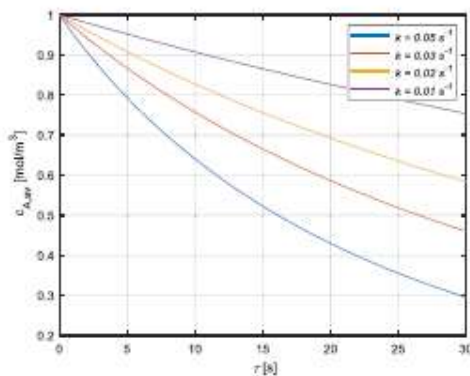


Fig. 5 – Average reactant concentration as a function of the residence time, varying systematically the kinetic constant value.  $D_A = 1 \cdot 10^{-11} \text{ m}^2/\text{s}$ ,  $R = 1.24 \cdot 10^{-4} \text{ m}$  and  $c_{A,0} = 1 \text{ mol/m}^3$ .

achieved. A better comparison can be visible in Fig. 1(right), where at the reactor wall a higher conversion is achieved higher compared with the one reached at the reactor center.

The average conversion calculated with Eq. 20 is plotted in Fig. 1(right), resulting in a conversion between the once calculated at the reactor radial coordinate extremes.

By reducing the value of the molecular diffusivity to  $D_A = 1 \cdot 10^{-12} \text{ m}^2/\text{s}$ , the gradients become steeper, as revealed in Fig. 2(left), leading to average conversion values closer to the ones obtained at the reactor center.

An opposite behavior is achieved when increasing the molecular diffusivity to  $D_A = 1 \cdot 10^{-9} \text{ m}^2/\text{s}$  (Fig. 2(right)), obtaining flatter profiles.

The influence of the reactor radius on the conversion gradients was investigated, by conducting different simulations, fixing the following parameters:  $D_A = 1 \cdot 10^{-11} \text{ m}^2/\text{s}$ ,  $k = 0.05 \text{ s}^{-1}$ , and  $c_{A,0} = 1 \text{ mol/m}^3$ . The results are reported in Fig. 3.

As revealed, by increasing the reactor radius, conversion gradients become steeper, while reducing it the conversion profiles are flatter, observation in line with theory as larger pipe leads to a longer diffusion path.

The feed concentration variation led to no change in conversion, as the reaction kinetics was fixed to a first-order equation. Therefore, the average concentration of the reactant along the residence time shows the trends reported in Fig. 4, revealing a faster consumption when a higher feed concentration is used. Simulations were conducted fixing  $D_A = 1 \cdot 10^{-11} \text{ m}^2/\text{s}$ ,  $k = 0.05 \text{ s}^{-1}$ , and  $R = 1.24 \cdot 10^{-4} \text{ m}$ .

Finally, the influence of the kinetic constant was checked on the reaction conversion, fixing  $D_A = 1 \cdot 10^{-11} \text{ m}^2/\text{s}$ ,  $R = 1.24 \cdot 10^{-4} \text{ m}$  and  $c_{A,0} = 1 \text{ mol/m}^3$ . The results reported in Fig. 5, show a logical trend, showing an increase in activity when the kinetic constant is higher.

## 2.2. Viscosity and density computations

As the model showed high flexibility, it was used to elaborate the experimental data collected in the laminar flow micro-reactor used for 1-octanol ethoxylation with KOH. For this purpose, molecular diffusivity must be estimated as one of the key parameters in correctly predicting the concentration gradients along the pipe radius.

For this purpose, ethylene oxide diffusivity was determined using the Scheibel correlation (Reid et al., 1987), Eq. 38.

$$D_{EO} = \frac{D_{EO}^* T}{\eta_{mix} V_{mix}^{0.7}} \quad (38)$$

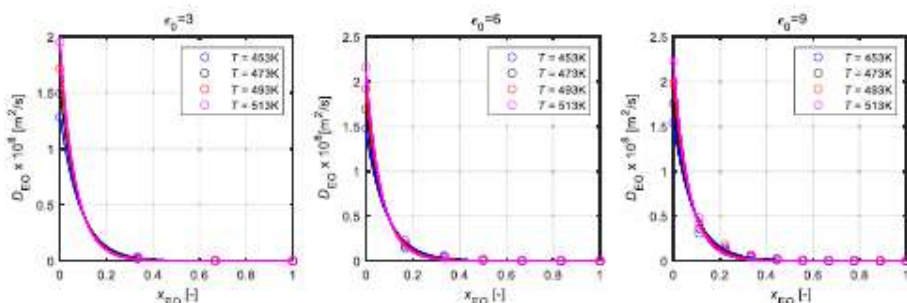


Fig. 6 – Evolution of ethylene oxide molecular diffusivity as a function of temperature, ethylene oxide conversion and initial ethylene oxide/1-octanol molar ratio. Symbols represent the calculated values with Eq. 38, lines the fitted values using Eqs. 43 and 44.



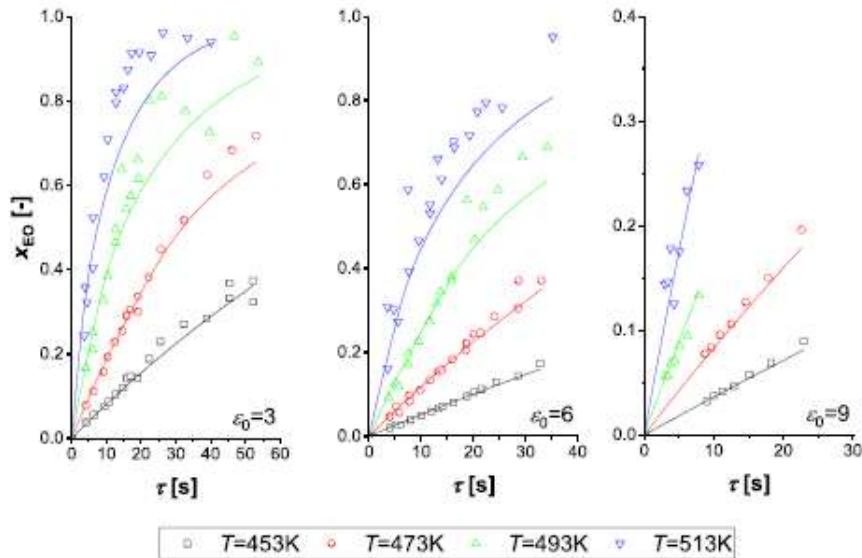


Fig. 7 – Data fit for experiments where both residence time and initial ethylene oxide/1-octanol molar ratio are varied as a function of temperature, in a range between 453 and 513 K. Symbols represent the experimental data, lines the calculated values.

Where,  $a_{ED} = 1.751 \cdot 10^{-16}$ .

The Scheibel correlation shows the dependence of the diffusion coefficient on the absolute temperature. Therefore, both the viscosity and the molar volume of the liquid mixture must be known. During the ethoxylation reaction, ethylene oxide is consumed, and oligomers are formed, consisting of chains of ethylene oxide added to one alcoholic molecule (i.e., 1-octanol). Thus, both the viscosity and the molar volumes of the liquid mixture are a natural function of the conversion degree.

Moreover, depending on the feed ethylene oxide/substrate molar ratio, different oligomers distribution can be obtained.

The molar volume can be easily calculated from the density liquid mixture, which was experimentally measured by Rupp et al. (2013a), obtaining a function of both  $x_{ED}$ ,  $T$  and  $\epsilon_0$ , using Eq. 39.

$$V_{mix} = \frac{M_{mix}}{\rho_{mix}} \tag{39}$$

With, the molecular weight of the mixture is defined as a function of the ethylene oxide conversion degree and the feed ethylene oxide/1-octanol molar ratio, as in Eq. 40.

$$M_{mix} = M_O + \epsilon_0 X_{ED} M_{EO} \tag{40}$$

The liquid mixture viscosity was calculated by weighting the ethylene oxide and the oligomer viscosity, by respectively the ethylene oxide conversion and the related complementary to one.

$$\ln(\eta_{mix}) = \ln(\eta_{EO})X_{ED} + \ln(\eta_{oligomer})(1 - X_{ED}) \tag{41}$$

The oligomer's viscosity was calculated using the Orrick and Erbar method (Reid et al., 1987), using the mixture density and molecular weight above mentioned, Eq. 42.

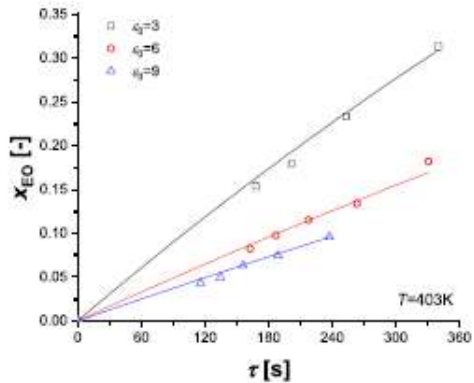


Fig. 8 – Data fit for experiments where both residence time and initial ethylene oxide/1-octanol molar ratio are varied at 403 K. Symbols represent the experimental data, lines the calculated values.

$$\ln(\eta_{oligomer}) = (A_{oligomer} + B_{oligomer}/T) + \ln(\rho_{mix} M_{mix}) \tag{42}$$

The correlation was tested for 1-octanol, obtaining less than 1 % deviation with the data retrieved from ChemCAD database (Chemstations, 2023).

To simplify the mathematical treatment, data were simulated varying both  $T$  and  $\epsilon_0$ , first at zero conversion, then varying the ethylene oxide conversion. The results are reported in Fig. 6, revealing a strong dependency of the diffusion coefficient with the conversion degree, as the viscosity of the product increases with conversion.

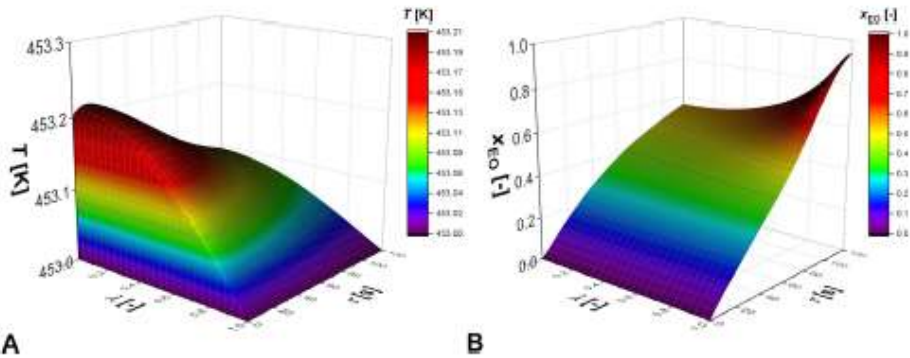


Fig. 9 - Temperature and EO conversion trends along the residence time and the dimensionless radial coordinate, fixing  $\epsilon_0 = 3$ ,  $K = 0.0066$  mol/mol,  $T_{\text{feed}} = T_w = 453$  K.

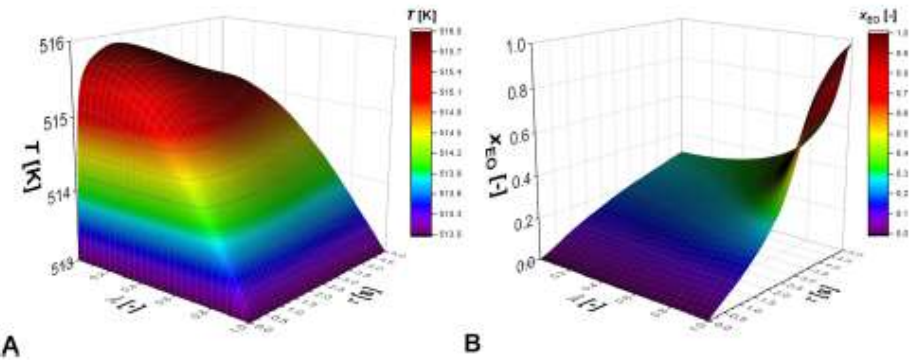


Fig. 10 - Temperature and EO conversion trends along the residence time and the dimensionless radial coordinate, fixing  $\epsilon_0 = 3$ ,  $K = 0.0066$  mol/mol,  $T_{\text{feed}} = T_w = 513$  K.

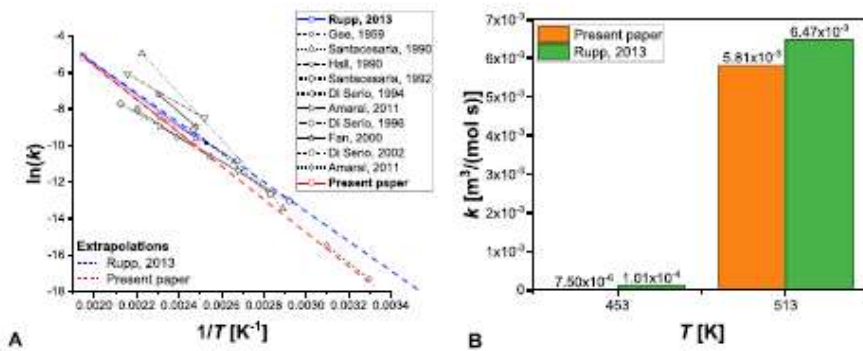


Fig. 11 - A. Comparison between the Arrhenius plot of different papers. B. Comparison between the kinetic constants obtained in the present paper and by Rupp et al., 2013.

The data calculated using Eq. 38 were fitted to introduce in the model a simpler equation, obtaining the agreements reported in Fig. 6 and the coefficients reported in Eqs. 43 and 44.

$$D_{EO,0} = (-8.32 \cdot 10^{-9} + 377 \cdot 10^{-12} r_0) + (111 \cdot 10^{-12} + 307 \cdot 10^{-15} r_0) T \quad (43)$$

$$D_{EO} = D_{EO,0} \exp(-67.75 \cdot 10^{-3} T x_{EO}) \quad (44)$$

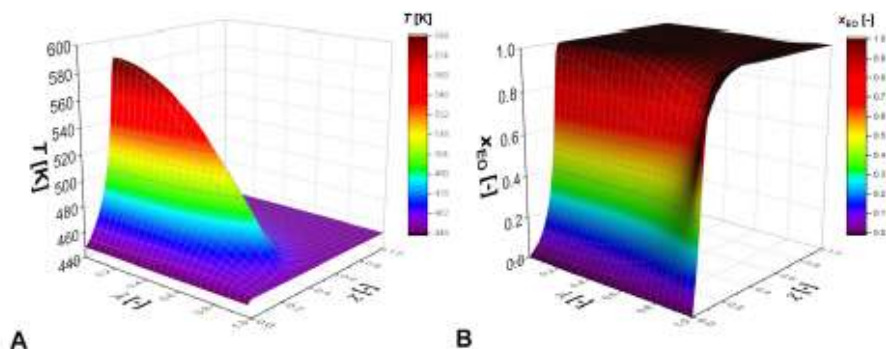


Fig. 14 – Temperature and ethylene oxide conversion trends along the dimensionless axial coordinate and the dimensionless radial coordinate for a reactor characterized by 9.0 mm inner diameter, imposing  $T_{\text{feed}} = T_w = 443$  K,  $\epsilon_0 = 1$ ,  $K = 0.001$  mol/mol.

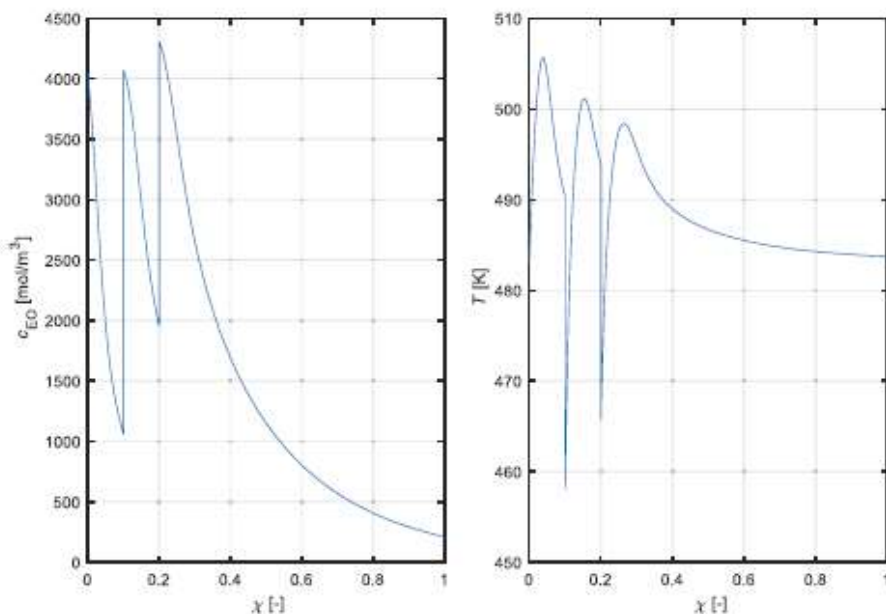


Fig. 15 – EO concentration and temperature profiles for a reactor working at  $T_{\text{feed}} = T_w = 483$  K,  $u = 0.05$  m/s,  $\epsilon_0 = 3$ , catalyst loading of  $K = 0.001$  mol/mol, reactor diameter of 9 mm and length of 50 m.

The increase in tube diameter could improve the productivity, but it could lead to a hot spot for the lowering of heat transfer efficiency. Thus, simulations were conducted using larger reactors, characterized by an internal diameter of 9 mm (Fig. 13), imposing  $T_{\text{feed}} = 453$  K,  $\epsilon_0 = 3$ ,  $K = 0.001$  mol/mol,  $L = 50$  m,  $u = 0.05$  m/s (Reynolds number < 3000). Several simulations were conducted by lowering the catalyst load, but the system was always characterized by a runaway behavior.

As revealed, high-temperature gradients are expected to occur when the diffusion path increases, leading to possible runaway risks.

Finally, an additional simulation was conducted simulating the performance of the system obtainable adopting always an inner diameter of 9 mm, thus simulating an industrial pipe, but with a lower EO feed ( $\epsilon_0 = 1$ ), assuming to add subsequently ethylene oxide at different reactors length (Fig. 14).



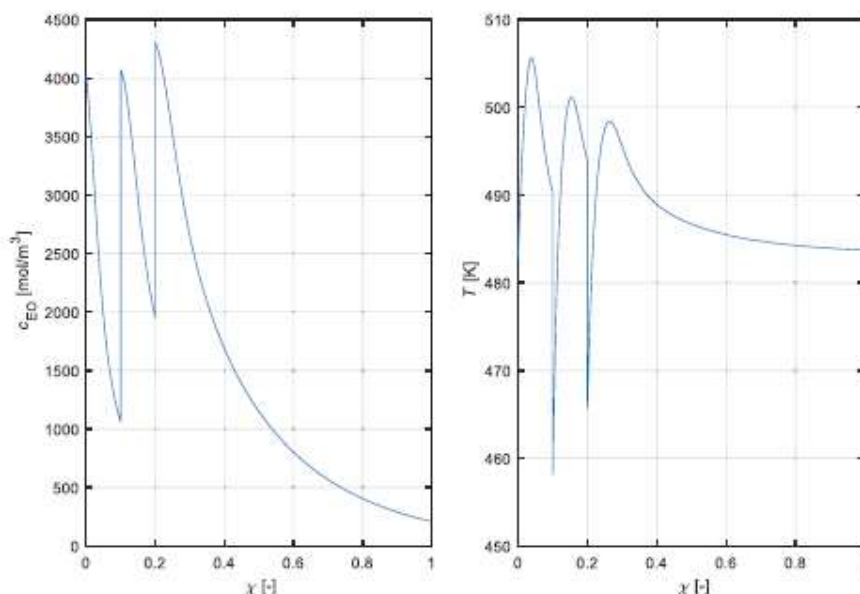


Fig. 16 – EO concentration and temperature profiles for a reactor working at  $T_{feed} = T_w = 483$  K,  $u = 0.05$  m/s, catalyst loading of  $K = 0.001$  mol/mol, reactor diameter of 9 mm and length of 50 m. Ethylene oxide feed is split into three streams, at 0, 10 % and 20 % of the pipe.

As revealed, also in this case the system is in runaway conditions.

#### 2.5. Simulation of reactors working in plug-flow regimes

A plug-flow model was implemented to simulate reactors working in conditions near to plug-flow conditions. The mass and energy balance equations adopted are reported in Eqs. 45 and 46.

$$\frac{u}{L} \frac{\partial c_{EO}}{\partial \chi} = \eta_1 r \quad (45)$$

$$\frac{u}{L} \frac{\partial T}{\partial \chi} = \frac{\Delta H r + UA_s(T - T_w)}{c_{p,mix} \rho_{mix}} \quad (46)$$

As revealed, the only unknown parameter of the model is the overall heat transfer coefficient ( $U$ ). To have an order of magnitude for a classical industrial pipe (9 mm internal diameter), data from the literature were taken to estimate the order of magnitude of this coefficient. Umbach reported the temperature profile along the axial coordinate for a coiled tube reactor characterized by a residence time of 25 s, a reactor length of 12.5 m, and a diameter of 9 mm, working with a jacket temperature range between 185 and 235 °C (Umbach and Stein, 1971). The authors reported that by working with  $\epsilon_0 = 1$  and a catalyst loading of  $K = 0.001$  mol/mol, a maximum temperature peak of 280 °C was recorded.

The developed mode was applied, estimating  $U = 0.4$  kW/(m<sup>2</sup> K), a value in line with the order of magnitude reported in the literature, being between 0.2 and 1.0 kW/(m<sup>2</sup> K) (Bell, 1978).

In this way, the parameter was fixed, and several simulations were conducted, imposing  $\epsilon_0 = 3$ , a pipe diameter of

9 mm, a feed fluid velocity of 0.05 m/s (Reynolds number = 90,000) and a catalyst loading of  $K = 0.001$  mol/mol, working with a feed temperature of 483 K. The length of the pipe was fixed at  $L = 50$  m. The result of the simulation is reported in Fig. 15.

As revealed, the temperature increase cannot be considered acceptable, thus, the EO feed was divided into three points, feeding  $\epsilon_0 = 1$  at the entrance of the pipe, and injecting other two equivalents in terms of ethylene oxide content at 10% and 20% of the pipe. Ethylene oxide was fed at room temperature in an adiabatic mixer. The results shown in Fig. 16 clearly demonstrate that it is possible to work at high conversion in safe conditions, the obtained productivity was calculated to be about 35,000 kg/(h m<sup>3</sup>), a value surely higher than the ones obtained using classical feed batch reactors (1000–300 kg/(h m<sup>3</sup>)) (Di Serio et al., 2005).

#### 4. Conclusions

In the present paper, a laminar flow reactor model was developed and successfully applied to describe the experimental data reported in the literature. The experimental data, derived from previous work, have been used to estimate reliable kinetic parameters. The exothermicity of the system was proved by additional simulations.

Larger reactors were considered, checking the possibility to conduct the operation at the industrial scale, demonstrating the high flexibility of the model and its power in predicting the alkoxylation system.

Final simulations were conducted using a plug flow model showing that it is possible to work at high conversion and in safe conditions by using a multi-feed approach, splitting the ethylene oxide stream in different positions of the pipe.

These results open the way to deeper experimental and theoretical investigation to arrive at a final industrial configuration for a continuous ethoxylation reactor.

### Funding

No funds were used to conduct the present study.

### Declaration of Competing Interest

The authors declare that they have no known competing financial interests or personal relationships that could have appeared to influence the work reported in this paper.

### Acknowledgments

Giusy Marotta is acknowledged for making the simulations for the parametric investigation.

### Author Contributions

Martino Di Serio and Vincenzo Russo wrote the original draft of the manuscript. The main conceptual ideas were drawn from the interactions between Martino Di Serio and Wiesław Hreczuch. The development of the artworks, the data elaboration and the formal analysis were conducted by Vincenzo Russo and Riccardo Tesser. The final draft was corrected by all the authors.

### References

- Amaral, G.M., Giudici, R., 2011. Kinetics and Modeling of Fatty Alcohol Ethoxylation in an Industrial Spray Loop Reactor. *Chem. Eng. Technol.* 34, 1635–1644. <https://doi.org/10.1002/CEAT.201100215>
- Bell, K., 1978. Estimate s & t exchanger design fast. Estimate s & t exchanger design fast.
- Chemstations, 2023. ChemCAD. v. 7.0 [WWW Document]. URL <https://www.chemstations.com/> (accessed 1.3.23).
- Hall, C.A., Agrawal, P.K., 1990. Separation of kinetics and mass-transfer in a batch alkoxylation reaction. *Can. J. Chem. Eng.* 68, 104–112. <https://doi.org/10.1002/CJCE.5450680113>
- Hermann, P.D., Cents, T., Klemm, E., Ziegenbalg, D., 2016. Simulation study of the ethoxylation of octanol in a microstructured reactor. *Ind. Eng. Chem. Res.* 55, 12675–12686. <https://doi.org/10.1021/acs.iecr.6b04110>
- Reid, R.C., Prausnitz, J.M., Poling, B.E., 1987. The properties of gases and liquids.
- Rupp, M., Ruback, W., Klemm, E., 2013a. Octanol ethoxylation in microchannels. *Chem. Eng. Process.: Process Intensif.* 74, 19–26. <https://doi.org/10.1016/j.cep.2013.09.012>
- Rupp, M., Ruback, W., Klemm, E., 2013b. Alcohol ethoxylation kinetics: Proton transfer influence on product distribution in microchannels. *Chem. Eng. Process.: Process Intensif.* 74, 187–192. <https://doi.org/10.1016/j.cep.2013.09.006>
- Rupp, M., Ruback, W., Klemm, E., 2013c. Octanol ethoxylation in microchannels. *Chem. Eng. Process.: Process Intensif.* 74, 19–26. <https://doi.org/10.1016/j.cep.2013.09.012>
- Santacesaria, E., di Serio, M., Lisi, L., Gelosa, G., 1990. Kinetics of nonylphenol polyethoxylation catalyzed by potassium hydroxide. *Ind. Eng. Chem. Fundam.* 29, 719–725.
- Santacesaria, E., Serio, M., di, Garaffa, R., Addino, G., 1992. Kinetics and mechanisms of fatty alcohol polyethoxylation. 1. The reaction catalyzed by potassium hydroxide. *Ind. Eng. Chem. Res.* 31, 2413–2418.
- Santacesaria, E., Tesser, R., di Serio, M., 2018. Polyethoxylation and polypropoxylation reactions: Kinetics, mass transfer and industrial reactor design. *Chin. J. Chem. Eng.* 26, 1235–1251. <https://doi.org/10.1016/j.cjche.2018.02.020>
- di Serio, M., di Martino, S., Santacesaria, E., 1994. Kinetics of fatty acids polyethoxylation. *Ind. Eng. Chem. Res.* 33, 509–514.
- di Serio, M., Tesser, R., Dimiccoli, A., Santacesaria, E., 2002. Kinetics of ethoxylation and propoxylation of ethylene glycol catalyzed by KOH. *Ind. Eng. Chem. Res.* 41, 5196–5206. <https://doi.org/10.1021/ie020082v>
- di Serio, M., Tesser, R., Santacesaria, E., 2005. Comparison of different reactor types used in the manufacture of ethoxylated, propoxylated products. *Ind. Eng. Chem. Res.* 44, 9482–9489. <https://doi.org/10.1021/ie0502234>
- di Serio, M., Russo, V., Santacesaria, E., Tesser, R., 2021. The evolution of the fed batch ethoxylation reactors to produce the non-ionic surfactants. *Front. Chem. Eng.* 3, 6. <https://doi.org/10.3389/FCENG.2021.644719>
- Tesser, R., Russo, V., Santacesaria, E., Hreczuch, W., di Serio, M., 2020. Alkoxylation for surfactant productions: toward the continuous reactors. *Front. Chem. Eng.* 2, 7. <https://doi.org/10.3389/FCENG.2020.00007>
- Umbach, W., Stein, W., 1971. Continuous alkoxylation process. *J. Am. Oil Chem. Soc.* 48, 394–397. <https://doi.org/10.1007/BF02637359>

Available online at [www.sciencedirect.com](http://www.sciencedirect.com)

Chemical Engineering Research and Design

journal homepage: [www.elsevier.com/locate/cherd](http://www.elsevier.com/locate/cherd)

IChemE

## Erratum



## Erratum to “Design of a continuous device for ethoxylation reaction: The choice between micro and milli scale” [Chem. Eng. Res. Des. 194 (2023) 550–562]

Vincenzo Russo<sup>a</sup>, Riccardo Tesser<sup>a,b</sup>, Wiesław Hreczuch<sup>c</sup>,  
Martino Di Serio<sup>a,d,\*</sup>

<sup>a</sup> Department of Chemical Sciences, University of Naples Federico II, 80126 Naples, Italy

<sup>b</sup> CIRCC, Consorzio Interuniversitario Reattività Chimica e Catalisi, 70126 Bari, Italy

<sup>c</sup> MEXEO, 47-200 Kędzierzyn-Koźle, Poland

<sup>d</sup> IROAST, Kumamoto University, 43201-6 Kumamoto, Japan

The publisher regrets that a typesetting error resulted in the duplication of the Fig. 16 in place of Fig. 15 in the published article.

The correct Fig. 15 is shown below.

The publisher would like to apologise for any inconvenience caused.

DOI of original article: <https://doi.org/10.1016/j.cherd.2023.04.051>

\* Corresponding author at: Department of Chemical Sciences, University of Naples Federico II, 80126 Naples, Italy.

E-mail address: [diserio@unina.it](mailto:diserio@unina.it) (M. Di Serio).

<https://doi.org/10.1016/j.cherd.2023.09.012>

0263-8762/© 2023 Institution of Chemical Engineers. Published by Elsevier Ltd. All rights reserved.

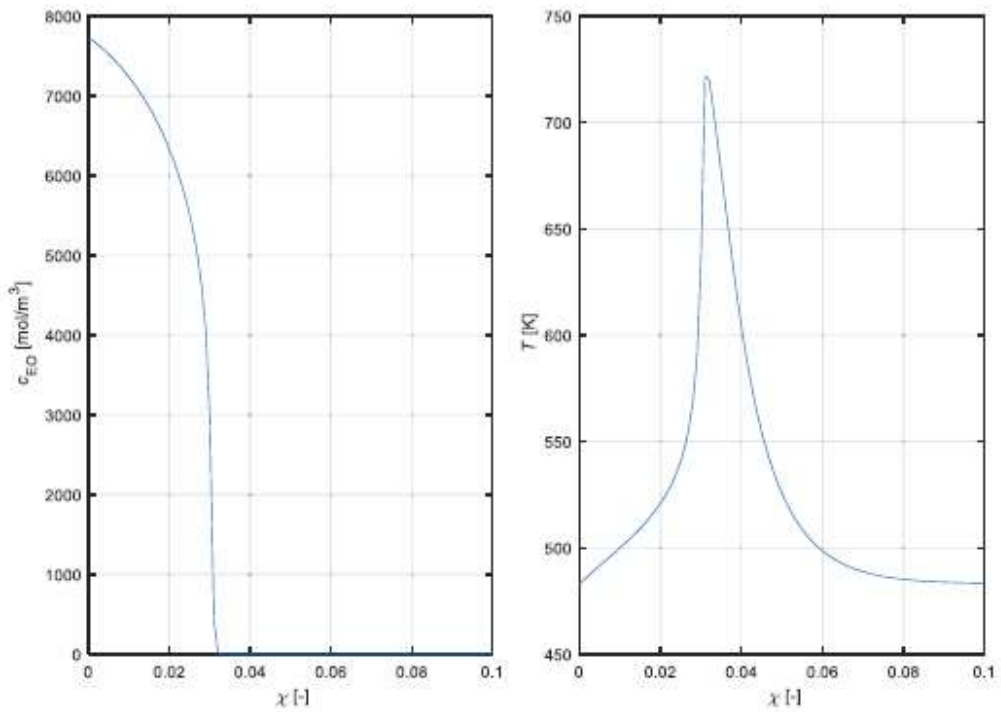


Fig. 15 - EO concentration and temperature profiles for a reactor working at  $T_{feed}=T_w=483$  K,  $u=0.05$  m/s,  $\epsilon_0=3$ , catalyst loading of  $K=0.001$  mol/mol, reactor diameter of 9 mm and length of 50 m.



## Articles 2-4. Frontiers Copyright Statement

[Terms and Conditions](#)

[Privacy Policy](#)

[Copyright Statement](#)

[Cookie Policy](#)

[Summary of Changes](#)

[Events Terms and Conditions](#)

# Frontiers Copyright Statement

Frontiers publishes its own journals (referred to here as **Frontiers Journals**) and journals owned by third parties (referred to here as **Hosted Journals**). When we refer to **Journals**, we include both Frontiers Journals and Hosted Journals.

In this Copyright Statement, **Websites** (with a capitalised W) refers to all Frontiers websites, including those of Hosted Journals. An **Owner** means Frontiers as owner of all Frontiers Journals, or the respective owner of a Hosted Journal.

All content included on these Websites (including Loop), such as text, graphics, logos, button icons, images, video/audio clips, downloads, data compilations and software, is the property of the person or entity who or which owned it prior to submission to Frontiers or to a Hosted Journal. If not owned by Frontiers or an Owner of a Hosted Journal, it is licensed to Frontiers Media SA ("Frontiers"), such Owner or its or their licensees and/or subcontractors.

The ownership of copyright in the text of individual articles (including research articles, opinion articles, book reviews, conference proceedings and abstracts) is not affected by its submission to or publication by Frontiers, whether for itself or for a Hosted Journal. Frontiers benefits from a general licence over all content submitted. Hosted Journal Owners benefit from a general licence over all content submitted to their respective Hosted Journals. Frontiers, Hosted Journal Owners and all their users benefit from a [Creative Commons CC-BY licence](#) over all content, as specified below.

Images and graphics not forming part of user-contributed materials are the property of or are licensed to Frontiers and may not be downloaded or copied without Frontiers' explicit and specific permission or in accordance with any specific copyright notice attached to that material.

The combination of all content on Frontiers websites, and the look and feel of the Frontiers websites, is the property of Frontiers Media SA.

As an author or contributor you grant permission to others to reproduce your articles, including any graphics and third-party materials supplied by you, in accordance with the Frontiers Terms and Conditions. The licence granted to third parties over all contents of each article, including third-party elements, is a Creative Commons Attribution ("CC BY") licence. The current version is CC-BY, version 4.0 (<http://creativecommons.org/licenses/by/4.0/>), and the licence will automatically be updated as and when updated by the Creative Commons organisation.

You may include a requirement to reproduce copyright notices but you may not restrict the right to reproduce the entire article, including third-party graphics. This means that you must obtain any necessary third-party consents and permissions to reproduce third-party materials in your articles submitted to Frontiers.

E-books are subject to the same licensing conditions as the articles within them.

Articles published prior to 25th May 2018: Please note that reproduction of third-party graphics and other third-party materials contained in articles published prior to 25th May 2018 may be subject to third-party notices prohibiting their reproduction without permission. You must comply with those notices.

Articles published prior to July 2012: The licence granted for these articles may be different and you should check the pdf version of any article to establish what licence was granted. If an article carries only a non-commercial licence and you wish to obtain a commercial licence, please contact Frontiers at [editorial.office@frontiersin.org](mailto:editorial.office@frontiersin.org).

Article metadata, as defined in [Frontiers' terms and conditions](#), are the property of Frontiers or the Owner of the respective Hosted Journal, and are licensed under [Creative Commons CC0](#) terms.

All software used on this site, and the copyright in the code constituting such software, and all intellectual property in all such elements, is the property of or is licensed to Frontiers and its use is restricted in accordance with the [Frontiers Terms and Conditions](#). All copyright, and all rights therein, are protected by national and international copyright laws.

Please also see the [Frontiers Terms and Conditions](#).

Copyright Statement updated with effect from 16th December 2020.

:

**Article 2. DiSerio, M., Russo, V., Santacesaria, E., & Tesser, R. (2021).  
The Evolution of the Fed Batch Ethoxylation Reactors to Produce the Non-Ionic  
Surfactants. *Frontiers in Chemical Engineering*, Vol. 3, Article 644719,  
<https://doi.org/10.3389/fceng.2021.644719>.**



## The Evolution of the Fed Batch Ethoxylation Reactors to Produce the Non-Ionic Surfactants

Martino Di Serio<sup>1</sup>, Vincenzo Russo<sup>1</sup>, Elio Santacesaria<sup>2</sup> and Riccardo Tesser<sup>1\*</sup>

<sup>1</sup>Department of Chemical Sciences, University of Naples Federico II, Naples, Italy, <sup>2</sup>Eurochem Engineering Srl, Milan, Italy

The most recent reactor technology to produce non-ionic surfactants via ethoxylation reaction is illustrated in the present work. The most advanced reactors are deeply illustrated for what concerns the working principle and the main performance. In detail, Venturi Loop Reactor (VLR), Spray Tower Loop Reactor (STLR) and Enhanced Loop Reactor (ELR) are depicted, and the related performance compared. ELR shows the highest flexibility, to reach the desired ethoxylation degree, and at the same time good performances comparable with the VLR. Moreover, ELR allows to reach high ethoxylation degree, as in this condition, a good mixing, in the case of high liquid expansion, is difficult to be achieved with the other reactors. Thus, it is possible to work at higher ethoxylation degree respecting safety issues. Finally, a comprehensive model was proposed to describe quantitatively the mentioned reactors. The model is characterized by a general validity and can be easily adapted to each specific reactor configuration.

**Keywords:** ethoxylation, reactors, reactor technology, non-ionic surfactants, scale-up

### INTRODUCTION

Starting from the patent assigned to I.G. Farbenindustrie (Schoeller and Wittwer, 1934) the production of non-ionic surfactant obtained by ethoxylation of fatty organic substances containing at least one reactive hydrogen has increased enormously. For example, nowadays more than 50% of world consumption of surfactants for household detergents application is represented by alcohol ethoxylates and alcohol ethers sulfates (Janshekar et al., 2010).

From the first used stirred jacketed reactor, during the time, new reactor types have been proposed on the market. The increase in safety, productivity and selectivity has been the driving force for the new reactor designs (Di Serio et al., 2005; Salzano et al., 2007; Di Serio, 2019) and we can consider the technological improvement in the ethoxylation reactors as a clear example of the process intensification (Stankiewicz and Moulijn, 2000).

Notwithstanding the new quite recent proposals for continuous reactor (Tesser et al., 2020), the ethoxylated products synthesis is still largely based on fed-batch reactors technology in various configurations.

A first classification of these reactors is possible by considering the dispersed phase (Dimiccoli et al., 2000). The ethylene oxide is bubbled in the liquid phase (stirred tank reactor, STR, or Venturi Loop Reactor, VLR (see Figure 1), or the liquid is sprayed in an atmosphere of gaseous ethylene

**Abbreviations:** CAT, catalyst; ELR, enhanced loop reactor; EO, ethylene oxide; STLR, spray tower loop reactor; STR, stirred tank reactor; SUB, substrate; VLR, venturi loop reactor.

### OPEN ACCESS

**Edited by:**  
Giuseppina Iervolino,  
University of Salerno, Italy

**Reviewed by:**  
Attila Egedy,  
University of Pannonia, Hungary  
Ernesto Salzano,  
University of Bologna, Italy  
Francesco Maestri,  
Politecnico di Milano, Italy

**\*Correspondence:**  
Riccardo Tesser  
riccardo.tesser@unina.it

**Specialty section:**  
This article was submitted to  
Chemical Reaction Engineering,  
a section of the journal  
*Frontiers in Chemical Engineering*

**Received:** 21 December 2020

**Accepted:** 01 February 2021

**Published:** 15 March 2021

**Citation:**  
Di Serio M, Russo V, Santacesaria E  
and Tesser R (2021) The Evolution of  
the Fed Batch Ethoxylation Reactors to  
Produce the Non-Ionic Surfactants.  
*Front. Chem. Eng.* 3:644719.  
doi: 10.3389/fceng.2021.644719



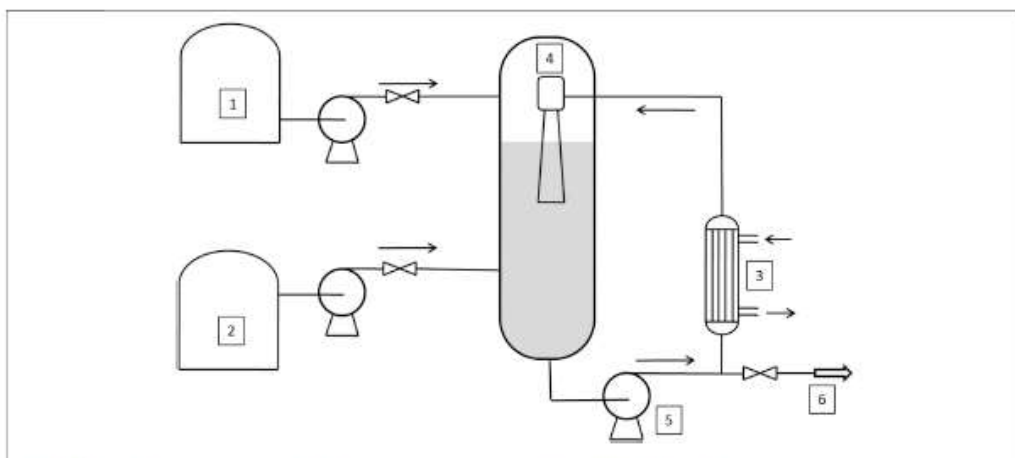


**FIGURE 1** | Venturi Loop Reactor (VLR). 1-2: tanks; 3: heat exchanger; 4: ejector; 5: recirculating pump; 6: outlet stream.

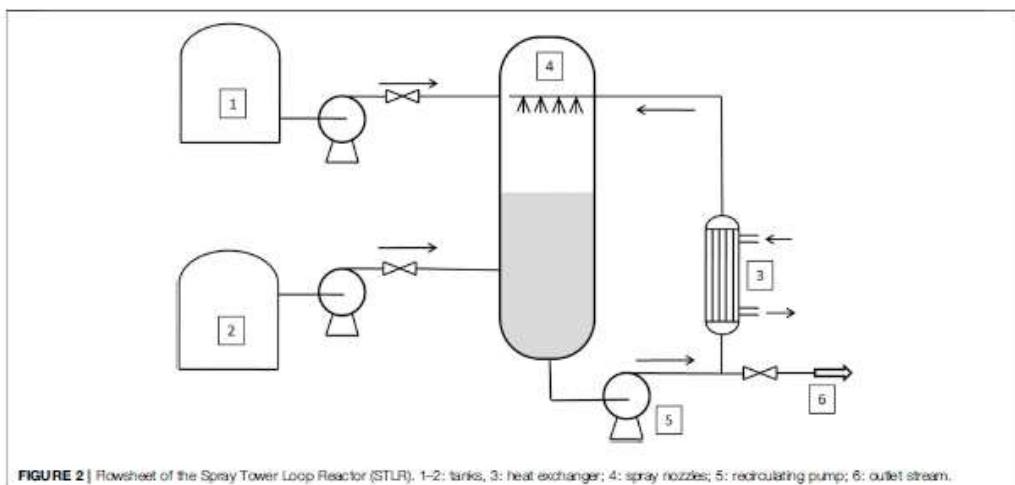


**FIGURE 2** | Flowsheet of the Spray Tower Loop Reactor (STLR). 1-2: tanks; 3: heat exchanger; 4: spray nozzles; 5: recirculating pump; 6: outlet stream.

(Spray Tower Loop Reactor, STLR) (see **Figure 2**). In general, the heat exchanger is located outside the reactor, on the circulation line, and a liquid recirculation pump is present, also in the case of the simple mixed reactor.

The main problem for this process is the difficulty in eliminating or minimizing mass-transfer and heat-transfer limitations, which are generally associated with conventional stirred tank alkoxylation reactors. The use of Venturi Loop Reactor (VLR) or Spray Tower Reactor (STLR) can solve these

problems, but they still have some drawbacks (Di Serio et al., 2005):

- (1) STLR: to achieve the maximum productivity in STLR a high recirculation flow rate is necessary. The required power input for a spray tower loop reactor is greater than that for a Venturi loop reactor.
- (2) VLR: Venturi loop reactor has some drawbacks related to the rigid geometrical parameters that must be satisfied as



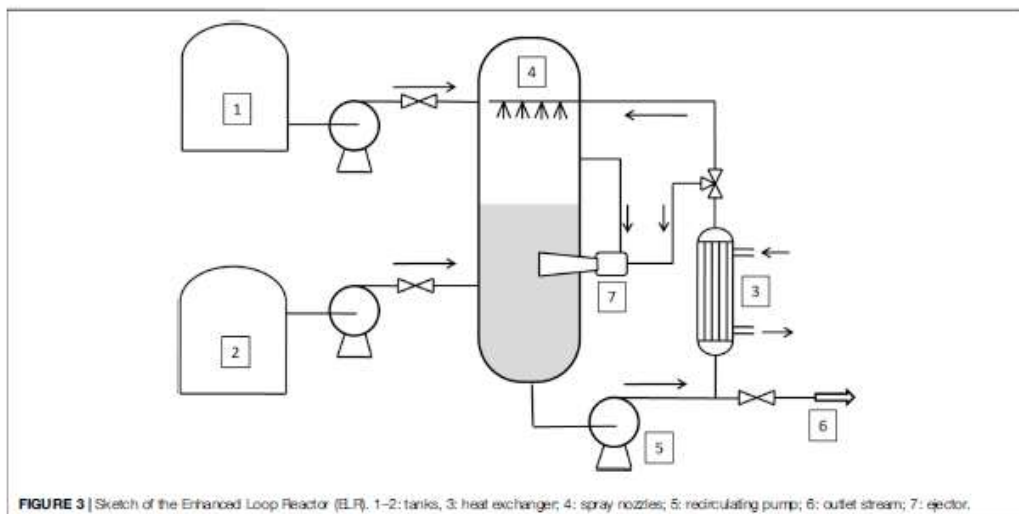


**FIGURE 3** | Sketch of the Enhanced Loop Reactor (ELR). 1–2: tanks; 3: heat exchanger; 4: spray nozzles; 5: recirculating pump; 6: outlet stream; 7: ejector.

concerns the dimensions of the reactor, the liquid level, and the nozzle length. As a matter of fact, the plants where VLR technology is used have in general two reactors: the first one works in the initial stage of the reaction (when the liquid level is low), and the other one is used for achieving high ethylene oxide/substrate molar ratio that corresponds to high increase in volume. Moreover, in the case of large reactors, the behavior of VLR can also become like that of STLR in terms of the power input required for liquid recirculation.

To overcome these drawbacks, a new reactor was proposed the Enhanced Loop Reactor (ELR) (see Figure 3) that represents a combination of the two best previously used technologies: Spray-Tower-Loop Reactor and the Venturi-Loop Reactor (Santacesaria et al., 2018)<sup>1</sup>. Thus, the main novelty of this paper is to introduce and describe the ELR, comparing its performance with both STLR and VLR.

In this paper we will compare the performances of the three cited technologies based on mathematical simulations of the reactors.

## DESCRIPTION OF THE REACTORS AND THE RELATED MATHEMATICAL MODEL

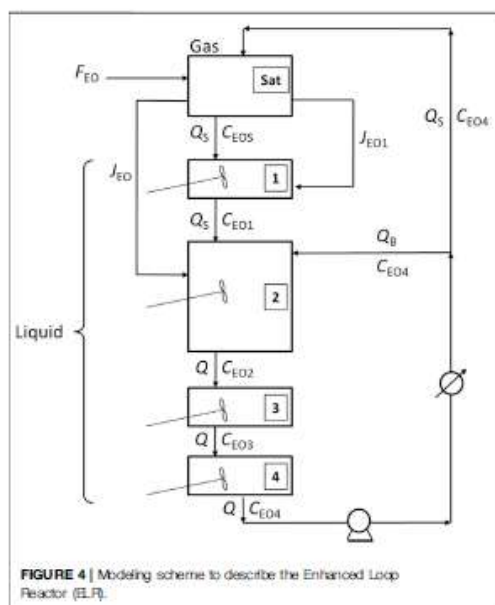
In the VLR, the pumped liquid passes through a nozzle that provides a high velocity jet of fluid to create suction of the gas. In a mixing tube, the high velocity jet attaches itself to the mixing tube wall, resulting in a rapid dissipation of kinetic energy, which creates an intensive mixing with the production of a fine

dispersion of gas bubbles in the liquid phase. The two-phase mixture that “jets” into the reaction autoclave also causes intensive mixing. Considering that the Hatta number of ethoxylation reactions is less than one, a Venturi Loop Reactor can be simulated by assuming it as a well-stirred isothermal reactor (Di Serio et al., 2005).

In STLR, the sprayed liquid is dispersed in the form of small liquid drops flying into the alkylene oxide gaseous atmosphere. Drops emerging from an efficient spray nozzle resulted as internally well-mixed drops, leading to a very high mass-transfer rate, and if the average flight time of the drops is long enough, these drops are completely saturated at the end of their flight (Tesser et al., 2020). The reaction occurs in the liquid column (Santacesaria et al., 1990; Santacesaria et al., 1999) and can be neglected the drops contribution to the reaction, since the flight time is extremely short if compared to the residence time in the liquid column. The liquid column can then be modeled assuming it as a plug-flow reactor in transient conditions as the concentration of dissolved alkoxyde changes with time and along the column itself. Hence, in these reactors, mass transfer and chemical reaction occur separately in two distinct zones: the mass-transfer zone, corresponding to the zone of drops flying across the gaseous atmosphere, and the reaction zone, corresponding to the slowly flowing liquid-phase collected at the bottom of the reactor and recirculated back to the spray nozzle (Di Serio et al., 2005).

The ELR has been simulated considering it as a STLR reactor on which, in the lower part of the reactor, is placed an ejector. In this case the total recirculating flow is divided, after the heat exchanger, in two streams: one of which is fed to the spray nozzle and the second to the ejector. Furthermore, the liquid flowing in the ejector suck up the gas from the reactor head and disperses it in the liquid phase in the form of bubbles which,

<sup>1</sup><https://www.desmetballestra.com/dsc/surfactants/ethoxylation-propoxylation>



rising upwards in the liquid column, further stir the liquid phase.

In this case the ELR, when the ethoxylation reaction is started, behaves like a STLR and when the liquid level reaches a prefixed value, circulation flow is splitted and the ejector is started. In this phase the behavior of the ELR is more similar to a VLR. This reactor configuration has the effect to merge the two most important advantage of both STLR and VLR: it is possible start the production with a very low quantity of substrate (like in the case of STLR) and a high efficiency in mass transfer is achieved with low power input (like in the case of VLR).

More details about the VLR and STLR mathematical model are reported elsewhere (Di Serio et al., 2005) and here only the main structure of the model is presented. The liquid column in the reactor can be assumed with a plug-flow behavior but is in transient conditions as the concentration changes both along the time and along the axial direction. For modeling purposes, the reactor can be schematized as a series of well mixed cells or liquid portions distributed along the liquid column, according to the well-known compartmental models (Egedy et al., 2013; Haag et al., 2018). In the scheme reported in Figure 4 the cells scheme related to ELR configuration is reported.

From this scheme it is possible to appreciate the characteristics of the reactor. After the heat exchanger on the circulation line, the flow is splitted into two portions: one of these is fed to the spray and the other one is sent to the ejector placed in the lower part of the reactor.

As revealed in Figure 4, four cells were assumed as an example of discretization. The model is certainly general and provides the possibility to impose a user-defined number of compartments,

depending on the axial dispersion degree that would describe the system, as in the general tank-in-series model. In the specific case, we assumed four cells as the liquid phase is well mixed by the ejector present in the bottom of the reactor. Thus, due to the mixing efficiency of the ejector, the liquid column is assumed as constituted by four separate cells which behavior is that of a dynamic CSTR reactor: the first upper cell one receive the liquid more or less saturated with EO in the spray chamber; the majority of the liquid is located in the cells two that is well mixed by the ejector; two additional relatively small cells three and four are located in the lower part of the reactor and become important in the final part of the operations, when the height of the liquid column is increased significantly. More generally, a higher number of cells can be considered both above and below the central cell two associated to the ejector.

In the scheme of Figure 4 also gas-liquid mass transfer flows are reported: the first,  $J_{EO1}$  is related to the spray chamber in which gaseous EO is transferred from gas-phase to liquid droplets emerging from nozzles; the second,  $J_{EO}$ , is due to the gas suction from ejector that transfer EO directly to the liquid phase of cell 2.

For the development of a general model based on the scheme reported in Figure 4, some assumptions can be adopted, as in the following points:

- (1) The spray nozzle is considered with a full efficiency in saturation. In the spray chamber, the entering liquid is fully saturated with EO.
- (2) The flow of liquid phase in the liquid column is simulated as a series of CSTR reactors (cells or compartments). The different distribution of cells volume can be used to represent different reactor configuration and fluid-dynamic conditions. For instance, as for the general tank-in-series model, depending on the axial dispersion degree, it is possible to choose a different number of compartments. In detail, a plug-flow fluid-dynamics can be simulated by a theoretically infinite number of cells, while a stirred tank with only one compartment. Thus, a high number of equal cells is used for a STLR while the case of ELR reactor the scheme of cells in Figure 4 is more suitable.
- (3) The expansion of the system volume, that occurs as ethoxylation proceeds, is assumed as equally distributed on all the cells in the reactor.
- (4) The overall volumetric circulation flowrate,  $Q$ , is assumed constant.
- (5) The feed of liquid EO from the external tank is assumed as completely vaporized in the saturation chamber of the reactor.
- (6) Some properties of the reacting mixture are assumed as constants or averaged with temperature, such as specific heat, heat of vaporization.
- (7) The reactor is perfectly insulated and no heat exchange with the surroundings is present.
- (8) The heat exchanger installed on the circulation line is assumed with infinite exchange capacity and the outlet temperature is fixed at a predefined value  $T_S$ .

Under these assumptions, the model of a generic cell is represented by a mass and heat balance equations as follows:



$$\frac{dn_{EO,j}}{dt} = Q(C_{EO,j-1} - C_{EO,j}) - V_j R_j, \quad (1)$$

$$\frac{dT_j}{dt} = \frac{Q}{V_j}(T_{j-1} - T_j) - \frac{R_j \Delta H_r}{\rho C_p}. \quad (2)$$

The specific model for the reactor can then be developed based on Eqs 1, 2 by considering for the specific reactor configuration.

A first differential equation in the model is used for calculating, as a global check, the overall quantity of ethylene oxide fed to the reactor per mole of substrate, during the entire fed-batch operation. This represents a counter and is defined as:

$$\frac{d\text{Count}}{dt} = \frac{F_{EO}}{n_{SUB,0}}. \quad (3)$$

Referring to the scheme in Figure 4, the mass balance for EO in this section of the reactor is:

$$\frac{dn_{EO,sub}}{dt} = F_{EO} + Q_{SPRAY}(C_{EON} - C_{EOS}) - J_{EO,V1} - J_{EO,EI} V_2, \quad (4)$$

where the mass transfer flows are defined by the following relations:

$$J_{EO} = \beta(C_{EOS} - C_{EO,1}), \quad (5)$$

$$J_{EO,EI} = \beta_{EJECT}(C_{EOS} - C_{EON-2}). \quad (6)$$

Another important relation is the account for the overall quantity of reacted EO. This equation can be written as follows:

$$\frac{dn_{EO}}{dt} = S, \quad (7)$$

where:

$$S = \sum_{j=1}^N V_j R_j. \quad (8)$$

As said before, the liquid EO is stored in a tank pressurized with an inert gas (usually nitrogen) and is fed to the reactor directly from this tank. The inert gas dissolved in liquid EO is then continuously fed to the reactor resulting in an accumulation of inert during the operation. The semi batch mass balance on inert gas is then:

$$\frac{dn_{N2}}{dt} = \frac{F_{EO} MW_{EO}}{H_{N2,sub}} (P_{atm} - P_{EO,sub,0}). \quad (9)$$

Material balance on cells is slightly different from one cell to another. The following differential equations represent the mass balances for cell 1 (Eq. 10), cell 2 (Eq. 11) and cells three and 4 (Eq. 12).

$$\frac{dn_1}{dt} = Q_{SPRAY}(C_{EOS} - C_{EO,1}) - R_1 V_1 + J_{EO} V_1, \quad (10)$$

$$\begin{aligned} \frac{dn_{EO,2}}{dt} = & Q_{SPRAY}(C_{EO,1} - C_{EO,2}) + Q_{EJECT}(C_{EOS} - C_{EO,2}) - R_{EO,2} V_2 \\ & + J_{EO,EI} V_2, \end{aligned} \quad (11)$$

$$\frac{dn_i}{dt} = Q(C_{EO,i-1} - C_{EO,i}) - V_i R_i. \quad (12)$$

In analogy with the material balance equations, the energy balance on the compartments can be written. For the first cell the energy balance assumes the following form:

$$\frac{dT_1}{dt} = -\frac{R_1 \Delta H}{\rho C_p} + \frac{Q_{SPRAY}}{V_1} (T_{SAT} - T_1). \quad (13)$$

For the central cell number two the energy balance is slightly different:

$$\frac{dT_2}{dt} = -\frac{R_2 \Delta H}{\rho C_p} + \frac{Q_{SPRAY}}{V_2} (T_1 - T_2) + \frac{Q_{EJECT}}{V_2} (T_3 - T_2). \quad (14)$$

The temperature of the two last bottom cells can be described by the two following ODEs:

$$\frac{dT_3}{dt} = -\frac{R_3 \Delta H}{\rho C_p} + \frac{Q}{V_3} (T_2 - T_3), \quad (15)$$

$$\frac{dT_4}{dt} = -\frac{R_4 \Delta H}{\rho C_p} + \frac{Q}{V_4} (T_3 - T_4). \quad (16)$$

The group of relations constituting the model represent a system of coupled ordinary differential equations that must be integrated in time starting from a suitable initial condition for each of the related dependent variables. However, the mentioned ODEs system cannot be solved without the addition of other algebraic constitutive equations that describe auxiliary variables such as pressure, liquid, and gas volume, EO solubility, reactive mixture density, kinetic expression and related parameters, etc. Moreover, some relations are necessary to calculate the right initial conditions in the reactor.

Initial nitrogen amount in the reactor can be evaluated as:

$$n_{N2,0} = P_{N2,0} \left( \frac{V_{G0}}{RT_0} + \frac{P_{N2,0} V_{L,0} \rho_{L,0}}{H_{N2,sub}} \right). \quad (17)$$

At each time step, the total pressure in the gas phase of the reactor can be evaluated, by the following relation:

$$P_{TOT} = (n_{EO,sub} + n_{N2,sub}) \frac{RT_{sub}}{V_G}. \quad (18)$$

For what concerns the kinetics, in the case of ethoxylation performed by using fatty alcohols as a starter in the presence of an alkaline catalyst, the following equation for overall EO consumption can be used (Santacesaria et al., 1992a; Santacesaria et al., 1992b; Di Serio et al., 1995; Di Serio et al., 2005):

$$R = k[\text{CAT}][\text{EO}], \quad (19)$$

where [CAT] is the catalyst concentration and [EO] is the liquid ethylene oxide concentration. In the simulations we have used the kinetic parameter recently proposed by Amaral and Giudici (Amaral and Giudici, 2011), who confirmed the reliability of our model in the description of STLR and proposed more accurate kinetic data for dodecanol ethoxylation:

$$k [m^3 \text{mol}^{-1} \text{s}^{-1}] = 4.07 \cdot 10^3 e^{-861.37/T}. \quad (20)$$

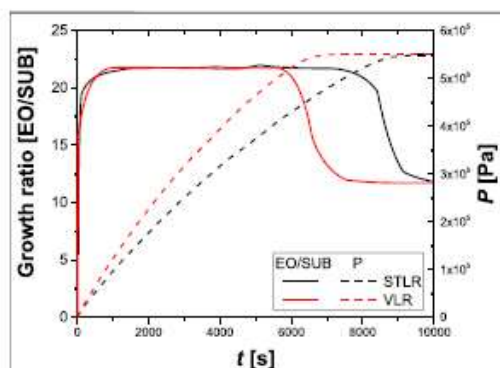


**FIGURE 5** | Calculated values of growth ratio and total pressure, in VLR, STLR operating in the same conditions. Reactor volume: 20 m<sup>3</sup>; total recirculating flow: 210 m<sup>3</sup>/h; maximum operating pressure: 5.5 bar; initial Nitrogen pressure: 1.2 bar; starter (dodecanol):500 kg; catalyst (KOH): 8 kg; exiting heat exchanger temperature: 178°C; final growth ratio:20.5.

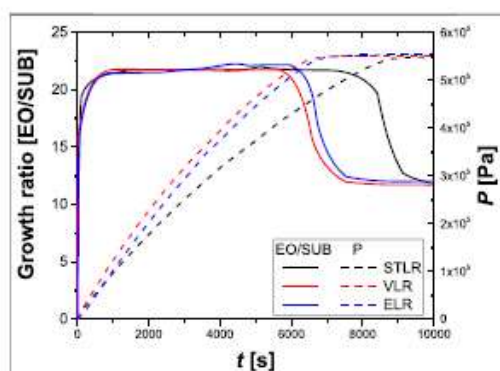


**FIGURE 6** | Calculated values of growth ratio and total pressure, in VLR, STLR, ELR operating in the same conditions. Reactor volume: 20 m<sup>3</sup>; total recirculating flow: 210 m<sup>3</sup>/h; maximum operating pressure: 5.5 bar; initial Nitrogen pressure: 1.2 bar; starter (dodecanol):500 kg; catalyst (KOH): 8 kg; exiting heat exchanger temperature: 178°C; final growth ratio:20.5.

To calculate the catalyst concentration [CAT] and liquid ethylene oxide concentration [EO] the physical (the EO solubility data and the density of the substrate and of the products) parameters have been calculated using previously reported equations and parameters (Santacesaria et al., 1992a; Santacesaria et al., 1992b; Di Serio et al., 1995; Di Serio et al., 2005).

## COMPARISON OF REACTORS

The comparison of the reactors was done considering reactor with the same total volume and using the same total

recirculating flow. In the case of VLR we idealize the reactor considering it well mixed in all the range of the simulation. As we said before, this is not true: at the beginning it is often necessary use a smaller reactor and when in the reactor there is a high amount of liquid also zones could exist in which the liquid is not well mixed.

In Figures 5, 6, the main results of the simulations are reported. For instance, the growth ratio of the ethoxylated product is reported as a function of the reaction time. The growth ratio is defined as the ethylene oxide moles added in the product per mole of substrate. Moreover,  $p$  is defined as the total pressure of the system.

The VLR has better performances than the STLR (see Figure 5), as in VLR the ethylene oxide average concentration in the liquid phase is higher than STLR. Since STLR behaves as a plug-flow reactor, it depletes ethylene oxide in the first upper portion of the liquid phase, while VLR, being a stirred vessel, increases the average EO content. However, the Venturi loop reactor has some drawbacks that are related to the necessity to have the geometrical parameters of the Venturi-type ejector within defined limits. As the simulations were conducted to keep a constant pressure of the system, the growth ratio approaches to a plateau value when the consumption of ethylene oxide decreases, indicating the stop of the ethylene oxide feed. Thus, the overall pressure decreases reaching the set value of the inert gas.

In ethoxylation reactions, as the liquid strongly increases as the reaction and a unique Venturi loop device becomes inadequate to handle the variation condition for the liquid level. For this reason, a multijet arrangement, with the jet starting to operate at different liquid levels, must be used for VLR in the ethoxylation.

In Figure 6 the performance of the ELR is reported. In this case the total recirculating flow was divided in two parts when liquid volume in the reactor was 3 m<sup>3</sup>. The one that supplied the spray nozzle was the 25% of the total while the remaining amount supplied the ejector.

As can be seen, the ELR has the same performances of the VLR, as they provide a similar mixing to the liquid phase, thus a similar ethylene oxide content. However, the Enhanced Loop Reactor has a high flexibility of the gas-liquid contacting devices that permit constant performances of the reactor during all the course of the production process and growth ratio up to 80 (see Figure 6).

## CONCLUSION

In the present paper, the behavior of different reactors for the ethoxylation of organic substrates was presented. In particular, the performance of three reactors was compared: Venturi Loop Reactor (VLR), Spray Tower Loop Reactor (STLR) and Enhanced Loop Reactor (ELR). The main conclusion of the present investigation is that ELR shows the highest flexibility among the presented approaches. In particular, the performance of ELR can be



considered comparable with VLR, but it allows to reach higher ethoxylation degree, that means a higher liquid expansion, warranting in the meantime a good mixing of such high volumes. This fact allows to work at full ethylene oxide per-pass conversion, with consequent improvements in the process safety and control.

The presented modeling approach allows the quantitative description of the three reactors. This model, based on a cell approach, allows to properly design reactors working at a desired ethoxylation degree. In perspective, with such a model, the operation conditions could be optimized, e.g. the split ratio between the flow rates feeding the spray nozzle and the ejector placed on the bottom of the reactor.

## REFERENCES

- Amaral, G. M., and Giudici, R. (2011). Kinetics and modeling of fatty alcohol ethoxylation in an industrial spray loop reactor. *Chem. Eng. Technol.* 34 (10), 1635–1644. doi:10.1002/cet.201100215
- Di Serio, M. (2019). Chemical reaction engineering as a bridge between nano and macro world. *Front. Chem. Eng.* 1, 1–2. doi:10.3389/fceng.2019.00002
- Di Serio, M., Tesser, R., Felippone, F., and Santacesaria, E. (1995). Ethylene oxide solubility and ethoxylation kinetics in the synthesis of nonionic surfactants. *Ind. Eng. Chem. Res.* 34, 4092–4098. doi:10.1021/ie00038a052
- Di Serio, M., Tesser, R., and Santacesaria, E. (2005). Comparison of different reactor types used in the manufacture of ethoxylated, propoxylated products. *Ind. Eng. Chem. Res.* 44, 9482–9489. doi:10.1021/ie0502234
- Dimicoli, A., Di Serio, M., and Santacesaria, E. (2000). Mass transfer and kinetics in spray-tower-loop absorbers and reactors. *Ind. Eng. Chem. Res.* 39, 4082–4093. doi:10.1021/ie000137y
- Egedy, A., Varga, T., and Chován, T. (2013). Compartment model structure identification with qualitative methods for a stirred vessel. *Math. Comput. Model. Dyn. Syst.* 19 (2), 115–132. doi:10.1080/13873954.2012.700939
- Haag, J., Gentré, C., Lemaître, C., and Lederc, J. (2018). Modelling of chemical reactors: from systemic approach to compartmental modelling. *Int. J. Chem. React. Eng.* 16 (8), 1–22. doi:10.1515/ijcre-2017-0172
- Janshakar, H., Rizvi, S. Q. A., and Inoguchi, Y. (2010). Surfactant household detergents and their raw material. CEH Report
- Salzano, E., Di Serio, M., and Santacesaria, E. (2007). The evaluation of risks of ethoxylation reactors. *Proc. Saf. Prog.* 26 (4), 304–311. doi:10.1002/prs.10212
- Santacesaria, E., Di Serio, M., Garaffa, R., and Addino, G. (1992a). Kinetics and mechanisms of fatty alcohol polyethoxylation. 1. The reaction catalyzed by potassium hydroxide. *Ind. Eng. Chem. Res.* 31, 2413–2418. doi:10.1021/ie00011a001
- Santacesaria, E., Di Serio, M., Garaffa, R., and Addino, G. (1992b). Kinetics and mechanisms of fatty alcohol polyethoxylation. 2. narrow-range ethoxylation

## DATA AVAILABILITY STATEMENT

The original contributions presented in the study are included in the article/Supplementary Material, further inquiries can be directed to the corresponding author.

## AUTHOR CONTRIBUTIONS

MS and RT wrote the original draft of the manuscript with support from ES. The main conceptual ideas were drawn from the interactions between MS and RT. The development of the artworks, the data elaboration and the formal analysis were conducted by VR and RT. The final draft was corrected by all the authors.

obtained with barium catalysts. *Ind. Eng. Chem. Res.* 31, 2419–2421. doi:10.1021/ie00011a002

Santacesaria, E., Di Serio, M., Liu, L., and Gelosa, D. (1990). Kinetics of nonylphenol polyethoxylation catalyzed by potassium hydroxide. *Ind. Eng. Chem. Res.* 29, 719–725. doi:10.1021/ie00101a002

Santacesaria, E., Tesser, R., and Di Serio, M. (2018). Polyethoxylation and polypropoxylation reactions: kinetics, mass transfer and industrial reactor design. *Chin. J. Chem. Eng.* 26 (6), 1235–1251. doi:10.1016/j.cjche.2018.02.020

Santacesaria, E., Di Serio, M., and Ingo, P. (1999). Mass transfer and kinetics in ethoxylation spray tower loop reactors. *Chem. Eng. Sci.* 54, 1499–1504. doi:10.1016/s0009-2509(99)00042-1

Schoeller, C., and Wittwer, M. (1934). *Assistants for the textile and related industries*. US1970578.

Stankiewicz, A. I., and Moulijn, J. A. (2000). Process intensification: transforming chemical engineering. *Chem. Eng. Prog.* 96, 22–34.

Tesser, R., Russo, V., Santacesaria, E., Hreczuch, W., and Di Serio, M. (2020). Alkoxylation for surfactant production: towards the continuous reactors. *Front. Chem. Eng.* 2, 1–7. doi:10.3389/fceng.2020.00007

**Conflict of Interest:** ES was employed by Eurochem Engineering Srl.

The remaining authors declare that the research was conducted in the absence of any commercial or financial relationships that could be construed as a potential conflict of interest.

Copyright © 2021 Di Serio, Russo, Santacesaria and Tesser. This is an open-access article distributed under the terms of the Creative Commons Attribution License (CC BY). The use, distribution or reproduction in other forums is permitted, provided the original author(s) and the copyright owner(s) are credited and that the original publication in this journal is cited, in accordance with accepted academic practice. No use, distribution or reproduction is permitted which does not comply with these terms.

## LIST OF SYMBOLS

$C_{i,j}$  Concentration of component  $i$  in cell  $j$  [mol/m<sup>3</sup>]

**Count** Amount of EO fed to the reactor [-]

$F$  EO molar feed rate [mol/s]

$C_p$  Specific heat [J/(kg K)]

$H$  Henry's constant [Pa m<sup>3</sup>/mol]

$J$  Mass transfer rate [mol/(m<sup>2</sup> s)]

$k$  Kinetic constant [m<sup>3</sup>/(mol s)]

$n$  Amount of substance [mol]

$P$  Pressure [Pa]

$Q$  Volumetric flow-rate [m<sup>3</sup>/s]

$R$  Reaction rate [mol/(m<sup>3</sup> s)]

$S$  Overall quantity of reacted EO [mol/s]

$t$  Time [s]

$T$  Temperature [K]

$V$  Volume [m<sup>3</sup>]

## Greek Symbols

$\beta$  Mass transfer coefficient [1/s]

$\Delta H_r$  Reaction enthalpy [J/mol]

$\rho$  Fluid density [kg/m<sup>3</sup>]

**Article 3. Tesser, R., Russo, V., Santacesaria, E., Hreczuch, W., & DiSerio, M. (2020). Alkoxylation for Surfactant Productions: Toward the Continuous Reactors.**

*Frontiers in Chemical Engineering*, Vol. 2, Article 7.

<https://www.semanticscholar.org/paper/Alkoxylation-for-Surfactant-Productions%3A-Toward-the-Tesser-Russo/a6b82dc93b5bf66cf4bd12f4e54c1c2dc9a34ef4>



## Alkoxylation for Surfactant Productions: Toward the Continuous Reactors

Riccardo Tesser<sup>1</sup>, Vincenzo Russo<sup>1,2</sup>, Elio Santacesaria<sup>3</sup>, Wieslaw Hreczuch<sup>4</sup> and Martino Di Serio<sup>1\*</sup>

<sup>1</sup> Department of Chemical Sciences, University of Naples Federico II, Naples, Italy, <sup>2</sup> Laboratory of Industrial Chemistry and Reaction Engineering, Åbo Akademi University, Turku, Finland, <sup>3</sup> Eurochem Engineering, Milan, Italy, <sup>4</sup> MEXEC, Kędzierzyn-Koźle, Poland

Alkoxylation is surely an important reaction as it is industrially used to produce surfactants. The actual technology is to convert ethylene oxide/propylene oxide with a long-chained alcohol, catalyzed by a homogeneous catalyst (e.g., KOH). Traditionally, the operation is conducted in semi-batch systems characterized by a low productivity. As the demand of surfactant production is increasing, it is natural to shift to a continuous process. In the present review article, the most recent efforts dealing with the alkoxylation processes in continuous are reported, analyzing critically the results reported in both the scientific and patent literature.

### OPEN ACCESS

#### Edited by:

Ernesto Salzano,  
University of Bologna, Italy

#### Reviewed by:

Mohsen Sarrafz,  
University of Adelaide, Australia  
Narendra Kumar,  
Åbo Akademi University, Finland

#### \*Correspondence:

Martino Di Serio  
dserio@unina.it

#### Specialty section:

This article was submitted to  
Chemical Reaction Engineering,  
a section of the journal  
Frontiers in Chemical Engineering

Received: 30 April 2020

Accepted: 07 July 2020

Published: 21 August 2020

#### Citation:

Tesser R, Russo V, Santacesaria E,  
Hreczuch W and Di Serio M (2020)  
Alkoxylation for Surfactant  
Productions: Toward the Continuous  
Reactors. *Front. Chem. Eng.* 2:7.  
doi: 10.3389/fbeng.2020.00007

**Keywords:** alkoxylation, scale-up, continuous reactor, microreactor, surfactant production

### INTRODUCTION

The alkoxylation reactions are generally performed in semi-batch gas-liquid reactors (Di Serio et al., 2005; Santacesaria et al., 2018), also in series, in which the catalyst and the substrate (alkyl phenols, fatty alcohols, organic acids, or amines) are initially charged (Di Serio et al., 2015). On the other hand, the epoxide (ethylene or propylene oxide) is added in fed-batch modality during the first step of the reaction course. Finally, the reaction is completed in a "digestion" step in which the residual epoxide, in gas and in the liquid phase, is completely reacted. This process strategy is a result of the high reactivity of alkoxides and to the high heat involved in alkoxylation reactions (around 90 kJ/mol). The use of semi-batch reactors, however, has some drawbacks that can be summarized in the following points: (1) the reactor volume is relatively high, and this aspect could represent a serious problem for safety issues (Gustin, 2000; Di Serio et al., 2005; Salzano et al., 2007a,b) owing to the high quantity of alkoxide present in the gas phase of the reactor at a certain time; (2) the productivity of the system is quite low for the various steps involved in a semi-batch process (reactant and catalyst charge, chemical reaction, products discharge); (3) the safety of the overall process is not optimal, a fact owing to possible epoxide accumulations that could easily lead to runaway reactions (Gustin, 2000; Di Serio et al., 2005; Salzano et al., 2007a,b).

A possible reactor configuration that could allow overcoming the mentioned drawbacks is the adoption of a continuous reactor that can be properly designed for the achievement of the desired alkoxylation degree and high productivity. The shift from the traditional semi-batch process to the continuous ones could really represent the start of a new era in the alkoxylation technologies (Santacesaria et al., 2018). Moreover, a continuous process must be designed to operate under high pressure, and this could represent a further advantage for the safety owing to the absence of a vapor phase (Di Serio et al., 2005) rich in alkoxide that could be more susceptible to ignition. The



**TABLE 1** | Summary of the typical reaction conditions and related results for different alkoxylation processes performed in continuous reactors.

Reactor	Alcohol (alkoxide)	C <sub>cat</sub> , wt. %	Type of catalyst	Alcohol/alkoxide	T <sub>max</sub> , °C	τ, s	P, kg/(h m <sup>3</sup> )	References
Cooled tubes	C <sub>12-14</sub> (EO/PO)	0.10	NaOCH <sub>3</sub>	1:1–1:6 mol/mol	287	25	120,000	Umbach and Stein, 1971
Cooled tubes	Sucrose (EO/PO)	0.40	KOH	11.4:5.8 w/w	180	600	–	Hinz and Dexheimer, 2002
Microchannels	Butanol (EO/PO)	3.00*	KOCH <sub>3</sub>	1:35 mol/mol	190	200	–	Hubel et al., 2010
Microchannels	Octanol (EO)	0.66*	KOH	1:3–1:6–1:9 mol/mol	240	50	12,600	Rupp et al., 2013a,b
Falling film multiple	n-Nonyl phenol (EO)	0.60	NaOH	1:7 mol/mol	220	160	22,000	Aigner et al., 2016
Microreactor	Butanol (EO)	5.00	KOH	1:9 mol/mol	150	300	–	Dessimoz, 2011
Stirred compartments	Polyoxypropylenetriol (PO)	0.05	DMC	1:4.2 w/w	120	15,000	324	Yamada et al., 2006
CSTR	C <sub>12</sub> (EO)	0.18	La(PO <sub>4</sub> ) <sub>3</sub>	1:1.4 w/w	170	7,200	450	McDaniel and Reese, 2007a
Two CSTR	C <sub>12-16</sub> (EO)	0.0144	DMC	1:1.4 w/w	130	12,960	255	McDaniel and Reese, 2007b
Two CSTR	Nonylphenol ethoxylate (EO)	0.0133	DMC	1:1.9 w/w	130	13,320	195	McDaniel and Reese, 2008b
CSTR + PFR	C <sub>26</sub> diol (EO)	0.3	DMC	1:9 w/w	140	21,600	150	Wils et al., 2014
CSTR + PFR	Glycerol alkoxyate (PO)	0.0058	DMC	1:4.2 w/w	125	8,700	372	Verwilt et al., 2008
CSTR + PFR	Glycerol (EO/PO)	0.4	DMC	1:10.3 w/w	160	25,200	130	Weston et al., 2012
Two CSTR	Glycerol (EO/PO)	0.002	DMC	1:2.7:33.1 w/w (EO/PO)	140	–	653	Lai et al., 2019

τ, residence time; P, productivity. \*mole.

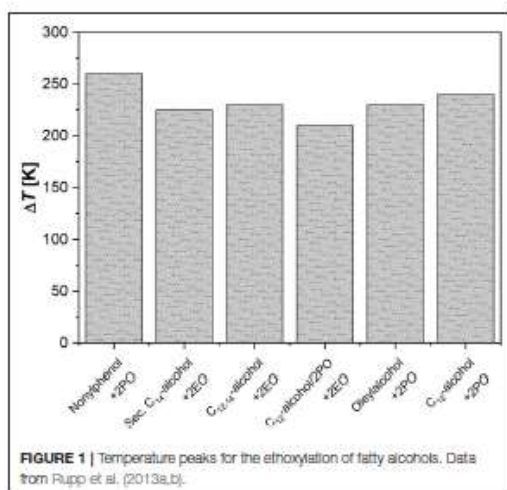


**FIGURE 1** | Temperature peaks for the ethoxylation of fatty alcohols. Data from Rupp et al. (2013a,b).

adoption of a sufficiently high pressure can ultimately keep the alkoxide in liquid state at the process temperature realizing high concentration with an improvement of the reaction rate.

In the scientific and patent literature, both traditional reactors, like the tubular ones, and more innovative reactor configurations, like microreactors, have been proposed for the continuous alkoxylation reactions. These last are particularly suitable for exothermic and multiphase reactions, thanks to the high heat and mass transfer exchange rate (Kralisch et al., 2012; Russo et al., 2013). Moreover, very recently, also stirred tank reactors in series or in combination with PFRs have been proposed as suitable for a continuous alkoxylation production process. In fact, whereas innovative microreactors showed superior performances in terms

of heat/mass transfer efficiency and in theoretical productivity, many authors still proposed the use of traditional reactor devices accepting the drawbacks (lower productivity, lower heat transfer efficiency) but gaining in the possibility for large-scale applications. On the other hand, the exploitation of microdevice advantages can be achieved through the concept of numbering-up (instead of scale-up) that involves, however, a complex setting and control. Hybrid emerging technologies, for example, annular thin film reactor (tube-in-tube arrangement) of corrugated plate heat exchanger reactor, could represent a good perspective in the industrial consolidation of continuous alkoxylation.

In the present paper, the state-of-the-art of such proposals is examined, compared, and extensively discussed, also considered for a possible industrial perspective in terms of productivity of different systems.

## DISCUSSION

From a literature survey of the last decades, several attempts in performing the alkoxylation process in continuous devices have been made. In Table 1, examples of the reaction conditions adopted by different authors are summarized and compared, also in terms of system productivity expressed as the quantity of product obtained per unit of time and per unit of reactor volume.

By using tubular reactors, even working under optimized process conditions of pressure and temperature, there are problems in the thermal control of the system. This fact has been solved by diluting the ethylene oxide concentration by splitting the feed at different points along the tubular reactor. This solution leads to drawbacks and difficulties owing to the necessity of a very complex process control system, particularly in the case of high numbering-up (replication of multiple reactor modules) (Umbach and Stein, 1971; Hinz and Dexheimer, 2002; Hubel et al., 2010; Nikbin et al., 2018).

A possible solution to the control of temperature can be the use of a coiled tubular reactor as suggested in a



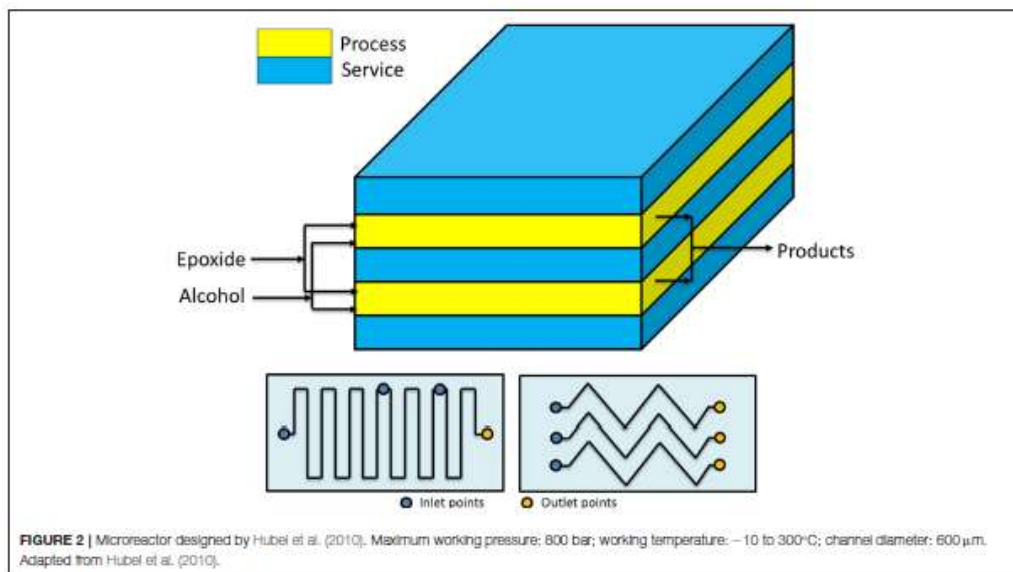
pioneering work of Umbach and Stein (Rupp et al., 2013a,b). In their investigation, these authors have tested ethoxylation and propoxylation reactions in two types of tubular reactors consisting in a stainless-steel tube of different diameters (6 and 9 mm) arranged as coils. With this experimental setup, the authors were able to obtain a complete conversion of alkoxides in very short residence times, in the range 15–150 s, which is much lower than the resident time characteristic of discontinuous processes. The system is operated under high pressure (60–100 bar) to maintain ethylene or propylene oxide in liquid state while the temperature of the feed is quite low (60–70°C).

The two reactors are designed with a very high  $L/D$  ratio (respectively, 2,500 and 1,400) for a better performance in heat removal; nevertheless, rather high temperatures were reached along the reactor with a characteristic profile. The achieved temperature peaks obtained with different systems tested by the authors can be observed in Figure 1.

As it can be seen, the maximum temperatures reached were in the range of 240–300°C. Even if only reactions with low alkoxylation degrees were tested in this investigation (2–4 mol alkoxide/mol substrate), the productivities obtained resulted very interesting, giving place to a product throughput up to 100–120 kg/h that corresponds to a monthly production of 60–70 tons and with a specific productivity of 120,000 kg/(h m<sup>3</sup>). The same concept has been developed for sucrose-based polyether production, in the patent by Hinz and Dexheimer (2002). These authors used concentrated aqueous solution of sucrose (60% by weight) as substrate to be epoxidized and various mixtures of EO and PO as epoxide mixture. The employed catalyst was KOH at 0.4 wt.%. For example, by using two reactor modules

connected in series, with a thermostating fluid, respectively at 140 and 180°C and with a feed ratio of sucrose solution and epoxides equal to 11.4:5.8, they obtain an average ratio of (EO, PO)/sucrose of around 5.2 mol/mol. The adopted reaction pressure was 36.5 bar.

The concept of using a reactor of high  $L/D$  ratio, for maximizing the heat removal efficiency, can be further stressed by passing to microreactors. Hubel et al. (2010) used different microchannel devices patented in 2010 to perform the alkoxylation of alcohols. The authors stated that microdevices are characterized by a very high efficiency in both mass and heat transfer. In this way, it is possible to run the reaction in safe conditions by using microplates, whose microchannels (capillaries of a 600  $\mu\text{m}$  hydraulic diameter) are optionally coated with catalysts, where alcohol and epoxide are mixed directly at the entrance of the plate (see Figure 2). In this way, the two solutions get totally mixed and temperature peaks are avoided. The described setups allow working in different configurations, characterized by the presence of heating/cooling plates that are alternated to plates where catalyst is present. The configurations differ in how the epoxide is fed to the reactor. In fact, it is possible to either feed the entire stream to the first plate or feed the mentioned stream in different points of the microreactor, keeping its concentration almost constant along the axial coordinate. The authors claim that a system like that can work at a temperature up to 400°C and at a pressure up to 800 bar, to keep the reaction media in liquid phase. From the different examples that the author reported, it is interesting to observe that by working with a residence time of 200 s at 190°C and 120 bar, it is possible to achieve 99.6% conversion.



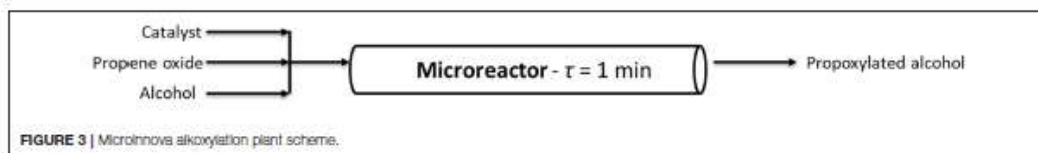


FIGURE 3 | Microreactor plant scheme.

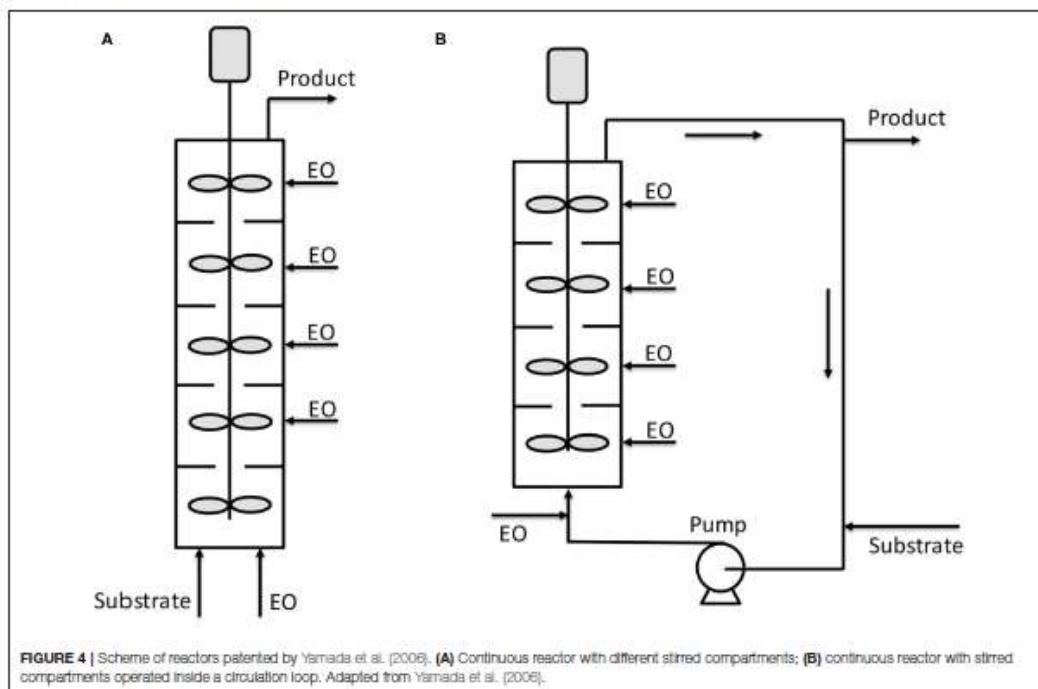


FIGURE 4 | Scheme of reactors patented by Yamada et al. (2006). (A) Continuous reactor with different stirred compartments; (B) continuous reactor with stirred compartments operated inside a circulation loop. Adapted from Yamada et al. (2006).

Different EO/butanol molar ratios were used between 9 and 65. The microreactors shown in Figure 2 have two possible channel structures for the reaction side that differ in geometry (one is zig-zagged, the other step-wised) and the possibility to feed fresh reactants also along different positions of the channel itself.

Moreover, the authors claim that a relatively high ethoxylation degree can be achieved in the microstructured device described previously. A molar ratio EO/alcohol of 35 with a polydispersity index of 1.06 was achieved by using the conditions reported in Table 1 and potassium methoxide (3 mol%) as catalyst. In this way, a very low concentration of unreacted EO (<10 ppm) was found in the reactor outlet stream.

In 2011, Anne-Laure Dessimoz reported data of a laboratory-scale microreactors for ethoxylation reactions, performing kinetic investigations at 250°C and 50 bar (Dessimoz, 2011), claiming a productivity higher than the conventional semi-batch reactors. An increase of a factor 2.5 was observed for productivity of a high-pressure two-phase reactor while

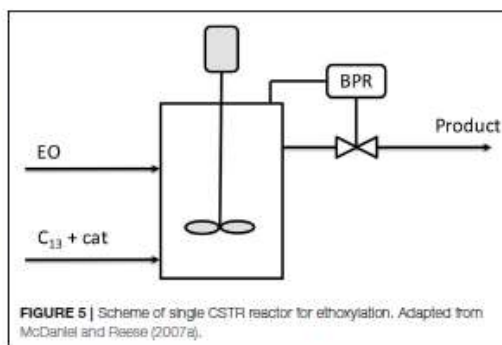
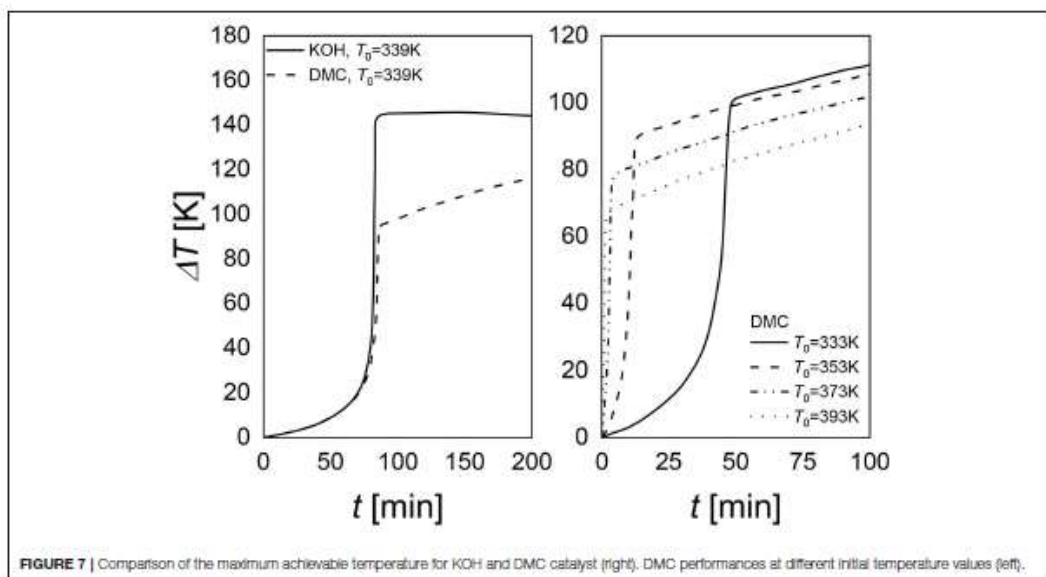
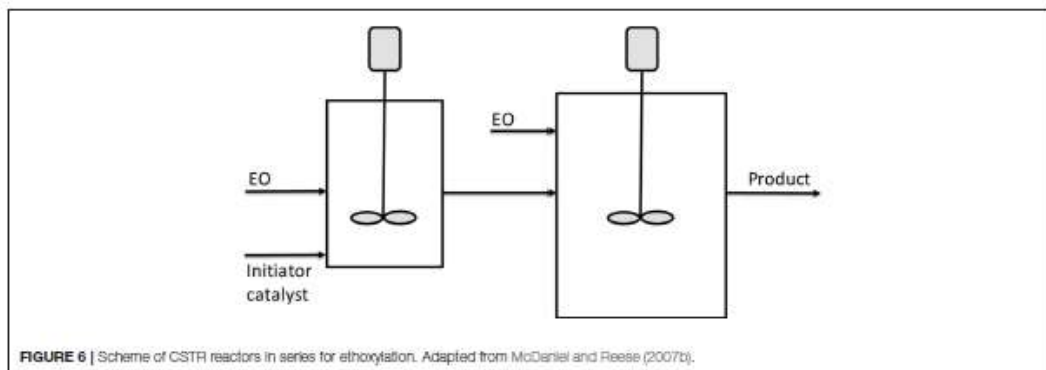


FIGURE 5 | Scheme of single CSTR reactor for ethoxylation. Adapted from McDaniel and Reese (2007a).

a factor of 6 was obtained in a multi-injection reactor in which ethylene oxide feed was split in multiple points along the reactor.



The same strategy was adopted by Rupp et al. (2013a,b) who studied octanol ethoxylation by using a single microchannel reactor immersed in a thermostatic bath. These authors performed an extensive experimental and modeling investigation on the possibility to continuously produce ethoxylated octanol, to a various degree, in a short residence time with interesting productivity results. The reactors used in this study are characterized by  $L/D$  ratio in the range 2,000–4,600 and are constituted by microchannels with diameters of respectively, 250 and 876  $\mu\text{m}$ . The feed to the reactor consists in two separate streams: one contains octanol and dissolved catalysts (potassium octanoate) and the other is ethylene oxide in the

desired ratio. Just before the reactor, a micromixer (SIMM V2 by IMM, Mainz) is installed to ensure a complete mixing and homogenization of the reactants. As before, the pressure was kept in the range 90–100 bar by means of a back-pressure regulator to ensure a liquid-phase reaction and the kinetic investigation of these authors covered the temperature range 130–240°C. In these operative conditions, a residence time of 50 s resulted enough to reach a complete conversion of ethylene oxide and to obtain an ethoxylation degree on octanol in the range 3–9. In this specific experimental device, the maximum throughput was 0.5  $\text{cm}^3/\text{min}$  that is very low; however, the productivity, defined as the amount of product obtained per hour



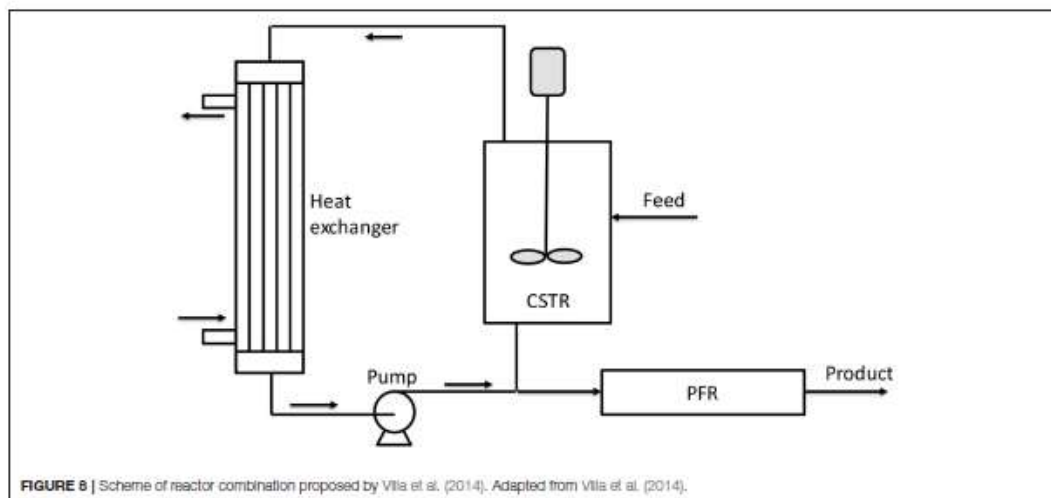


FIGURE 8 | Scheme of reactor combination proposed by Villa et al. (2014). Adapted from Villa et al. (2014).

and per cubic meter of reactor, is on the contrary very high:  $12,600 \text{ kg}/(\text{h}\cdot\text{m}^3)$ .

The problem of the low productivity of microreactors in the alkoxylation reaction has been recently faced and solved by the Microinova Engineering GmbH, using a microstructured chemical reactor developed by the Institut für Mikrotechnik Mainz (IMM) GmbH with innovative fabrication techniques reported in Krtschil et al. (2013). The reactor is built with the concept of modularity which allows the manufacture of different reactors according to the requirements of the process (see sketch in Figure 3). Microinova has designed and built an alkoxylation plant with a productivity of  $20 \text{ kg}/\text{h}$ . This plant is now on stream and a new plant with a productivity of  $200 \text{ kg}/\text{h}$  is in assembly. The authors claim that working with their multiple plate microreactor, it is possible to scale down the reaction times from 12 h to 1 min, keeping the same product characteristics, with an intensification factor of about 700.

Other kinds of reactors are also present in the literature which structure is more traditional with respect to the already presented microchannel or microstructured reactors. For example, Yamada et al. (2006) patented a tubular reactor constituted by different plates stirred by dynamic impellers. Both the epoxide and initiator/catalyst mixture are fed from the bottom and the vessel is kept under pressure by an external vessel pressurized with nitrogen. The reactor can be operated also by feeding ethylene oxide in the different stirred sections of the reactor body (see Figure 4A). A second configuration is also shown, where the mentioned reactor is placed in a loop (see Figure 4B). This last setup could be particularly interesting as a heat exchanger can be installed on the circulation line improving the reaction heat removal. In the patent of Yamada et al. (2006), different examples are reported and among them is worth to note a case in which a reactor configuration like the scheme of Figure 4A was used. The reactor (6.5 cm of internal diameter)

was constituted by 10 compartments each of them of  $100 \text{ cm}^3$  and operated at  $120^\circ\text{C}$  and 15 bar. The authors worked with the double metal cyanide catalyst (DMC), zinc hexacyanocobaltate complex, first patented by General Tires in 1960's and widely used in alkoxylation reactions (McDaniel and Reese, 2007a). The stirring speed was 900 rpm, DMC was used as catalyst with a concentration of 0.05 wt.% in the initiator. The feed was  $2 \text{ g}/\text{min}$  of polyoxypropylentriol as initiator and PO was adopted as epoxide. This last was fed at a rate of  $1.68 \text{ g}/\text{min}$  to each 1, 3, 5, 7, and 9<sup>o</sup> compartments. After 30 min of operation, the reactor reached stationary conditions with a complete conversion of PO and with a polydispersity index of 1.12 and with a productivity of  $624 \text{ kg}/(\text{h}\cdot\text{m}^3)$ .

The strategy to employ CSTR reactor for continuous ethoxylation, instead of tubular reactor, has been extensively studied by (McDaniel and Reese, 2007a,b, 2008a,b). Two interesting examples are reported here to illustrate the approach based on the CSTR reactor. In the first example, a single CSTR reactor of around  $1,900 \text{ cm}^3$  of volume and equipped with thermal and pressure controls was used to conduct an ethoxylation at  $170^\circ\text{C}$  at 3 bar with  $\text{La}(\text{PO}_4)$  as catalyst (McDaniel and Reese, 2007a). The scheme of this reactor is reported in Figure 5.

The reactor, initially charged with an ethoxylated  $\text{C}_{13}/\text{EO} = 6.5$ , was fed with  $8.34 \text{ g}/\text{min}$  of EO and  $5.83 \text{ g}/\text{min}$  of a mixture  $\text{C}_{13}/\text{catalyst}$ . With a residence time of 2 h, a complete conversion of EO was reached and the product was characterized with a polydispersity index of 1.12. In a second example, the same authors adopted the strategy of multiple-stage reactors in series with intermediate feed of EO. The scheme is illustrated in Figure 6.

The two reactors schematized in Figure 7 have a volume of respectively, 4.5 and 9 L. DMC was used as catalyst with a concentration of 144 ppm. The first reactor was fed with 23.95

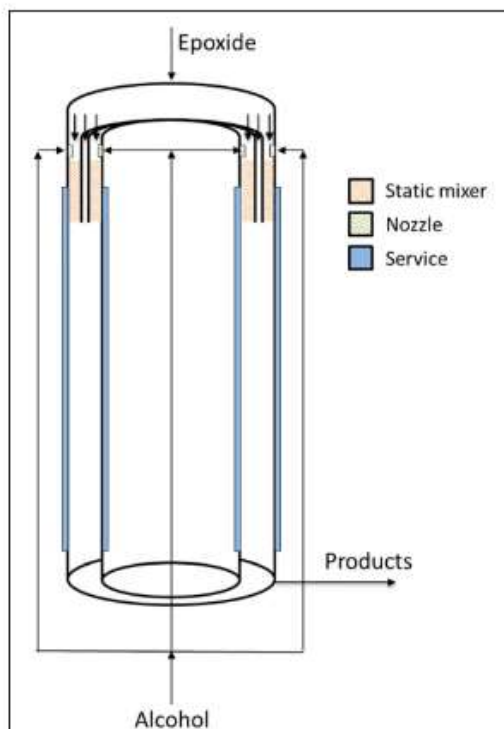


**FIGURE 9** | Concentric tubular reactor in which an annular space is present. Adapted from Aigner et al. (2016).

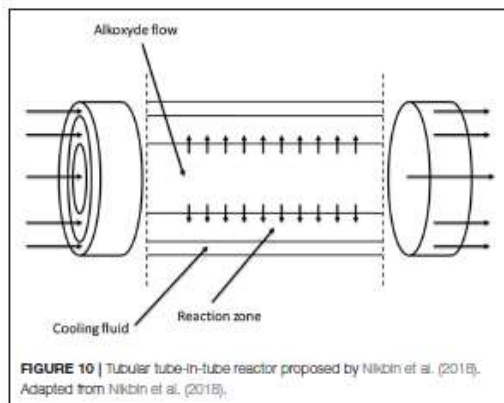


**FIGURE 10** | Tubular tube-in-tube reactor proposed by Nikbin et al. (2018). Adapted from Nikbin et al. (2018).

g/min of initiator (ethoxylate of Neodol 25) and catalyst in a first stream and with 16.7 g/min of EO in a second stream. A further feed of 16.7 g/min of EO was fed to the second

bigger reactor. An overall molar ethoxylation degree of 6.6 was obtained with a residence time of 1.5 h in the first reactor and 2.1 h in the second. Finally, a polydispersity index of 1.10 was obtained for the product stream. The same apparatus described in **Figure 6** was used by McDaniel and Reese (2008a,b) for the continuous ethoxylation of a different initiator, based on nonylphenol ethoxylate and with DMC catalyst. At 130°C and 3.5 bar, a productivity of 195 kg/(h m<sup>3</sup>) was obtained.

Verwijs et al. (2008), Weston et al. (2012), Villa et al. (2014) showed another interesting aspect of DMC catalyst that could favor their industrial application. These catalysts are thermally deactivated, a fact that increases the safety of the process. By working with this catalyst, it is possible to reduce the maximum temperature that the system can reach. In **Figure 7**, it is possible to observe that KOH leads to a higher temperature than DMC. Moreover, starting from different initial temperatures, it is possible to reach different maximum temperatures (**Figure 8**, left plot). As it is evident, a slope of temperature increase is still present but very smooth. Thus, it is possible to take all the safety procedures to stop the reaction (Dessimoz, 2011).

All these considerations can be better understood if we consider that in **Figure 8**, the  $\Delta T$  is reported as a multiplication factor with respect to the initial temperature (a value of 2 means that the temperature was doubled with respect to the initial). These authors reported a different example in their patent as a reaction in liquid phase under pressure adopting a CSTR reactor enclosed in a circulation loop and a tubular reactor used as digester of the unreacted monomer (PO). By using glycerol alkoxyate as initiator and propylene oxide as monomer, an overall productivity of 372 kg/(h m<sup>3</sup>) was obtained at relatively low temperature (110°C in CSTR and 125°C in PFR).

For what concerns reactor configuration, in the patent of Villa et al. (2014), different loop continuous systems are proposed and, among them, one is particularly promising and is represented schematically in **Figure 8**. In an example reported by these authors, two reactors (CSTR and PFR) with a volume of 28 and 25 L, respectively, were used to process a diol of 400 Da and obtain a product of 4,000 Da that corresponds to an EO/S molar ratio of about 80. The catalyst concentration of 25 ppm and reaction temperature of 140°C were used as other conditions. A high circulation flow rate of 7,500 kg/h was adopted to minimize temperature and concentration differences (maximum  $\Delta T = 1^\circ\text{C}$ ). With a residence time of 3 h in each reactor, the authors obtained a residual EO concentration in the loop of 0.3% and a product with a polydispersity index of 1.11.

In 2016, Aigner et al. filed a patent claiming a new reactor technology dedicated to the continuous alkoxylation reaction of a generic substrate with active hydrogen atoms (Aigner et al., 2016). The reactor is designed as a concentric tubular reactor in which an annular space is obtained for performing the reaction continuously (see sketch in **Figure 9**). In this way, the annular gap reaction volume (width 6.5 mm, diameter 5 inches, length 5 m) is very similar to a thin film with enhanced properties of thermal exchange and able to achieve safe operation. Such a reactor system is characterized by a  $L/D$  ratio of about 770 and is able to achieve a product throughput of 250 kg/h (7 mol EO/mol n-nonyl phenol) in correspondence to



a residence time of roughly 160 s and with a productivity of 22,000 kg/(h·m<sup>3</sup>). The authors claim the possibility to complete the reaction either in a separate tank or in the same reactor by introducing a higher volume at its bottom. In this way, products of different properties can be produced. Despite the fact that this reactor was built in a quite complex way, it opens the perspective of a real industrial utilization in the field of alkoxylation technology.

In the patent of Lai et al. (2019), two CSTR reactors connected in series allowed to obtain a polyether constituted by EO/PO copolymer (Hreczuch et al., 2016) using DMC as catalyst (20 ppm) at a temperature of 140°C. Glycerol was used as starter and in the final product a weight ratio PO/EO of 12 was obtained.

Another very interesting reactor configuration was proposed by Nikhin et al. (2018). The continuous reactor was assembled as three concentric tubes (tube-in-tube setup) schematically represented in Figure 10. In the inner, small-diameter tube, alkoxide is fed and can be distributed along the reactor axis at different axial positions; in the intermediate annular section, the reaction zone, the starter is fed and the reaction occurs with alkoxide coming from holes in the inner tube. Between the larger external tube and the intermediate one, the cooling fluid is fed allowing an optimal temperature control.

With this configuration, the authors described the use of a very long reactor (200 m) with a volume of 50 m<sup>3</sup>. The reactor was operated in three sections to demonstrate the flexibility of the operation: in the first 50 m, PO was fed through the holes of internal tube; in the next 104 m, EO was added in the same way and the remaining 46 m were used as cooking section.

## REFERENCES

- Aigner, R., Hirsch, D., and Lagnaz, A. (2016). *Process and Apparatus for Continuous High Temperature Short-Time Alkoxylation (Ethoxylation, Propoxylation) of Chemical Substances With Active Hydrogen Atoms*. US9242217B2.
- Dessimoz, A. L. (2011). *Intensification of gas/liquid chemical synthesis using microreactors and new operating windows* (Ecole Polytechnique Fédérale De Lausanne, Thèse N. 5142). EPFL, Lausanne, Switzerland.
- Di Serio, M., Tesser, R., Russo, V., Turco, R., Vitiello, R., Sun, Y., et al. (2015). Catalysts for the ethoxylation of esters. *J. Surfactants Deterg.* 18, 913–918. doi: 10.1007/s11743-015-1719-1
- Di Serio, M., Tesser, R., and Santacesaria, E. (2005). Comparison of different reactor types used in the manufacture of ethoxylated, propoxylated products. *Ind. Eng. Chem. Res.* 44, 9482–9489. doi: 10.1021/ie0502234
- Gustin, J. (2000). "Safety of ethoxylation reactions," in *ICHEM Symposium Series No. 147* (Manchester), 19.
- Herfeld, W., Hessel, V., and Löwe, G. (2000). *Microreactors: New Technology for Modern Chemistry*. New York, NY: Wiley-VCH. doi: 10.1002/3527601953
- Hinz, W., and Dexheimer, E. M. (2002). *Continuous Process for the Production of Sucrose-Based Polyether Polyols*. US6380367B1.
- Hreczuch, W., Chrusciel, A., Dabrowska, K., Di Serio, M., and Yongqiang, S. (2016). Characteristics of block copolymers of methyl oxirane and oxirane derivatives of 2-ethylhexanol as obtained with KOH and dimethylcyanide type catalyst. *Tenside Surfactants Deterg.* 53, 259–264. doi: 10.3139/113.110431
- Hübel, R., Markowicz, G., Reckisik, M., Rudek, M., Wewers, D., and Zeller-Schuldes, F. (2010). *Alkoxylation in Microstructured Capillary Reactors*. US7858829B2.

## CONCLUSION

If we consider the recent findings reviewed in this paper, a promising perspective is nowadays available for performing alkoxylation reactions in continuous modality. It has been demonstrated that specifically designed continuous reactors can furnish very good performances in terms of productivity and for ensuring safe operation in the adopted conditions. The reactors are characterized by sufficient flexibility to achieve different alkoxylation degrees being, in this way, suitable for different productions. The obtained productivity is sufficiently high to guarantee, also considering reactor modularity, the possibility of useful industrial applications. Employing these emerging technologies, a new era in alkoxylation technology could start in the near future.

In perspective, more experimental and theoretical activities are needed to confirm the interesting data that emerged from the preliminary results reported in this review to achieve the conceptualization of new open process windows for the alkoxylation reaction, realizing prototypes solving the numbering-up issues (Herfeld et al., 2000). Moreover, it must be pointed out that these achievements in the improvement of microreactor technology will give a sure help in solving the new emerging COVID-19 challenges, which require safer and more localized specialized production.

## AUTHOR CONTRIBUTIONS

MD drew the initial idea of the work and directed the workgroup composed by the other authors, who gave the same contribution as each of them edited part of the review. All authors contributed to the article and approved the submitted version.

- Kralisch, D., Streckmann, L., Ott, D., Krtischil, U., Santacesaria, E., Di Serio, M., et al. (2012). Transfer of the epoxidation of soybean oil from batch to flow chemistry guided by cost and environmental issues. *ChemSusChem* 5, 300–311. doi: 10.1002/cssc.201100445
- Krtischil, U., Hofmann, C., Lob, P., Schutt, C., Schorch, P., and Streuber, M. (2013). Novel manufacturing techniques for microstructured reactors in industrial dimensions. *Green Process. Synth.* 2, 451–463. doi: 10.1515/gps-2013-0066
- Lai, J., Wray, W. D., Lenahan, R. A., Reese, J. R., and Morrison, D. M. (2019). *Systems and Processes for Producing Polyether Polyols*. US10258953B2.
- McDaniel, K. G., and Reese, J. R. (2007a). *Continuous Process for the Production of Ethoxylates*. EP2223953A1.
- McDaniel, K. G., and Reese, J. R. (2007b). *High Productivity Alkoxylation Processes*. EP2325230A1.
- McDaniel, K. G., and Reese, J. R. (2008a). *Continuous Processes for the Production of Alkylphenol Ethoxylates*. US0132728A1.
- McDaniel, K. G., and Reese, J. R. (2008b). *High Productivity Alkoxylation Processes*. US0167501A1.
- Nikhin, N. N., Villa, C. M., Remacha, M. J. N., Khan, I., Heat, W. H., Pendergast, J. G., et al. (2018). *Alkoxylation Process Using Tubular Reactor*. WO2018/057438A1.
- Rupp, M., Ruback, W., and Klemm, E. (2013a). Alcohol ethoxylation kinetics: proton transfer influence on product distribution in microchannels. *Chem. Eng. Process. Process Intensif.* 74, 187–192. doi: 10.1016/j.cep.2013.09.006
- Rupp, M., Ruback, W., and Klemm, E. (2013b). Octanolethoxylation in microchannels. *Chem. Eng. Process. Process Intensif.* 74, 19–26. doi: 10.1016/j.cep.2013.09.012

- Russo, V., Protasova, L., Turco, R., de Croon, M. H. J. M., Hessel, V., and Santacesaria, E. (2013). Hydrogen peroxide decomposition on manganese oxide supported catalyst: from batch reactor to continuous microreactor. *Ind. Eng. Chem. Res.* 52, 7668–7676. doi: 10.1021/ie303543x
- Salzano, E., Di Serio, M., and Santacesaria, E. (2007a). The evaluation of risks of ethoxylation reactors. *Process Saf. Prog.* 26, 304–311. doi: 10.1002/prs.10212
- Salzano, E., Di Serio, M., and Santacesaria, E. (2007b). The role of recirculation loop on the risk of ethoxylation processes. *J. Loss Prev. Process Ind.* 20, 238–250. doi: 10.1016/j.jlp.2007.03.016
- Santacesaria, E., Tesser, R., and Di Serio, M. (2018). Polyethoxylation and polypropoxylation reactions: kinetics, mass transfer and industrial reactor design. *Chin. J. Chem. Eng.* 26, 1235–1251. doi: 10.1016/j.cjche.2018.02.020
- Umbach, W., and Stein, W. (1971). Continuous alkoxylation process. *IAOCS* 48, 394–397. doi: 10.1007/BF02637359
- Verwijs, J. W., Weston, J. W., Papadopoulos, W. J. S., Elwell, R. J., and Villa, C. M. (2008). *Continuous Process and System of Producing Polyether Polyols*. US7378559B2.
- Villa, C. M., Weston, J. W., Jain, P., Thompson, L. H., and Masy, J.-P. (2014). *Continuous Loop Flow Process for Polyether Polyol Production*. US8912364B2.
- Weston, J. W., Villa, C. M., Masy, J.-P., and Seavey, K. C. (2012). *Method for Continuously Producing Low Equivalent Weight Polyols Using Double Metal Cyanide Catalysts*. US0283483A1.
- Yamada, K., Kasahara, N., Toyota, Y., Suzuki, C., Ikai, S., and Hatano, H. (2006). *Method for Continuously Producing a Polyether*. US7012164B2.

**Conflict of Interest:** ES was employed by the company Eurochem Engineering. WH was employed by the company MEXEO.

The remaining authors declare that the research was conducted in the absence of any commercial or financial relationships that could be construed as a potential conflict of interest.

Copyright © 2020 Tesser, Russo, Santacesaria, Hreczuch and Di Serio. This is an open-access article distributed under the terms of the Creative Commons Attribution License (CC BY). The use, distribution or reproduction in other forums is permitted, provided the original author(s) and the copyright owner(s) are credited and that the original publication in this journal is cited, in accordance with accepted academic practice. No use, distribution or reproduction is permitted which does not comply with these terms.



# Chemical Reaction Engineering as a Bridge Between Nano and Macro World

Martino Di Serio\*

Department of Chemical Sciences, Polytechnic and Basic Sciences School, University of Naples Federico II, Naples, Italy

**Keywords:** chemical reaction engineering, reactor, thermodynamics, kinetics, catalysis

Chemical Reaction Engineering started its history with the development of refinery and petrochemical industry at the beginning of the last century (Levenspiel, 1980). To come to commercial scale, laboratory data needs to be transferred toward industrial applications. That optimization of process performance demands for the merge of fundamentals sciences (chemistry, physics, mathematics—reactor modeling) in a new applied discipline: Chemical Reaction Engineering (CRE) (Levenspiel, 1998; Froment et al., 2010; Scott Fogler, 2016). In the recent decades, an increasing trend is observed in the use of biology and particularly biocatalysis for application in biotechnology (Bischoff, 1966; Katoh et al., 2015).

The main fields of chemistry belonging to CRE are thermodynamics, kinetics and catalysis (Levenspiel, 1998; Froment et al., 2010; Scott Fogler, 2016). The classical kinetic approach provides the development of know-how about the conduction of a kinetic test, drawing the lines about the correct definition of the minimum number of experiments needed to understand the kinetics of a reaction network (Salmi et al., 2010; Santacesaria and Tesser, 2018). The main concern of this approach is the need to determine kinetic parameters from the collected data, most likely defining a reaction mechanism. The experimental data implementation is becoming nowadays more and more sophisticated, moving to a deeper understanding of the micro-scale of a reaction. To describe the observed chemical phenomena, the underlying physical phenomena need also to be considered (Ramachandran and Chaudhari, 1983; Dudukovic et al., 1999).

Currently, the boundary in CRE is pushed from the macro-meso-micro- to the nano-electronic scale (Lerou and Ng, 1996; Šivec et al., 2019). This is enabled by advances made in the development of experimental equipment for investigation. For instance, nowadays it is possible to follow the kinetics of a reaction with *in-situ* operando techniques allowing the determination of realistic reaction mechanism (Gracia et al., 2003; Frenken and Groot, 2017; Li et al., 2019). To describe the phenomena at the nano scale it is necessary to use a quantum mechanics approach. Increasingly, DFT is coupled with kinetic modeling, coined microkinetic, demonstrating high predictability of the reaction kinetics (Alexopoulos et al., 2016; Hussain Motagamwala et al., 2019). In the future, efforts in this field are expected to provide important insights into molecular phenomena and to foster process improvement.

A great disruptive transformation of reactor design has made its way from academia to industrial use. New concepts are now available, such as:

- the intensification of the processes with multifunctional reactors (Cho et al., 1980; Taylor and Krishna, 2000; Rodrigues et al., 2012; Gallucci et al., 2013; Russo et al., 2018)
- the opening of the novel process windows by microreactors (Kiwi-Minsker and Renken, 2005; Hessel, 2009);
- the use of alternative way to transfer energy to the reactive system (mainly with microwaves or cavitation reactors; Nüchter et al., 2004; Gogate, 2008).

## OPEN ACCESS

### Edited and reviewed by:

Fengqi You,  
Cornell University, United States

### \*Correspondence:

Martino Di Serio  
dserio@unina.it

### Specialty section:

This article was submitted to  
Chemical Reaction Engineering,  
a section of the journal  
*Frontiers in Chemical Engineering*

**Received:** 20 September 2019

**Accepted:** 15 October 2019

**Published:** 31 October 2019

### Citation:

Di Serio M (2019) Chemical Reaction  
Engineering as a Bridge Between  
Nano and Macro World.  
*Front. Chem. Eng.* 1:2.  
doi: 10.3389/fceng.2019.00002



All the above new concepts have the same objective: on the one hand to optimize the processes by reducing the required energy and waste and, on the other hand, to increase the safety. Yet, although they can offer more novel process windows, with only a part of that having been released,—the new types of reactors slowly change the way of carrying processes.

Also concerning macro-scale processing substantial efforts have been made to improve technical instrumentations, allowing the precise determination of the physical properties of fluids and solids inside the reactors (e.g. tomography, high resolution IR camera, MRI imaging) (Kumar et al., 1997; Gladden et al., 2003; Rafique et al., 2004). Therefore, the classical approach of describing physical phenomena in simple terms is moving in a more sophisticated and realistic direction: from the use of dimensionless numbers to computational fluid-dynamics. Classically, for example, when simulating continuous reactors, the momentum balance equations are neglected, and the fluid-dynamics is described in terms of pressure-drop correlations. This approach is usually valid, but what if the geometry of the packing is non-conventional? What if the fluid-dynamics is far from being classical? It has been demonstrated that CFD modeling can be coupled with a classical kinetic approach to consider irregular geometries of non-conventional packing materials, such as foams (Della Torre et al., 2016).

These approaches are at the forefront of CRE: scientists specialized in physical chemistry and fluid-dynamics develop tools for the deep investigation of the fundamentals of the cited disciplines. It is evident that classical CRE is the joining link between the two approaches.

## REFERENCES

- Alexopoulos, K., John, M., Van der Borgh, K., Galvita, V., Reyniers, M.-F., and Marin, G. B. (2016). DFT-based microkinetic modeling of ethanol dehydration in H-ZSM-5. *J. Catal.* 339, 173–185. doi: 10.1016/j.jcat.2016.04.020
- Anastas, P. T., and Zimmerman, J. B. P. (2003). Design through the 12 principles of green engineering. *Environ. Sci. Technol.* 37, 94–101A. doi: 10.1021/es032373g
- Bischoff, K. B. (1966). Optimal continuous fermentation reactor design. *Can. J. Chem. Eng.* 44, 281–284. doi: 10.1002/cjce.5450440507
- Cho, B. K., Carr, R. W., and Aris, R. (1980). A continuous chromatographic reactor. *Chem. Eng. Sci.* 35, 74–81. doi: 10.1016/0009-2509(80)80072-8
- Constable, D. J. C., Gonzalez, M., and Morton, S. A. (2016). "Towards more sustainable chemical engineering processes: integrating sustainable and green chemistry into the engineering design process." *Sustainability in the Design, Synthesis and Analysis of Chemical Engineering Processes*, eds G. Ruiz-Mercado and H. Cabezas (Oxford, UK: Butterworth-Heinemann), 1–34. doi: 10.1016/B978-0-12-802032-6.00001-3
- Della Torre, A., Lucci, F., Montenegro, G., Onorati, A., Dimopoulos Iggenschwiler, P., Tronconi, E., et al. (2016). CFD modelling of catalytic reactions in open-cell foam substrates. *Comput. Chem. Eng.* 92, 55–63. doi: 10.1016/j.compchemeng.2016.04.031
- Dudukovic, M. P., Larachi, F., and Mills, P. L. (1999). Multiphase reactors – revisited. *Chem. Eng. Sci.* 54, 1975–1995. doi: 10.1016/S0009-2509(98)00367-4
- Frekn, J., and Groot, I. (2017). *Operando Research in Heterogeneous Catalysis*. Cham: Springer. doi: 10.1007/978-3-319-44439-0
- Froment, G. F., Bischoff, K. B., and De Wilde, J. (2010). *Chemical Reactor Analysis and Design*, 3rd Edn. New York, NY: John Wiley and Sons.
- Gallucci, F., Fernandez, E., Corengia, P., and van Sint Annaland, M. (2013). Recent advances on membranes and membrane reactors for hydrogen production. *Chem. Eng. Sci.* 92, 40–66. doi: 10.1016/j.ces.2013.01.008

In the development of CRE the evolution of computational tools (both hardware and software) is gaining a fundamental role. Computational times are becoming ever shorter, high performance calculators are released virtually every day, supporting the development of reliable and more sophisticated kinetic and reactor models. Great efforts have been made in the past to develop adequate mathematical models. The research in the field is still taking on new challenges for chemical reaction engineering (Varma and Morbidelli, 1997; Rasmuson et al., 2014).

What is the *Grand Challenge of CRE*? The main challenge is to build a reliable bridge from the nano to the macro scale, that allows to predict the behavior of a whole chemical process, starting from its definition by scratch. To do this it is certainly necessary to continue researching the boundaries (the nano dimensions and the detailed description of fluid dynamics phenomena) without compromising the use of classical approaches. It must be remembered that often the simplest approaches lead to the faster and to the most reliable results (KISS principle—keep it simple, stupid). Both fundamental and applied research are equally important to achieve the final objective: to develop new chemical processes for the sake of increasing safety and decreasing depletion of natural resources and the total environmental impact, following the 12 principles of green engineering (Anastas and Zimmerman, 2003) and sustainable process design (Constable et al., 2016).

## AUTHOR CONTRIBUTIONS

MD devised the manuscript concept and writing.

- Gladden, L. P., Lim, M. H. M., Mantle, M. D., Seiderman, A. J., and Stitt, E. H. (2003). MRI visualisation of two-phase flow in structured supports and trickle-bed reactors. *Catal. Today* 79–80, 203–210. doi: 10.1016/S0920-5861(03)00006-3
- Gogate, P. R. (2008). Cavitation reactors for process intensification of chemical processing applications: a critical review. *Chem. Eng. Process.* 47, 515–527. doi: 10.1016/j.ccep.2007.09.014
- Gracia, F. J., Bollmann, L., Wolf, E. E., Miller, J. T., and Kropf, A. J. (2003). *In situ* FTIR, EXAFS, and activity studies of the effect of crystallite size on silica-supported Pt oxidation catalysts. *J. Catal.* 220, 382–391. doi: 10.1016/S0021-9517(03)00296-3
- Hessel, V. (2009). Novel process windows – gate to maximizing process intensification via flow chemistry. *Chem. Eng. Technol.* 32, 1655–1681. doi: 10.1002/ceat.200900474
- Hussain Motagamwala, A., Ball, M. R., and Dumesic, J. A. (2019). Microkinetic analysis and scaling relations for catalyst design. *Ann. Rev. Chem. Biomol. Eng.* 9, 413–450. doi: 10.1146/annurev-chembioeng-060817-084103
- Katoh, S., Horiuchi, J., and Yoshida, F. (2015). *Biochemical Engineering: A Textbook for Engineers, Chemists and Biologists*, 2nd Edn. Weinheim: Wiley-VCH. doi: 10.1002/9783527684984
- Kiwi-Minsker, L., and Renken, A. (2005). Microstructured reactors for catalytic reactions. *Catal. Today* 110, 2–14. doi: 10.1016/j.cattod.2005.09.011
- Kumar, S. B., Moslemian, D., and Dudukovic, M. P. (1997). Gas-holdup measurements in bubble columns using computed tomography. *AIChE J.* 43, 1414–1425. doi: 10.1002/aic.690430605
- Lerou, J. J., and Ng, K. M. (1996). Chemical Reaction Engineering a multiscale approach to a multiobjective task. *Chem. Eng. Sci.* 51, 1595–1614. doi: 10.1016/0009-2509(96)00022-X
- Levenspiel, O. (1980). The coming-of-age of chemical reaction engineering. *Chem. Eng. Sci.* 35, 1821–1839. doi: 10.1016/0009-2509(80)80132-1

- Levenspiel, O. (1998). *Chemical Reaction Engineering, 3rd Edn.* New York, NY: John Wiley and Sons.
- Li, X., Yang, X., Zhang, J., Huang, Y., and Liu, R. (2019). *In situ/operando* techniques for characterization of single-atom catalysts. *ACS Catal.* 9, 2521–2531. doi: 10.1021/acscatal.8b04937
- Nächter, M., Ondruschka, B., Bonrath, W., and Gum, A. (2004). Microwave assisted synthesis – a critical technology overview. *Green Chem.* 6, 128–141. doi: 10.1039/B310502D
- Rafique, M., Chen, P., and Duduković, M. P. (2004). Computational modeling of gas-liquid flow in bubble columns. *Rev. Chem. Eng.* 20, 225–375. doi: 10.1515/REVCE.2004.20.3-4.225
- Ramachandran, P. A., and Chaudhari, R. V. (1983). *Three Phase Catalytic Reactors.* London: Gordon and Breach Science Publishers.
- Rasmuson, A., Andersson, B., Olsson, L., and Andersson, R. (2014). *Mathematical Modeling in Chemical Engineering.* Cambridge: Cambridge University Press. doi: 10.1017/CBO9781107279124
- Rodrigues, A. E., Pereira, C. S. M., and Santos, J. C. (2012). Chromatographic reactors. *Chem. Eng. Technol.* 35, 1171–1183. doi: 10.1002/ceat.201100696
- Russo, V., Tesser, R., Rossano, C., Vitiello, R., Turco, R., Salmi, T., et al. (2018). Chromatographic reactor modelling. *Chem. Eng. J.* 377, 119692. doi: 10.1016/j.cej.2018.08.078
- Salmi, T. O., Mikkola, J. P., and Warna, J. P. (2010). *Chemical Reaction Engineering and Reactor Technology.* Boca Raton, FL: CRC Press. doi: 10.1201/9781439894859
- Santacesaria, E., and Tesser, R. (2018). *The Chemical Reactor from Laboratory to Industrial Plant.* Cham: Springer International Publishing AG. doi: 10.1007/978-3-319-97439-2
- Scott Fogler, H. (2016). *Elements of Chemical Reaction Engineering, 5th Edn.* Boston, MA: Prentice Hall.
- Švec, R., Grlič, M., Huš, M., and Likozar, B. (2019). Multiscale modeling of (hemi)cellulose hydrolysis and cascade hydrotreatment of 5-hydroxymethylfurfural, furfural, and levulinic acid. *Ind. Eng. Chem. Res.* 58, 16018–16032. doi: 10.1021/acs.iecr.9b00898
- Taylor, R., and Krishna, R. (2000). Modelling reactive distillation. *Chem. Eng. Sci.* 55, 5183–5229. doi: 10.1016/S0009-2509(00)00120-2
- Varma, A., and Morbidelli, M. (1997). *Mathematical Methods in Chemical Engineering.* Oxford: Oxford University Press.

**Conflict of Interest:** The author declares that the research was conducted in the absence of any commercial or financial relationships that could be construed as a potential conflict of interest.

Copyright © 2019 Di Serio. This is an open-access article distributed under the terms of the Creative Commons Attribution License (CC BY). The use, distribution or reproduction in other forums is permitted, provided the original author(s) and the copyright owner(s) are credited and that the original publication in this journal is cited, in accordance with accepted academic practice. No use, distribution or reproduction is permitted which does not comply with these terms.

## Article 5. Copyright Elsevier.



RightsLink

[Sign in/Register](#)



### Polyethoxylation and polypropoxylation reactions: Kinetics, mass transfer and industrial reactor design

**Author:** E. Santacesaria, R. Tesser, M. Di Serio

**Publication:** Chinese Journal of Chemical Engineering

**Publisher:** Elsevier

**Date:** June 2018

*© 2018 The Chemical Industry and Engineering Society of China, and Chemical Industry Press. All rights reserved.*

### Journal Author Rights

Please note that, as the author of this Elsevier article, you retain the right to include it in a thesis or dissertation, provided it is not published commercially. Permission is not required, but please ensure that you reference the journal as the original source. For more information on this and on your other retained rights, please visit: <https://www.elsevier.com/about/our-business/policies/copyright#Author-rights>

[BACK](#)

[CLOSE WINDOW](#)

© 2024 Copyright - All Rights Reserved | [Copyright Clearance Center, Inc.](#) | [Privacy statement](#) | [Data Security and Privacy](#)  
| [For California Residents](#) | [Terms and Conditions](#) Comments? We would like to hear from you. E-mail us at [customer-care@copyright.com](mailto:customer-care@copyright.com)



**Article 5. Santacesaria, E., Tesser, R., & DiSerio, M. (2018). Polyethoxylation and polypropoxylation reactions: Kinetics, mass transfer and industrial reactor design. *Chinese Journal of Chemical Engineering*, 26(6), 1235–1251. <https://doi.org/10.1016/j.cjche.2018.02.020>.**

Chinese Journal of Chemical Engineering 26 (2018) 1235–1251



Contents lists available at ScienceDirect

Chinese Journal of Chemical Engineering

journal homepage: [www.elsevier.com/locate/CJChE](http://www.elsevier.com/locate/CJChE)



Article

## Polyethoxylation and polypropoxylation reactions: Kinetics, mass transfer and industrial reactor design



E. Santacesaria<sup>1,\*</sup>, R. Tesser<sup>2</sup>, M. Di Serio<sup>2</sup>

<sup>1</sup> Eurochem Engineering srl, Via Godogno 5, IT-20139 Milan, Italy

<sup>2</sup> University of Naples "Federico II", Department of Chemical Sciences, Via Cinthia, IT-80126 Naples, Italy

### ARTICLE INFO

#### Article history:

Received 8 November 2017

Received in revised form 7 February 2018

Accepted 9 February 2018

Available online 21 March 2018

#### Keywords:

Ethoxylation

Propoxylation

Kinetics

Mass transfer

Spray tower loop reactor

### ABSTRACT

Ethoxylation and propoxylation reactions are performed in the industry to produce mainly non-ionic surfactants and ethylene oxide (EO)–propylene oxide (PO) copolymers. Both the reactions occur in gas–liquid reactors by feeding gaseous EO, PO or both into the reactor containing a solution of an alkaline catalyst (KOH or NaOH). Non-ionic surfactants are produced by using liquid starters like fatty alcohols, fatty acids or alkyl-phenols, while when the scope is to prepare EO–PO copolymers the starter can be a mono- or multi-functional alcohol of low molecular weight. Both reactions are strongly exothermic, and EO and PO, in some conditions, can give place to runaway and also to explosive side reactions. Therefore, the choice of a suitable reactor is a key factor for operating in safe conditions. A correct reactor design requires: (i) the knowledge of the kinetic laws governing the rates of the occurring reactions; (ii) the role of mass and heat transfer in affecting the reaction rate; (iii) the solubility of EO and PO in the reacting mixture with the non-ideality of the reacting solutions considered; (iv) the density of the reacting mixture. All these aspects have been studied by our research group for different starters of industrial interest, and the data collected by using semibatch well stirred laboratory reactors have been employed for the simulation of industrial reactors, in particular Gas–Liquid Spray Tower Loop Reactors.

© 2018 The Chemical Industry and Engineering Society of China, and Chemical Industry Press. All rights reserved.

### 1. Introduction

Polyethoxylation and polypropoxylation reactions are normally performed, in industry, for preparing non-ionic surfactant and polymers [1–3]. Both the reactions are highly exothermic ( $\sim 83.7 \text{ kJ} \cdot \text{mol}^{-1}$ ) and requires an efficient heat exchange to avoid the hazard of runaway that is particularly dangerous for the possible intervention, at high temperature, of explosive side reactions related to ethylene or propylene oxide decomposition [4,5]. In all cases the reaction needs a starter, that is, a molecule having a more or less acid terminal proton. The starter can be a hydrophobic molecule, in the case of producing surfactants or a hydrophilic molecule of low molecular weight for producing polymers.

Polyethoxylation and polypropoxylation are normally promoted by an alkaline catalyst like KOH, NaOH or related alkoxides previously dissolved in the starter. The reaction is normally studied in laboratory by using well-mixed semibatch reactors. Ethylene oxide (EO) or propylene oxide (PO) or both are gradually added to the solution of an alkaline catalyst in the liquid starter previously heated at the reaction temperature,

normally kept in a range of 120–200 °C. EO and PO, in the mentioned conditions of temperature, quickly evaporate and are partitioned between gas and liquid phases. The reaction occurs in liquid phase between the starter and the gaseous reagent dissolved into the starter. The pressure of the gas phase is kept constant at a level of 0.2–0.5 MPa by continuously feeding the alkylene oxide reagent. To study the reaction kinetics, it is important, first of all, to create a large gas–liquid interface area to avoid mass transfer limitation. Moreover, considering that the reaction occurs in the liquid phase, it is opportune to know how the EO and PO solubility changes by changing pressure, temperature and chemical composition of the reaction environment. It is opportune to achieve the EO, PO solubility data by experiments independent of the kinetic study or by using predictive methods. Another important point to be considered in the kinetic study is that the volume of the reaction mixture increases as the polyalkoxylation reaction proceeds. As a consequence, it is necessary to know how the density of the liquid phase changes with the reaction extent and the temperature. A kinetic model, for interpreting correctly the behavior of the polyalkoxylation reactions, must consider both the mentioned effects and must be developed on the basis of the alkoxylation reaction mechanism. In this review, the kinetic approach for the ethoxylation and propoxylation of many different starters, performed in laboratory semibatch gas–liquid well-stirred reactors, is described in detail together with the agreement achieved between the developed kinetic models and the experimental obtained

\* Corresponding author.

E-mail address: [info@eurochemengineering.com](mailto:info@eurochemengineering.com) (E. Santacesaria),

[riccardo.tesser@unina.it](mailto:riccardo.tesser@unina.it) (R. Tesser), [diserio@unina.it](mailto:diserio@unina.it) (M. Di Serio).

URL: <http://www.eurochemengineering.com> (E. Santacesaria).

results. Then, it will be shown how the kinetic models and related parameters can be usefully employed for simulating the behavior of industrial reactors, in particular, the Spray Tower Loop Reactors.

## 2. Kinetics in the Literature

A lot of kinetic runs have been performed in laboratory by the research group of the authors by using different starters and alternatively EO or PO. The different runs have been performed with the aim to evaluate:

- 1) the effects of both the acidity of the starter and the nucleophilicity of the corresponding anions [6–8].
- 2) the effect of the type of involved hydroxyls using respectively 1- and 2-octanol as starters [9].
- 3) the effect of low molecular weight hydrophilic and polyfunctional starters, such as ethylene and tetraethylene glycols [10].
- 4) the behavior of propylene oxide in comparison with ethylene oxide [9,10].

More details about the performed runs are reported in Fig. 1.

### 2.1. Laboratory reactor for studying the kinetics

The kinetics of polyalkoxylation have been studied by using a thermostated well-mixed semibatch reactors equipped with a magnetic driven stirrer sucking the gas and dispersing it in small bubbles inside the liquid phase. The large interface area developed by stirring avoids reaction rate suffered from mass transfer limitation. EO or PO are pressurized in a bottle with nitrogen and automatically fed to the reactor kept at constant moderate pressure of 0.2 or 0.3 MPa. Small samples of the reacting liquid were withdrawn at different times and analyzed by HPLC. A scheme of the employed apparatus is in Fig. 2.

## 3. Alkoxylation Reaction Mechanism (S<sub>N</sub>2)

The catalyst precursor KOH or NaOH is added to the starter and reacts with it forming in situ the true catalyst and water. Water must be

removed by heating under vacuum the reaction mixture, because, it acts as an undesired starter giving place to a side reaction. Then, when the reaction temperature is reached, ethylene or propylene oxide or both are added and the polymerization reaction starts. The initiation step occurs with an S<sub>N</sub>2 mechanism followed by further reaction steps of propagation occurring with the same mechanism. The product is formed thanks to the proton transfer reaction that is an equilibrium fast reaction. The described reaction mechanism is summarized in the scheme of Fig. 3 [11].

This is a living polymer because no termination occurs and in the presence of the catalyst the reaction starts again when we add ethylene or propylene oxide. The reaction can be definitively stopped only by neutralizing the alkaline catalyst with an acid.

## 4. Polyalkoxylation Kinetic Model Describing a Semibatch Well-stirred Reactor

On the basis of the described mechanism a kinetic model can be written. We can define first of all, an equation describing the substrate consumption and then a series of equations describing respectively the formation and disappearing of any single oligomer and, at last, an equation giving the overall consumption of the alkylene oxide. Then we can consider also the eventual contribution of the mass transfer limitation by equating the overall reaction rate to the mass transfer rate. If the reactor is not perfectly isothermal we have to evaluate also the change of temperature inside the reactor by solving the heat balance equation reported in Fig. 4.

To solve this system of differential equations we need to know, first of all, the expressions of the reaction rates that are present in the system. Considering the reaction mechanism we can write for the initiation and propagation rates second order kinetic laws, such as

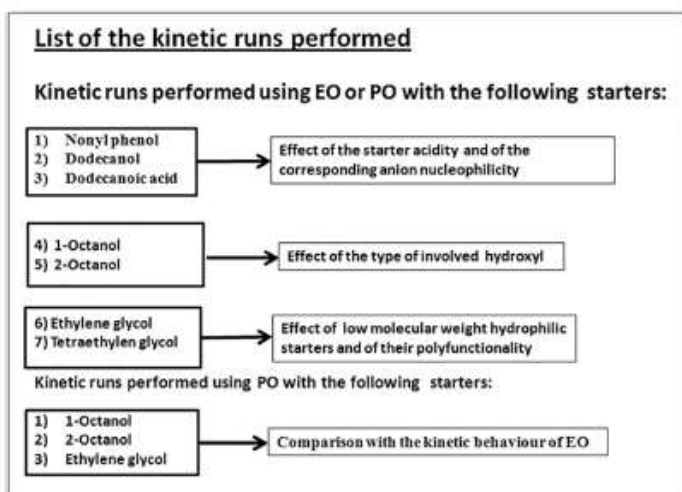
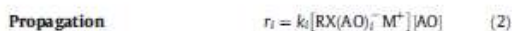


Fig. 1. List of the performed kinetic runs and the related scope.

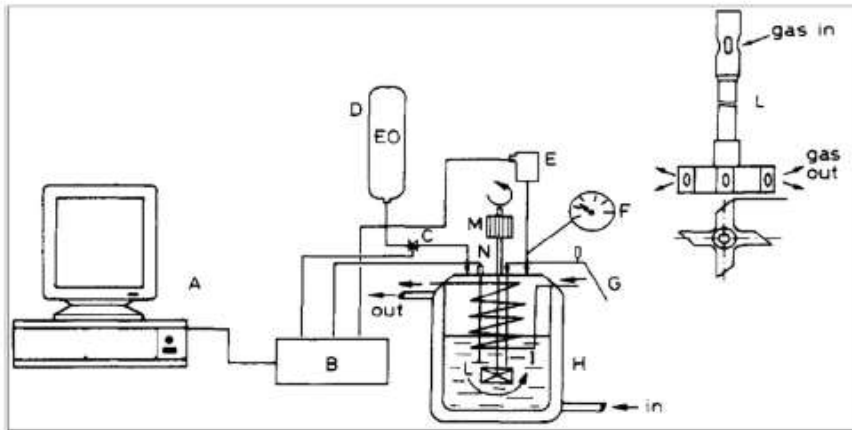


Fig. 2. Scheme of the laboratory reactor for studying polyalkoxylation reactions. A = Computer; B = Computer interface; C = on-off solenoid valve; D = EO bottle; E = Pressure transducer; F = Manometer; G = Line for samples; H = Jacketed reactor; I = Freezing coil; L = Holed stirrer; M = Magnetic driven stirrer; N = Thermocouple. Reprinted with permission from [7] copyright (1992) American Chemical Society.

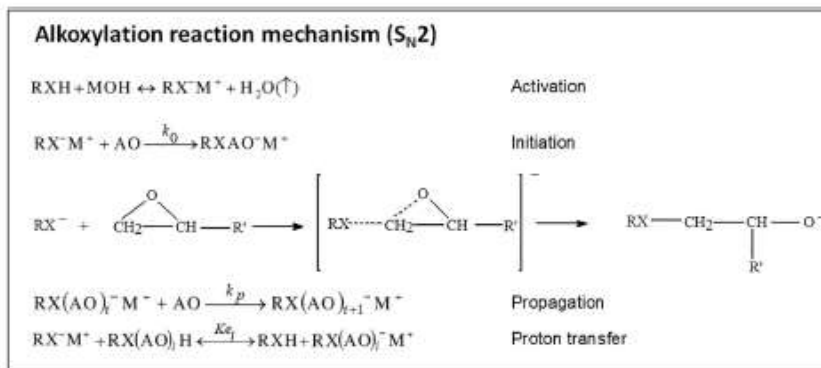


Fig. 3. Polyalkoxylation reaction mechanism.

**Polyalkoxylation kinetic model describing a semibatch gas-liquid well stirred reactor**

Substrate consumption	$\frac{d[RXH]}{dt} = -r_0$
Oligomers formation or consumption	$\frac{d[RX(AO)_iH]}{dt} = r_{i-1} - r_i \quad i = 1, \dots, n$
Overall alkylene oxide consumption	$\frac{dn_{AO}}{dt} = -V_L \sum_{i=0}^n r_i = J$
Gas-liquid mass transfer rate	$J = \beta_L ([AO]_g - [AO]_b)$ with $\beta_L = k_L a_L$
Heat balance for not isotherm reactor	$\frac{d(\rho C_p T)}{dt} = -(\sum_{i=0}^n r_i) \Delta H - q$ $q$ = heat removed from the system by the heat exchanger

Fig. 4. Kinetic model describing a semibatch well-stirred reactor.



Moreover, as the reaction products are obtained through the proton transfer equilibria, we assume all these reactions at equilibrium and introduce the corresponding equilibrium constants.

$$\text{Proton transfer equilibria} \quad K_{el} = \frac{[\text{RXH}][\text{RX}(\text{AO})_i^- \text{M}^+]}{[\text{RX}(\text{AO})_i\text{H}][\text{RX}^- \text{M}^+]} \quad (3)$$

Initial conditions are:  $t = 0$ ,  $[\text{RXH}] = [\text{RXH}]^0$ ,  $[\text{RX}(\text{AO})_i\text{H}] = 0$ ,  $n_{\text{AO}} = 0$ ,  $T = T_i$ .

But we have some other problems to solve before starting with the calculations:

- 1) The concentrations appearing in the expressions of the kinetic model change along the time, not only as a consequence of the reaction but also because the liquid volume of the reacting mixture changes during the reaction.
- 2) The solubility of the alkylene oxide changes, too, with the pressure, temperature and polymer composition, and we need to know how this change occurs.
- 3) At last, the catalyst is partitioned between the unreacted starter anion and the growing chains ethoxylated anions.

This last problem can be solved by introducing in the catalyst mass balance a reasonable approximation expressed by these relations:

$$[\text{RXH}] + [\text{RX}^- \text{M}^+] = [\text{RXH}] \quad \text{and} \quad [\text{RX}(\text{AO})_i\text{H}] + [\text{RX}(\text{AO})_i^- \text{M}^+] = [\text{RX}(\text{AO})_i\text{H}] \quad (4)$$

As a consequence we have:

$$[\text{RX}^- \text{M}^+] = \frac{[\text{RXH} \cdot B^*]}{[\text{RXH}] + \sum_{i=1}^n K_{el} [\text{RX}(\text{AO})_i\text{H}]} \quad \text{and} \quad [\text{RX}(\text{AO})_i^- \text{M}^+] = K_{el} [\text{RX}^- \text{M}^+] \frac{[\text{RX}(\text{AO})_i\text{H}]}{[\text{RXH}]} \quad (5)$$

where  $B^*$  is the overall catalyst concentration. Densities and solubilities must be determined with independent experiments [11,12] or by predictive calculations as described in the following chapter.

### 5. Effect of Density Change on the Kinetics

As before mentioned, we have to evaluate how the density changes as a function of the number of adducts and of the temperature by interpolating, for example, the experimental data with a polynomial empirical expression like the following one:

$$\rho = A + B \left( \frac{EO_{\text{units}}}{[\text{RXH}^{\text{H}^+}]} \right) + C \left( \frac{EO_{\text{units}}}{[\text{RXH}^{\text{H}^+}]} \right)^2 + D \left( \frac{EO_{\text{units}}}{[\text{RXH}^{\text{H}^+}]} \right)^3 + E T \quad (6)$$

**Table 1**

Empirical parameters to describe the densities of different hydrophobic substrates and related ethoxylated mixtures [11,12]

Substrate	A	B	C	D	E	$EO_{\text{units}}$
Nonylphenol + nEO	0.95	$2.33 \times 10^{-2}$	$-5.33 \times 10^{-4}$	$-6.38 \times 10^{-5}$	$-6.5 \times 10^{-4}$	10
Dodecanol + nEO	0.86	$2.50 \times 10^{-2}$	$-4.76 \times 10^{-4}$	$-2.69 \times 10^{-5}$	$-7.7 \times 10^{-4}$	15
Dodecanoic acid + nEO	0.93	$3.29 \times 10^{-2}$	$3.20 \times 10^{-3}$	$-1.02 \times 10^{-3}$	$-8.0 \times 10^{-4}$	4

**Table 2**

Empirical parameters of the Wilson model experimentally found for different substrates

Substrate	$A_{12}$	$B_{12}$	$C_{12}$	$A_{21}$	$B_{21}$	$C_{21}$
Nonylphenol + nEO	4.010	$1.797 \times 10^{-1}$	$1.351 \times 10^{-2}$	$8.987 \times 10^{-1}$	$-4.423 \times 10^{-2}$	$5.329 \times 10^{-4}$
Dodecanol + nEO	13.00	$9.611 \times 10^{-1}$	$-1.967 \times 10^{-2}$	$-4.069 \times 10^{-1}$	$4.714 \times 10^{-2}$	$-1.340 \times 10^{-3}$
Dodecanoic acid + nEO	5.917	1.042	$1.584 \times 10^{-4}$	$8.678 \times 10^{-2}$	$-4.272 \times 10^{-3}$	$-4.200 \times 10^{-6}$

The values of the coefficients A to E, experimentally determined for some different substrates, are reported in Table 1.

### 6. Effect of AO Solubility on the Kinetics

The alkylene oxide solubility in the reaction mixture can be considered as a pseudo-binary system: one component being the alkylene oxide and the other a more or less ethoxylated substrate considering the average number of ethoxy groups [12,13]. The vapor phase can normally be considered ideal, but the liquid phase is usually, characterized by high non-ideality, therefore, the equilibrium alkylene oxide molar fraction in liquid phase is given by the Raoult equation, while the Antoine equation can be used for determining the corresponding equilibrium vapor pressure:

$$\text{Raoult equation} \quad x_{\text{AO}} = \frac{P \gamma_{\text{AO}}}{P_{\text{AO}}^0 \gamma_{\text{AO}}} \quad (7a)$$

$$\text{Antoine equation} \quad P_{\text{AO}}^0 = \frac{\exp \left[ \frac{16.74 - \frac{2568}{T - 29.01}}{760} \right]}{760} \quad (7b)$$

The interpretation of experimental data can be made by using the Wilson or the NRTL methods that performs very well. Here are reported, as example, the Wilson equations containing the binary interaction parameters  $\Lambda_{12}$  and  $\Lambda_{21}$ :

$$\ln \gamma_1 = - \ln(x_1 + x_2 \Lambda_{12}) + x_2 [\Lambda_{12} / (x_1 + x_2 \Lambda_{12}) - \Lambda_{21} / (x_2 + x_1 \Lambda_{21})] \quad (8)$$

$$\ln \gamma_2 = - \ln(x_2 + x_1 \Lambda_{21}) + x_1 [\Lambda_{12} / (x_1 + x_2 \Lambda_{12}) - \Lambda_{21} / (x_2 + x_1 \Lambda_{21})] \quad (9)$$

Then, the binary interaction parameters can be correlated with the average number of alkylene oxide groups  $n_{\text{AO}}$ :

$$\Lambda_{12} = A_{12} + B_{12} n_{\text{AO}} + C_{12} n_{\text{AO}}^2 \quad \Lambda_{21} = A_{21} + B_{21} n_{\text{AO}} + C_{21} n_{\text{AO}}^2 \quad (10)$$

In Table 2 the parameters experimentally found for different substrates are reported.

In the absence of experimental data, the well-known predictive methods such as UNIFAC or ASOG can be used.

### 7. Effect of the Catalyst Anion Nucleophilicity and Starter Acidity

The molecule acidity and the different nucleophilicity of the starter anions have a dramatic effect on the kinetic behavior [11], as it can be appreciated in Fig. 5.

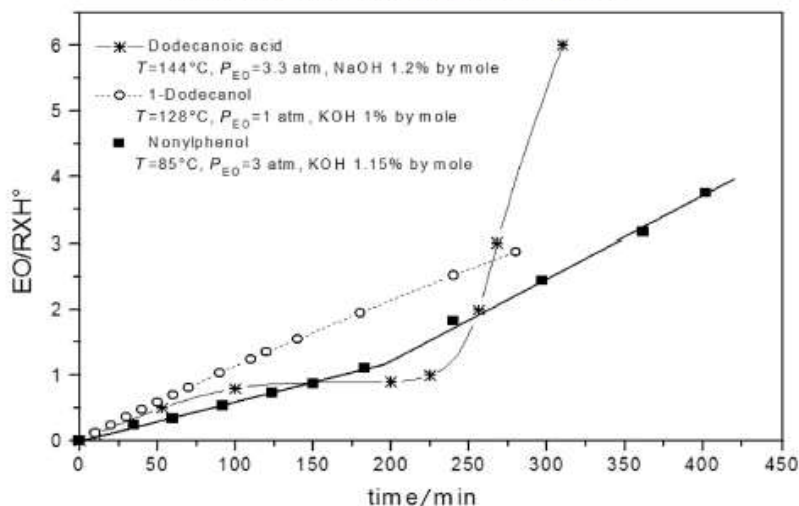


Fig. 5. The effect of acidity of the starter and of nucleophilicity of the corresponding anion on the ethoxylation activity (1 atm = 101.325 kPa) [11].

In Fig. 5, the kinetic behavior observed for respectively 1-dodecanol, dodecanoic acid and nonylphenol are reported for comparison. Dodecanol has a quasi linear trend of the ethylene oxide consumption, nonylphenol shows two consecutive linear trends, while, dodecanoic acid has an initial curve going toward a plateau followed by a linear trend in which the reaction rate increases very much with respect to the initial reaction rate. It has been observed that dodecanoic acid [8] gives place initially to a reaction that is not catalyzed by KOH. The reaction initially is promoted by the acidity of the starter and the reaction, therefore, occurs also in the absence of KOH. When the first adduct completely neutralized the dodecanoic acidity, the reaction, catalyzed by KOH, starts with a rate similar to the one observed for dodecanol. This behavior can be well appreciated in Fig. 6.

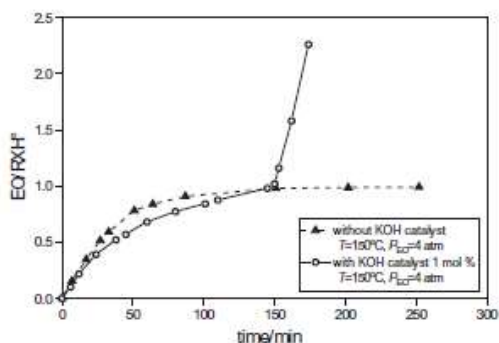


Fig. 6. Peculiar kinetic behavior of fatty acids in the ethoxylation. Reprinted with permission from [8] Copyright (1994) American Chemical Society (1 atm = 101.325 kPa).

In Fig. 7, the kinetic behavior of dodecanol observed in three different runs, performed at  $2 \times 10^5$  Pa of pressure and at three different temperatures is reported [7]. In the same figure an example of oligomer distribution related to Run 1 is also reported. Points are experimental data, lines are calculated with the previously described kinetic model.

Only three parameters are necessary to describe the ethoxylation of a starter constituted by a primary alcohol like dodecanol, because, initiation rate is approximately equal to the rates of all the successive propagation steps. Moreover, the proton exchange equilibrium constant is a unique value independently of chain length and temperature. Therefore, the kinetic parameters experimentally determined for dodecanol are [7]:

$$\ln A_i = \ln A_p = 20.3 \pm 0.30$$

$$\Delta E_i = \Delta E_p = (55.56 \pm 0.95) \text{ kJ} \cdot \text{mol}^{-1} \quad K_{e1} = 4.65$$

The behavior of the kinetic and equilibrium constant with the temperature can be appreciated in Fig. 8.

In Fig. 9, the kinetic behavior of nonylphenol [6] for some runs performed by changing both the temperature and the pressure are reported. In the same figure, an example of oligomer distribution related to run 4 is also reported. As before, points are experimental; lines are calculated always with the previously described kinetic model but with different kinetic parameters.

In this case, the initiation rate is clearly different from the successive propagation steps. This occurs, because, the nonylphenol hydroxyl has a greater acidity and the corresponding anion has a lower nucleophilicity than the primary alcohol formed in the successive propagation steps. Therefore, the initiation kinetic constant is different from the constants of the propagation steps.

Hence, two different kinetic constants and related activation energies and a proton transfer equilibrium parameter and related enthalpy change are necessary, in this case, to describe all the nonylphenol ethoxylation kinetic runs.



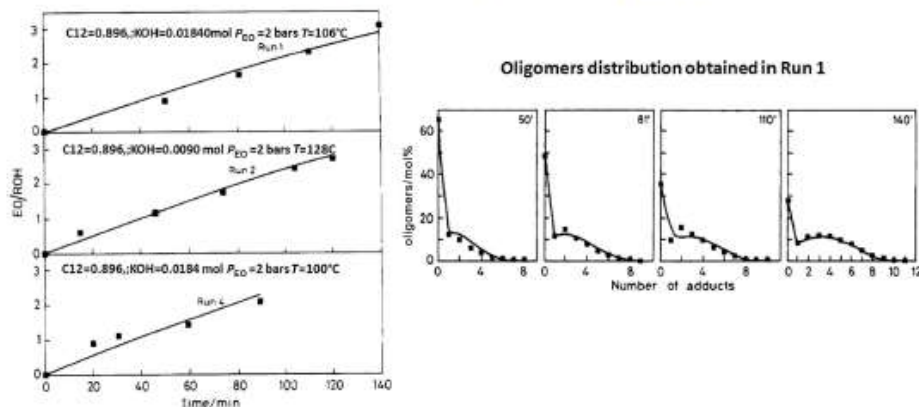


Fig. 7. The kinetic behavior of the starter dodecanol at different temperatures and catalyst concentrations. Reprinted with permission from [7] Copyright (1992) American Chemical Society (1 bar =  $10^5$  Pa).

#### Kinetic parameters determined

$$A_i = (2.16 \pm 0.06) \times 10^{13} \text{ cm}^3 \cdot \text{mol}^{-1} \cdot \text{min}^{-1} \quad \Delta E_i = (102.88 \pm 2.34) \text{ kJ} \cdot \text{mol}^{-1}$$

$$A_p = (2.67 \pm 1.10) \times 10^{16} \text{ cm}^3 \cdot \text{mol}^{-1} \cdot \text{min}^{-1} \quad \Delta E_p = (107.90 \pm 52.26) \text{ kJ} \cdot \text{mol}^{-1}$$

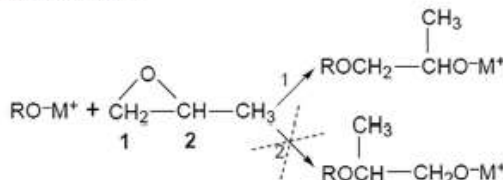
$$K_e = (3.10 \pm 0.12) \times 10^{-12} \quad \Delta H_e = (-91.00 \pm 1.80) \text{ kJ} \cdot \text{mol}^{-1}$$

It is interesting to point out that the difference in the kinetic constant of the initiation step with respect to the propagation one has a dramatic

effect on the oligomers distribution, as shown in Fig. 10. As it can be seen, in this figure, 1-dodecanol shows a broad oligomers distribution and a large amount of un-reacted alcohol if compared with nonylphenol [13].

#### 8. Propoxylation Mechanism and the Kinetics of PO with EO

On a theoretical basis the asymmetric characteristics of the propylene oxide molecule could generate, when ring opening reaction occurs, a primary or a secondary alcohol, as a consequence of the nucleophilic attack to respectively the methylene group 1 or the methyne group 2.



But by  $^{13}\text{C}$  NMR analysis, it is possible to demonstrate that the contribution of route 2 is negligible. Therefore, reaction with PO gives place exclusively to a secondary alcohol. In order to compare the reactivity of primary and secondary alcohols in both ethoxylation and propoxylation, a series of runs have been made using respectively 1- and 2-octanol as starters in both ethoxylation and propoxylation [9,14,15]. The results can be appreciated in the plots of Fig. 11.

As it can be seen, two limit conditions of reactivity can be recognized in Fig. 11 corresponding respectively to the reaction of a primary alcohol with EO (higher activity) and to the reaction of a secondary alcohol with PO (lower activity). These two systems, although having different reactivities, are quite similar in behavior, because the hydroxyl that formed after any step of polymerization has the same characteristics, that is, the primary alcohol reacting with EO remains primary, while the secondary alcohol reacting with PO remains secondary. The consequence is that there is no difference between initiation and propagation

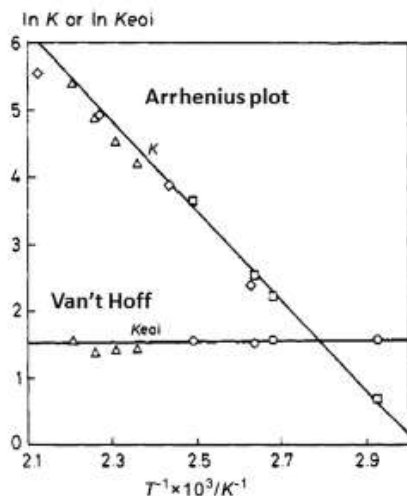


Fig. 8. Arrhenius and Van't Hoff plots for the parameters of dodecanol ethoxylation. Reprinted with permission from [7] Copyright (1992) American Chemical Society.

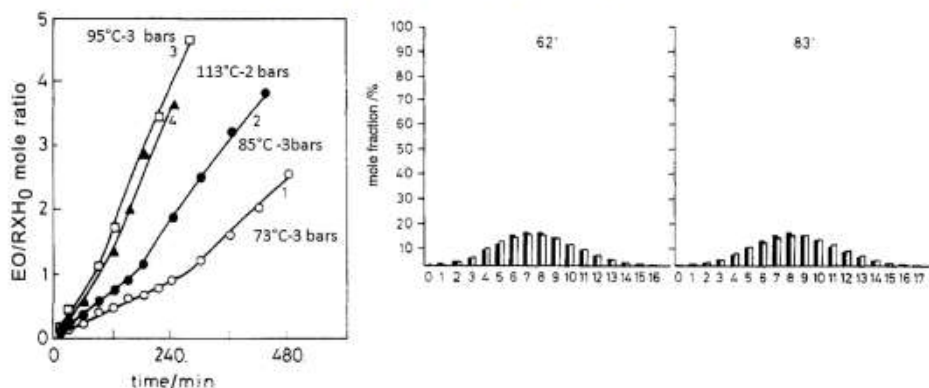


Fig. 9. The kinetic behavior of the starter nonylphenol at different temperatures, pressures and catalyst concentrations: (KOH = 0.015 mol/0.785 mol of NP (run 1,2,3), KOH = 0.083/0.759 of NP (run 4)). Reprinted with permission from [6] Copyright (1990) American Chemical Society (1 bar = 10<sup>5</sup> Pa).

kinetic constants. On the contrary, when a secondary alcohol (2-octanol) is subjected to ethoxylation, a primary alcohol is formed. In this case, initiation and propagation constants are different, but the propagation constant is equal to the one observed for the system starting with a primary alcohol. In the case of a primary alcohol submitted to propoxylation, from a primary alcohol a secondary one is obtained, and again, the initiation has a constant different from propagation, but the propagation step constant is the same as the system starting from secondary alcohol. In other words, at a given temperature only 4 kinetic parameters can describe with a satisfactory approximation all the kinetic behaviors of the considered systems. In conclusion, when a change occurs from primary to secondary alcohol or vice versa we need at least two kinetic constants to describe the system but one only parameter is necessary when no change occurs. So, we can identify four different

occurring reactions with their own kinetic behavior and related kinetic constant:

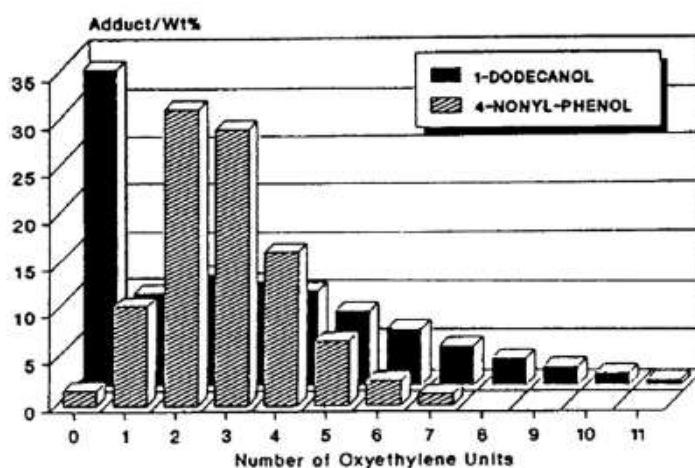
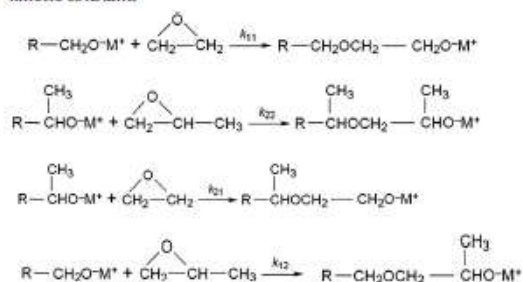


Fig. 10. The effect of the difference in the kinetic constant of initiation and propagation on the oligomers distribution [13].

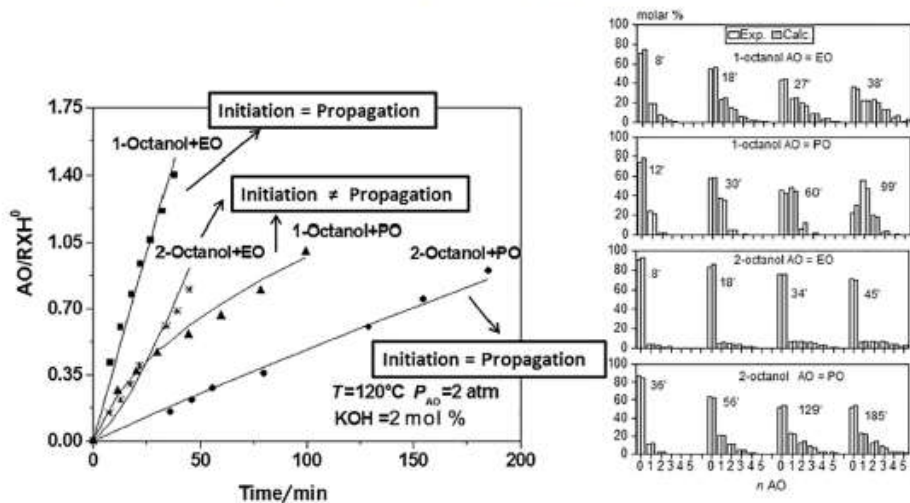


Fig. 11. Kinetic behavior observed for the reaction of 1- and 2-octanol with respectively ethylene and propylene oxide [18].

The kinetic constants for each reaction type are reported in Table 3. For what concerns the proton transfer equilibrium constants, these parameters seem independent of temperature and chain length and the values experimentally found are:

$$K_{e11} = 2.0 \pm 0.3, K_{e12} = 3.5 \pm 0.4, K_{e21} = 2.2 \pm 0.2, K_{e22} = 2.5 \pm 0.3$$

Table 3

Kinetic constants for describing all the reaction occurring in the ethoxylation and propoxylation of both 1 and 2 octanol

Kinetic constants	ln A	$\Delta E/(kJ \cdot mol^{-1})$
$k_{11}$	$20.52 \pm 0.25$	$54.39 \pm 7.5$
$k_{12}$	$22.69 \pm 0.03$	$65.27 \pm 2.1$
$k_{21}$	$23.83 \pm 0.14$	$70.29 \pm 4.2$
$k_{22}$	$25.10 \pm 0.19$	$79.50 \pm 7.9$

The effect of the type of hydroxyl on the EO and PO activity can be well appreciated in the Arrhenius plot of Fig. 12. As it can be seen, we can write that  $k_{11} \gg k_{12} > k_{21} > k_{22}$ .

Again, it is opportune to point out that as in the previous examples for simulating all these systems we need to evaluate, with independent experiments, how density changes with the polymerization degree and the temperature, evaluating the parameters of an empirical polynomial correlation. For example, the densities parameters determined by regression for both 1- and 2-octanol reacting with ethylene or propylene oxide are reported in Table 4.

For completing the kinetic analysis, we have also to evaluate the EO/PO solubilities in both the starter and the corresponding ethoxylated mixture. In this case, the solubility values have been estimated by using the predictive method UNFAC, and the obtained values for a pressure of 0.2 MPa are reported in Table 5. As it can be seen, PO is twice more soluble than EO, and this represents a problem for the safety of the reactors working with PO.

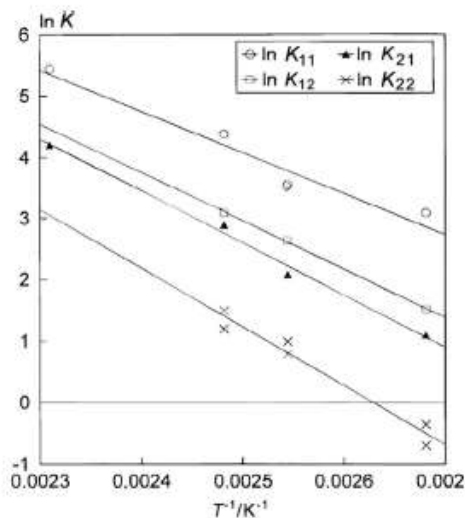


Fig. 12. A comparison of the activity found for the ethoxylation and propoxylation of 1- and 2-octanol respectively. Reprinted with permission from [9] Copyright (1996) American Chemical Society.

Table 4

Empirical parameters for determining the density of the mixtures of oligomers obtained by ethoxylation and propoxylation of 1- and 2-octanol

Starter	Epoxide	A	B	C	$\Delta T / ^\circ C$
1-Octanol	EO	0.860	0.07	$9.0 \times 10^{-4}$	100–130
1-Octanol	PO	0.860	0.05	$9.0 \times 10^{-4}$	100–130
2-Octanol	EO	0.826	0.14	$7.0 \times 10^{-4}$	100–100
2-Octanol	PO	0.826	0.06	$7.0 \times 10^{-4}$	100–130

$$d = A + Bn + CT \text{ (g} \cdot \text{cm}^{-3}\text{)}$$



**Table 5**

Solubilities of EO and PO in 1- and 2-octanol and related oligomers mixtures determined by LNFAC

Substrate	Epoxide	Conc. $\times 10^{-3}/\text{mol}\cdot\text{cm}^{-3}$			
		100 °C	120 °C	130 °C	160 °C
1-Octanol	EO	1.4	0.91	0.77	
1-Octanol + 1 EO	EO	1.4	0.86	0.73	
1-Octanol	PO	2.7	1.80	1.40	
1-Octanol + 1 PO	PO	2.5	1.20	1.00	
2-Octanol	EO	1.4	0.89	0.79	0.42
2-Octanol + 1 EO	EO	1.6	1.00	0.87	0.49
2-Octanol	PO	2.6	1.60	1.30	
2-Octanol + 1 PO	PO	2.0	1.20	0.99	

## 9. Effect of Using Low Molecular Starters

### 9.1. Ethoxylation of ethylene glycol and tetraethylene glycol

Let us consider now the effect on the kinetics of low molecular weight hydrophilic starters. In Fig. 13, the kinetic runs of polyethoxylation using respectively ethylene glycol and tetraethylene glycol, as starters at different temperature are reported [10]. From these figures it is possible to observe that the reaction rate is slightly declining with the starter ethylene glycol, while is just a straight line starting with tetraethylene glycol. The conclusion is that in the first case, we need at least two kinetic parameters for the complete simulation, while in the second case, one only parameter is enough. In Fig. 14 are reported, in an Arrhenius type plot, the kinetic constants of the initiation and propagation reactions for the polyethoxylation of ethylene glycol. Initiation and propagation constants are equal for tetraethylene glycol corresponding to the propagation constant of ethylene glycol.

On the same plot are reported for comparison also the kinetic constants determined for the ethoxylation of 1-octanol and 1-dodecanol. As it can be seen, the data points fall on the straight line, confirming that the propagation constant is approximately the same for a primary alcohol independently of the type of starter (hydrophobic or hydrophilic) and of the chain length.

The best fitting kinetic parameters are:

$$k_i = A_i e^{-\Delta E_i/RT} \quad \ln A_i = 37.5 \pm 2.6$$

$$\Delta E_i = (90.8 \pm 7.9) \text{ kJ} \cdot \text{mol}^{-1}$$

$$k_p = A_p e^{-\Delta E_p/RT} \quad \ln A_p = 28.0 \pm 1.4$$

$$\Delta E_p = (66.1 \pm 4.6) \text{ kJ} \cdot \text{mol}^{-1}$$

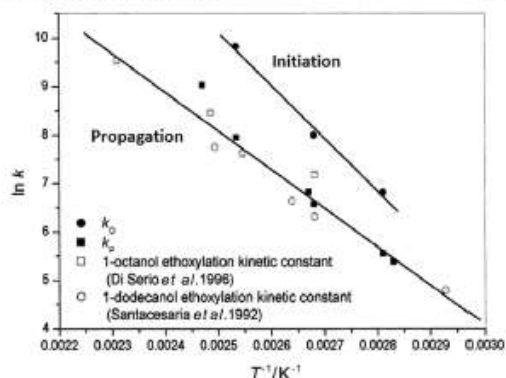
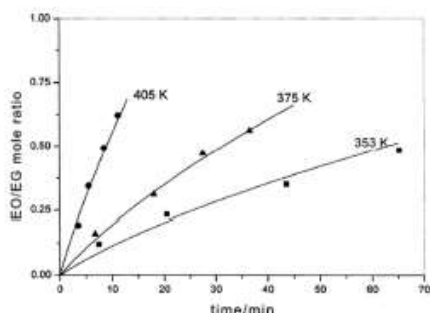


Fig. 14. Arrhenius type plot for the ethoxylation of ethylene glycol. The plot is valid also for the starter tetra-ethylene glycol. Reprinted with permission from [10] Copyright (2002) American Chemical Society.

### 9.2. Propoxylation of ethylene glycol

The reaction of PO with ethylene glycol [10] gives place to an asymmetric mono-adduct (A1). A further reaction with propylene oxide can give two types of bi-adducts: one symmetric (S2) and another asymmetric (A2). The asymmetric compound A2 follows two different growing routes, while S2 has only one possibility of reaction as can be seen in the scheme of Fig. 15.

The kinetic model of propoxylation is slightly different with respect to the model initially described in this work. By considering the mechanism reported in Fig. 15, we have one initiation rate but two different propagation routes, one followed by the symmetric molecules and another one followed by the asymmetric molecules. Therefore, we can write:

Initiation

$$\frac{d[EG]}{dt} = -r_{op} \quad (11)$$

Asymmetric propagation,

$$\frac{d[A_1]}{dt} = r_{op} - r_{1ps} - r_{1pa} \quad \dots \quad \frac{d[A_2]}{dt} = r_{1pA} - r_{1ps} - r_{1pa} \quad (12)$$

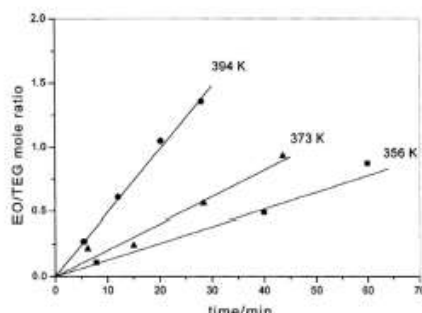


Fig. 13. Ethoxylation of low molecular weight starts, that is, ethylene glycol and tetra-ethylene glycol. Reprinted with permission from [10] Copyright (2002) American Chemical Society.



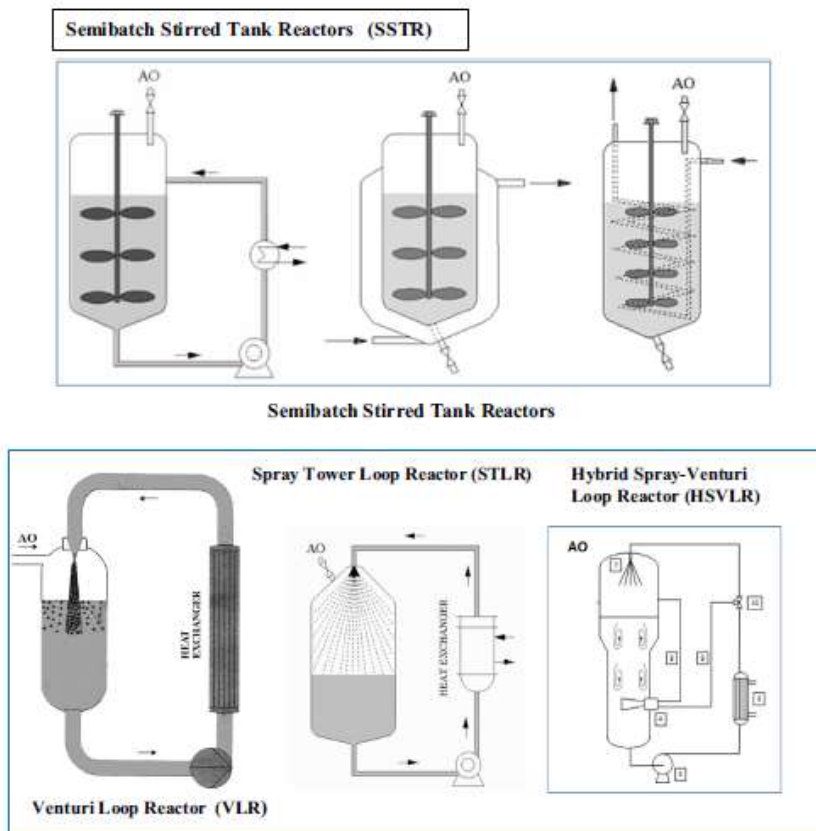


Fig. 17. Simplified schemes of the reactors most used in industry in polyalkoxylation processes [18].

reactor, in which hydrogen gas was sucked by the Venturi tube. It has been then adapted to alkoxylation, but EO and PO are sucked as liquid into the Venturi tube and there vaporize with an exceptional increase of volume. This gas is pressurized into the mixer and gives place to a high gas–liquid interface area inside the reactor. Therefore, this reactor can be considered as a well-mixed gas–liquid reactor and treated with models similar to the already seen isothermal laboratory reactors [15]. The only problem of this reactor is the project of the Venturi tube suitable for this specific application [16].

In all the described reactors, for favoring EO or PO mass transfer, the gas is bubbled into the liquid phase. On the contrary, the Spray Tower Loop Reactors (or Pressindustria-Scientific Design reactors) are singular, because in these reactors the liquid is sprayed in an atmosphere of gaseous EO or PO, that is, the liquid is the dispersed phase [17–20]. Recently, Desmet-Ballestra launched a Hybrid Spray-Venturi Loop Reactor that coupled the advantages of the Venturi Loop Reactor with those of the Spray Tower Loop Reactor.

### 11. Modeling of the Spray Tower Loop Reactor (STLR)

In Fig. 18, a Spray Tower Loop Reactor is sketched. There are two distinct zones of the reactor: the mass transfer zone and the

reaction zone. In the mass transfer zone, the gaseous reagent diffuses into the fine droplets emerging from the spray nozzles. Then, the droplets, more or less saturated with EO or PO, arrive on the top of the liquid pool and start to react. Passing from the top to the bottom of the liquid phase bulk the EO/PO concentration is reduced as a consequence of the reaction according to a Plug Flow pattern. In the meantime, the temperature increases from the top to the bottom due to the reaction heat released. Passing the liquid phase through the external heat exchanger the desired reaction temperature is restored. In optimal conditions, the droplets are completely saturated and contain EO or PO corresponding to their solubility at the reaction temperature.

The saturation level of the drops can be evaluated with a rigorous approach to calculate the average allylene oxide concentration  $C_{AO}^T$  at the end of the drop flight by solving the following differential equation:

$$\frac{dC_{AO}}{dt} = k_L a_L (C_{AO}^* - C_{AO}) \quad (16)$$

where  $t$  corresponds to flight time of the drops going from 0 to the average flight time  $t_{avr}$ . To make the integration we have to know:



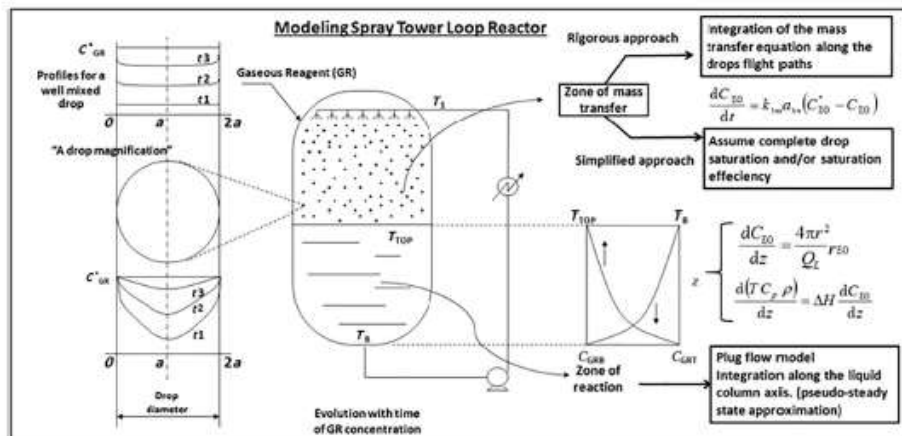


Fig. 18. The scheme of a Spray Loop Reactor with the magnification of the sprayed liquid drops.

(i) the equilibrium solubility of AO ( $C_{AO}$ ); (ii) the average specific surface of the drops ( $a_{lm}$ ), (iii) the average flight time ( $t_{fm}$ ), (iv) the average liquid side mass transfer coefficient ( $k_{lm}$ ) and (v) the AO concentration in the recirculated sprayed liquid entering into the spray nozzle ( $C_{AO}^i$ ). The parameter  $k_{lm}$  and  $a_{lm}$  are estimated with the methods described later in the text. The EO consumption during the absorption into the drops is negligible because the flight time is very small if compared with the residence time of the liquid pool.

The drops, more or less saturated with AO, fall on the liquid surface forming a layer that begins to react and moves toward the bottom of the reactor. The AO concentration along the liquid column can be calculated together with the temperature profile, by assuming the approximation of a plug-flow behavior and by integrating the equation of mass and heat balance from the top of the liquid column ( $z = 0$ ) to the bottom ( $z = h_L$ ). The assumption of a plug flow-like behavior is justified by the observation that the increase of the temperature from the top to the bottom is in agreement with the extent of AO conversion per passage and by the observation that by increasing the residence time of the liquid inside the reactor the difference increases. Then, by assuming a pseudo steady-state condition for the mentioned profiles, the mass and the heat balance can be expressed with the following ordinary differential equations:

$$\frac{dC_{AO}}{dz} = -\frac{4\pi r^2}{Q_L} r_{AO} \quad (17)$$

$$\frac{d(T, C_p, \rho)}{dz} = \frac{\Delta H}{C_p \rho} \frac{dC_{AO}}{dz} \quad (18)$$

The integration of this system of equations can be made by considering the liquid column divided into  $N$  vertical slides that are integrated as standalone reactors keeping boundary conditions between them. This procedure of discretization is useful for increasing the accuracy of the calculations. The advantage is that the integration duration to have the new concentration and temperature profile is  $N$  time lower. In particular, also the gas-phase behavior can be updated after a time equal to  $1/N$  the value of the residence time. This feature has shown improvement especially during fast transients and instability condition simulation. Normally values of  $N = 10$  or  $20$  are enough for obtaining satisfactory results.

For working in optimal conditions it is necessary:

- 1) To know for a given spray nozzle how fast is the EO/PO mass transfer rate, that is, what is the degree of saturation of the droplets falling on the liquid column.
- 2) To evaluate the optimal residence time of the liquid inside the reactor on the basis of the conversion per pass.
- 3) To know what is the temperature profile inside the liquid column.

As we have no information about the performances of the in-line spray nozzles, we have studied this specific problem for answering to the question: how much saturated are the drops falling on the liquid column? For studying all these aspects a spray tower loop laboratory reactor schemed in Fig. 19 have been developed. As it can be seen, in the reactor there is only one spray nozzle inserted in a cylindrical reactor of well-known geometry. A recirculation pump and a heat exchanger allow control over the reaction temperature.

This reactor has been employed for studying and comparing:

- (i) the absorption of  $CO_2$  in an alkaline solution.
- (ii) the absorption of ethylene oxide in dodecanol, containing KOH as catalyst.

The scope is to compare the rates of these two reactions whose kinetics are quite different but well-known, to establish the performance of the spray nozzle in saturating the droplets. The reaction of  $CO_2$  is an extremely fast reaction, normally occurring inside the boundary liquid film and characterized by the presence of an enhancement factor greater than one, while polyethoxylation is a relatively slow reaction, occurring in the liquid bulk, which enhancement factor is equal to about 1. We have experimentally determined, first of all, the droplets size distribution by employing a Laser Scattering technique and feeding water at the spray nozzle (see Fig. 20). In this way, we evaluated the Sauter Mean Diameter of the drops.

The Sauter mean diameter obtained by using water was then corrected for obtaining the corresponding value for the starter dodecanol, then from the Sauter diameter we determined the specific surface area and hence the overall surface area of the flying drops. Then, we examined the geometry of the system [17,20] to evaluate both the average flight time and the average path length of the drops

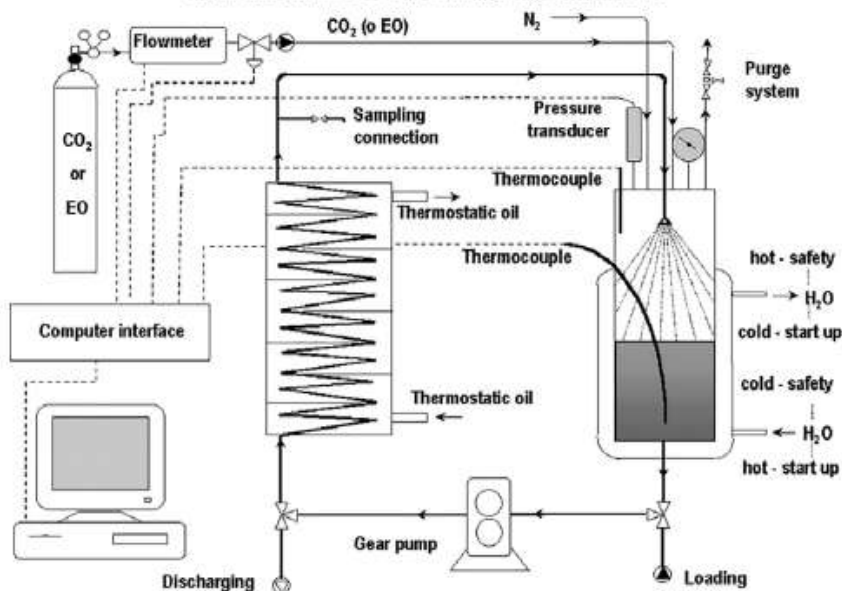


Fig. 19. Scheme of a Laboratory Spray Tower Loop Reactor. Reprinted with permission from [19] Copyright (2000) American Chemical Society.

before the impact on the liquid surface or on the walls of the reactor (see Fig. 21).

The motion of the drops had been considered uniformly accelerated with a speed determined by integrating the following equation:

$$\frac{dx}{dt} = t \left[ g \frac{(\rho - \rho_G)}{\rho} - 3 C_D \left( \frac{dx}{dt} \right)^2 \frac{\rho_G}{\rho D_{32}} \right] + v_0 = v \quad (19) \quad v_0 = \varphi \sqrt{\frac{2\Delta P}{\rho}} \quad (20)$$

considering both the effect of the gravity and that of a friction coefficient  $C_D$  function of the Reynolds number.  $v_0$  is the initial drops velocity corresponding to:

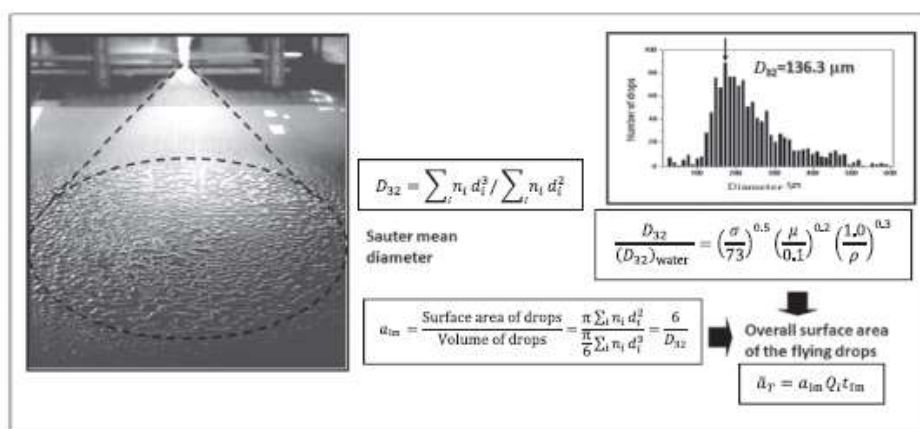


Fig. 20. Determination of drop size distribution with a Laser Scattering Technique and evaluation of the average Sauter diameter  $D_{32}$ . Reprinted with permission from [19] Copyright (2000) American Chemical Society.



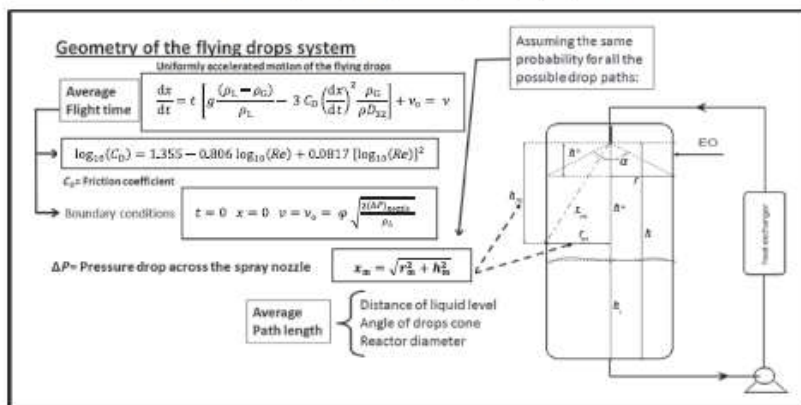


Fig. 21. Determination of the Average Path Length of the drops on the basis of geometrical aspects. Reprinted with permission from [20] Copyright (2005) American Chemical Society.

The length of the path has been calculated on the basis of geometrical aspects as the distance of the liquid level, the angle  $\alpha$  of the spray cone of drops and the reactor diameter.

The problem of a gas diffusion in a spherical drop has already been treated in the literature: one case considering the drop internally well-mixed [21], and another case considering the drop internally stagnant [22,23]. The mathematical description is summarized in Fig. 22.

Both the proposed models have been tested to describe respectively the absorption of  $\text{CO}_2$  in water and in an alkaline solution and the adsorption of EO in dodecanol + KOH catalyst. In Fig. 23 some results obtained for the physical absorption of  $\text{CO}_2$  in water are reported. In the first plot are shown some calculations to evaluate how the drop saturation occurs along the time by respectively assuming that the drop is either well-mixed or stagnant. In the same plot, is reported also an estimation of the drop speed during their flight. As can be seen, the drop life is of the order of some milliseconds. In the second plots, the simulations of two performed experimental run as examples. As is

seen the simulation is satisfactory if we consider the drops internally well-mixed, while the agreement for the stagnant model is poor. In conclusion, the drops emerging from the spray nozzles are internally turbulent.

Let us consider now the behavior of  $\text{CO}_2$  absorption in a sprayed alkaline solution. As previously mentioned, the reaction of  $\text{CO}_2$  with NaOH solution has been largely studied by many different researchers [23–25], but nobody studied this reaction in a spray tower loop reactor. The  $\text{CO}_2$  absorption in this case is the consequence of the two extremely fast reactions:

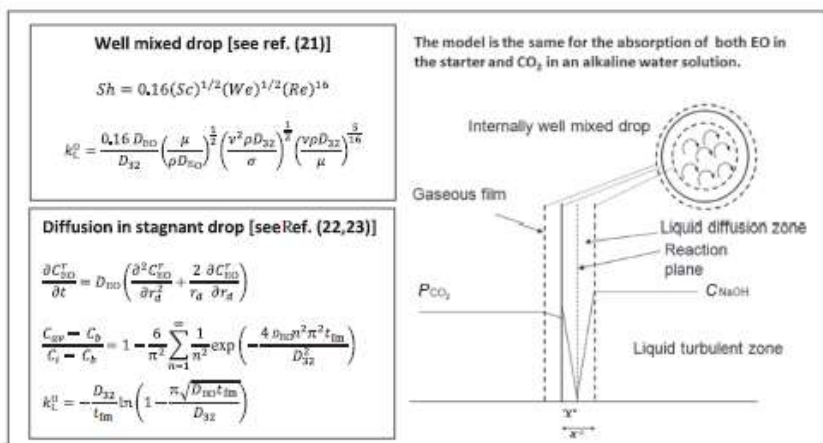


Fig. 22. The problem of gas diffusion in a spherical drop and the solutions in the literature.

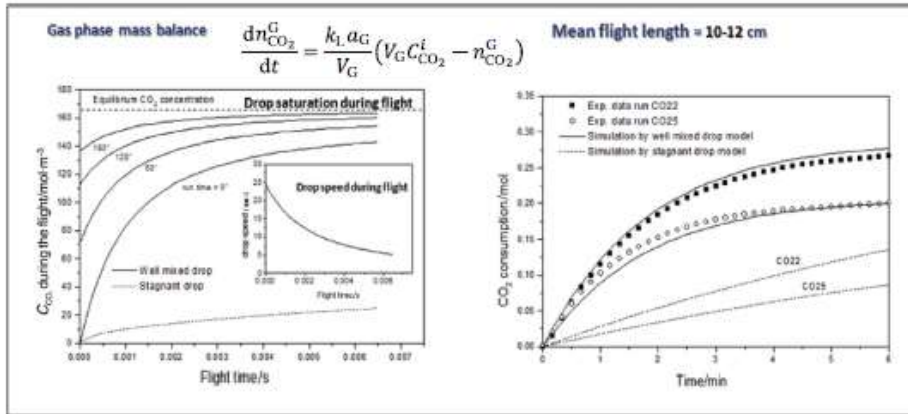


Fig. 23. Kinetics of physical absorption of  $\text{CO}_2$  in water. Comparison of the models with drops stagnant and internally well-mixed. Reprinted with permission from [19] Copyright (2000) American Chemical Society.

The kinetic law for the overall absorption is of the second order, while the mass transfer rate can be expressed as reported in the following expression containing the enhancement factor  $E$ :

$$-V \frac{d[\text{OH}^-]_b}{dt} = 2Ek_1 a_G C_{\text{CO}_2}^i \quad (22)$$

In Fig. 24 the collected experimental points and the calculated simulation line by assuming the drops well-mixed are reported. In the same plot for comparison, is also reported the physical absorption of  $\text{CO}_2$  in water, that is, absorption in the absence of the reaction.

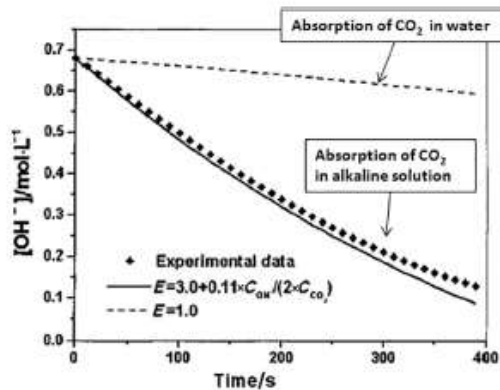


Fig. 24. Kinetics of  $\text{CO}_2$  absorption in an alkaline solution. Reprinted with permission from [19] Copyright (2000) American Chemical Society.

As it can be seen, the effect of the reaction on the mass transfer rate is dramatic. For describing correctly the experimental curves we have introduced an enhancement factor correlation that is a function of both the alkalinity of the solution and of the  $\text{CO}_2$  solubility:

$$E = A + B \left( \frac{[\text{OH}^-]_b}{2 C_{\text{CO}_2}^i} \right) = 3.0 + 0.11 \left( \frac{[\text{OH}^-]_b}{2 C_{\text{CO}_2}^i} \right) \quad (23)$$

For physical absorption in water  $E = 1$ .

Some ethoxylation runs have been performed in a Pilot Spray Tower Loop Reactor by using dodecanol and nonylphenol respectively as starters. The runs, reported in Fig. 25 have been interpreted with the already described kinetic model by using the parameters found as the best for these reactions. Again, we have considered the drops either well-mixed or stagnant. As it can be seen, the best agreement has been obtained by considering the drops internally well mixed in both cases. In the same slide are also reported, as example, the simulations of the evolution of the EO pressure in the reactor and of the temperature measured at the bottom of the liquid column. As can be seen, the agreement of the kinetic model is excellent.

The same kinetic model has then been used also for simulating an industrial reactor running. The reaction in industrial reactors is characterized by three different periods that we can call: (1) Peaking; (2) Reacting and (3) Cooking. Peaking corresponds to the feeding of a small pulse of EO and has the scope to check the functionality of the reactor. As a matter of fact during the peaking (or picking?) period the pressure increases after the EO pulse addition and then decreases as a consequence of the EO reaction. Then, EO is fed with a constant flow rate until the amount of the corresponding number of adducts desired is reached. At this point starts the cooking period in which all the EO accumulated in the reactor must be eliminated by the reaction. All the mentioned operations have been successfully simulated with the described model and also the temperatures, measured at the bottom of the liquid column, are well-fitted, too. A correct simulation of the EO concentration respectively at the head and at the bottom of the liquid column is very important for safety purpose having the scope to estimate what is the accumulation of ethylene oxide inside the reactor.

## 12. Conclusions

The kinetics of ethoxylation and propoxylation have been studied by using many different starters. Ethoxylation and propoxylation have been classified as relatively slow gas–liquid reactions with a Hatta Number = 1. As a consequence, the two films theory can be applied for interpreting mass transfer rates. Venturi Loop Reactors (VLR) are characterized by a dispersion of the gas (EO and/or PO) into the liquid and mass transfer occurs together with the reaction. The kinetic behavior of this reactor is similar to the one of well-mixed semibatch reactors.

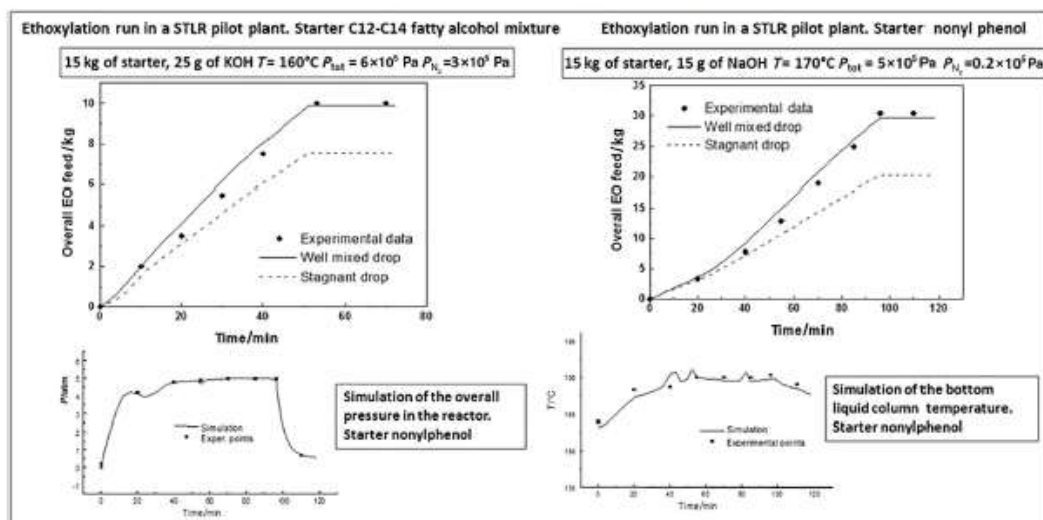


Fig. 25. Simulation of a Pilot Spray Tower Loop Reactor by using a mixture of fatty alcohol and in alternative nonylphenol as starters. The model and the kinetic parameters are the ones previously reported in this work. To assume the drops internally well stirred gives the best simulation results. Modified from [19] Copyright (2000) American Chemical Society (1 atm = 101.325 kPa).

A rigorous mathematical model has been developed to simulate the Spray Tower Loop Reactors for determining:

- The degree of saturation of the drops;
- The amount of reaction occurring inside the liquid column;
- The change of temperature along the liquid column.

The model has shown that with efficient spray nozzles the drops are completely saturated at the end of their flight. This allows to greatly simplify the mathematical model. The developed model has a more general use because can be applied also to the modeling of spray tower absorber.

#### Nomenclature

$A_i$	Pre-exponential factor of the initiation reaction, $\text{cm}^3 \cdot \text{mol}^{-1} \cdot \text{s}^{-1}$
$[AO]$	Concentration of the alkylene oxide in the liquid phase, $\text{mol} \cdot \text{cm}^{-3}$
$A_p$	Pre-exponential factor of the propagation reaction, $\text{cm}^3 \cdot \text{mol}^{-1} \cdot \text{s}^{-1}$
$a_L$ or $a_{lin}$	Average specific interfacial surface area of drops, $\text{cm}^2 \cdot \text{cm}^{-3}$
$a_t$	Total interfacial surface area of flying drops, $\text{cm}^2$
$B^*$	Catalyst concentration, $\text{mol} \cdot \text{cm}^{-3}$
$C_{AO}$	Bulk AO concentration, $\text{mol} \cdot \text{cm}^{-3}$
$C_{AO}$	Interface gas-liquid equilibrium AO concentration, $\text{mol} \cdot \text{cm}^{-3}$
$C_D$	Friction coefficient
$C_{CO_2}$	$\text{CO}_2$ concentration at the gas liquid interface, $\text{mol} \cdot \text{cm}^{-3}$
$C_p$	Liquid specific heat, $\text{J} \cdot \text{g}^{-1} \cdot \text{C}^{-1}$
$D_{EO}$	EO diffusion coefficient, $\text{cm}^2 \cdot \text{s}^{-1}$
$D_{32}$	Sauter diameter, cm
$d_i$	Diameter of $i$ fraction drops, cm
$E$	Enhancement factor
$g$	Gravity acceleration, $\text{cm}^2 \cdot \text{s}^{-2}$
$J$	Gas-liquid mass transfer rate, $\text{mol} \cdot \text{cm}^{-3} \cdot \text{s}^{-1}$
$K_e$	Equilibrium constants of the proton exchange reaction

$k_i$	Constant rate of initiation, $\text{cm}^3 \cdot \text{mol}^{-1} \cdot \text{s}^{-1}$
$k_L$	Average mass transfer gas-liquid coefficient, $\text{cm} \cdot \text{s}^{-1}$
$k_p$	Constant rate of propagation, $\text{cm}^3 \cdot \text{mol}^{-1} \cdot \text{s}^{-1}$
$n_{AO}$	Average number of alkylene oxide units for starter molecule
$n_i$	Number of drops with diameter $d_i$
$P$	Total gaseous pressure, MPa
$P_{AO}^*$	AO vapor pressure
$Q_R$	Liquid re-circulation rate, $\text{cm}^3 \cdot \text{s}^{-1}$
$Re$	Reynold Number ( $D_{32} v \rho / \mu$ )
$[RXH^*]$	Initial starter concentration, $\text{mol} \cdot \text{cm}^{-3}$
$[RXH]$	Starter concentration, $\text{mol} \cdot \text{cm}^{-3}$
$[RX^- M^+]$	Concentration of the ionic form of the starter, $\text{mol} \cdot \text{cm}^{-3}$
$[RX(AO)_i H]$	Oligomer concentration with $i$ adducts of AO in the chain, $\text{mol} \cdot \text{cm}^{-3}$
$[RX(AO)_i^- M^+]$	Concentration of the ionic form of the oligomer concentration with $i$ adducts of AO in the chain, $\text{mol} \cdot \text{cm}^{-3}$
$r$	Reactor radius, cm
$r_{AO}$	Rate of substrate consumption in spray tower loop reactor, $\text{mol} \cdot \text{cm}^{-3} \cdot \text{s}^{-1}$
$r_i$	Rate of oligomer " $i$ " formation or consumption, $\text{mol} \cdot \text{cm}^{-3} \cdot \text{s}^{-1}$
$r_b$	Rate of substrate consumption in semibatch conditions, $\text{mol} \cdot \text{cm}^{-3} \cdot \text{s}^{-1}$
$Sc$	Schmidt Number ( $\mu / \rho D_A$ )
$Sh$	Sherwood Number ( $k_L D_{32} / D_A$ )
$T$	Temperature, K
$t$	Time, s
$t_{200}$	Average flight time, s
$V_L$	Liquid volume, $\text{cm}^3$
$v$	Drops velocity, $\text{cm} \cdot \text{s}^{-1}$
$v_0$	Initial drops velocity, $\text{cm} \cdot \text{s}^{-1}$
$We$	Weber Number ( $v^2 \rho D_{32} / \sigma$ )
$x$	Flying pathway, cm
$x_{AO}$	AO liquid phase molar fraction
$x_{in}$	Average path of sprayed drops, cm
$y_{AO}$	AO gas phase molar fraction
$z$	Spray tower loop reactor length, cm



$\alpha$	Spray cone width angle
$\beta_L$	$k_{iL}$ = Overall gas liquid mass transfer coefficient, $s^{-1}$
$\gamma_{AO}$	AO activity coefficient in liquid phase
$\Delta H$	Reaction enthalpy change, $kJ \cdot mol^{-1}$
$\Delta E_i$	Activation energy of the initiation reaction, $kJ \cdot mol^{-1}$
$\Delta E_p$	Activation energy of the propagation reaction, $kJ \cdot mol^{-1}$
$\Delta P$	Pressure drop of the liquid through the nozzle, MPa
$\mu_G$	Gas viscosity, $Pa \cdot s^{-1}$
$\mu_L$	Liquid viscosity, $g \cdot cm^{-1} \cdot s^{-1}$
$\rho$ or $\rho_L$	Liquid density, $g \cdot cm^{-3}$
$\rho_G$	Gas density
$\sigma$	Surface tension, $g \cdot s^{-2}$
$\varphi$	Spray efficiency factor (dimensionless)

### Acknowledgments

Thanks are due to the valuable help of all the students of Master Degree that worked on the topic. Thanks are due to Pressindustria, Scientific Design and Desmet Ballestra for the financial support to the researches described in this work.

### References

- [1] F.E. Bailey, J.V. Koleske, Polyoxyalkylene: Ullmann's Encyclopedia of Industrial Chemistry, vol. A21, VCI: Verlagsgesellschaft, (1992) 579–589.
- [2] M.J. Schick, Nonionic Surfactants, Surfactants; Science Series, vol. 1, Marcel Dekker, New York, 1967.
- [3] Nico M. Van Os (Ed.), Nonionic Surfactants: Organic Chemistry, Surfactant Science Series, vol. 72, Marcel Dekker Inc., New York, (1997).
- [4] G. Mulé, La Rivista Italiana delle Sostanze Grasse, vol. LXVII, 1990 447.
- [5] A.A. Pekalski, J.E. Zevenbergen, M. Bmithwaite, S.M. Lemkowitz, H.J. Pasman, Explosive decomposition of ethylene oxide at elevated condition: effect of ignition energy, nitrogen dilution, and turbulence, *J. Hazard. Mater.* 118 (1–3) (2005) 19–34.
- [6] E. Santacesaria, M. Di Serio, L. Lisi, D. Gelosa, Kinetics of Nonylphenol Polyethoxylation catalyzed by potassium hydroxide, *Ind. Eng. Chem. Res.* 29 (1990) 719–725.
- [7] E. Santacesaria, M. Di Serio, R. Garaffa, G. Addino, Kinetics and mechanism of fatty alcohol polyethoxylation, the reaction catalyzed by potassium hydroxide, *Ind. Eng. Chem. Res.* 31 (1992) 2413–2418.
- [8] M. Di Serio, S. Di Martino, E. Santacesaria, Kinetics of fatty acids polyethoxylation, *Ind. Eng. Chem. Res.* 33 (1994) 509–514.
- [9] M. Di Serio, G. Vairo, P. Iengo, F. Felippone, E. Santacesaria, Kinetics of ethoxylation and propoxylation of 1- and 2-octanol catalyzed by KOH, *Ind. Eng. Chem. Res.* 35 (1996) 3848–3853.
- [10] M. Di Serio, R. Tesser, A. Dimiccoli, E. Santacesaria, Kinetics of ethoxylation and propoxylation of ethylene glycol catalyzed by KOH, *Ind. Eng. Chem. Res.* 41 (2002) 5196–5206.
- [11] E. Santacesaria, P. Iengo, M. Di Serio, Catalytic and kinetic effects in ethoxylation processes, in: D.R. Karsa (Ed.), Design and Selection of Performance Surfactants, Sheffield Academic Press, 1999.
- [12] M. Di Serio, R. Tesser, F. Felippone, E. Santacesaria, Ethylene oxide solubility and ethoxylation kinetics in synthesis of nonionic surfactants, *Ind. Eng. Chem. Res.* 34 (1995) 4092–4098.
- [13] E. Santacesaria, M. Di Serio, R. Tesser, Role of ethylene oxide solubility in the ethoxylation processes, *Catal. Today* 24 (1995) 23–28.
- [14] E. Santacesaria, M. Di Serio, R. Tesser, Production of ethylene oxide/propylene oxide block copolymers, in: Uri Zoller, Paul Soosis (Eds.), Handbook of Detergents, Part F, Surfactant Science Series, vol. 142, (2009).
- [15] E. Santacesaria, M. Di Serio, P. Iengo, Kinetic and reactor simulation for polyethoxylation and polypropoxylation reactions, in: G.F. Froment, K.C. Waugh Eds., Reaction Kinetics and the Development of Catalytic Process, Elsevier Science B.V. 1999, pp. 267–274.
- [16] L. Van Dierendonck, J. Zahradnik, V. Linek, Loop Venturi reactors, a feasible alternative to stirred tank reactors? *Ind. Eng. Chem. Res.* 37 (1998) 734–738.
- [17] E. Santacesaria, M. Di Serio, P. Iengo, Mass transfer and kinetics in ethoxylation spray tower loop reactors, *Chem. Eng. Sci.* 54 (1999) 1489–1504.
- [18] A. Dimiccoli, M. Di Serio, E. Santacesaria, Key factor in ethoxylation and propoxylation technology, SRD CESTO, Proceedings, World Surfactant Congress, Firenze, vol. 1, 2000, pp. 99–110.
- [19] A. Dimiccoli, M. Di Serio, E. Santacesaria, Mass transfer and kinetics in spray-tower-loop absorbers and reactors, *Ind. Eng. Chem. Res.* 39 (2000) 4082–4093.
- [20] M. Di Serio, R. Tesser, E. Santacesaria, Comparison of different reactor types used in the manufacture of ethoxylated, propoxylated products, *Ind. Eng. Chem. Res.* 44 (25) (2005) 9482–9489.
- [21] V. Srinivasan, R.C. Aiken, Mass transfer to droplets formed by the controlled breakup of a cylindrical jet-physical absorption, *Chem. Eng. Sci.* 43 (12) (1988) 3141–3150.
- [22] J. Crank, The Mathematics of Diffusion, Clarendon Press, Oxford, 1958.
- [23] A.I. Johnson, A.E. Hamielec, D. Ward, A. Golding, End effect corrections in heat and mass transfer studies, *Can. J. Chem. Eng. Sci.* 8 (1958) 201–215.
- [24] G. Astaria, Mass Transfer with Chemical Reaction, Elsevier Publishing Company, New York, 1967.
- [25] P.V. Danckwerts, Gas-Liquid Reactions, McGraw Hill Co., New York, 1970.

## Appendix 2

### Articles 1 to 5 Declarations of co-authors on the substantive contribution to the articles

#### Table of contents:

Article	Pages
1. Russo, V., Tesser, R., Hreczuch, W., & <b>DiSerio, M.</b> (2023). Design of a continuous device for ethoxylation reaction: The choice between micro and milli scale. <i>Chemical Engineering Research and Design</i> . 194 (2023) 550–562, <a href="https://doi.org/10.1016/j.cherd.2023.04.051">https://doi.org/10.1016/j.cherd.2023.04.051</a> .	195 – 198
2. <b>DiSerio, M.</b> , Russo, V., Santacesaria, E., & Tesser, R. (2021). The Evolution of the Fed Batch Ethoxylation Reactors to Produce the Non-Ionic Surfactants. <i>Frontiers in Chemical Engineering</i> , Vol. 3, Article 644719, <a href="https://doi.org/10.3389/fceng.2021.644719">https://doi.org/10.3389/fceng.2021.644719</a> .	199 – 202
3. Tesser, R., Russo, V., Santacesaria, E., Hreczuch, W., & <b>DiSerio, M.</b> (2020). Alkoxylation for Surfactant Productions: Toward the Continuous Reactors. <i>Frontiers in Chemical Engineering</i> , Vol. 2, Article 7. <a href="https://www.semanticscholar.org/paper/Alkoxylation-for-Surfactant-Productions%3A-Toward-the-Tesser-Russo/a6b82dc93b5bf66cf4bd12f4e54c1c2dc9a34ef4">https://www.semanticscholar.org/paper/Alkoxylation-for-Surfactant-Productions%3A-Toward-the-Tesser-Russo/a6b82dc93b5bf66cf4bd12f4e54c1c2dc9a34ef4</a>	203 – 207
4. <b>M DiSerio</b> (2019), Chemical reaction engineering as a bridge between nano and macro world, <i>Frontiers in Chemical Engineering</i> , Vol. 1, Article 2, <a href="https://www.frontiersin.org/articles/10.3389/fceng.2019.00002/full">https://www.frontiersin.org/articles/10.3389/fceng.2019.00002/full</a> .	208
5. Santacesaria, E., Tesser, R., & <b>DiSerio, M.</b> (2018). Polyethoxylation and polypropoxylation reactions: Kinetics, mass transfer and industrial reactor design. <i>Chinese Journal of Chemical Engineering</i> , 26(6), 1235–1251. <a href="https://doi.org/10.1016/j.cjche.2018.02.020">https://doi.org/10.1016/j.cjche.2018.02.020</a> .	209 - 211

Napoli, 26.07.2024

Dr. Russo, Vincenzo,  
University of Naples Federico II  
Department of Chemical Science, via Cintia 4  
80126, Napoli, Italy

Statement of substantive contribution  
to the article

I declare that at work:

Russo, V., Tesser, R., Hreczuch, W., & DiSerio, M. (2023).  
Process intensification for ethoxylation Reaction: the choice between micro and milli scale.  
*Chemical Engineering Research and Design*, 194, 550–562.

Martino Di Serio and Vincenzo Russo wrote the original draft of the manuscript. The main conceptual ideas were drawn from the interactions between Martino Di Serio and Wiesław Hreczuch. The development of the artworks, the data elaboration and the formal analysis were conducted by Vincenzo Russo and Riccardo Tesser. The final draft was corrected by all the authors.

Signature of the coauthor:

.....  
  
.....  
Dr. V. Russo

Napoli, 26.07.2024

D.Sc. Wiesław Hreczuch,  
MEXEO  
Energetyków 9 Street  
47-225 Kędzierzyn-Koźle, Poland

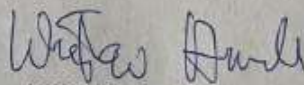
Statement of substantive contribution  
to the article

I declare that at work:

Russo, V., Tesser, R., Hreczuch, W., & DiSerio, M. (2023).  
Process intensification for ethoxylation Reaction: the choice between micro and milli scale.  
*Chemical Engineering Research and Design*, 194, 550–562.

Martino Di Serio and Vincenzo Russo wrote the original draft of the manuscript. The main conceptual ideas were drawn from the interactions between Martino Di Serio and Wiesław Hreczuch. The development of the artworks, the data elaboration and the formal analysis were conducted by Vincenzo Russo and Riccardo Tesser. The final draft was corrected by all the authors.

Signature of the coauthor:



.....  
Dr. W. Hreczuch



Napoli, 26.07.2024

Prof. Tesser, Riccardo  
University of Naples Federico II  
Department of Chemical Science, via Cintia 4  
80126, Napoli, Italy

Statement of substantive contribution  
to the article

I declare that at work:

Russo, V., Tesser, R., Hreczuch, W., & DiSerio, M. (2023).  
Process intensification for ethoxylation Reaction: the choice between micro and milli scale.  
*Chemical Engineering Research and Design*, 194, 550–562.

Martino Di Serio and Vincenzo Russo wrote the original draft of the manuscript. The main conceptual ideas were drawn from the interactions between Martino Di Serio and Wiesław Hreczuch. The development of the artworks, the data elaboration and the formal analysis were conducted by Vincenzo Russo and Riccardo Tesser. The final draft was corrected by all the authors.

Signature of the coauthor:



.....  
Prof. Riccardo Tesser

Napoli, 26.07.2024

Prof. Di Serio, Martino  
University of Naples Federico II  
Department of Chemical Science, via Cintia 4  
80126, Napoli, Italy

Statement of substantive contribution  
to the article

I declare that at work:

Russo, V., Tesser, R., Hreczuch, W., & DiSerio, M. (2023).  
Process intensification for ethoxylation Reaction: the choice between micro and milli scale.  
*Chemical Engineering Research and Design*, 194, 550–562.

Martino Di Serio and Vincenzo Russo wrote the original draft of the manuscript. The main conceptual ideas were drawn from the interactions between Martino Di Serio and Wiesław Hreczuch. The development of the artworks, the data elaboration and the formal analysis were conducted by Vincenzo Russo and Riccardo Tesser. The final draft was corrected by all the authors.

Signature of the coauthor:

  
Prof. Martino Di Serio

Napoli, 26.07.2024

Dr. Russo, Vincenzo,  
University of Naples Federico II  
Department of Chemical Science, via Cintia 4  
80126, Napoli, Italy

Statement of substantive contribution  
to the article

I declare that at work:

Di Serio, M., Russo, V., Santacesaria, E., & Tesser, R. (2021).  
The Evolution of the Fed Batch Ethoxylation Reactors to Produce the Non-Ionic Surfactants.  
*Frontiers in Chemical Engineering*, 3.

Martino Di Serio and Riccardo Tesser wrote the original draft of the manuscript with support from Elio Santacesaria. The main conceptual ideas were drawn from the interactions between Martino Di Serio and Riccardo Tesser. The development of the artworks, the data elaboration and the formal analysis were conducted by Vincenzo Russo and Riccardo Tesser. The final draft was corrected by all the authors.

Signature of the coauthor:

..........  
Dr. V. Russo

Napoli, 26.07.2024

Prof. Elio Santacesaria  
Eurochem Engineering  
Via Codogno 10  
20139 Milano, Italy

Statement of substantive contribution  
to the article

I declare that at work:

Di Serio, M., Russo, V., Santacesaria, E., & Tesser, R. (2021).  
The Evolution of the Fed Batch Ethoxylation Reactors to Produce the Non-Ionic Surfactants.  
*Frontiers in Chemical Engineering*, 3.

Martino Di Serio and Riccardo Tesser wrote the original draft of the manuscript with support from Elio Santacesaria. The main conceptual ideas were drawn from the interactions between Martino Di Serio and Riccardo Tesser. The development of the artworks, the data elaboration and the formal analysis were conducted by Vincenzo Russi and Riccardo Tesser. The final draft was corrected by all the authors



Signature of the coauthor:

.....  
Prof. E. Santacesaria

Napoli, 26.07.2024

Prof. Tesser, Riccardo  
University of Naples Federico II  
Department of Chemical Science, via Cintia 4  
80126, Napoli, Italy

Statement of substantive contribution  
to the article

I declare that at work:

Di Serio, M., Russo, V., Santacesaria, E., & Tesser, R. (2021).  
The Evolution of the Fed Batch Ethoxylation Reactors to Produce the Non-Ionic Surfactants.  
*Frontiers in Chemical Engineering*, 3.

Martino Di Serio and Riccardo Tesser wrote the original draft of the manuscript with support from Elio Santacesaria. The main conceptual ideas were drawn from the interactions between Martino Di Serio and Riccardo Tesser. The development of the artworks, the data elaboration and the formal analysis were conducted by Vincenzo Russi and Riccardo Tesser. The final draft was corrected by all the authors

Signature of the coauthor:



.....  
Prof. Riccardo Tesser

Napoli, 26.07.2024

Prof. Di Serio, Martino  
University of Naples Federico II  
Department of Chemical Science, via Cintia 4  
80126, Napoli, Italy

Statement of substantive contribution  
to the article

I declare that at work:

Di Serio, M., Russo, V., Santacesaria, E., & Tesser, R. (2021).  
The Evolution of the Fed Batch Ethoxylation Reactors to Produce the Non-Ionic Surfactants.  
*Frontiers in Chemical Engineering*, 3.

Martino Di Serio and Riccardo Tesser wrote the original draft of the manuscript with support from Elio Santacesaria. The main conceptual ideas were drawn from the interactions between Martino Di Serio and Riccardo Tesser. The development of the artworks, the data elaboration and the formal analysis were conducted by Vincenzo Russi and Riccardo Tesser. The final draft was corrected by all the authors

Signature of the coauthor:

  
.....  
Prof. Martino Di Serio

Napoli, 26.07.2024

Dr. Russo, Vincenzo,  
University of Naples Federico II  
Department of Chemical Science, via Cintia 4  
80126, Napoli, Italy

Statement of substantive contribution  
to the article

I declare that at work:

Tesser, R., Russo, V., Santacesaria, E., Hreczuch, W., & Di Serio, M. (2020).  
Alkoxylation for Surfactant Productions: Toward the Continuous Reactors.  
*Frontiers in Chemical Engineering*, 2(7)

Martino Di Serio drew the initial idea of the work and directed the workgroup composed by the other authors, who gave the same contribution as each of them edited part of the review. All authors contributed to the article and approved the submitted version.

Signature of the coauthor:

  
.....  
Dr. V. Russo



Napoli, 26.07.2024

D.Sc. Wiesław Hreczuch,  
MEXEO  
Energetyków 9 Street  
47-225 Kędzierzyn-Koźle, Poland

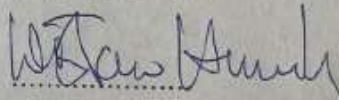
Statement of substantive contribution  
to the article

I declare that at work:

Tesser, R., Russo, V., Santacesaria, E., Hreczuch, W., & Di Serio, M. (2020).  
Alkoxylation for Surfactant Productions: Toward the Continuous Reactors.  
*Frontiers in Chemical Engineering*, 2(7)

Martino Di Serio drew the initial idea of the work and directed the workgroup composed by the other authors, who gave the same contribution as each of them edited part of the review. All authors contributed to the article and approved the submitted version.

Signature of the coauthor:



Dr. W. Hreczuch

Napoli, 26.07.2024

Prof. Elio Santacesaria  
Eurochem Engineering  
Via Codogno 10  
20139 Milano, Italy

Statement of substantive contribution  
to the article

I declare that at work:

Tesser, R., Russo, V., Santacesaria, E., Hreczuch, W., & Di Serio, M. (2020).  
Alkoxylation for Surfactant Productions: Toward the Continuous Reactors.  
*Frontiers in Chemical Engineering*, 2(7)

Martino Di Serio drew the initial idea of the work and directed the workgroup composed by the other authors, who gave the same contribution as each of them edited part of the review. All authors contributed to the article and approved the submitted version

Signature of the coauthor:



.....  
Prof. E. Santacesaria

Napoli, 26.07.2024

Prof. Tesser, Riccardo  
University of Naples Federico II  
Department of Chemical Science, via Cintia 4  
80126, Napoli, Italy

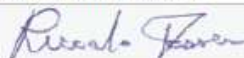
Statement of substantive contribution  
to the article

I declare that at work:

Tesser, R., Russo, V., Santacesaria, E., Hreczuch, W., & Di Serio, M. (2020).  
Alkoxylation for Surfactant Productions: Toward the Continuous Reactors.  
*Frontiers in Chemical Engineering*, 2(7)

Martino Di Serio drew the initial idea of the work and directed the workgroup composed by the other authors, who gave the same contribution as each of them edited part of the review. All authors contributed to the article and approved the submitted version

Signature of the coauthor:



Prof. Riccardo Tesser

Napoli, 26.07.2024

Prof. Di Serio, Martino  
University of Naples Federico II  
Department of Chemical Science, via Cintia 4  
80126, Napoli, Italy

Statement of substantive contribution  
to the article

I declare that at work:

Tesser, R., Russo, V., Santacesaria, E., Hreczuch, W., & Di Serio, M. (2020).  
Alkoxylation for Surfactant Productions: Toward the Continuous Reactors.  
*Frontiers in Chemical Engineering*, 2(7)

Martino Di Serio drew the initial idea of the work and directed the workgroup composed by the other authors, who gave the same contribution as each of them edited part of the review. All authors contributed to the article and approved the submitted version

Signature of the coauthor:

  
Prof. Martino Di Serio

Napoli, 26.07.2024

Prof. Di Serio, Martino  
University of Naples Federico II  
Department of Chemical Science, via Cintia 4  
80126, Napoli, Italy

Statement of substantive contribution  
to the article

I declare that at work:

Di Serio, M. (2019)  
Chemical reaction engineering as a bridge between nano and macro world  
*Frontiers in Chemical Engineering* 1(2), 31.

Martino Di Serio is the unique author of the paper

Signature of the author:



Prof. Martino Di Serio

Napoli, 26.07.2024

Prof. Elio Santacesaria  
Eurochem Engineering  
Via Codogno 10  
20139 Milano, Italy

Statement of substantive contribution  
to the article

I declare that at work:

Santacesaria, E., Tesser, R., & Di Serio, M. (2018).  
Polyethoxylation and polypropoxylation reactions: Kinetics, mass transfer and industrial  
reactor design.  
*Chinese Journal of Chemical Engineering*, 26(6), 1235–1251

Elio Santacesaria drew the initial idea of the work and directed the workgroup composed by  
the other authors, who gave the same contribution as each of them edited part of the review.  
All authors contributed to the article and approved the submitted version.

Signature of the coauthor:



.....  
Prof. E. Santacesaria

Napoli, 26.07.2024

Prof. Tesser, Riccardo  
University of Naples Federico II  
Department of Chemical Science, via Cintia 4  
80126, Napoli, Italy

Statement of substantive contribution  
to the article

I declare that at work:

Santacesaria, E., Tesser, R., & Di Serio, M. (2018).  
Polyethoxylation and polypropoxylation reactions: Kinetics, mass transfer and industrial  
reactor design.  
*Chinese Journal of Chemical Engineering*, 26(6), 1235–1251

Elio Santacesaria drew the initial idea of the work and directed the workgroup composed by  
the other authors, who gave the same contribution as each of them edited part of the review.  
All authors contributed to the article and approved the submitted version.

Signature of the coauthor:

  
.....  
Prof. Riccardo Tesser



Napoli, 26.07.2024

Prof. Di Serio, Martino  
University of Naples Federico II  
Department of Chemical Science, via Cintia 4  
80126, Napoli, Italy

Statement of substantive contribution  
to the article

I declare that at work:

Santacesaria, E., Tesser, R., & **Di Serio, M.** (2018).  
Polyethoxylation and polypropoxylation reactions: Kinetics, mass transfer and industrial  
reactor design.  
*Chinese Journal of Chemical Engineering*, 26(6), 1235–1251

Elio Santacesaria drew the initial idea of the work and directed the workgroup composed by  
the other authors, who gave the same contribution as each of them edited part of the review.  
All authors contributed to the article and approved the submitted version.

Signature of the coauthor:

  
Prof. Martino Di Serio